

**INSTITUTO POTOSINO DE INVESTIGACIÓN
CIENTÍFICA Y TECNOLÓGICA, A.C.**

POSGRADO EN CIENCIAS APLICADAS

**Environmental Applications of Functionalized
Activated Carbon with Iron Oxyhydroxide
Nanoparticles.**

Tesis que presenta

Javier Antonio Arcibar Orozco

Para obtener el grado de

Doctor en Ciencias Aplicadas

En la opción de

Ciencias Ambientales

Director de la Tesis:

Dr. José René Rangel Méndez

San Luis Potosí, S.L.P., diciembre de 2013.



Constancia de aprobación de la tesis

La tesis “*Environmental applications of functionalized activated carbon with iron oxyhydroxide nanoparticles*” presentada para obtener el Grado de Doctor en Ciencias Aplicadas en la opción de Ciencias Ambientales fue elaborada por **Javier Antonio Arcibar Orozco** y aprobada el **dieciseis de diciembre de dos mil trece** por los suscritos, designados por el Colegio de Profesores de la División de Ciencias Ambientales del Instituto Potosino de Investigación Científica y Tecnológica, A.C.

Dr. José René Rangel Méndez
Director de la tesis

Dra. Ma. Catalina Alfaro de la Torre
Miembro del Comité Tutorial

Dr. Miguel Avalos Borja
Miembro del Comité Tutorial

Dr. Vladimir Alonso Escobar Barrios
Miembro del Comité Tutorial



Créditos Institucionales

Esta tesis fue elaborada en la División de Ciencias Ambientales del Instituto Potosino de Investigación Científica y Tecnológica, A.C., bajo la dirección del Dr. José René Rangel Méndez.

Durante la realización del trabajo el autor recibió una beca académica del Consejo Nacional de Ciencia y Tecnología (232598) y del Instituto Potosino de Investigación Científica y Tecnológica, A. C.

La investigación desarrollada en esta tesis fue financiada por el proyecto: SEP-CB-2008-01-105920 bajo la dirección del Dr. José René Rangel Méndez, y se encuentra dentro del marco de investigación de la solicitud 219794 del fondo SEP-CONACYT.

El autor agradece el apoyo otorgado por la División de Ciencias Ambientales del Instituto Potosino de Investigación Científica y Tecnológica, A.C, para la presentación del trabajo en conferencias internacionales y nacionales.



Instituto Potosino de Investigación Científica y Tecnológica, A.C.

Acta de Examen de Grado

El Secretario Académico del Instituto Potosino de Investigación Científica y Tecnológica, A.C., certifica que en el Acta 021 del Libro Primero de Actas de Exámenes de Grado del Programa de Doctorado en Ciencias Aplicadas en la opción de Ciencias Ambientales está asentado lo siguiente:

En la ciudad de San Luis Potosí a los 16 días del mes de diciembre del año 2013, se reunió a las 09:30 horas en las instalaciones del Instituto Potosino de Investigación Científica y Tecnológica, A.C., el Jurado integrado por:

Dr. Miguel Avalos Borja	Presidente	IPICYT
Dra. Ma. Catalina Alfaro de la Torre	Secretario	UASLP
Dr. José René Rangel Méndez	Sinodal	IPICYT
Dr. Vladimir Alonso Escobar Barrios	Sinodal	IPICYT

a fin de efectuar el examen, que para obtener el Grado de:

DOCTOR EN CIENCIAS APLICADAS
EN LA OPCION DE CIENCIAS AMBIENTALES

sustentó el C.

Javier Antonio Arcibar Orozco

sobre la Tesis intitulada:

Environmental applications of functionalized activated carbon with iron oxyhydroxide nanoparticles

que se desarrolló bajo la dirección de

Dr. José René Rangel Méndez

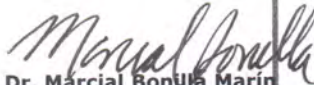
El Jurado, después de deliberar, determinó

APROBARLO

Dándose por terminado el acto a las 12:00 horas, procediendo a la firma del Acta los integrantes del Jurado. Dando fe el Secretario Académico del Instituto.

A petición del interesado y para los fines que al mismo convengan, se extiende el presente documento en la ciudad de San Luis Potosí, S.L.P., México, a los 16 días del mes de diciembre de 2013.


Mtra. Ivonne Lizette Cuevas Vélez
Jefa del Departamento del Posgrado


Dr. Marcial Bonilla Marín
Secretario Académico



Dedicatoria

Le dedico esta tesis doctoral a mis padres y mi hermana, que durante estos 4 años y medio me han apoyado de una forma que solamente la familia puede hacerlo, por aguantarme durante mis ratos de mal humor, aceptarme, comprenderme y creer en mí sin importar lo ridículas que fueran mis decisiones y actitudes.

Así mismo dedico este trabajo a 2 de las personas que con su ejemplo de tenacidad, perseverancia y fortaleza, han representado para mí esa dosis diaria de energía para levantarme sin importar cuántas veces caiga, para ser un roble en la tempestad, para saber que mi momento es ahora, que quizá no nací para ganar pero sí que nací para intentar, esas personas son mis abuelos: Josefina Montaña Guzmán y Antonio Arcibar Martínez.

Para ustedes mi más grande agradecimiento y mi dedicatoria.

Agradecimientos

A mis **padres y hermana** por darme el apoyo incondicional y la comprensión que solamente la familia puede darte.

A mis **amigos** que con su entusiasmo y compañía siempre han sabido mantenerme centrado en la realidad, llenado de energía y equilibrado en mi vida diaria. Les agradezco por su amistad incondicional y por dejarme ser parte de sus vidas.

A mis **amigos del IPICYT**: *Erika, Liz, Emilia, Gaby, Marco, Fátima, Pablo, Mayra, Nancy, Julián, José Luis, Josué, Jorge, Miguel, Guillermo* y los que me faltan. Por aceptarme como soy y haberme ayudado con sus críticas, buen humor y apoyo.

A mis **excompañeros**: *Bernardo, José Luis, Nancy, El Memo, Cesar, Paola, Mayra, Lalo y Alma* que con su ejemplo y dirección me orientaron en mi fase de formación para adentrarme en el mundo de la ciencia y la investigación. En especial al Dr. Cesar Nieto Delgado y al Dr. Pablo Delgado que quizá sin saberlo, con su ejemplo me han motivado para ser una persona crítica y productiva que busca superarse en el día a día.

A mis **compañeros del grupo**: *Litza, Héctor, Aurora, Charly, Alejandra y Esmeralda* que con sus siempre atinados comentarios, valiosas opiniones y sus diversos puntos de vista me han ayudado a mejorar mi trabajo de tesis y además me han compartido de su conocimiento.

A los **técnicos** de las divisiones de Ciencias Ambientales y Materiales Avanzados: Juan Pablo Rodas, Guillermo Vidriales, Gladis Labrada, Beatriz Rivera, Nicolás Cayetano y en especial a las técnicas: *Dulce Partida y María del Carmen Rocha* que siempre me ayudaron con disponibilidad y alegría.

A los **laboratorios nacionales**: LANBAMA y LINAN y en especial al Dr. Miguel Avalos Borja por su ayuda durante la caracterización del material.

A **Jennifer Eckerly** que me ayudó durante la redacción en inglés de la tesis y de prácticamente todos mis artículos de investigación.

A la **Dra. Teresa Badosz** y a mis amigos de *The City College*: *Anna, Mykola, Benoit, Mikolaj, Rajiv, Niyi, Amani, Nana y Svetlana* que me acogieron durante mi estadía en USA y además contribuyeron a mi formación con sus sabias enseñanzas y su opinión siempre crítica.

Finalmente al **Dr. René Rangel Méndez** por aceptarme en su grupo de trabajo, compartirme de sus conocimientos y formarme como doctor, además le agradezco ese especial apoyo que siempre me dio no solo como asesor, sino como amigo.

A todos ellos:

¡MUCHAS GRACIAS!...

Contents

Constancia de aprobación de la tesis	ii
Créditos institucionales	iii
Acta de examen	iv
Dedicatorias	v
Agradecimientos	vi
Contents	vii
List of Tables	xii
List of Figures	xiv
Resumen	xxi
Abstract	xxiii
Structure of this thesis	xxv

CHAPTER 1: Introduction

1.1. Pollution of air and water	2
1.2. Arsenic and sulfur, priority pollutants of water and air	2
1.3. Methodologies of pollution control	6
1.3.1. Arsenic removal	6
1.3.2. Desulfurization	7
1.3.2.1. Ultra-deep desulfurization	8
1.3.2.2. Adsorptive ultra-deep desulfurization	9
1.3.3. Interference of nitrogen compounds and adsorptive denitrogenation	10
1.4. Fundamentals of adsorption	12
1.4.1. Nature of physisorption forces	13
1.4.2. Surface complexation	15
1.4.2.1. Inner sphere complexes	15
1.4.2.2. Reactive adsorption	17
1.4.3. Adsorption equilibrium	18
1.4.3.1. Langmuir isotherm	18
1.4.3.2. Brunauer-Emmet and Teller (BET) isotherm	19
1.4.3.3. Freundlich isotherm	20
1.4.3.4. Other adsorption models	20
1.4.4. Adsorption kinetics	22
1.4.5. Adsorbent materials	23
1.5. Activated carbon	23
1.5.1. Structure	24
1.5.2. Chemistry	27
1.5.3. Application of the adsorption operation in activated carbon	28
1.5.3.1. Adsorption in liquid phase	29
1.5.3.2. Adsorption from gas phase	35
1.5.4. Constrains of activated carbon	30
1.6. Tailoring activated carbon	31

1.6.1.	Iron oxyhydroxides	32
1.6.2.	Advantages of iron oxyhydroxide-AC adsorbents	34
1.6.3.	Methodologies to incorporate iron oxyhydroxides on activated carbon.	35
1.6.3.1.	Impregnation	35
1.6.3.2.	Incipient wetness impregnation	36
1.6.3.3.	Precipitation	36
1.6.3.4.	Salt evaporation	36
1.6.3.5.	Fe(II) oxidation	37
1.6.3.6.	Forced hydrolysis	37
1.6.4.	Forced hydrolysis, from solution to particles	38
1.6.5.	Forced hydrolysis in the presence of activated carbon	40
1.7.	The importance of the nano-scale	41
1.8.	The capping agent effect	42
1.9.	State of the art	44
1.9.1.	Removal of arsenic from aqueous solution	44
1.9.2.	Removal of SO ₂ from gas phase	44
1.9.3.	Adsorptive desulfurization from diesel fuel	48
1.10.	Motivation for this research	48
1.11.	Hypothesis	49
1.12.	Objectives	49
1.12.1.1.	General objective	49
1.12.1.2.	Specific objectives	50

CHAPTER 2: Effect of Particle Size of Ferric Oxyhydroxides on the As(V) Removal from Water.

Abstract	52
2.1. Introduction	52
2.2. Experimental	55
2.2.1. Materials and chemicals	55
2.2.2. Activated carbon modification	55
2.2.3. Adsorption experiments	56
2.2.4. Materials characterization	56
2.3. Results and discussion	58
2.3.1. Adsorption experiments	58
2.3.2. Material characterization	61
2.3.3. Possible contribution of phosphate as capping agent	69
2.4. Conclusions	74

CHAPTER 3: Influence of Iron Content, Surface Area and Charge Distribution in the Arsenic Removal.

Abstract	76
3.1. Introduction	76
3.2. Experimental	78
3.2.1. Materials and chemicals	78
3.2.2. Activated carbons oxidation and alkaline treatment	79
3.2.3. Iron modified activated carbons	80
3.2.4. Materials characterization	80
3.2.5. Arsenic(V) adsorption test	81
3.2.6. Statistical analyses	81
3.3. Results and discussion	82
3.3.1. Material characterization	82
3.3.2. Arsenic adsorption test	90
3.3.3. Effect of the adsorbent surface charge on As(V) uptake	95
3.4. Conclusions	98

CHAPTER 4: Role of Iron Particle Size in the Reactive Adsorption of SO₂.

Abstract	101
4.1. Introduction	101
4.2. Experimental	104
4.2.1. SO ₂ dynamic adsorption experiments	104
4.2.2. Material characterization	105
4.3. Results and discussion	106
4.3.1. Materials characterization	106
4.3.2. Dynamic adsorption experiments	109
4.4. Conclusions	124

CHAPTER 5: Desulfurization of Model Diesel Fuel: Effect of Tert-Butylbenzene and Naphthalene Concentrations.

Abstract	126
5.1. Introduction	126
5.2. Experimental	128
5.2.1. Experimental setup	128
5.2.2. Material characterization	129
5.3. Results and discussion	131
5.4. Conclusions	148

CHAPTER 6: Model Diesel Denitrogenation: Sulfur Compounds Effect.

Abstract	150
6.1. Introduction	150
6.2. Experimental	152
6.2.1. Materials and chemicals	152
6.2.2. Materials characterization	153
6.2.3. Adsorption isotherms	154
6.2.4. Compounds determination	154
6.3. Results and discussion	155
6.3.1. Materials characterization	155
6.3.2. Adsorption experiments	159
6.3.2.1. Single adsorption of indoline and quinoline	160
6.3.2.2. Competitive adsorption of indoline-quinoline	162
6.3.2.3. Effect of sulfur compounds on indoline and quinoline uptake	162
6.3.3. Adsorption mechanism	170
6.4. Conclusions	173

CHAPTER 7: Final Remarks

7. Final Remarks	174
------------------	-----

CHAPTER 8: Final Conclusions, perspectives and scientific products

8.1. Final Conclusions	184
8.2. Perspectives	188
8.3. Scientific products	190
8.3.1. List of publications	190
8.3.2. Attendance to conferences	191
8.3.3. Conference proceedings	192

References

References	193
------------	-----

Appendixes

Appendix A	224
Appendix B	226
Appendix C	229

List of Tables

Table 1.1 Methodologies of arsenic removal from water.	7
Table 1.2 Strategies for gas and diesel desulfurization.	9
Table 1.3 Models of surface complexation.	21
Table 1.4 Iron oxyhydroxide allotropes and highlighted properties.	33
Table 1.5 Effect of phosphate during the hydrolysis of ferric ions.	43
Table 1.6 Highlighted recent studies focused in the removal of arsenic from water in iron modified activated carbons.	46
Table 1.7 Selected works related with the desulfurization of diesel fuel by activated carbon.	47
Table 2.1 Parameters of Langmuir and Freundlich isotherms for arsenic removal in selected materials at 25 °C and pH 7.	61
Table 2.2 Pore volume of carbon samples calculated from nitrogen adsorption isotherms at 77 K by DFT.	63
Table 2.3 Species distribution of the solution employed during carbon modification.	71
Table 3.1 Textural features of materials studied.	86
Table 3.2 Paired Student's t-test of transformed Q As(V) values.	90
Table 3.3 Results of the multiple regression analysis showing the factor coefficients of the variables and the selection criteria. The selected model is denoted by *.	93
Table 4.1 Surface areas and pore volumes of the initial and exhausted	108

samples.

Table 4.2 pK _a positions, number of groups (in parentheses (mmol/g)), and surface pH values for the initial and exhausted samples.	111
Table 4.3 SO ₂ adsorption capacities of the materials studied and water uptake during the prehumidification.	113
Table 5.1. Composition of the different model diesel fuels.	130
Table 5.2 Summarized of the adsorption capacities and selectivities of breakthrough curves.	136
Table 5.3 Parameters of surface area and pore volume of materials.	139
Table 5.4 Species identified after furan extraction from the surfaces of samples after exposure to MDF.	146
Table 6.1 Physical surface properties of studied materials.	158
Table 6.2 Elemental content of studied materials.	160
Table 6.3 Langmuir and Freundlich parameters and Standard deviation of adsorption experiments.	161
Table 7.1 Comparison of the adsorption capacities reported in similar works.	178
Table 7.2 Adsorption capacities of SO ₂ adsorbents, took from reference [47].	181

List of Figures

Figure 1.1 Schematization of the world health problem of arsenic around the world.	4
Figure 1.2 Representation of the problems related to the presence of sulfur in air due to the burning of fossil fuels, mainly diesel fuel.	5
Figure 1.3 Concept of the two stages, adsorptive denitrogenation and desulfurization, in one and two bed systems.	11
Figure 1.4 Lennard-Jones potential for an adsorbate molecule.	13
Figure 1.5 Polar interactions of adsorbates and solid surfaces.	15
Figure 1.6 Geometries of coordination complexation between metal oxidants and ligands.	17
Figure 1.7 Illustration of mass transference resistances on porous solids.	22
Figure 1.8 Starting from a macroscopic point of view in A) , the scanning electron image in B) shows macroporosity associated to carbons, and by means of transmission images C)-F) amorphous nature of graphite sheets in activated carbon [119]. The edges of the layers contain various oxygenated functionalities as represented in G) , modified from [118].	25
Figure 1.9 Representations of the porous structure of activated carbon. A) <i>The Norit</i> model showing the formation of porous where the layer is stabilized by oxygen functionalities. B) <i>Potato chip model</i> representing porosity in activated carbon. C) <i>negative branched tree model</i> representing pore interconnectivity in activated carbon, adapted from	26

Reynoso and March [117].

Figure 1.10 Concentration profile and evolution of the MTZ in the GAC packed columns. 30

Figure 1.11 Different linkages of octahedral in Fe^{III} and their Fe-Fe distances, adapted from. 34

Figure 1.12 Possible interactions between iron and oxygen groups in activated carbon A) carboxylic, B) phenolic, C) lactonic and D) carbonyl. 40

Figure 2.1 A) Effect of hydrolysis time, temperature and molar ratio PO_4/Fe on the As(V) adsorption capacity (at 25° C, pH 7 and C_0 of 4.5 mg/L), standard error of central point is 0.038(1.67%) and **B)** Pareto chart of the experimental design. 59

Figure 2.2 Surface response of arsenic(V) adsorption capacity (25 °C, pH 7 and C_i of 4.5 mg/L) as function of molar ratio and hydrolysis time at 80 °C. 60

Figure 2.3 Arsenic(V) adsorption isotherms at 25 °C and pH 7. 60

Figure 2.4 Synthetized materials at 80°C and at a hydrolysis time of 60 h: **A)** arsenic adsorption capacity; **B)** BET surface area, **C)** Iron content and **D)** Phosphorous content. 62

Figure 2.5 Surface adsorption capacity as a function of the molar ratio PO_4/Fe . The linear equation is: adsorption = 0.0005*MR+0.003. 63

Figure 2.6 A) STEM image of GAC. **B)** EDS of GAC, (no iron was detected). **C)** STEM image of ACM, arrows indicate nanoparticles. **D)** EDS of ACM particles, indicating the presence of Fe. **E)** STEM image of ACM 64

1P: **F)** EDS of ACM 1P, indicating the presence of Fe ($K\alpha$ and $K\beta$ transitions). **G)** Fourier filtered image of selected area in **E)**.

Figure 2.7 Surface charge distributions of studied materials at room temperature. 66

Figure 2.8 XRD patterns of studied materials with a step size of $0.02^\circ 2\theta$ at 10 s per step. 68

Figure 2.9 Adsorption and stabilization of the surface charge by anions **A)** without capping agent, **B)** in the presence of the capping agent and **C)** adsorption of ferrous ions in the surface of activated carbon without the capping agent and **D)** in the presence of the capping agent. This effect contributes at a higher adsorption and to a better distribution of iron species on activated carbon. 72

Figure 2.10 Adsorption of phosphate anions on the surface of the growing IOH nanoparticles. 73

Figure 3.1 Point of zero charge (pH_{PZC}) of un-modified and modified activated carbons. 83

Figure 3.2 pK_a distribution of dissociated groups on the surface of the CS and CF. 84

Figure 3.3 Iron content of activated carbons before and after modification. 85

Figure 3.4 A) SEM image of the surface of CS5.0h-MP, **B)** Colored contour of iron nanoparticles inside the red square. The particles inside yellow line are in the range of 6-7 nm. 87

Figure 3.5 Arsenic(V) adsorption capacity of modified and unmodified 89

activated carbons carried out at a starting concentration of 4 ppm As(V), pH 7 and 25°C.

Figure 3.6 Relationships between arsenic adsorption capacity of the adsorbents under study and their pH_{PZC} , surface area, micropore volume and iron content. 91

Figure 3.7 **A)** Developed empiric model that describes the arsenic adsorption capacity as a function of the iron content and pH_{PZC} . **B)** Predicted versus measured adsorption capacity. **C)** Importance of activated carbon features over the arsenic adsorption capacity. 95

Figure 3.8 Arsenate (As(V)) adsorption mechanism on modified activated carbons with: **A) Acidic properties.** Most of the carbon surface remains negatively charged causing an electrostatic repulsion of anions preventing the adsorption of some arsenates onto iron oxyhydroxide particles. **B) Basic properties.** The positive surface charged attracts arsenates allowing their interaction with iron oxyhydroxide particles and with basic groups by electrostatic interactions. 97

Figure 3.9 Surface charge distribution of CF-MP and CW-MP at 25°C. 98

Figure 4.1 Experimental setup to adsorb SO₂. 105

Figure 4.2 **A)** TEM image of AC-M, **B)** STEM image of AC-MP and **C)** Fourier Transform image of the dotted area in Figure B; the arrows indicate iron nanoparticles of about 2.5-4 nm. 107

Figure 4.3. Nitrogen adsorption isotherms of studied materials. 109

Figure 4.4 Pore size distributions for the initial samples and those 110

exposed to SO₂ in moist and dry conditions.

Figure 4.5 SO₂ breakthrough curves for the studied materials measured 112
in moist **(A)** and dry **(B)** conditions.

Figure 4.6 The DTG curves for the initial samples and those exposed to 115
SO₂ in moist and dry conditions.

Figure 4.7 Proton binding curves of the materials before and after 117
exposure to SO₂ in moist and dry conditions.

Figure 4.8 Schematic representation of the anchorage of iron 119
oxyhydroxides on oxygenated groups of the carbon matrix.

Figure 4.9 Role of the iron particle size in the SO₂ uptake. **A)** adsorbed 123
SO₂ interacts with chemisorbed oxygen and water to form H₂SO₄. **B)** Iron
deposition causes a decrease in the adsorption capacity, owing to the
screening of surface groups by larger iron nanoparticles. **C)** Capping
agent utilization decreases iron nanoparticle size, and thus increases the
number of adsorption centers and their distribution.

Figure 5.1 Breakthrough curves of **(A)** DBT on GAC, **(B)** DMDBT on 132
GAC, **(C)** DBT on ACM 1P and **(D)** DMDBT onto ACM 1P.

Figure 5.2. Breakthrough curves of naphthalene and TBB from MDFLC 134
(A) and of DBT and DMDBT on regenerated materials exposed to MDFLC
(B).

Figure 5.3 Contour plots that reflect the effects of naphthalene and tert- 138
butylbenzene on the adsorption capacities of DBT on ACM-1P **(A)**,
DMDBT on ACM 1P **(B)**, DBT on ACF **(C)**, and DMDBT on ACF **(D)**.

Inside numbers indicate the sulfur uptake in mg-S/L.

Figure 5.4 Comparison of the differences between the adsorption capacities of the initial and regenerated samples. 140

Figure 5.5 DTG curves in nitrogen for GAC and ACM 1P before and after exposure to the different MDFs. 142

Figure 5.6 Pore size distributions for the materials before and after adsorption from MDFLC and for ACM 1P after regeneration. 143

Figure 5.7 XRF for materials before and after regeneration. 143

Figure 5.8 Proton binding curve of studied materials before and after exposure to MDFMH. 144

Figure 5.9 pK_a distribution of materials in [Figure 5.8](#). 145

Figure 6.1 Electron transmission images of the ACM 1P material. **A)** and **B)** images show the presence of nanoparticles ranging from 1 to 10 nm. The elemental mapping of the marked zone in **C)** corroborates the presence of iron that is associated with oxygen of the adsorbent material. 156

Figure 6.2 Surface area distribution of GAC and ACM 1P described by DFT. 157

Figure 6.3 Proton-binding curve for released ions from the surface of studied materials. 159

Figure 6.4 Single adsorption isotherms of **A)** indoline and **B)** quinoline over studied materials at 25°C. 163

Figure 6.5 Competitive adsorption isotherms of **A)** indoline and **B)** quinoline at 25°C. 164

Figure 6.6 Adsorption isotherms of A) indoline and B) quinoline in competition with 50 ppm-S.	165
Figure 6.7 Adsorption capacities of indoline and quinoline of GAC and ACM 1P in presence of a nitrogen contaminant and two sulfur compounds.	166
Figure 6.8 DBT and DMDBT adsorption capacities of carbon materials at several nitrogen concentrations.	169
Figure 6.9 A) π - π interactions among quinoline and graphitic layers in carbon. B) Nitrogen in indoline is more capable of interacting with iron nanoparticles.	171
Figure 6.10 Charge of hydrogens in the indoline molecule, obtained in ChemBioDraw 12 (Hückel-charge calculation).	172

RESUMEN

Aplicaciones Ambientales de Carbón Activado Modificado con Nanopartículas de Hidro(óxidos) de Hierro.

El arsénico y el azufre son contaminantes prioritarios que determinan la calidad del agua y el aire. La remoción de arsénico y la desulfuración (de gas y diésel) mediante carbón activado es una opción atractiva como técnica de mitigación ambiental. Sin embargo, existen algunas limitaciones relacionadas con la capacidad y la selectividad de adsorción del carbón activado que deben ser superadas. La funcionalización del carbón activado con hidro(óxidos) de hierro tiene el potencial de remover selectivamente los contaminantes mencionados, sin embargo, el mayor reto durante la funcionalización del material es el anclaje de nanopartículas reactivas sobre su superficie.

Este trabajo demostró que es posible reducir el tamaño de partícula de hidro(óxidos) de hierro anclados en carbón activado hasta 2 nm, mediante el uso de fosfato como agente acomplejante durante la hidrólisis forzada del cloruro férrico, que a su vez, permite que el material modificado adsorba arsénico y azufre de las fases líquida y gas.

El material modificado tiene una elevada área específica de 900 m²/g y aproximadamente 1% de hierro, en la forma de pequeñas nanopartículas de hidro(óxidos) de aproximadamente 2 nm. Los resultados demostraron que el fosfato actúa únicamente como un agente acomplejante, disminuyendo el tamaño de partícula de los hidro(óxidos) de hierro y dejando los sitios activos disponibles para la adsorción de moléculas. La disminución en el tamaño de partículas (30 a 2 nm) ancladas en el carbón activado incrementó 60% la capacidad de adsorción de arsénico(V). Se propone que a pH 7, dos mecanismos de adsorción de arsénico(V) operan simultáneamente en materiales modificados con hierro: 1. intercambio de ligandos entre los arsenatos y las nanopartículas de hidro(óxidos) de hierro y 2. atracción electrostática entre arsenato y grupos superficiales básicos del adsorbente.

Por otra parte, la funcionalización del carbón activado con hierro aumentó su capacidad de adsorción reactiva de dióxido de azufre en una corriente gaseosa. Nanopartículas de hierro brindaron una alta concentración de sitios de adsorción para las moléculas de dióxido de azufre y con esto, se incrementó la capacidad de adsorción en un 80%. Además, la incorporación de las nanopartículas de hidro(óxido) de hierro permitió la formación de Fe₂(SO₄)₃ en la superficie del

adsorbente, lo que contribuyó a una menor acidificación del medio después de la eliminación del dióxido de azufre.

La funcionalización del carbón activado también fue efectiva para la adsorción y oxidación de compuestos azufrados de un diésel modelo. La incorporación de hierro tiene dos propósitos: disminuir la adsorción de mono y di aromáticos, y provee un centro de oxidación para moléculas adsorbidas.

Finalmente fue demostrado que los compuestos nitrogenados (quinolina e indolina) disminuyen la capacidad de desulfuración de los materiales de carbón modificados con hierro de un diésel modelo sintético. El material modificado presentó una mayor afinidad para la remoción de compuestos nitrogenados que azufrados, especialmente para la remoción del compuesto nitrogenado con un doble anillo aromático (quinolina). Debido a la preferencia por la remoción de compuestos nitrogenados, es factible que el material sintetizado en esta investigación sirva para la desnitrogenación de diésel modelo en una etapa previa a desulfuración.

Los resultados presentados en ésta tesis doctoral demuestran el gran potencial de la funcionalización de carbón activado con nanopartículas de hidro(óxidos) de hierro, para la remoción de arsénico y azufre de las fases líquida y gas. Este estudio representa un gran avance en el desarrollo de materiales adsorbentes basados en nanotecnología para la remoción de contaminantes prioritarios en efluentes líquidos y gaseosos.

PALABRAS CLAVE:

Carbón activado, nanopartículas, hidro(óxidos) de hierro, adsorción, arsénico, adsorción reactiva, azufre, diésel, desulfuración, desnitrogenación.

ABSTRACT

Environmental Applications of Functionalized Activated Carbon with Iron Oxyhydroxide Nanoparticles.

Arsenic and sulfur are key pollutants whose presence determines the quality of water and air systems, respectively. Arsenic removal and desulfurization (of gas and diesel fuel) by activated carbon is an attractive option for pollution control. However, some limitations related to the capacity and selectivity of activated carbons must be overcome. The functionalization of activated carbon with iron oxyhydroxide has the potential of selectively removing those contaminants; however, a major challenge for material functionalization is the incorporation of reactive nanoparticles on its surface.

This work demonstrated that it is possible to decrease the particle size, up to 2 nm, of iron oxyhydroxides anchored on activated carbon by using phosphate as a capping agent during ferric chloride forced hydrolysis, which in turn allowed the modified adsorbent to uptake arsenic and sulfur from liquid and gas phase.

The modified material has a large surface area of 900 m²/g and a low iron content of about 1%, consisting of small nanoparticles of about 2 nm. The results demonstrated that phosphate is acting only as a capping agent, decreasing the particle size of iron oxyhydroxides and leaving the active sites on these available for adsorption of pollutants. The decrease in iron particle size from 30 to 2 nm, anchored on activated carbon led to an increase in arsenic(V) uptake of about 60%. It is also proposed that at pH 7 two arsenic(V) adsorption mechanisms can be carried out simultaneously in iron-modified activated carbons: a ligand interchange between arsenates and iron oxyhydroxide nanoparticles and electrostatic attraction between arsenate and the adsorbent basic surface groups.

On the other hand, the functionalization of activated carbon with iron increased its reactive adsorption capacity of sulfur dioxide from gas phase. Iron nanoparticles provided highly dispersed adsorption sites for sulfur dioxide molecules and thus increased the adsorption capacity by about 80%. Furthermore, the incorporation of reactive iron oxyhydroxides enabled the formation of Fe₂(SO₄)₃ on the adsorbents surface, which dismissed the acidification of the medium after sulfur dioxide elimination.

The functionalization of activated carbons with iron nanoparticles was also effective for the adsorption and oxidation of sulfur compounds from model diesel fuel. Iron incorporation serves a dual purpose: it decreases the uptake of mono- and di-aromatics and provides an oxidation center for adsorbed molecules.

Finally, nitrogen compounds (quinoline and indoline) were shown to decrease the iron-modified materials uptake of sulfur compounds from model diesel. The modified material showed a promising performance for diesel denitrogenation, especially for removing the non-planar nitrogen molecules. This study also suggests that it is feasible to perform denitrogenation and desulfurization of diesel fuel with the modified material in a single or simultaneous stage.

The results presented in this doctoral thesis demonstrated the great potential of the activated carbon functionalization with iron oxyhydroxide nanoparticles in the removal of hazardous arsenic and sulfur compounds from liquid and gas phase. This study represents a major step forward in the development of efficient adsorbents, based on nanotechnology to remove key pollutants from liquid and gaseous effluents.

KEYWORDS.

Activated carbon, nanoparticles, iron oxyhydroxides, adsorption, arsenic, reactive adsorption, sulfur, diesel, desulfuration, denitrogenation.

STRUCTURE OF THIS THESIS

This doctoral thesis is organized as follows:

Chapter 1 contains: the background of the doctoral thesis; an overview of the problematic of key pollutants of water (arsenic) and air (sulfur); methodologies to control pollution, emphasizing on the adsorption process; a description of activated carbon and the methodologies to modify it with iron oxyhydroxides. At the end of the chapter, it is included a brief description of the state of the art in the arsenic and sulfur adsorption on activated carbon.

Chapter 2 describes the modification of the activated carbon, and the selection of the best conditions for the forced hydrolysis of Fe(III), including phosphate as capping agent, to optimize the uptake of arsenic(V) on the modified adsorbent. Evidence of the presence of iron oxyhydroxide nanoparticles on the carbon surface is also included.

Chapter 3 describes the inferences of the intrinsic properties of the activated carbon (surface area, iron content and point of zero charge) on the removal of arsenic(V) from aqueous solution is described. This chapter includes also the empiric model that describes the best condition any activated carbon must have to enhance its arsenic uptake.

Chapter 4 includes the removal of SO₂ from gas phase over raw activated carbon and activated carbon modified with two iron particles sizes. The dynamic adsorption capacities under standard conditions and the role of the particle size in

the uptake and oxidation of SO₂ were determined. Finally an oxidation/adsorption mechanism was proposed.

[Chapter 5](#) reports the effect of the incorporation of iron nanoparticles on the desulfurization performance of activated carbon. The adsorption capacities obtained at dynamic conditions, correlated with the presence of several concentrations of mono- and di-aromatics in the model diesel fuel, are reported. Also evidences of the oxidation effect of iron were included.

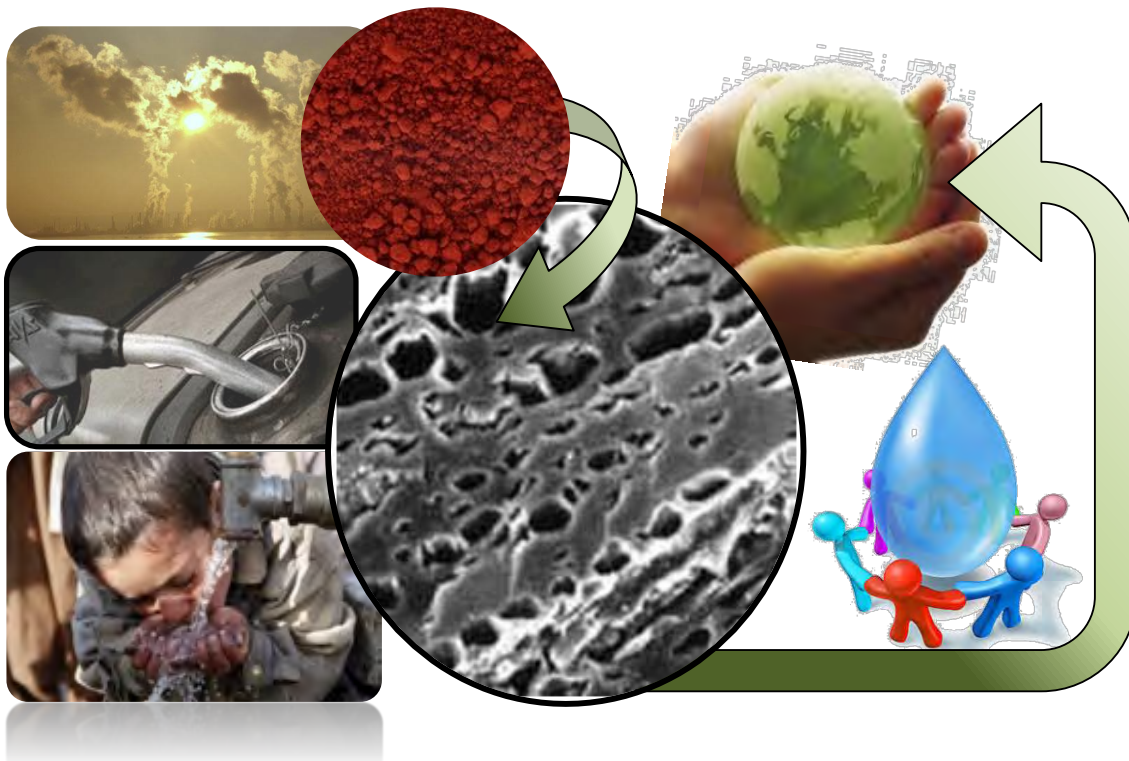
[Chapter 6](#) includes the effect of the nitrogen compounds quinoline and indoline on the removal of 4,6-dimethyldibenzothiophene (DMDBT) and dibenzothiophene (DBT) from diesel fuel by raw and iron-modified activated carbon. Since materials were more akin to nitrogen than sulfur compounds, the denitrogenation capacity was reported.

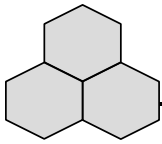
[Chapter 7](#) reports a general discussion of the results included in Chapters 2-6, while a final conclusion is provided in *Chapter 8*, along with the work perspectives and a list of the scientific products obtained during the doctoral studies.

Chapter 1

Introduction

In this work was studied the removal of As(V) and sulfur form liquid and gas phase by activated carbon modified with iron oxyhydroxide nanoparticles. A brief description of the pollution issue of these compounds and all scientific background are provided in this Chapter.





1.1 POLLUTION OF AIR AND WATER

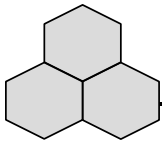
The extraordinary increase of anthropogenic activities has created a great demand for natural resources and the pollution of several systems, especially water and air. The rate at which resources are removed and pollutants are accumulated in natural systems has led to the pollution of natural systems in which such contaminants are a priority to remove.

Nowadays the removal of priority pollutants from liquid and gas phases represents one of the greatest scientific and technological challenges of the new century.

Among priority pollutants two that stand out due to their high toxicity and difficulty to remove are arsenic from aqueous solution and sulfur from air, and since these compounds occur on a global scale several countries around the world have a major interest in their removal.

1.2 ARSENIC AND SULFUR, PRIORITY POLLUTANTS OF WATER AND AIR

Water is the most valuable resource for life and human been; due to the expansion of both rural and urban spaces, water supplies are being affected. Sometimes pollution has a non-anthropogenic origin which makes the issue much more challenging to identify and solve. This is the case of water pollution caused by arsenic that is considered the largest mass poisoning in the history [1]; nowadays arsenic is one of the highest priority pollutants to remove from water supplies.



The ingestion of arsenic is causing serious health problems worldwide [2-5] (Figure 1.1). Among the affected countries are: Bangladesh [4,6-9], India [6], Vietnam [10,11], Thailand [12], Taiwan, Mongolia, China, Argentina, Chile, Bolivia, Brazil, Mexico, Germany, Hungary, and USA [5]. Estimates indicate that millions of people around the world are ingesting water with arsenic concentrations of up to 300 µg/L [13], high enough to incite a wide range of diseases like arsenicosis, keratosis, hyperkeratosis, cancer, etc. [2,14,15]. To abate the arsenic problem, environmental organizations around the world decreased the maximum allowable limits of arsenic in water. The World Health Organization (WHO) recommends a maximum permissible limit of arsenic in water of 10 ppb in drinking water. Reaching this low allowable limit requires the implementation of highly efficient and low cost technologies that allow the polishing of contaminated effluents. The main health problems caused by arsenic-contaminated water are schematized in Figure 1.1.

On the other hand, sulfur is one of the main air pollutants whose presence contributes to the formation of acid rain [16,17], destruction of foliage cover, increase in particulate matter formation, abrasion of buildings, and monuments [18]. Moreover, a broad range of health problems is also linked to sulfur dioxide emissions into the atmosphere as for example asthma, an increased risk of premature births, and lung cancer [19]. The main source of SO₂ is the burning of fossil fuels, especially diesel oils [20,21]. Therefore, the removal of SO₂ directly from emission sources and desulfurization of fossil fuels are major environmental problems to abate.

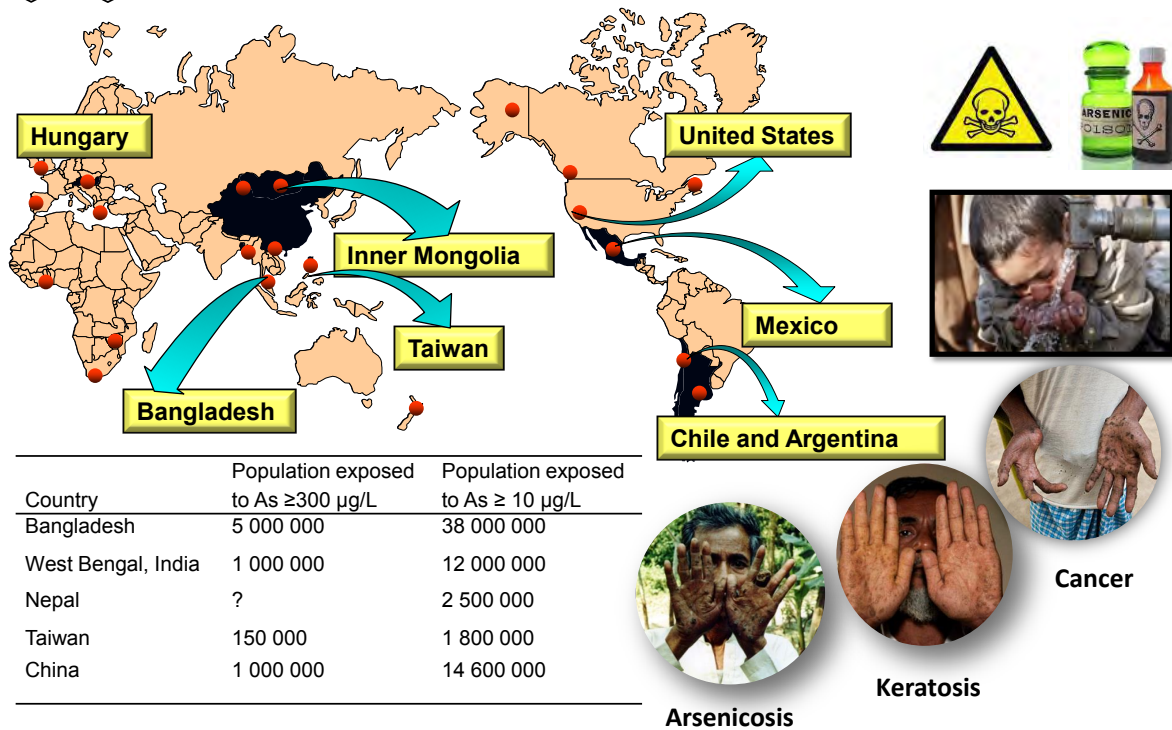
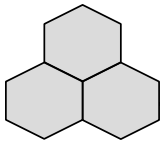
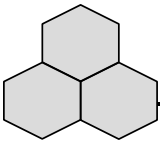


Figure 1.1 Schematization of the world health problem of arsenic around the world, adapted from [2] and [13].

Fossil fuel desulfurization is a topic that has garnered great attention during the last decade, not only due to environmental implications related to the SO_2 release, but also because sulfur deposition diminishes the lifetime of the catalytic converters in vehicles. For this reason in 2006 the EPA announced its plan to decrease the maximum limit of sulfur content in all types of fuels [22-26]. One of the most critical reductions was the one applied to diesel, since this fuel contains high concentration of sulfur [26].

Because there is still a growing demand for this fuel, a trend that is projected to continue over the upcoming years (Figure 1.2), the problem became even more alarming when in 2010 the ultra-clean fuels program of the EPA required the sulfur



content in non-road diesel oil to be less than 15 ppm . Since such levels are technologically and economically difficult to achieve via hydrodesulfurization (Described later in section 1.3.2) [27-30], diesel fuel desulfurization will be one of the most critical and major issues to solve in the years to come. The issues related to the sulfur presence in air and diesel fuel are outlined in Figure 1.2.

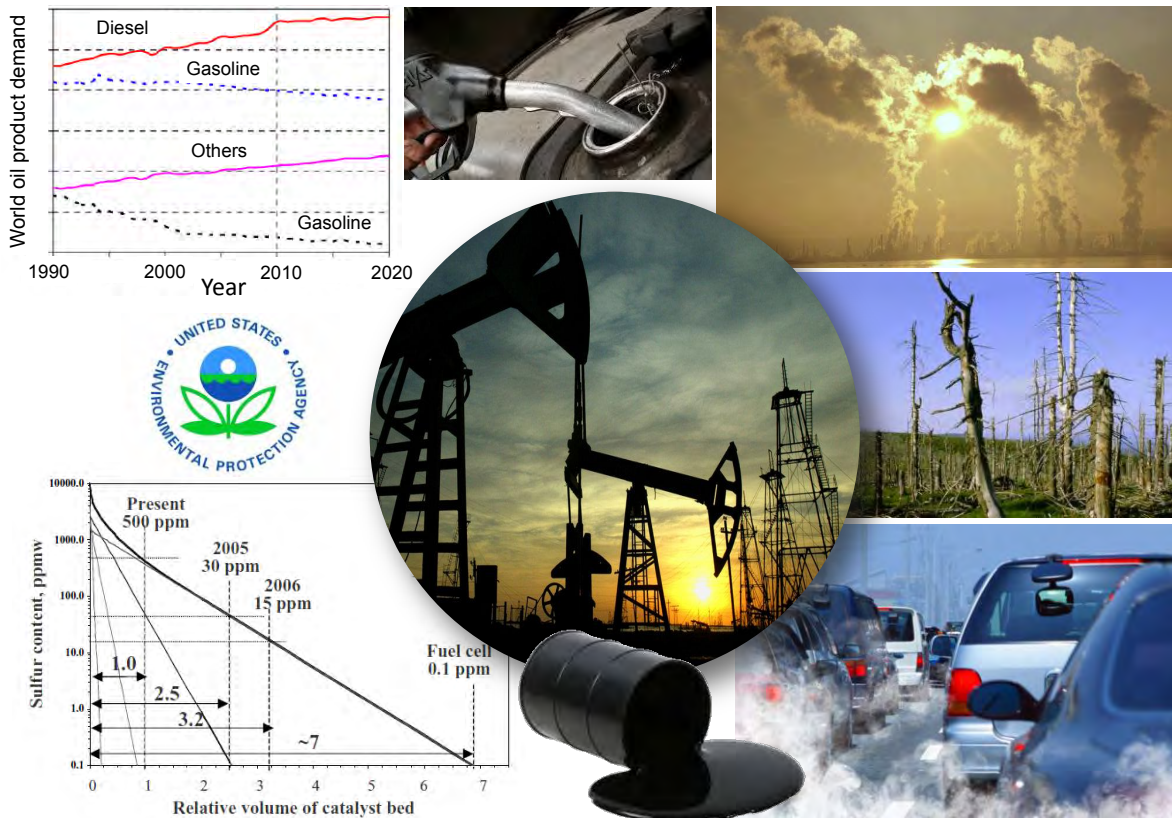
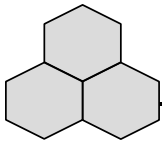


Figure 1.2 Representation of the problems related to the presence of sulfur in air due to the burning of fossil fuels, mainly diesel fuel, adapted from [22].



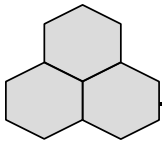
1.3 METHODOLOGIES OF POLLUTION CONTROL

1.3.1 ARSENIC REMOVAL

Arsenic removal from aqueous solution is a big challenge due to the high levels of purification needed to reach safe levels of arsenic for human ingestion. There are various methodologies available for arsenic removal; their efficiency depends on the characteristics of natural water, the volume to be treated and the objective concentrations. In [Table 1.1](#) is provided a brief list of technological approaches to the removal of arsenic and a discussion of the advantages and disadvantages of each one.

Among listed technologies for arsenic pollution control, adsorption arises as one of the most attractive options. Numerous studies and reviews have reported the benefits of the adsorption process during arsenic removal [[14,31,34,36-45](#)], depending on the physicochemical properties of the adsorbent material; in this matter metal oxyhydroxides and carbon-modified materials stand out as attractive options due to their high adsorption capacity and selectivity. Nevertheless, there are still some challenges to overcome in the development of efficient materials that are capable of selectively removing arsenic from aqueous solution.

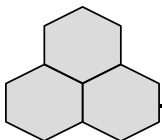
Hitherto were discussed the pollution control methodologies for arsenic, one of the key contaminants in water. The following sections describe the strategies of control of sulfur that can be present in gas phase and in fossil fuels

**Table 1.1** Methodologies of arsenic removal from water.

Methodology	Discussion
Coagulation-Flocculation	A chemical agent “coagulant” is added to the polluted water and As(V) is removed in the colloidal suspension. Commonly coagulants for As removal are: alum, ferric chloride, ferric sulfate, chitin, and polymers [31]. C-F removes anions non-selectively its actual efficiency of removal is highly dependent on the raw water quality [14].
Ion Exchange	A polymeric resin interchanges negative charged ions with the solution immobilizing arsenic [32]. However, the price of such ionic exchangers is still high and the problem of arsenic ingestion remains in margined communities.
Membrane Filtration and Reverse Osmosis	During membrane filtration a high pressure flow is passed through a microporous membrane. Only small particles can pass through, allowing water filtration. MF and RO are expensive technologies for water purification that can remove all arsenic; however, its usage is only justified when the removal of several compounds is required.
Precipitation	Precipitation of arsenate with chemical agents is one of the most commonly methods for water purification. Common precipitants are: alum [31], and iron [33]. Lime softening also removes arsenic, but its usage is only justified when water softening is required [31]. The arsenic is separated with the sludge after sedimentation; however, the high volume of waste generated and its disposal makes precipitation hard to apply for arsenic removal.
Adsorption	Adsorption is probably the most sustainable technique that can be applied to the removal of arsenic from aqueous solutions [34,35]. The success of the operation depends on the concentration of arsenic in the influent, the volume of water to be treated and the adsorption capacity of the adsorbent.

1.3.2 DESULFURIZATION

The methodology of anthropogenic sulfur control can be achieved by removing the sulfur compounds (SO₂) directly from the source and by removing the sulfur compounds from fuels before the burning process. The methodologies of SO₂

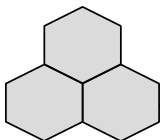


removal from the gas phase and the desulfurization of diesel, one of the most important fuels, are briefly described in [Table 1.2](#). It is worth mentioning that nowadays one of the biggest challenges in desulfurization is to achieve the ultra-deep desulfurization of diesel fuel.

1.3.2.1 Ultra-deep desulfurization

According to Song [\[66\]](#) the approaches to ultra-deep desulfurization are:

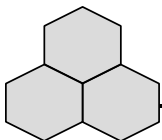
1. *Improving the catalytic activity by a new catalyst for HDS.* New catalyzers capable of enhancing hydrogenation of the aromatic ring of thiophenes that includes the incorporation of acidic features to induce methylation from 4 and 6 positions of the thiophenes. New catalyzers have been developed by companies such as Azko Nobel, Criterion, ExxonMobil, etc.
2. *Tailoring the reaction and process conditions.* The tuning of parameters as space velocity, temperature and pressure.
3. *Designing new configurations.* Reactor configurations of HDS have been reviewed by Sie [\[67\]](#). The development of new refination reactors in one or two stages may enhance the desulfurization of diesel fuel; however, refractory compounds are still hard to remove from the current streams.
4. *Develop new processes.* These have been proposed for ultra-deep desulfurization, among which adsorptive desulfurization is one of the most attractive options for diesel ultra-deep desulfurization [\[68\]](#).

**Table 1.2** Strategies for gas and diesel desulfurization.

Methodology	Discussion
Removal of SO₂ from gas phase	
Scrubbers and catalytic oxidation of SO₂.	In scrubbers the acidity of SO ₂ gas is neutralized by a basic solution and salts are formed [46]. For high-volume SO ₂ production, the oxidation of SO ₂ is preferred. The SO ₂ is then passed through a catalytic bead containing metal oxides (e.g. Al ₂ O ₅) that produce SO ₃ , which is reacted in water promoting the formation of H ₂ SO ₄ .
SO₂ adsorption	Preferred at low concentration of SO ₂ , the implementation of adsorbents as activated carbon is desired due to the low cost and easier application [47-62]. During SO ₂ uptake, H ₂ SO ₄ is formed on the surface of carbons [46,47,57,63] resulting in the acidification of the medium and the rusted of the pipe line of the depuration process. The development of carbon materials that might remove SO ₂ without causing acidification of the adsorbent system is still the subject of numerous studies.
Removal of sulfur compounds from diesel fuel	
Hydro-desulfurization (HDS)	The distilled fraction of diesel is passed through a catalytic bead and contacted with H ₂ at high temperatures. Sulfur compounds of diesel react with hydrogen forming H ₂ S that later is removed and recovered from the current stream [64,65]. This method has been traditionally very efficient for the removal of large amounts of sulfur from fuel streams; however (due to the presence of refractory compounds) in order to comply with the new environmental regulations it is estimated that this process requires a scaling of about 3-5 times in the catalytic reactors [22,30], limiting its implementation for ultra low diesel production. The alternative is to implement an ultra-deep desulfurization process.

1.3.2.2 Adsorptive ultra-deep desulfurization

It has been proposed that refractory sulfur compounds might be removed from current streams by adsorption at normal conditions, reaching zero concentration of



sulfur in the stream without altering the properties of the diesel fuel. The challenge in the material design (adsorbent) includes stable materials that might uptake a large amount of refractory sulfur compounds selectively.

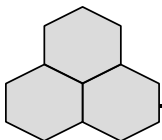
Many studies agree that the presence of refractory sulfur compounds in diesel (due to their concentration and difficulty to remove) is represented by the incidence of dibenzothiophene (DBT) and 4,6-dimethyldibenzothiophene (4,6 DMDBT) [30,69-71]. Hence, desulfurization experiments normally focus on the removal of these compounds.

The presence of nitrogen compounds in diesel plays a key role, since these might strongly decrease the performance of desulfurization materials [72,73]. This effect is described in the following section.

1.3.3 INTERFERENCE OF NITROGEN COMPOUNDS AND ADSORPTIVE DENITROGENATION

Several studies of diesel desulfurization have demonstrated that the presence of even small amounts of aromatic nitrogen compounds such as indole, aniline, and specially quinoline and indoline have an important inhibitory effect on sulfur removal because nitrogen compound tends to adsorb over active groups removing sites for sulfur compounds [72-75]. On the other hand the removal of nitrogen compounds (denitrogenation) is also required by environmental organizations to abate the release of NO_x to the atmosphere.

It has been proposed [76-79] that depending on the adsorbent properties nitrogen and sulfur compounds might be removed in adsorbents either simultaneously or in a



previous stage to desulfurization (Figure 1.3). Therefore, adsorptive denitrogenation from diesel fuel is of the utmost importance in order to evaluate the extent of desulfurization inhibition or to develop materials for selective adsorptive denitrogenation.

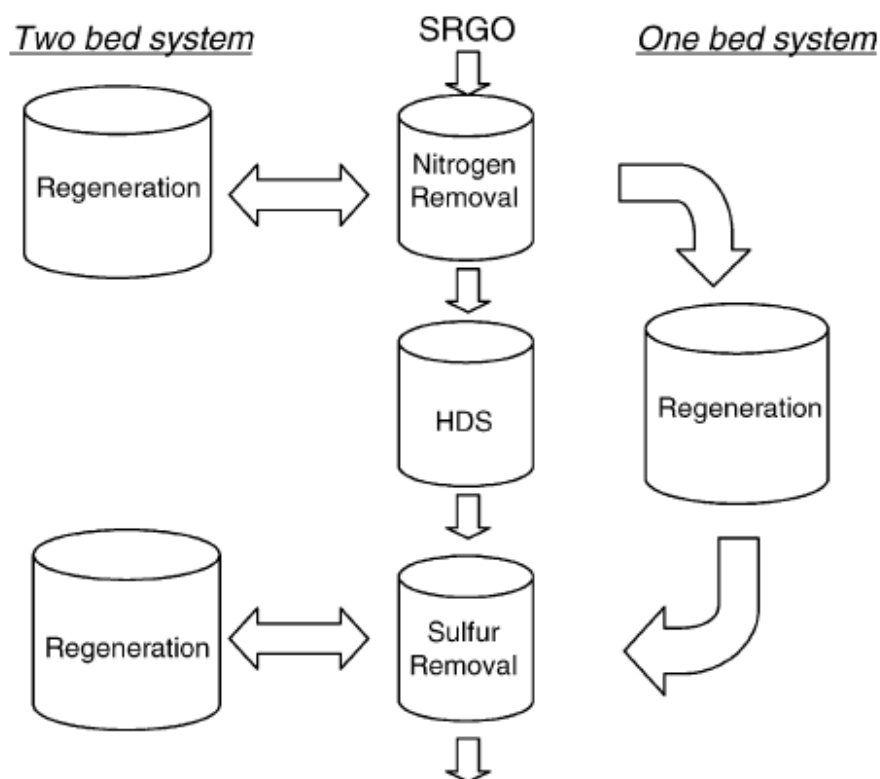
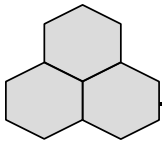


Figure 1.3 Concept of the two stages, straight run gas-oil (SRGO) adsorptive denitrogenation and desulfurization, in one and two bed systems, adapted from [79].

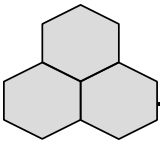
As mentioned above, one of the most attractive options of arsenic and sulfur pollution control is adsorption. The next describe the theoretical background and the fundamentals of adsorption.



1.4 FUNDAMENTALS OF ADSORPTION

Adsorption is the term associated to an interfacial process of mass transference molecules (adsorbate) from a fluid phase (liquid or gas) to a solid surface (adsorbent). When the adsorbates are in contact with a solid surface, those fill the pores of the adsorbent in order to balance the surface tension of the solid. The process continues until thermodynamically the system is in equilibrium. The adsorbate remains adsorbed by the action of several forces embracing Van der Waals-like and columbic forces, polar interactions, and several types of specific bonds. Both shorter range (repulsive) and longer range (attractive) forces are balanced when the adsorption equilibrium is reached. The extent of the force between adsorbate-adsorbent is described by the Lennard-Jones potential (LJP) [80]. That defines the attractive and repulsive forces acting over a molecule as a function of its distance over the surface. Figure 1.4 describes the LJP of a typical adsorption process, as can be observed, when the adsorbent is approaching the surface of the solid, this passes through a minimum of energy known as the potential well ($U(r_0)$) in which it is balanced with the surface energies of the solid. The energy associated with the process is the heat of adsorption.

Depending on the adsorbate-adsorbent interaction energy the adsorption might be classified in physisorption and chemisorption. Physisorption is normally associated with the “non-specific” attraction of molecules by secondary forces such as electrostatic attraction (i.e. Van der Waals forces). The energy of adsorption is lower than 20 Kcal/mol [81] and the nature of the process is in principle reversible. On the other hand the term chemisorption implies the formation of a “specific” bond



between the adsorbent surface and the adsorbate. The energies associated are in the same order as chemical reactions (20-100 Kcal/mol) and are restricted to a monolayer formation.

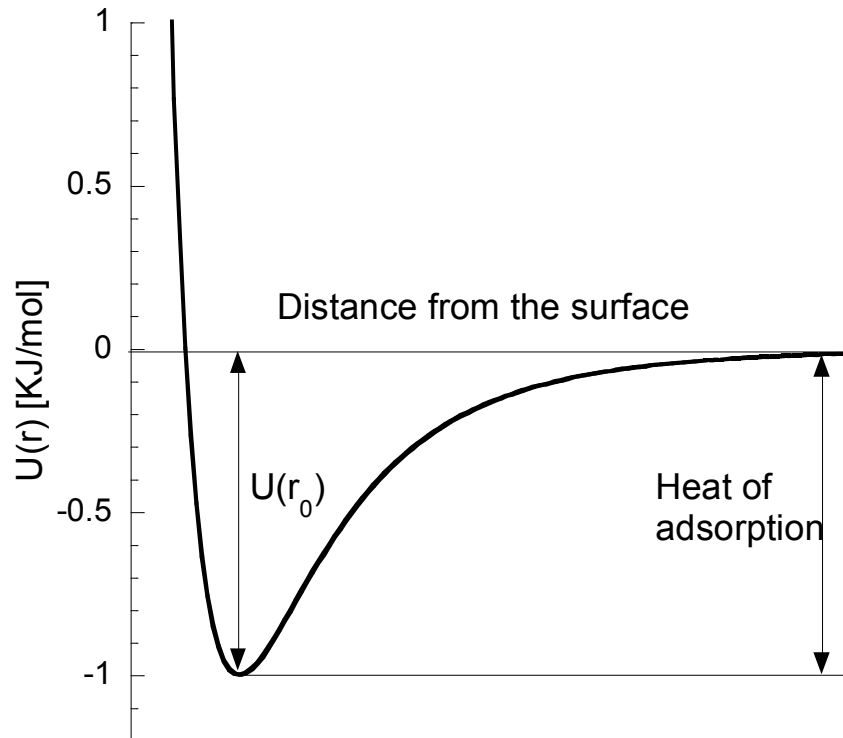
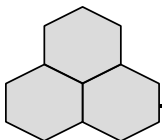


Figure 1.4 Lennard-Jones potential for an adsorbate molecule.

1.4.1 NATURE OF PHYSISORPTION FORCES

Physisorption is the interaction of adsorbates and surfaces by Van der Waals-like forces originated from the interaction of dipoles, quadrupoles and London forces (dispersive forces). These interactions are present in all types of mater and always act as attractive forces between adjacent atoms.



A chemical dipole is a permanent localization of the charge in a molecule as a result of its dipolar moment [82]. When two molecules with dipoles approach each other they undergo a repulsion or attraction force depending on the dipole charge. The dipole-dipole forces are then attraction forces between the positive and the negative sides of the molecules (Figure 1.5 A).

Although some molecules do not present dipolar moment, they have a quadrupolar moment in which their interaction involves symmetrical molecules with atoms of different electronegativity like CO_2 , leading in dipole-quadrupole and quadrupole-quadrupole interactions (Figure 1.5 B).

The other component of the physical adsorption is the formation of instantaneous dipoles in the so-called dispersion forces or London forces. In nonpolar molecules the electronic distribution is not uniform. A dipolar moment is induced when a molecule approaches another in which the electrons are temporarily located out of the symmetry arrangement, leading to a temporal dipole attraction [80]. Even when instantaneous dipoles last few seconds its overall force is of attraction (Figure 1.5 C).

Hydrogen bond is a stronger form of dipole interaction. When hydrogen is bonded with an electronegative atom, the molecule strongly polarizes leading to the hydrogen with a positive charge that is strongly attracted to non-sharing electrons of other electronegative atom [82] (Figure 1.5 D).

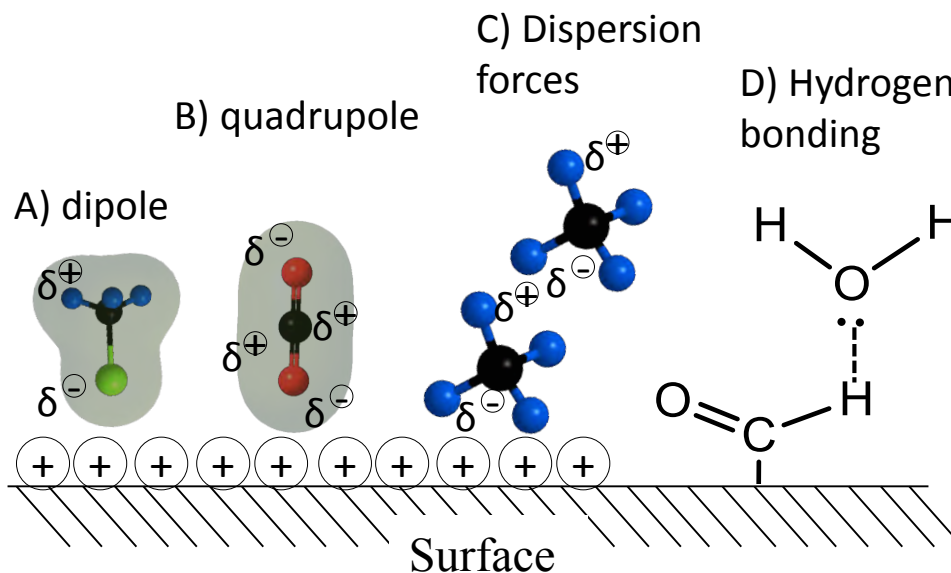
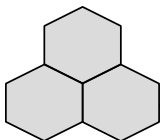


Figure 1.5 Polar interactions of adsorbates and solid surfaces.

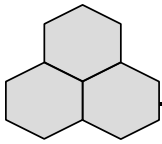
1.4.2 SURFACE COMPLEXATION

Surface complexation occurs between surface reactive groups and adsorbate molecules that can be in liquid or gas phase. The concept of surface complexation is crucial for the understanding of the uptake of several adsorbents, especially for anions such as arsenate or arsenite.

Below is a description of the most important chemical reactions occurring either in liquid or gas phase at the surface of adsorbents.

1.4.2.1 Inner sphere complexes

In aqueous solution, ions are surrounded by water molecules forming hydration spheres. An inner sphere complex is formed when the first shell of hydration of the adsorbate is replaced and the ion forms a direct bond with the surface of the solid [83]. This process is different from physical adsorption in which ions are bonded

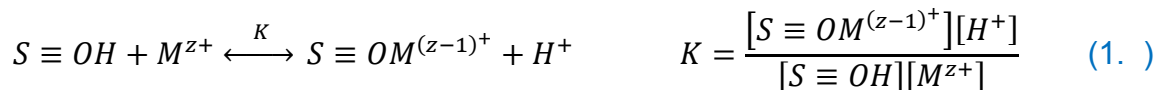


with the surface without losing their first coordination shell. The nature of inner sphere complexes depends on the charge of the adsorbing ion.

Since anions are ligands, they have one or more atoms with a lone pair of electrons and can act as donor in coordinate bonds. The ligand (L^-) is then replaced by the reactive specific group (i.e. hydroxyl) located on the surface of the adsorbent (Rxn. 1.1).



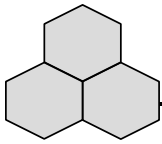
On the other hand, cations (M^{z+}) are bonded directly with the surface groups displacing protons rather than by a ligand interchange, as for anion uptake.



Hence, the equilibrium reaction of ions can be expressed in terms of the surface complexation constants. Several studies have been conducted to determine the complexation constants of well-defined systems, for example the work of Dzombak and Morel [84] that comprises a compendium of complexation reactions of anions and cations over the surface of ferrihydrite.

Several studies have proved that the coordination of ions can be conducted by means of several coordination geometries, as shown in Figure 1.6 for the hydroxyl present in the surface of metal oxides adsorbents.

Finally, other organic and non-ionic inorganic molecules might be bonded to the surface of the solid by the action of several chelating agents that are designed for



specific adsorbate-adsorbent systems. For example, the uptake of mercury by chelating agents that are present in the surface of interchange resins [85].

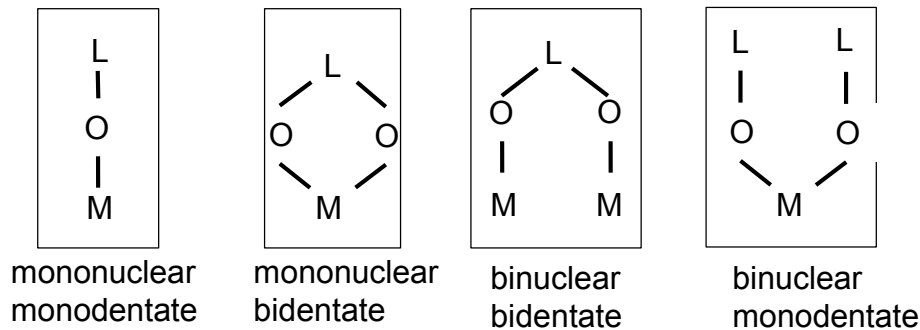
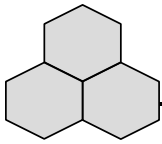


Figure 1.6 Geometries of coordination complexation between metal oxidants and ligands.

1.4.2.2 Reactive adsorption

Reactive adsorption is a process in which the adsorbate first reacts with specific groups located on the surface of a solid, changing its chemical nature and then bonded by physical or chemical forces over its surface.

Recently Sharma et al. [86] reviewed the potential of reactive adsorption in environmental applications especially for gas oxidation/reduction/uptake and for fuel desulfurization. For example, it is well known that SO_2 uptake by activated carbons occurs first via oxidation of adsorbed SO_2 with chemisorbed oxygen leading to the formation of reactive SO_3 that forms H_2SO_4 with water contact; finally H_2SO_4 is adsorbed by electrostatic interactions on the surface of carbons.



Another instance is the oxidation of dibenzothiophenes for active oxygen on the surface of activated carbons resulting in the formation of sulfoxides and sulfones that remain strongly adsorbed by polar interactions [87].

1.4.3 ADSORPTION EQUILIBRIUM

Adsorption equilibrium is described by plotting the equilibrium concentration in the fluid phase (liquid or gas) versus the adsorbed mass in the solid; data are obtained experimentally in batch adsorbers and the temperature, pH and electrolyte concentration are maintained constant. The plot receives the name of adsorption isotherm. Experimentally a certain mass of the solid is contacted with a solution containing an established concentration of the adsorbate; once the concentration in solution is constant a mass balance in the reactor yields the adsorbed mass for the adsorbent (Q_{ads}):

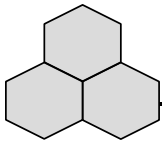
$$Q_{ads} = \frac{V}{m_{ads}} * (C_0 - C_f) \quad (\text{eqn. 1.1})$$

Where V is the reactor volume, m_{ads} is the adsorbent mass C_0 is the adsorbate starting concentration and C_f is the adsorbate final concentration.

The amount adsorbed and in solution can be adjusted by several equations that describe specific isotherms systems. The most common are described as follows:

1.4.3.1 Langmuir equation

The Langmuir equation was developed in 1917 [88] by assuming that the adsorbates are located on the surface of the solid forming a monolayer without interacting with other adsorbed molecules.



The equation is:

$$q = \frac{q_m K_L C_e}{1 + K_L C_e}, \quad (\text{e n.1.})$$

where q is the adsorption capacity at the equilibrium concentration C_e , is the Langmuir constant, and q_m is the adsorption capacity of the monolayer.

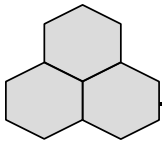
1.4.3.2 Brunauer-Emmet and Teller (BET) equation

The BET adsorption isotherm [89] was developed from the formulation of the Langmuir isotherm for the adsorption of gases. If the surface is composed of several kinds of spaces the total coverage of the surface consists of multilayers of condensed adsorbate. The BET equation can be represented for the adsorption in gas phase as:

$$\frac{P}{q(P_s - P)} = \frac{1}{bq_m} + \left(\frac{1}{bq_m}\right)(b - 1)\left(\frac{P}{P_s}\right), \quad (\text{e n.1.3})$$

where P is the pressure of the system, P_s is the saturation pressure at the adsorption temperature, q_m is the adsorbed amount at the monolayer formation, and b is a constant that depends on the isotherm shape.

This equation has become very popular due to its employment to calculate a material surface area. If the adsorbate dimensions are known and the surface covered by a single adsorbed molecule can be determined, then the surface area of the materials is obtained by plotting $P/[q(P_s - P)]$ versus P/P_s . The range of validity of BET equation is at low relative pressures (P/P_s , 0.05-0.3) [90].



1.4.3.3 Freundlich isotherm

The Freundlich isotherm does not take into consideration that the coverage of molecules must approach a monolayer [91]. The main consideration of the Freundlich equation is that the energy distribution for the adsorption sites is exponential. The Freundlich equation is

$$q = K C_e^{1/n}, \quad (\text{e n. 1.})$$

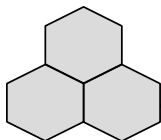
where n is a constant related with the surface heterogeneity and K is the Freundlich constant that is a measure of the adsorption intensity or the ability of the system to accept molecules [92].

1.4.3.4 Other adsorption isotherm models

There are many other adsorption models available in the literature that have been applied successfully for describing the adsorption of specific molecules in particular systems either in gas or liquid phase. A summary of such models that include two and three parameters can be found elsewhere in references [92,100,101].

However such models do not explain the chemical reactions implied in the uptake process (chemisorption), and only adjust experimental data to empirical models or specific theories. In order to explain the surface reactions implied during the adsorption process, some adsorption models have been developed and are condensed in Table 1.2. The basis of these models is the acquisition of charge of a solid when is immersed in a liquid phase that arises from the following factors [93]:

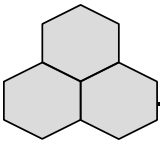
1) *Chemical reactions at the surface*, 2) *Lattice imperfections and isomorphous*



replacements, 3) Adsorption of hydrophobic species or surfactants, and 4) Protons adsorption [94].

Table 1.3 Models of surface complexation.

Model	Description
Electric double layer	Developed by Stern in 1923 [93] that suggested that two layers or ions are formed around the solid to stabilize the formed surface charge. The first one is compact (similar to a monolayer) and is made of ions from the opposite charge to the surface with the same potential, this layer is similar to the described earlier by Helmholtz. The second layer is formed of ions of several charges in which its potential decreases exponentially as the ions are away from the surface. The second layer is normally named diffuse layer and was described by the first time by Gouy-Chapman [95,96]. This model was utilized by Dzombak and Morel [84] for anions adsorption on ferrihydrite, for Evanko and Dzombak [97] for aromatic compounds adsorption, for Ali and Dzombak [98] to the adsorption of Cu and Ca, and for Marmier et al. [99] for the adsorption of Yb and Ni on magnetite.
Triple layer model	Developed by Yates et al. [102] and Davis [103], is an expanded Stern-Grahame model in which the adsorbed ions are placed as partially solvated ions in the inner Helmholtz layer. Adjacent to this inner plane is the outer Helmholtz plane and outside is the diffuse layer. This model was applied by Davis and Leckie [103] to the adsorption of several cations and anions on ferrihydrite.
Four layer model	This model locates the several adsorbed ions on different planes. It has been used to model adsorption of phosphate, citrate and selenite [104] and competitive adsorption of Ca and Cd on ferrihydrite [105].
CD-MUSIC model	This is an extension of the MUSIC model developed by the Riedmsdijk group. The model takes into account that the charge is distributed over the interfacial region over several electrostatic planes. The model has been applied for the adsorption of several systems, such as adsorption of organic acids, sulphate, fulvic acids, benzene, among others [106].



1.4.4 ADSORPTION KINETICS

The adsorption models and isotherms provide information about the adsorption in terms of equilibria; however, another factor that determines the adsorption efficacy is the kinetic or rate at which it takes place.

The adsorption of a molecule can happen in three stages: 1) *External or film diffusion*: the adsorbate passes from the bulk solution through the boundary layer to the surface of the adsorbent. 2) *Internal diffusion (molecular transport)*: during this stage the adsorbate is transported from the external surface of the solid through the pores until the adsorption site, and 3) *the actual adsorption process* (Figure 1.7).

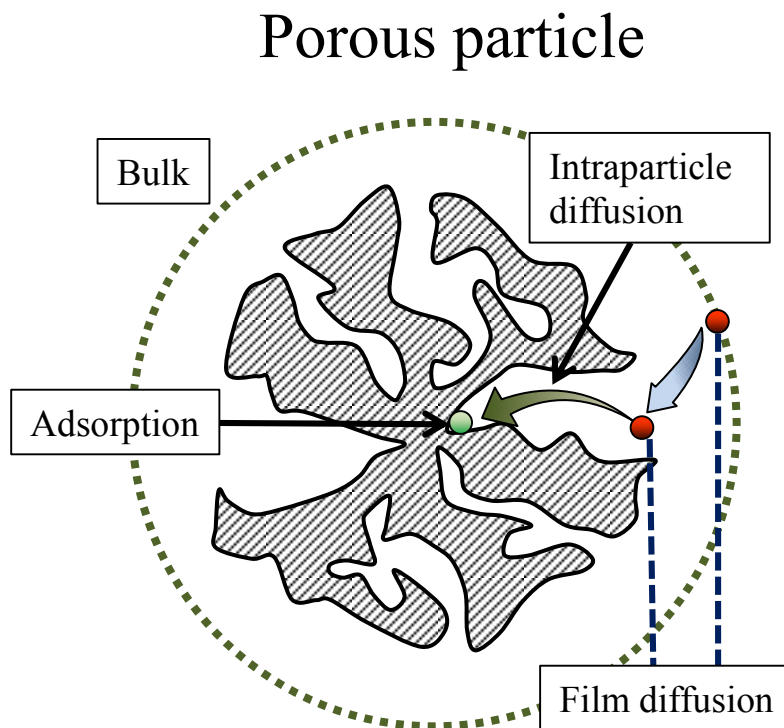
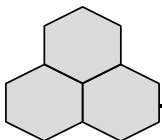


Figure 1.7 Illustration of mass transference resistances on porous solids.



There are many models that describe the rate at which a molecule is transported from the bulk until its adsorption site (Figure 1.7). Any of these makes specific assumptions depending on which of the three stages controls the adsorbates uptake. The kinetics models are classified in Appendix A, and can be consulted in references [111-115].

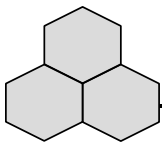
1.4.5 ADSORBENT MATERIALS

There are several available materials for the removal of inorganic arsenic from water and sulfur compounds either from gas or from an organic phase such as diesel fuel. The most commonly used materials are: zeolites [37,107-109], silica based adsorbents, polymers, metal organic frameworks, metal oxyhydroxides [110] and activated carbon [116].

Activated carbon is the most widely employed and popular adsorbent material [116]. The success of its application lies in its excellent physicochemical properties that make it an ideal adsorbent. Below is a description of activated carbon, its operation and its modification for enhancing its adsorptive properties.

1.5 ACTIVATED CARBON

There is not a single definition for activated carbon, albeit it is generally accepted that activated carbon is the name given to all amorphous carbonaceous materials having a large surface area and porosity. It is precisely their porous structure and the chemistry associated with them the most important properties of activated carbons that allow them having hundreds of several applications and furthermore, to be tailored to meet specific objectives.



Activated carbon consists of disordered (or microcrystalline arrangement) graphitic layers with plenty of structural defects that confer it porosity [116,117]. The carbon atoms on the edges of the graphitic layers are normally bonded with heteroatoms forming reactive groups. Those reactive groups located in the carbon layers along with the π system of the basal plane of graphite are responsible for the active sites in activated carbon [118]. Figure 1.8 represents the activated carbon porosity and chemical surface.

1.5.1 STRUCTURE

The porous structure of activated carbon is very diverse and many models have attempted to explain the details of it. One of the simplest pioneering models of carbon structure is the *Norit model* [117] (Figure 1.9 A), in which carbon is formed by misaligned graphitic layers; some of these are removed by activation processes leading to the formation of pores in activated carbon.

Another simple model that outlines pore structure and surface area of activated carbons is the “*potato chips model*”, represented in Figure 1.9 B. The shape of the potato spaces (pores) depends on the shape and size of the chips (graphitic layers). Since there are no two chips of same size and shape, each pore will have special properties, sizes and textures. Pore interconnectivity in activated carbon can be explained in another simple model, the “*negative branched tree model*” represented in Figure 1.9 C that outlines how pores of different size and shape are connected among themselves.

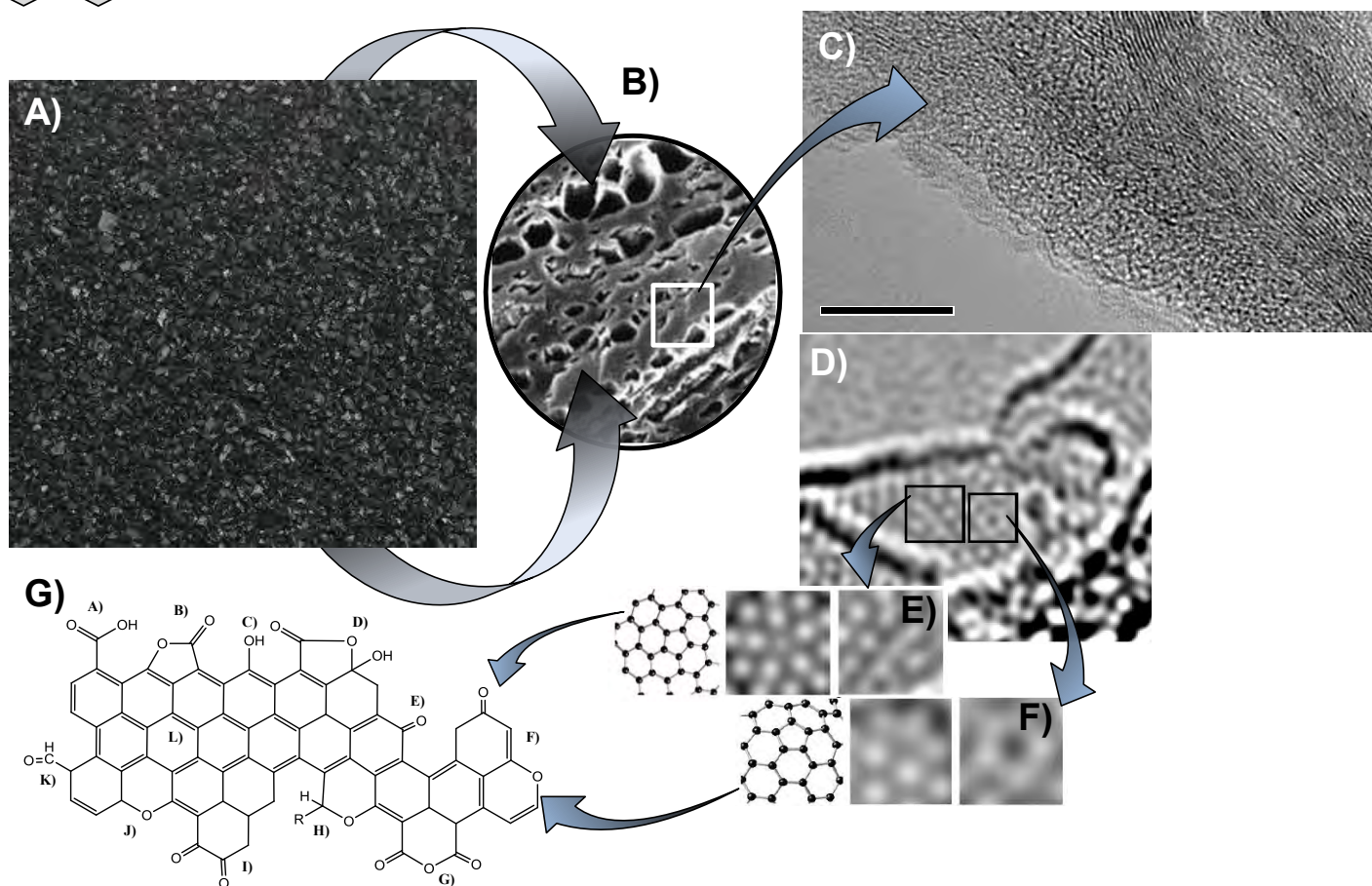
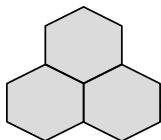
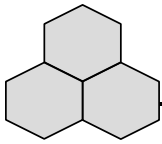


Figure 1.8 Starting from a macroscopic point of view in **A)**, the scanning electron image in **B)** shows macroporosity associated to carbons, and by means of transmission images **C)-F)** amorphous nature of graphite sheets in activated carbon [119]. The edges of the layers contain various oxygenated functionalities as represented in **G)**, modified from [118].

Many other carbon models and detailed information related to them are provided in the book of Reynoso and Marsh [117].

The pores might be classified according the criterion proposed by Dubinin [120] that is now accepted by the IUPAC. According to this classification micropores are less than 2 nm in width, mesopores are between 2 and 50 nm and macropores are



bigger than 50 nm. The adsorption energy depends on the kind of pores in which is carried out: in micropores is larger than in mesopores because of the overlapping of adsorption forces from the opposite walls of the micropores.

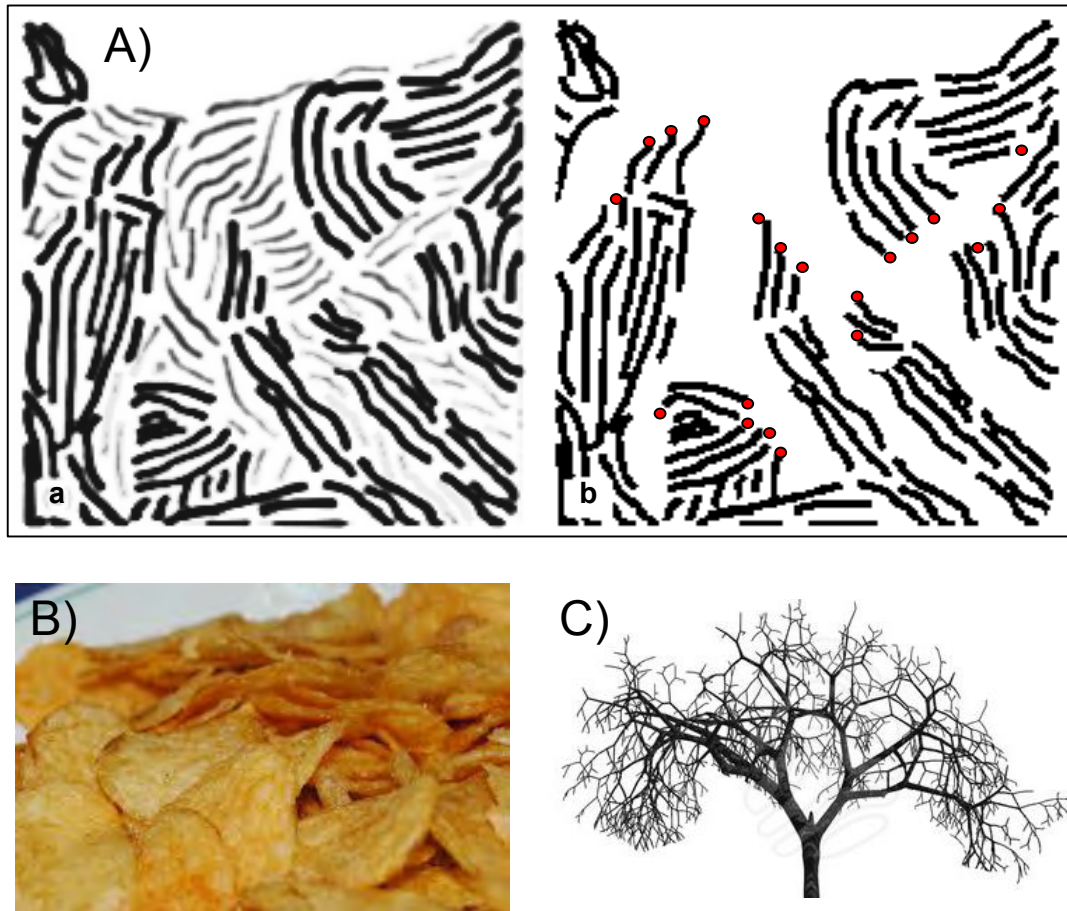
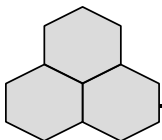


Figure 1.9 Representations of the porous structure of activated carbon. **A)** *The Norit model* showing the formation of porous where the layer is stabilized by oxygen functionalities. **B)** *Potato chip model* representing porosity in activated carbon. **C)** *negative branched tree model* representing pore interconnectivity in activated carbon, adapted from Reynoso and March [117].

As shown in [Figure 1.8](#) activated carbons normally contain a large amount of pores that are responsible for its extraordinarily high surface area. Different pores sizes in



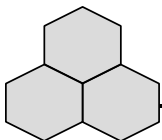
carbons are necessary for specific applications moreover, sometimes not only high surface areas and large pore volumes are required also sharp pore size distribution (PSD) is required.

Hence pore development and its control in activated carbons is a big issue of great scientific interest. The control and characterization of activated carbon porosity have been the subject of numerous studies, where methodologies for controlling pore size, shape and volume during carbons production-activation have been discussed and reviewed [121].

1.5.2 CHEMISTRY

The surface chemistry of activated carbons has also been the subject of several studies and reviews [118]. Most of the chemical surface features of activated carbons are conferred by the incorporation of oxygen functional groups during the activation process. During the activation process some graphitic layers are removed from the carbon, leaving vacant sites that in order to become stable chemisorb oxygen. The diversity of the oxygen containing groups on graphitic edges is responsible for most of the surface chemistry of activated carbons.

The incorporation of oxygen functionalities has repercussion on the hydrophobicity, chemical behavior, affinity, and amphoteric behavior of activated carbons. Generally, activated carbons contain low oxygen content and a normal procedure to increase its content is to oxidize their surface by reacting with an oxidant agent, typically nitric acid [122]. The oxidation of carbon surfaces yields the incorporation of a great number of acidic and basic oxygenated groups. The most common groups are A) carboxyl, B) lactone, C) phenol, D) lactole, E) ketone, F) pyrone, G)



carboxyl anhydrous, H) chromene, I) quinone, J) ether and K) carbonyl-like, and are outlined in [Figure 1.8 G](#). It has been reported that groups from A) to D) have acidic properties mean while groups E) to K) are mainly basic. The overall sum of any of the previous groups grants to activated carbon either basic or acidic properties.

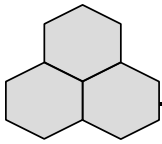
1.5.3 APPLICATION OF THE ADSORPTION PROCESS IN ACTIVATED CARBON

1.5.3.1 Adsorption in liquid phase

The removal of pollutants from liquid phase depends on the particle size of the AC, if very small particles (smaller than 24 μm , [\[123\]](#)) are employed, it is preferred to perform the adsorption in batch adsorbent reactors. The use of powder-activated carbon (PAC) is preferred when removing taste and odor compounds and also pesticides and micropollutants from water, due to the convenience of the application, and to the low treated volume [\[123\]](#).

In batch reactors the polluted liquid is loaded to the reactor and then the PAC is added in enough amounts to reach an objective concentration. The amount of PAC added can be determined by the adsorption equilibrium data and [Equation 1.1](#). The PAC is rapidly mixed and once equilibrium is reached, the settled PAC is separated from the treated liquid.

If a large volume of water needs to be treated and/or a long operation is necessary, the usage of granular activated carbon (GAC) in a continuous process conducted in packed columns is preferred. The most commonly employed configuration



implies that the polluted liquid is loaded in the top of the packed column, and as the operation advances, the materials become exhausted. During the operation a zone is identified in which the uptake is taking place, known as *mass transference zone* (MTZ). When the MTZ reaches the end of the column some pollutant are detected in the column outlet, this stage is identified as the breakthrough point (Figure 1.10). Moreover when the MTZ leaves the column, the outlet and inlet concentration of the objective pollutant is the same, indicating that the material is exhausted and need to be replaced or regenerated.

1.5.3.2 Adsorption from gas phase

The removal of hazardous compounds from gas phase by activated carbons is normally carried out in adsorption scrubbers or packed columns. The polluted gas is normally passed through the packed column against gravity at some pressure; as the pressure of the system increases more molecules adsorb over the surface of the AC, normally a dismissal of the system pressure leaves in the desorption of the adsorbed molecules if only physical forces are involved during the process. The extent to which the contaminants are removed strongly depends on the gas pressure, the concentration of the contaminant and the water content of the gas phase that might promote chemisorption reactions on the surface of the carbons [46]. Analogously to liquid uptake, the MZT is identified, and the breakthrough and saturation points are identified. A normal procedure to evaluate the extent of the physical and the chemical adsorption consists of decreasing the adsorption pressure and evaluating the amount of desorbed molecules.

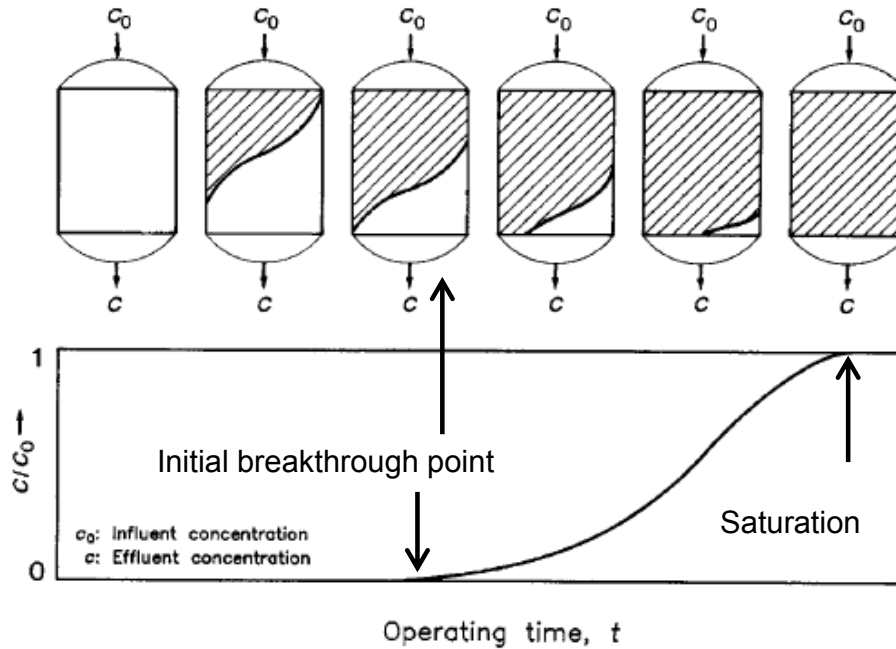
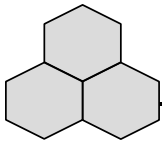
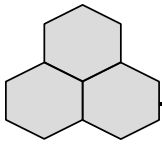


Figure 1.10 Concentration profile and evolution of the MTZ in the GAC packed columns.

1.5.4 CONSTRAINTS OF ACTIVATED CARBON

Even when the advantages of using AC are demonstrated there are some limitations related to arsenic removal and desulfurization.

For arsenic removal, the main constraint of AC is its lack of capacity and selectivity. Since As is normally present as an anion or arsenate (As(V)) or arsenite (As(III)) it is necessary to develop a basic charge surface that attracts arsenic by electrostatic forces [124]. The inorganic content of activated carbons also plays an important role: studies have demonstrated that in order to increase the arsenic adsorption capacity from aqueous solution the content of mainly iron and aluminum and inorganic content are relevant [125,126]. In order to overcome this limitation,



activated carbon is modified to increase its capacity for the removal of inorganic arsenic from water.

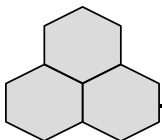
In the removal of SO_2 from gas phase one of the greatest limitations of activated carbons is the acidification of the medium after the uptake. As mentioned in [Table 1.2](#), SO_2 adsorption leads to the formation of H_2SO_4 on the surface of activated carbon that contributes to the rusting of pipelines and scrubbers. To avoid such limitations it is necessary to modify the AC in order to promote reactive adsorption and decrease the acidity formed after the operation.

Another constraint of activated carbon is its lack of selectivity for specific compounds like the removal of sulfur compounds from diesel fuel, which when contacted with AC some other compounds besides sulfur are removed (such as paraffins, aromatics and nitrogen compounds) from the diesel stream, changing the properties of the diesel fuel. In this matter the modifications of activated carbon are carried out to increase its selectivity [\[127-131\]](#).

1.6 TAILORING ACTIVATED CARBON

The versatility of the activated carbons chemical surface not only has a great impact on its adsorptive properties, but it also allows it to be tailored to specific applications.

Besides the carbon oxidation, other chemical modifications are carried out in order to increase the adsorptive properties of ACs. These modifications include the incorporation of foreign compounds such as N, S, P, and metal oxides, especially iron oxyhydroxides (IOH).



Iron oxyhydroxides are preferred over other metal oxides, because they are very easy to synthesize and (since iron is one of the most abundant elements in the earth's crust) they are cheaper to produce than other metal oxides [83]. Also, due to their chemical properties they are very effective for the adsorption/degradation of several compounds. The most important characteristics and properties of IOH are described in the following section.

1.6.1 IRON OXYHYDROXIDES

Iron oxyhydroxides are found in natural systems and readily produced in laboratory. Iron is present in a Fe(III) and Fe(II) state valence and its oxides and hydroxides are normally grouped in a great family of 16 allotropes called iron oxyhydroxides (IOH), the most important of which are summarized in Table 1.4.

Due to their reactive hydroxyl groups IOH are especially important in adsorption and catalysis fields [83].

The structure of IOH consists of packed arrays of anions; the most common are *hexagonal closed packing* (hcp) and *cubic close packing* (ccp). The anions are stacked in a particular crystallographic structure with a mean distance of anion layers of about 0.23-0.25 nm. In ideal packed anions the O-O distance is 0.304 nm for Fe(II), whereas for Fe(III) is 0.29 nm in octahedral and 0.33 nm in tetrahedral coordination [83]. The Fe-Fe distances depend on the kind of connection. In Figure 1.11 the different linkages and their Fe-Fe distances are represented. Those connections give the IOH their particular crystal structures, configurations, and dimensions that are related to their adsorptive and catalytic properties.

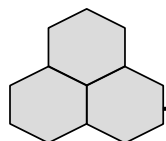




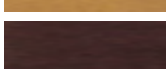








Table 1.4 Iron oxyhydroxide allotropes and highlighted properties.

Mineral name	Formula	Crystal system	Type of magnetism	Colour /Appearance	ΔG formation KJ/mol	Solubility product*
Goethite	α -FeOOH	Orthorhombic	Antiferromag.		-488.6	40-44
Lepidocrite	γ -FeOOH	Orthorhombic	Antiferromag.		-477.7	42
Akageneite	β -FeOOH	Monoclinic	Antiferromag.		Unknown	34.8
Schwertmannite	$Fe_{16}O_{16}(OH)_y(SO_4)_z \cdot nH_2O$	Tetragonal	Antiferromag.		-	-
Feroxyhyte	δ -FeOOH	Hexagonal	Ferrimag.		Unknown	Unknown
Ferrihydrite	$Fe_5HO_8 \cdot 4H_2O$	Hexagonal	Speromag.		-699	38-39.5
Bernalite	$Fe(OH)_3$	Orthorhombic	-		-	-
Hematite	α - Fe_2O_3	Rhombohedral Hexagonal	Weakly ferromag. or antiferromag.		-742.7	42.2-43.3
Magnetite	Fe_3O_4 (Fe(II) Fe ₂ (III) O ₄)	Cubic	Ferrimag.		-1012.6	35.7
Maghemite	γ - Fe_2O_3	Cubic or tetragonal	Ferrimag.		-711.1	40.4
Wustite	FeO	Cubic	Antiferromag.		-251	Unknown

* (pFe+pOH) see ref [83]

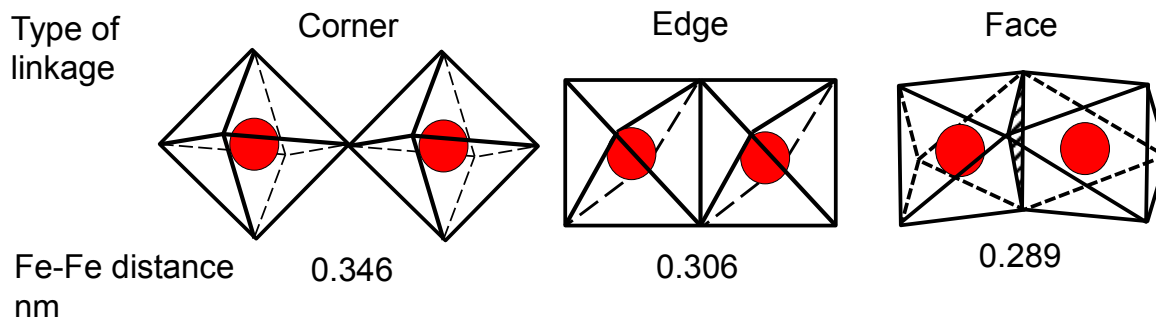
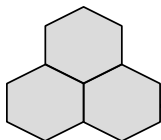


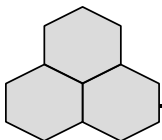
Figure 1.11 Different linkages of octahedral in Fe(III) and their Fe-Fe distances, adapted from [83].

For the adsorption process, crystalline phases as goethite and hematite are preferred; because these phases are the final product of IOH aging and therefore great stability of these phases is expected after adsorption.

1.6.2 ADVANTAGES OF IRON OXYHYDROXIDE-ACTIVATED CARBON MATERIALS

The development of hybrid materials containing the high surface area and the chemical stability of activated carbons and the reactivity and selectivity of the IOH can lead to the design of new materials capable of selectively removing contaminants from liquid phase.

Numerous studies have demonstrated that when iron is added on the surface of the AC there is an enhancement of its adsorptive properties, improving the uptake of many adsorbates from several phases. From water solution pollutants as perchlorate [132], methylene blue [133], phenol and cyanide [134], phosphate [135], chromium [136], and arsenic [37] have been successfully removed by iron-



activated carbons. On the other hand, hazardous sulfur and nitrogen compounds from gas phase have been adsorbed onto iron-modified activated carbon [50,137]. The catalytic effect of iron has been reported by oxidation [138,139] and hydrogenation reactions [140].

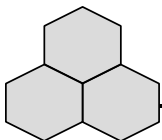
The extent of the increase in the reactive properties of iron-modified activated carbon depends on the shape, size, and pore properties of introduced IOH, in this respect the applied methodology to modify carbon materials is of utmost importance.

1.6.3 METHODOLOGIES TO INCORPORATE IRON OXYHYDROXIDES ON ACTIVATED CARBON

The development of an efficient methodology to iron incorporate on activated carbon is nowadays the subject of numerous studies. Below is a brief list of highlighted methodologies.

1.6.3.1 Impregnation

The methodology consists of precipitating the iron oxyhydroxides and then mixing them with AC under certain conditions. Zhang et al [141] mixed FeCl_4 and FeSO_4 with a 5 M solution of NaOH and then impregnated a commercial AC. Yu et al [142] mixed a 0.125 M FeCl_3 solution, adjusted at pH 4, with GAC at 70°C until 10% of the total volume was evaporated. Liu et al. [143] mixed bamboo AC with 0.01 M NaOH, washed it and then mixed it with a solution 0.1 M FeCl_3 adjusted at pH 2.5 and shook for 24 h.



1.6.3.2 Incipient wetness impregnation

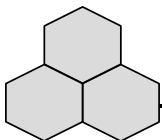
Incipient wetness is a special impregnation method that consists of mixing AC with a solution in the volume necessary only to fill the materials pores, then mixing and drying. Jang et al. [144] tailored AC by mixing 1-1.5 mL of a $\text{Fe}(\text{NO}_3)_3$ solution with 1g of AC, and then mixing thoroughly follow by evaporation at 60°C for 12 h.

1.6.3.3 Precipitation

The precipitation includes the mixing of AC with an iron salt. Then the solution pH is gradually increase of pH leading to the precipitation of the IOH over the surface of the AC. The resultant material depends on the precipitation agent, and the synthesis conditions. Mondal et al. [126,145] precipitated a 2.5% FeCl_3 solution with NaOH at 70°C . Chen et al. [146] precipitated a 2M $\text{Fe}(\text{NO}_3)_3$ solution with NaOH and then the solution was heated at 105°C overnight. Ganizadezh et al. [147] precipitated a FeCl_3 solution with NaOH until a pH of 8.5 and then the solution was rapidly mixed with GAC. Deliyanni and Bandosz [148] mixed AC with $\text{Fe}(\text{NO}_3)_3$ and used $(\text{NH}_4)_2\text{CO}_3$ as a precipitation agent that was added dropwise using a dosimetric pump until reaching a final pH of 8.

1.6.3.4 Salt evaporation

This method consists of impregnation of AC with a Fe salt followed by complete evaporation of the solution and the deposit of Fe(III) species on the surface of the AC. This method was used by Chen et al. [146] for the complete evaporation of a $\text{Fe}(\text{NO}_3)_3$ salt. Likewise, Mackenzie et al. [149] mixed AC with $\text{Fe}(\text{NO}_3)_3$ and shook it overnight. The water was removed in a rotatory evaporator and then transferred



into a glass reactor and heated at 350°C under N₂ atmosphere to promote dehydration.

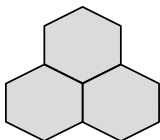
1.6.3.5 Fe(II) oxidation

The methodology of Fe(II) oxidation consists of the impregnation of Fe(II) ions and the subsequent oxidation that decreases the solubility of the Fe allowing its incorporation into the AC. Hristovski et al. [150] pretreated GAC with KMnO₄ and then brought it into contact with a 1 M solution of FeSO₄ for 6h. During the reaction adsorbed Mn(IV) is reduced to Mn(II) and Fe(II) is oxidized to Fe(III) [135].

1.6.3.6 Forced hydrolysis

Forced (or thermal) hydrolysis of ferric and ferrous ions has been amply studied; however their use for the modification of activated carbons has been rarely reported. The first study in this matter was the one conducted by Fierro et al. [151] in which commercial ACs were oxidized by several treatments and then contacted with a solution 0.05 M FeCl₃ at 80°C for 1-24 h.

However, in order to successfully employ the modified adsorbent, this must have chemical stability, which implies stable bonds between iron and the surface of activated carbon. This avoids the loss of the active phase that might be saturated with hazardous compounds. In this sense the forced hydrolysis of ferric ions has demonstrated to be one of the most advantageous for the modification of activated carbon. This methodology has been a subject of recent studies by our research group [152,153] finding that small nanoparticles can be anchored in AC when high temperatures and iron concentration are employed; the resultant material has high



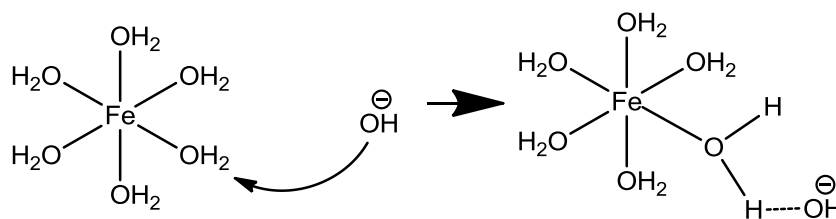
adsorptive properties and excellent chemical stability with less iron content than adsorbents modified with other methodologies.

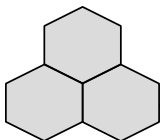
Due to the importance of forced hydrolysis for activated carbon functionalization, this methodology is described in detail in the following section.

1.6.4 FORCED HYDROLYSIS FROM SOLUTION TO PARTICLES

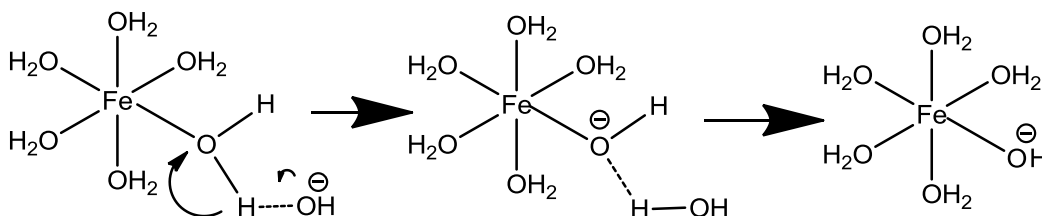
From the earlier works of the Matijevic research group [154] in the 70's, many studies have been focused on studying the forced hydrolysis of Fe(III) ions, and a complete revision was carried out by Flynn [155]. It has been reported that by increasing the temperature of a Fe(III) solution, several IOH can be obtained including: goethite [156,157], hematite [154,157-159], lepidocrite [160], akageneite [161-163], maghemite [164], magnetite [164,165] and amorphous oxides [166].

When a metal polyvalent ion such as Fe(III) is in solution, this coordinates with water molecules forming hexa-aquo complexes as $[\text{Fe}(\text{OH}_2)_6]^{3+}$, the condensation of iron oxyhydroxides occurs in a two-stage reaction based on the hexa-aquo complexes. The first stage is called *initiation* and proceeds by olation with elimination of water and formation of hydroxo-bridges [167]; this step occurs via acid-base, oxidation-reduction reactions or by increasing the solution temperature as in *forced hydrolysis* [168].





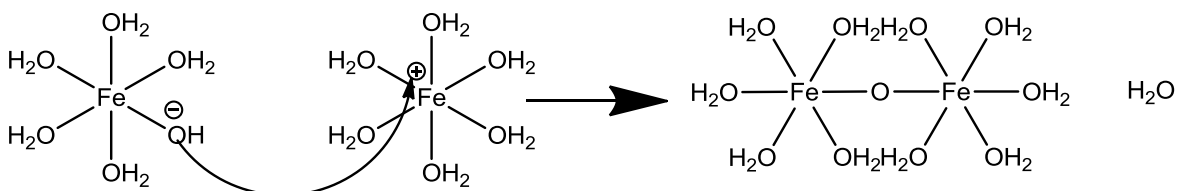
However, the hydrogen bond network in liquid promotes the release of the OH^- ion and the reaction proceeds through a nucleophilic attack of the aquo ligand by hydroxyl, leaving the ligand negatively charged:



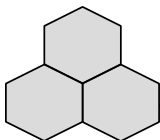
The extent of the reaction depends on the speciation of the iron(III) species. Hydroxylation is the initial stage of the process and the hydroxylated complex is the precursor of the condensation products.

As soon as the hydroxylated species are formed in solution, the condensation may take place giving way to the *propagation step* that is conducted for the formation of oxygenated bridges between cations (oxolation) [168].

The reactions occur by a nucleophilic attack between the hydroxylated complex and the oxo ligand complex:



The reaction continues until it thermodynamically reaches the minimum energy state and the particle condensates.



1.6.5 FORCED HYDROLYSIS IN THE PRESENCE OF ACTIVATED CARBON

Since activated carbon contains oxygen groups on its surface, it is hypothesized that the oxygen in carbons acts as a nucleation center for the anchorage and condensation of the iron oxyhydroxide nanoparticles. [Figure 1.12](#) shows the possible bonds between oxygenated groups and iron aquo-complexes.

The incorporation of iron occurs by adsorption of the Fe(III) aquo complexes from solution over oxygenated groups and afterwards the increase in temperature promotes oxolation reactions and incorporation of iron on the surface of the AC.

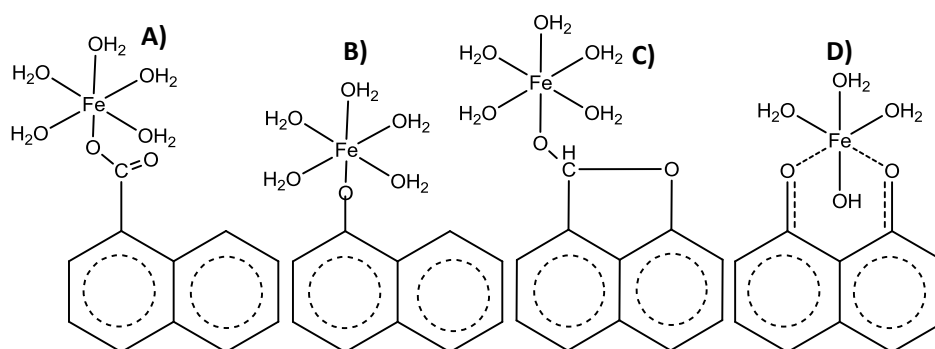
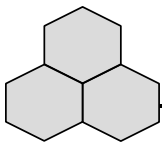


Figure 1.12 Possible interactions between iron and oxygen groups in activated carbon A) carboxylic, B) phenolic, C) lactonic and D) carbonyl.

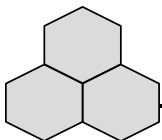
As mentioned before, not many studies of carbon modification have been conducted by means of forced hydrolysis. Those studies have reported particle sizes of IOH that range from 2 to 500 nm. The size, of the particles formed will depend on the thermodynamic conditions of the forced hydrolysis. The crystal phase of the anchored IOH nanoparticles might be determined by X-Ray Diffraction (XRD) experiments on the synthesized material that also can be a useful tool for monitoring any change in the crystalline structure with time (aging).



1.7 THE IMPORTANCE OF THE NANO-SCALE

The size of metal particles can be considered a determinant factor for the adsorption of various molecules onto activated carbon. When very large metal particles are deposited on the surface, they can lead to pore blocking and low adsorption capacity. On the other hand, when nanoparticles are deposited onto the surface of the material adsorbent, the pores can still be accessible and both physical adsorption and chemisorption can enhance a separation process.

Several studies have reported the benefits of the incorporation of very small nanoparticles onto the activated carbon. Zhang et al. [169] reported that smaller particles are more likely to adsorb other molecules in order to become more stable. Yean et al. [170] reported that a decrease in the size of magnetite particles from 300 nm to 20 nm led to an increase of about 200 % in the arsenite adsorption, which was attributed to an increase in the availability of adsorption sites; these results were corroborated by Auffman et al. [42] who observed that when the particle size of maghemite decreased to less than 20 nm, the arsenic adsorption capacity was enhanced four fold. Stara and Matolin's [171] reported that Pd particles of 27 and 2.5 nm supported on alumina affects differently the adsorption of CO. They reported that the activation energy for CO desorption is particle-size dependent and it decreases with the particle size. Zhang and co-workers [172] found a dramatic increase in the response and sensitivity of SnO₂(CuO) sensors, when the particle size was in the range of nanometers.



Therefore, the anchorage of particles of nanometric size on activated carbons is of great importance in order to obtain materials with high density of active surface groups without significantly decreasing their surface area, optimizing their adsorptive and catalytic properties.

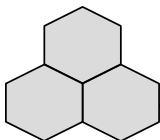
1.8 THE CAPPING AGENT EFFECT

While it is reported that the forced hydrolysis might produce nanoparticles, several methodologies have been applied to reduce the particle size of IOH. One that has been corroborated includes the addition of additives (capping agents) during thermal hydrolysis, which induces a change in the particle size, shape and crystal phase of IOHs.

Several chemical agents have been used to either increase or decrease the particle size of IOHs, for example: surfactants [173], amino acids [174], polymers [175], silicon [176], heavy metals [177] and phosphate. Among them phosphates is an attractive capping agent since it has been reported to decrease the particle size of iron oxyhydroxides.

One of the first works related to the employment of phosphate for controlling the hydrolysis of iron oxyhydroxides was conducted by Rose et al. [178]; the authors reported that the presence of Cl^- and PO_4^{3-} ions in the first and the second coordination sphere inhibits the linkage of the iron octahedral during hydrolysis.

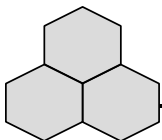
Later, Ishiwaka [179] reported a particle size decrease of $\beta\text{-FeOOH}$ from 20 nm to less than 5 nm when adding HPO_4^{2-} during forced hydrolysis (Table 1.5). Likewise Kandori [180] synthesized particles of FePO_4 by forced hydrolysis and observed a



decrease in particle size from 200 nm to less than 50 nm when increasing the molar ratio of PO_4/Fe . To the best of our knowledge, this is the first work that reports the use of a capping agent to decrease the particle size of IOH in the presence of a porous matrix like activated carbon where porosity can affect the properties of the resultant material.

Table 1.5 Effect of phosphate during the hydrolysis of ferric ions.

Image		Description	Ref
		Particles formed by Fe(II) oxidation in the presence of HPO_4^{2-} .	[179]
		Particles formed by Fe(III) forced hydrolysis in the presence of HPO_4^{2-} .	[179]
		Particles formed in the presence of a) $\log[\text{H}_3\text{PO}_4] = -1.5 \text{ M}$ and b) $\log[\text{H}_3\text{PO}_4] = -2.5 \text{ M}$ at 40°C for 16 h.	[180]



1.9 STATE OF THE ART

1.9.1 REMOVAL OF ARSENIC FROM AQUEOUS SOLUTION

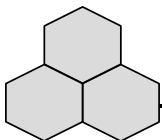
A great range of materials have been studied for the removal of arsenic in either As(III) and As(V) valence states, most of them can be found in several reviews [37,44,45].

Recently the functionalization of activated carbon with iron has been a great interest for the removal of arsenic from aqueous solution. Table 1.6 resumes the most recent works related to the removal of arsenic as well as the observations during material synthesis and adsorption performance. A deeper discussion of key works is provided in the Introduction and discussion sections of Chapter 2 and Chapter 3.

1.9.2 REMOVAL OF SO₂ FROM GAS PHASE

The removal of SO₂ from gas phase by activated carbons has been extensively studied, key studies [49,50,57,58,60-62] specially the carried out by Prof. Bandosz research group [46-48] have reported that crucial factors for SO₂ uptake are the activated carbon porosity, surface chemistry, and the presence of air and water during the adsorption process.

In 2002 Davini [52] studied the incorporation of iron derivatives to activated carbon for the removal of SO₂, finding an increase in the uptake as the iron content of the carbon increases. The maximum adsorption capacity of 120 mg-S/g-C was obtained at an iron content of 1.3 %. Later in 2003 Yang and Yang [63] reported by



molecular orbital calculations that the structural incorporation of SO_2 in activated carbon is thermodynamically favorable ($\Delta G < 0$). The reactive adsorption occurs in three steps: adsorption of SO_2 in basic surface groups, oxidation of SO_2 to SO_3 by chemisorbed oxygen and H_2SO_4 formation by water. The formation of H_2SO_4 represents a problem for depuration systems due to the difficulty for the disposal of acidic wastes in a long-term operation. Those studies demonstrated the importance of the activated carbon surface chemistry during SO_2 uptake, after that several studies were focused in the modification of the carbons surface to enhance the adsorption capacities of carbonaceous materials and to promote the reactive adsorption of SO_2 , avoiding the acidification of the medium.

In 2007 two studies reported that SO_2 can be immobilized by iron oxyhydroxides; Baltrusaitis et al. [181] determined that in the absence of air and water adsorbed SO_2 is transformed to sulfite (SO_3^{2-}) and in the presence of humidity it is transformed to SO_3^{2-} and sulfate (SO_4^{2-}). Meanwhile Fu et al. [182] reported that SO_2 is oxidized to SO_4^{2-} that coordinates with iron oxyhydroxides by means of mono and bi-dentate complexes, in the absence of O_2 no SO_4^{2-} was formed. However those studies do not report the adsorption capacities or the elimination efficiencies for SO_2 removal.

A direct comparison between SO_2 adsorption capacities is difficult, since most of the studies have different adsorption conditions of temperature, concentration, pressure, etc. Recently Seredych et al. [183] reported an extraordinary SO_2 adsorption capacity of 118 mg/g at a concentration of 1000 ppm w of SO_2 in zinc (hydr)oxide/graphite oxide composites.

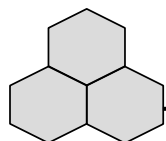


Table 1.6 Highlighted recent studies focused in the removal of arsenic from water in iron modified activated carbons.

Methodology of iron incorporation in activated carbon	Observations on material characterization	Adsorption conditions	Observations on adsorption experiments	Ref
Precipitation of Fe ³⁺ and Fe ²⁺ salts with NaOH followed from solution evaporation	Low iron loading (22 and 34 mg(Fe)/g ads). Loss of about 300-500 m ² /g after modification.	4.5 ppm As(V), pH 3,5 and 7 T 298, 318 and 338 K.	Negligible adsorption capacity at pH 7. At pH 3 and 5 mg/L the adsorption capacities was 4.6 and 2.8 for Fe(III) and Fe(II) respectively.	[184]
Bamboo charcoal Impregnated with 0.5M Fe(NO ₃) ₂	Increase in the surface area of 300 m ² /g after modification. No iron percentages were reported.	As(III) and As(V) in the pH range of 0-14.	Very low adsorption capacities of 0.019 and 0.001 mg/g for arsenite and arsenate at C _{eq} =5 mg/L.	[185]
Precipitation of 10% Fe ₂ (SO ₄) ₃ with 5% NaOCl followed of a calcination at 500°C.	Decrease of about 400 m ² /g after the modification. Incorporation of 5.5% Fe as magnetite and amorphous oxide. No information about particle size was provided.	As(III) in dynamic conditions at pH 7 and 25°C.	No breakthrough curves or volumes treated were reported an adsorption capacity of 1.32 mg/g at 0.2mg/L is reported.	[186]
Oxidation with KMnO ₄ and iron impregnation with 0.2M FeSO ₄ for 24 h.	Loss of less than 100 m ² /g and increase in total pore volume after modification. An extraordinary amount of iron was incorporated (32%) with a pH _{PZC} of 3.6.	As(V) at room temperature without pH control.	Adsorption capacity of 16 mg/g at 1 mg/L. The uptake by iron loading was similar to other studies (108-84 mg-As/g-Fe).	[187]
Bamboo charcoal mixed with 0.01M NaOH and then impregnated with 0.1M FeCl ₃ at pH 2.5.	Same S ^{BET} area after modification with pore reduction. Decrease in pH _{PZC} from 7.4 to 5.0 with an iron loading in carbon of 7.7%. No information of particle size was provided.	As(III) and As(V) at 25°C and pH from 2 to 10.	No interference for pH for As(III) adsorption, maximum uptake of As(V) at pH 3-4. Higher adsorption capacities for As(V) than As(III) (7.8 and 3.0 mg/L) at 5 mg/L.	[143]
Multi-step impregnation of GAC with 0.5M FeCl ₂ .	Increase in the iron content with the repetitions in the treatment. Iron loading up to 12% with 6-46% of iron lixiviating at pH<4.	As(V) at pH 7 with NaHCO ₃ as buffer medium.	The best performance was observed at an iron content of 4.2%. Q As(V) at pH 7 and C _{eq} 5ppm of 1.87 mg/g.	[188]
Precipitation of a Fe(NO ₃) ₃ salt with NH ₄ OH.	Relative lose decrease in the SBET after modification, iron loading up to 8.5 and surface charge of the materials around 6.5.	High As(V) conc. ranged from 10 to 150 ppm, at pH 7 and 25°C.	Maximum uptake at pH 6 in the oxidized and modified material. As(V) uptake at C _{eq} 5 ppm of 5.7 mg/g.	[189]

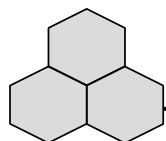
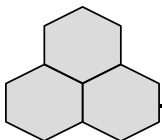


Table 1.7 Selected works related with the desulfurization of diesel fuel by activated carbon.

Material	Diesel Fuel	Adsorbate	Concentration range	Maximum adsorption capacity	Ref.
Oxidized activated carbon cloth	n-heptane	DBT and 4,6 DMBT	0-100 mg-S/g Fuel.	DBT = 35 mg-S/g ads 4,6 DMBT = 50 mg-S/g ads	[190]
Commercial activated carbon maxsorb1	Model diesel fuel	DBT and 4,6 DMBT	320 ppm w	DBT = 0.4 mmol/g 4,6 DMBT = 0.65 mmol/g	[191]
Activated carbon treated with H ₂ SO ₄	n-heptane	DBT	220 mg/dm ³	DBT = 47.1 mg/g	[192]
Coconut shell activated carbon	Decane-hexadecane 1:1	DBT and 4,6 DMBT	20 ppm w	DBT = 18.6 mg/g DMBT = 21.4 mg/g	[193]
HNO ₃ oxidized activated carbon	Hydrotreated diesel from Chennai Petroleum Corporation	4-MDBT 4,6-DMBT	11 ppm of 4-MDBT and 128 ppm of 4,6-DMBT	2.83 mg S/g	[194]
Mesoporus activated carbon	Real diesel provided by Singapore Refinery Co. Ltd.	4,6 DMBT and other non-determined	400 ppm w-S That contains 300 ppm of 4,6 DMBT.	Real diesel = 3.5 mg-S/g A,.	[130]
Activated carbon modified with PdCl ₂	Model diesel fuel	2-MBT and BT	250 ppm-S	Total desulfurization capacity of 0.184 mmol-S/g	[195]
Ag/Cu/Fe loaded activated carbon	n-octane	DBT	376 ppm w	Around 8.4 mg/g	[196]
Activated carbon modified with Fe and Cu	Decane-hexadecane with naphthalene and 1-Methylnaphtalane	DBT and 4,6 DMBT	20 ppm w	Total desulfurization capacity of AC-Cu= 10.28 and AC-Fe=8.37 mg-S/g AC	[197]



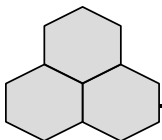
1.9.3 ADSORPTIVE DESULFURIZATION FROM DIESEL FUEL

During the last decade there has been an increase in the studies related to the adsorptive desulfurization of diesel fuel by activated carbons. Since a model diesel, adsorbates and adsorption conditions are selected by particular criteria for the research groups, a direct comparison among the diverse studies reported in the literature is hard to make. However, selected works that are similar to the reported in this thesis are provided in [Table 1.7](#).

1.10 MOTIVATION OF THIS RESEARCH

The increase in human activities has resulted in the presence of key pollutants that determine the quality of air and water. Among these compounds two of the most important are arsenic and sulfur, which pollute water and air, respectively. It has been postulated that both compounds can be efficiently removed from liquid and gas phase by adsorption onto several materials. However, the more strict environmental regulations require the implementation of more efficient and accessible materials capable of polishing the polluted effluents.

It was thought that the blend of the chemical and physical properties of activated carbon and the high selectivity and capacity of iron oxyhydroxides could lead in the synthesis of a promising material to uptake arsenic and sulfur with adequate mechanical stability. However, previous reports related to this subject had been demonstrated that most of the times when activated carbon is modified with iron oxyhydroxide clusters are formed, blocking pores and decreasing the materials adsorptive properties. Therefore, the main motivation of this research was to



anchored iron oxyhydroxide nanoparticles (<2 nm) on activated carbon, taking advantage of capping agents recently used in nanotechnology, to keep as much of the original surface area of the carbon material and at the same time to introduce a high concentration of active sites to synthesize an adsorbent material with high adsorption capacity for key pollutants in liquid and gas phases.

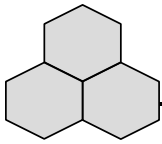
1.11 HYPOTHESIS

The implementation of phosphate as capping agent during the forced hydrolysis of Fe(III) salts will decrease the particle size of iron oxyhydroxides anchored on activated carbon, and hence, the adsorption capacity of key pollutants such as arsenic and sulfur compounds in liquid and gas phases will increase due to the incorporation of highly reactive hydroxyl groups that can bond with arsenic by ligand interchange and with sulfur by specific reactions.

1.12 OBJECTIVES

1.12.1 GENERAL OBJECTIVE

To incorporate iron oxyhydroxide nanoparticles on the surface of activated carbon, by means of the thermal hydrolysis of ferric chloride with the assistance of phosphate as a capping agent, to increase its adsorption capacity for arsenic and sulfur compounds from liquid and gas phase.



1.12.2 SPECIFIC OBJECTIVES

To determine the synthesis conditions of the thermal hydrolysis of FeCl_3 in the presence of PO_4 enhancing the higher As(V) removal by the modified AC.

To characterize the synthesized materials and corroborate the presence of iron oxyhydroxide nanoparticles on their surface.

To determine the key properties of the modified activated carbon that influence the As(V) adsorption from aqueous solution and that maximize the adsorptive properties of the synthesized material.

To determine the adsorption capacity of iron-modified activated carbon for removing SO_2 gas and relate it to the iron oxyhydroxide particle size.

To determine the desulfurization capacity of un-modified and iron-modified activated carbon by using a synthetic model diesel.

To study the effect of organic compounds, naturally present in diesel fuel, on the desulfurization capacity of un-modified and iron-modified activated carbons.

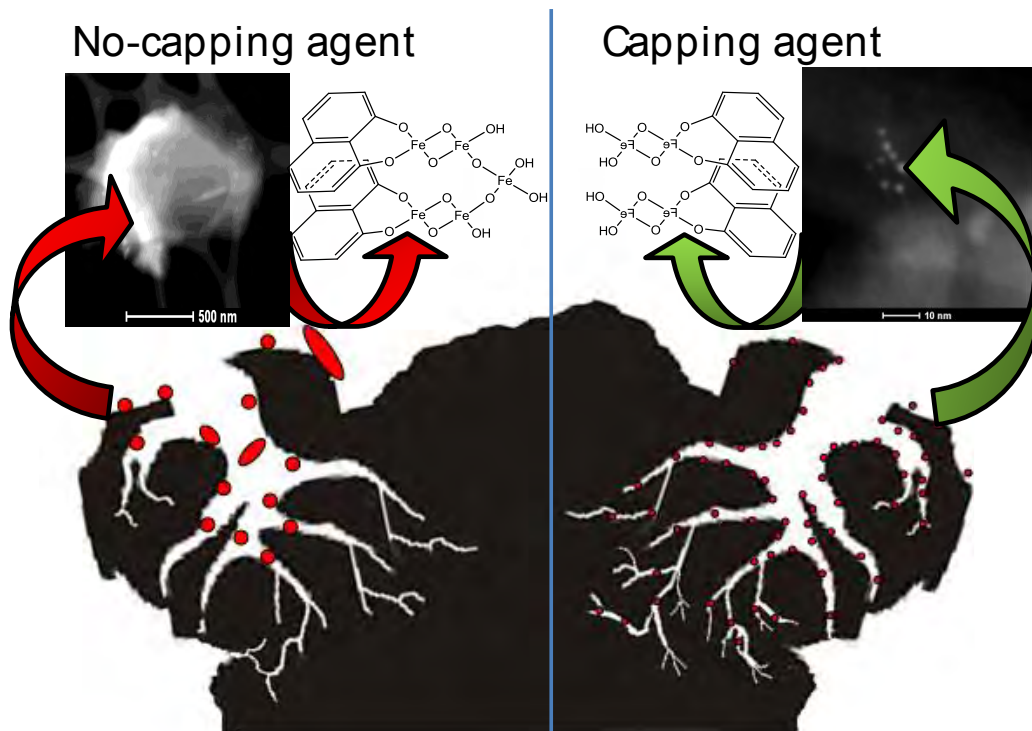
To determine if the iron nanoparticles anchored in activated carbon cause further oxidation of adsorbed sulfur compounds.

To study the influence of the nitrogen aromatic compounds quinoline and indoline on the desulfurization capacity of un-modified and iron-modified activated carbon.

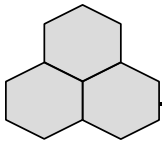
Chapter 2

Effect of Particle Size of Ferric Oxyhydroxides on the As(V) Removal from Water

Implementation of PO_4 during $FeCl_3$ forced hydrolysis decreased the particle size of IOH anchored in activated carbon enhancing its As(V) adsorption capacity.



This chapter was adapted from: *Effect of phosphate on the particle size of ferric oxyhydroxides anchored onto activated carbon: As(V) removal from water*, Environmental Science and Technology, 2012, 46 (17), 9577-9583.

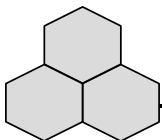


Abstract

The surface area of iron oxyhydroxides is a key factor when removing arsenic from water. However, research related to this matter shows that this issue has not been explored in detail. The use of capping agents is a viable method to synthesize iron oxyhydroxide nanoparticles; however, this method to our knowledge has not been applied for the anchorage of iron oxyhydroxide nanoparticles on activated carbon (AC). In the present work, the addition of PO_4 (as a capping agent) in forced hydrolysis of FeCl_3 in AC was investigated. Results revealed that the surface area of modified materials reached a maximum of about $900 \text{ m}^2/\text{g}$ with a molar ratio PO_4/Fe of 0.1. Moreover, microscopy studies indicate a size range of iron nanoparticles from 2 to 300 nm, where the smallest particles are attained at the highest concentration of PO_4 . The surface charge distribution of modified samples became less positive, however the As removal increased, indicating that electrostatic interaction is not the controlling sorption mechanism. Modified samples showed a 40% increase on As(V) adsorption capacity when using a molar ratio PO_4/Fe of 1.5. The proposed method allowed anchoring of iron oxyhydroxides nanoparticles on AC, which have a high As(V) adsorption capacity (5 mg/g).

2.1 INTRODUCTION

Since the pioneering work of Reed et al. [198], hybrid carbon-iron materials have garnered great attention for arsenic removal. The incorporation of iron to the

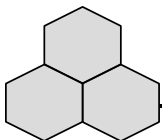


carbon matrix includes several technologies resulting in the synthesis of materials with a large range of properties having different performances for As removal.

Payne and Abdel-Fattah [36] impregnated activated carbon with a FeSO_4 salt reporting an As(V) adsorption capacity of 0.8 mg/g after modification. At acidic conditions the adsorption capacity dramatically decreased, due to the dissolution of incorporated Fe. An impregnation of activated carbon with $\text{FeCl}_3/\text{FeSO}_4$ was also applied by Zhang et al. [141], after modification surface area was reduced in a 20% with an increase of about 8% in iron content. An improvement in arsenic(V) adsorption capacity from 44 to 67 mg/g after modification at very high arsenic concentrations (up to 375 mg/L) was reported.

By using the forced hydrolysis methodology Fierro et al. [199] were capable to anchor nanoparticles at the surface of AC. A maximum arsenic(V) adsorption capacity of 0.028 mg/g was obtained with a 2.2% of iron in AC. After that, iron deposition causes clusters formation decreasing the available sites for arsenic adsorption; the particle size in the material with the highest adsorption capacity was smaller than 50 nm.

Nieto et al. [153] reduced the iron particle size anchored in AC by controlling the time, temperature and iron concentration during forced hydrolysis. The iron percentages obtained were in the range of 0.73 to 5.27 %. However, the maximum arsenic adsorption capacity (3.25 mg/g) was obtained for the activated carbon with 1.37 % of iron. This material presented a decrease in the specific surface area of less than 100 m^2/g due to the deposition of very small iron particles (2-10 nm).

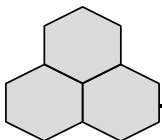


Those studies emphasize the importance of the iron particle when removing arsenic from aqueous solution.

Controlling the hydrolysis process allows to control the structure and the size of the nuclei of colloids formed. However, the major challenge in controlling the hydrolysis of Fe(III) ions is the very low energy state of this process, thus nucleation and propagation steps are highly spontaneous [178]. This constrain can be avoided by using complexing or capping agents such PO_4^{3-} that as mentioned before, reduces the particle size of the iron oxyhydroxides (IOHs) formed. In addition, the work of Rose et al. [178] emphasizes the usage of PO_4 during FeCl_3 hydrolysis. The authors reported that in the Fe- PO_4 system the number of Fe1 neighbors is maintained lower than 1 at difference of the Fe-Cl system in which the neighbors reaches 1.5 for higher hydrolysis ratios. This indicates that the presence of PO_4 ligands hinder the polymerization of Fe.

To the best of our knowledge, we were the first to use capping agents to decrease IOHs particle in the presence of porous matrices like activated carbon where porosity can affect the properties of the resultant material.

The aim of the present work was to study the effect of phosphate as capping agent, on the anchorage of IOHs nanoparticles onto granular activated carbon (GAC), with the purpose of obtain materials with well-dispersed iron nanoparticles and with a high arsenic adsorption capacity. Three synthesis factors were studied: hydrolysis temperature (80, 90 and 110 °C), hydrolysis time (48, 60 and 72 h) and molar ratio of phosphate to iron (0-1.5). The resultant materials were tested to adsorb arsenic(V) from aqueous solution, and selected adsorbents materials were



characterized by nitrogen physisorption, chemical content, microscopy, charge distribution and XRD. A Box-Behnken experimental design was chosen to determine the significance of the parameters studied, and a surface response that describes the arsenic adsorption capacity was obtained.

2.2 EXPERIMENTAL

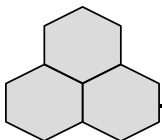
2.2.1 MATERIALS AND CHEMICALS

All the chemical reagents used in this study (FeCl_3 , H_3PO_4 , Na_2HAsO_4 , HNO_3 , NaOH , HCl and H_2SO_4) were reagent grade. The granular activated carbon (GAC), Filtrasorb (F-400, lot 1) provided by Calgon, was reduced to a particle diameter of 250-500 μm (30 X 60 U.S. mesh), washed with double deionized water and then dried at 90°C for 24 h.

2.2.2 ACTIVATED CARBON MODIFICATION

Activated carbons were modified by contacting 0.5 g of GAC in 14 mL serological bottles with 10 mL of a reagent solution, which was prepared by mixing FeCl_3 , H_3PO_4 and H_2O to obtain a desired molar ratio (MR) PO_4/Fe . An iron concentration of 3 M was kept constant in all the experiments. The serological bottles were hermetically sealed and placed in a stove (Thermo Scientific 6909) at constant temperature (80, 95, and 110 °C) for 48, 60, and 72 h, respectively.

After the modification, the materials were rinsed with double deionized water until iron, phosphate, and chlorine were not detected in solution. Finally, modified GACs were dried at 90 °C for 24 h. These materials were named ACM and ACM XP for



the GACs modified with iron and with iron plus phosphate, accordingly, where X stands for the molar ratio PO_4/Fe .

2.2.3 ADSORPTION EXPERIMENTS

Adsorption experiments were carried out in 50 mL Falcon conical flasks, in which 25 mg of raw or treated GAC were immersed in a solution containing a known concentration of arsenic(V). The pH was kept constant at 7 by adding 0.1 N NaOH or HNO_3 . After equilibrium was reached, samples were centrifuged and the remaining arsenic in solution was determined by inductively coupled plasma atomic emission spectroscopy (ICP-AES), by a Varian spectrometer 730-ES, at a wavelength of 188.98 nm. Finally, the adsorption isotherms of selected materials were adjusted by the Freundlich and Langmuir models.

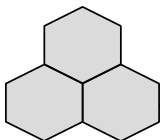
2.2.3 MATERIALS CHARACTERIZATION

Surface area and pore volume

Surface area and pore size distribution were calculated from the corresponding nitrogen adsorption isotherm at 77 K determined by a Micromeritics Accelerated Surface Area and Porosimetry (ASAP) analyzer 2020. The specific surface area was calculated using the BET isotherm, and the pore size distribution was determined by using the density functional theory (DFT) protocol.

Iron and phosphorous content

Iron and phosphate content in materials was determined according to Nieto et al. [153] after acid digestion in a microwave (Milestone, Ethos 1). This digestion was carried out as follows: 50 mg of material were placed in a silicone container and then 20 mL of an acid solution ($\text{HCl}:\text{H}_2\text{SO}_4$, 5:1) were added. The container was closed and heated to 150 °C at a rate of 10 °C per minute; and maintained



constant for 1 h. The remaining solution was diluted to 50 mL and then analyzed. The iron concentration was obtained by atomic absorption spectroscopy (AAS) in a PerkinElmer AAnalyst 400 at a wavelength of 271.9 nm, and the phosphorous amount was determined by ICP-AES at a wavelength of 213.618 nm.

Microscopy studies

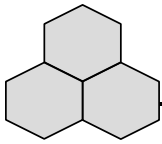
Microscopic studies were carried out on a Tecnai FEI 300 transmission electron microscope (TEM) operated at 300 kV. The sample was reduced to powder, suspended in isopropanol and then sonicated for 5 minutes. Finally, the samples were mounted in a Cu TEM grid. Elemental analysis and elemental mapping were carried out by EDS on the same equipment.

Surface charge distribution and point of zero charge

Surface charge distribution and point of zero charge (pH_{PZC}) were obtained by an automatic titrator Metler Toledo (PL 70) according to Chen et al. [200]: 50 mg of sample was brought into contact with 50 mL of 0.1 M NaCl and 1.5 mL of 0.1 M HCl. The recipient was saturated with N_2 gas for 3 minutes and then stirred for 12 hours, in order to guarantee that equilibrium was reached. Then, a titration with 0.1 M NaOH was carried out under a nitrogen atmosphere to avoid CO_2 interferences. Blank experiments were conducted without the addition of material. The ion released was calculated with the following equation:

$$\frac{C (V_m V_b)}{m} \quad (\text{e n. .1})$$

Where: IR are the ions released [mol/g], V_m is the sample volume necessary to achieve a certain pH value [mL], V_b is the blank volume necessary to achieve the same pH value as the sample [mL] and m is the sample mass titrated [g].



X-Ray diffraction studies

XRD patterns were obtained in a Bruker D8 diffractometer using a $\text{CuK}\alpha$ radiation ($\lambda = 1.5406 \text{ \AA}$). Samples were reduced to a mesh size < 90 , and then the powder was placed in the XRD sample port. The patterns were obtained with a step size of 0.02° 2θ at 10 s per step.

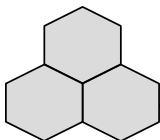
2.2.4 Distribution of species

Species distribution was calculated in Visual MINTEQ 3.0 free version, using the specific ion interaction theory (SIT) to estimate the activity coefficients of high concentrated electrolytes in solution [201].

2.3 RESULTS AND DISCUSSION

2.3.1 ADSORPTION EXPERIMENTS

Figure 2.1.A shows that when adding phosphate as a capping agent (filled symbols), the arsenic adsorption capacity increased (open symbols). Moreover, the Pareto chart of the experimental analysis (Figure 2.1.B) shows the significance ($P < 0.05$) of molar ratio PO_4/Fe (MR) and hydrolysis time (T) on the As(V) adsorption capacity of modified GACs, contrary to the hydrolysis temperature (T_e) as also observed in Figure 2.1A. Hence, 80°C was chosen to anchor iron oxyhydroxides on GACs. The surface response (Figure 2.2.) shows that the maximum As(V) adsorption capacity at 25°C , pH 7 and initial concentration (C_0) of 4.5 mg/L is obtained at a MR of 1 and at a hydrolysis time of 60 h. To consider the effect of initial concentration, arsenic(V) adsorption isotherms were determined for samples GAC, ACM and ACM 1P (Figure 2.3.). The lines on this graph correspond to the



Freundlich model, which best fit the experimental data (Langmuir and Freundlich parameters are provided in Table 2.1). It can be observed that after the GAC was modified with iron (ACM), the adsorption capacity increased by about 20%. However, when phosphate was used as a capping agent at a MR of 1 (ACM 1P), the As(V) adsorption capacity increased 90% compared to GAC and 69% in contrast to ACM. Moreover, a maximum adsorption capacity of 5 mg/g was obtained for ACM 1P, which is in the top range compared to that of other iron based adsorbent materials (see Table 1.6) and references [37,151,188,202,203].

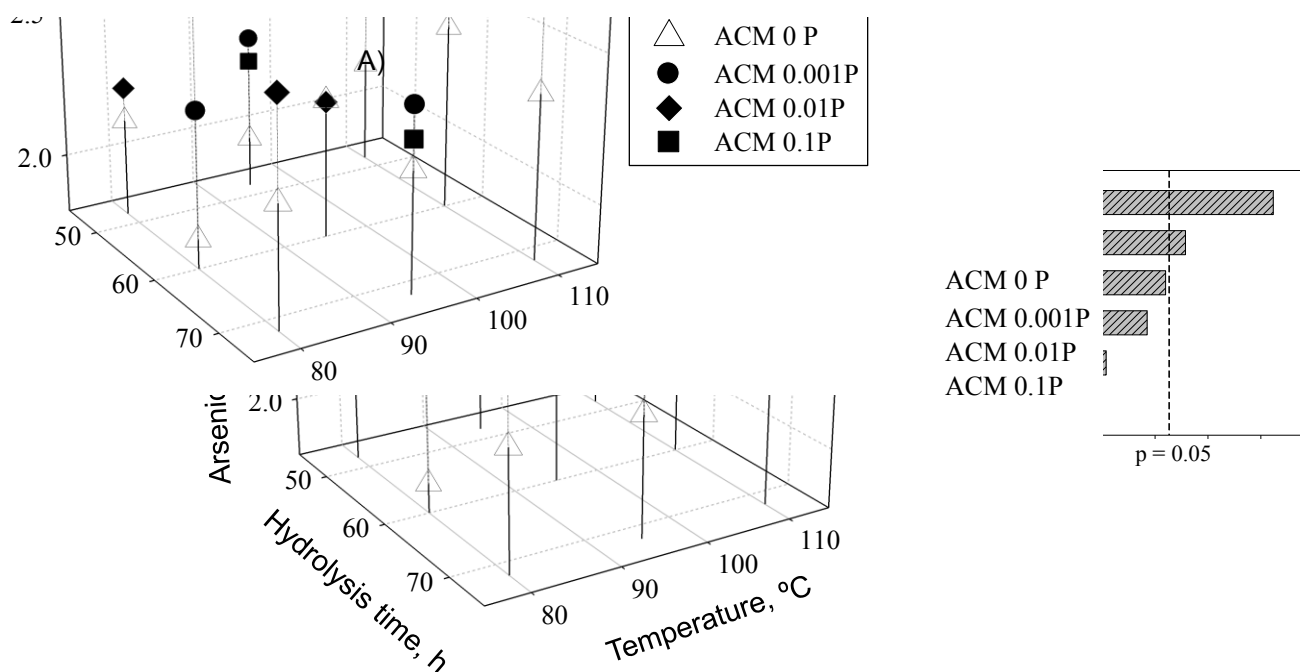


Figure 2.1 A) Effect of hydrolysis time, temperature and molar ratio PO_4/Fe on the As(V) adsorption capacity (at 25° C, pH 7 and C_0 of 4.5 mg/L), standard error of central point is 0.038(1.67%) and **B)** Pareto chart of the experimental design.

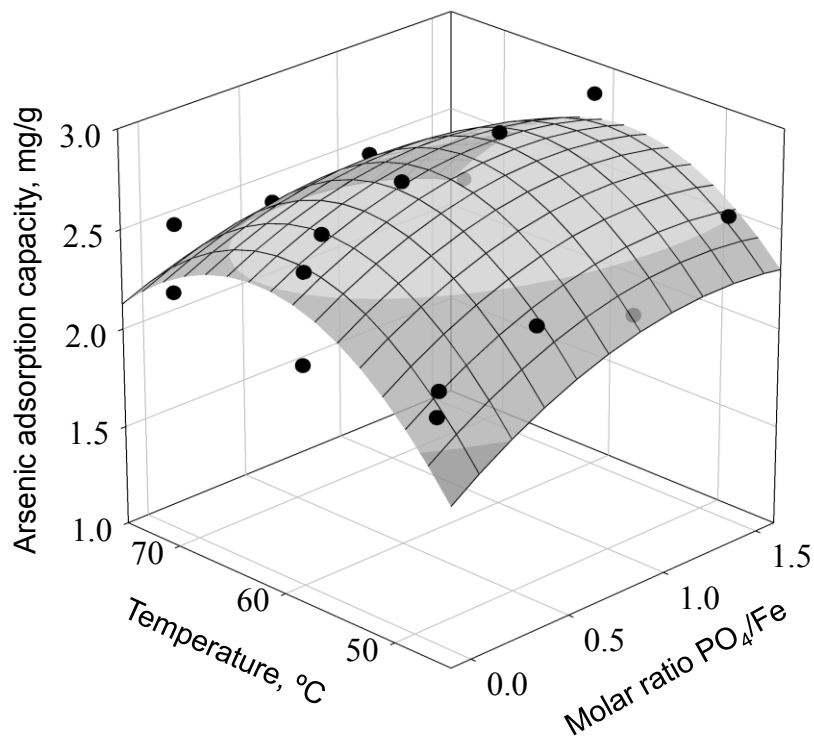
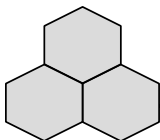


Figure 2.2 Surface response of arsenic(V) adsorption capacity (25 °C, pH 7 and Ci of 4.5 mg/L) as function of molar ratio and hydrolysis time at 80 °C.

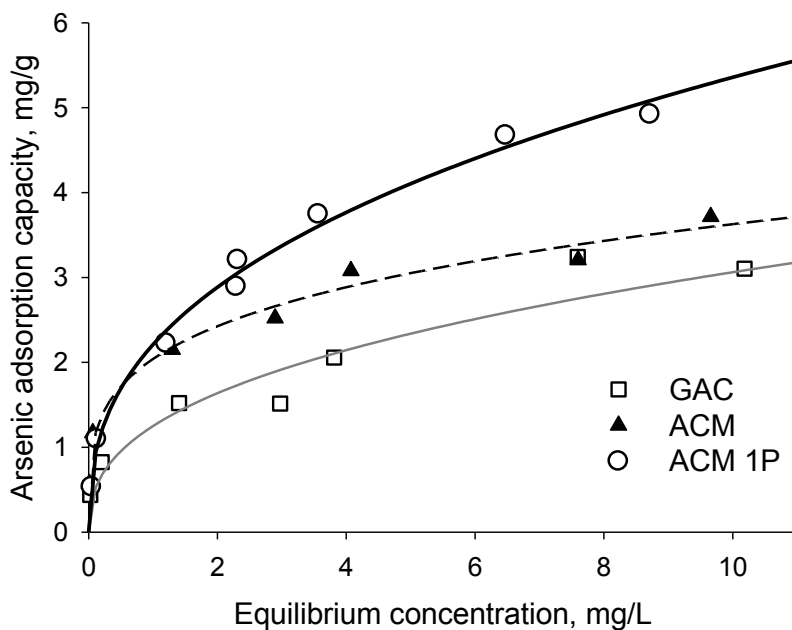


Figure 2.3 Arsenic(V) adsorption isotherms at 25 °C and pH 7.

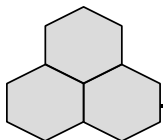


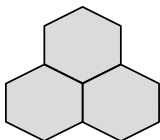
Table 2.1 Parameters of Langmuir and Freundlich isotherms for arsenic removal in selected materials at 25 °C and pH 7.

Sample	Langmuir		R	Freundlich		R
	Q _m	K _L		K _F	n	
GAC	4.27	0.28	0.92	1.25	2.57	0.960
ACM	3.08	7.68	0.92	2.04	4.00	0.991
ACM 1P	6.04	0.48	0.98	2.21	2.6	0.995

2.3.2 MATERIALS CHARACTERIZATION

In order to understand the differences on arsenic adsorption capacity of the modified materials, the surface area, iron and phosphorous content of these adsorbents were concentrated in [Figure 2.4](#). The surface area of GAC is 830 m²/g, but this increased by 30 m²/g when it was modified with iron, which can be due to the anchorage of IOHs nanoparticles (iron content changed from 0.2 % to 1.33%).

[Table 2.2](#) shows that the mesopore volume slightly increased. On the other hand, when the capping agent was added, the As(V) adsorption capacity increased ([Figure 2.4.A](#)). Also the BET surface area showed a maximum of 900 m²/g ([Figure 2.4.B](#)) at a MR of 0.1 at which the iron content was 1% ([Figure 2.4C](#)). The micropore volume increased under these conditions ([Table 2.2](#)), indicating that iron nanoparticles are small enough to create microporosity between them, thereby increasing surface area. As the MR continued increasing (>0.1) the surface area started to decrease, and iron content slightly increased reaching a maximum of



1.22 % at a MR of 1.5 (Figure 2.4.C). This increase in the iron content was accompanied by a decrease in micropore volume due to the ultramicropores obstruction in the GAC, indicating that IOH nanoparticles are small enough to penetrate the narrowest micropores. However, the adsorption capacity showed a plateau around a MR of 1 (Figure 2.4.C), indicating that it is not affected, despite the decreasing micropore volume, due to the continuous decrease of IOH particle size.

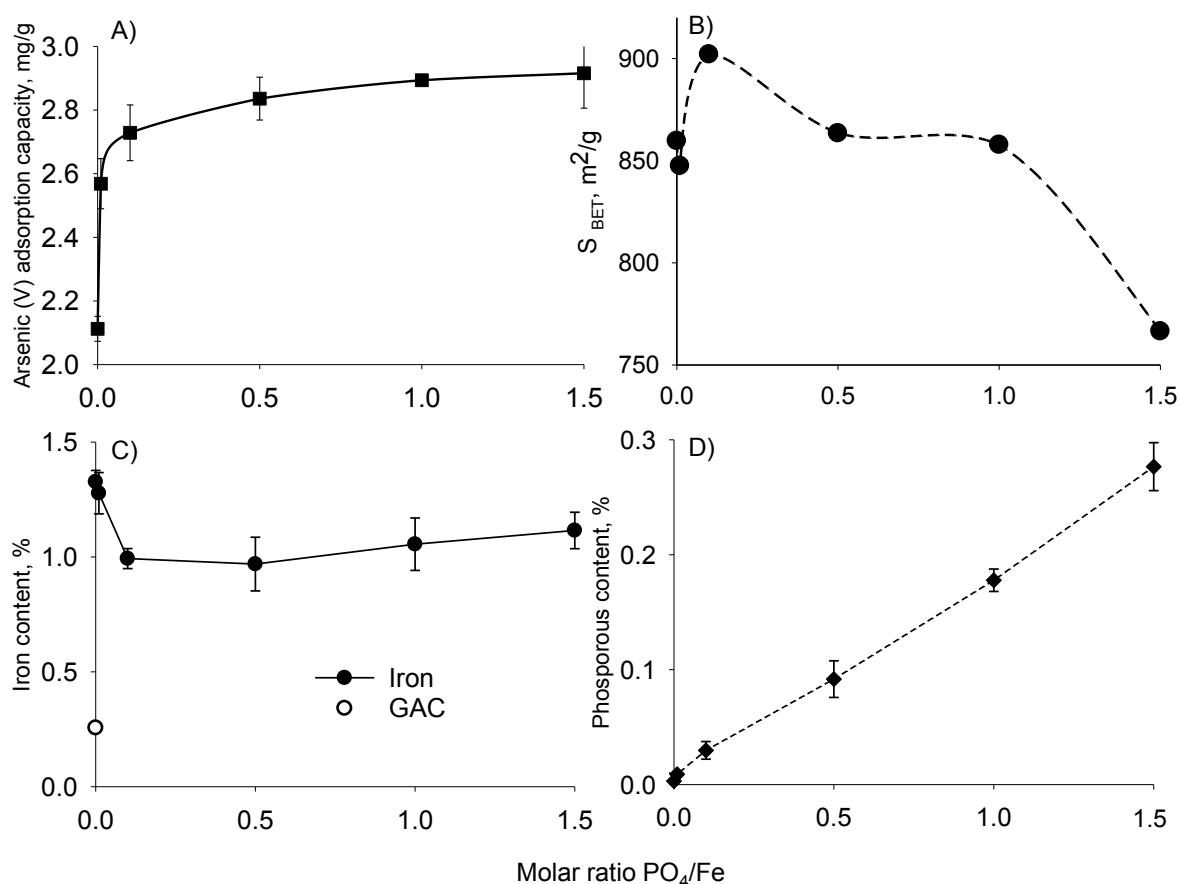


Figure 2.4 Synthetized materials at 80°C and at a hydrolysis time of 60 h: **A)** arsenic adsorption capacity; **B)** BET surface area, **C)** Iron content and **D)** Phosphorous content.

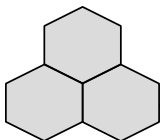


Table 2.2 Pore volume of carbon samples calculated from nitrogen adsorption isotherms at 77 K by DFT.

Sample	$V_{<10\text{\AA}}$ (cm^3/g)	V_{mic} (cm^3/g)	V_{mes} (cm^3/g)	V_t (cm^3/g)
GAC	0.204	0.305	0.070	0.379
ACM	0.201	0.305	0.087	0.399
ACM0.1P	0.215	0.333	0.087	0.426
ACM1.0P	0.183	0.260	0.071	0.338
ACM 1.5P	0.164	0.244	0.065	0.316

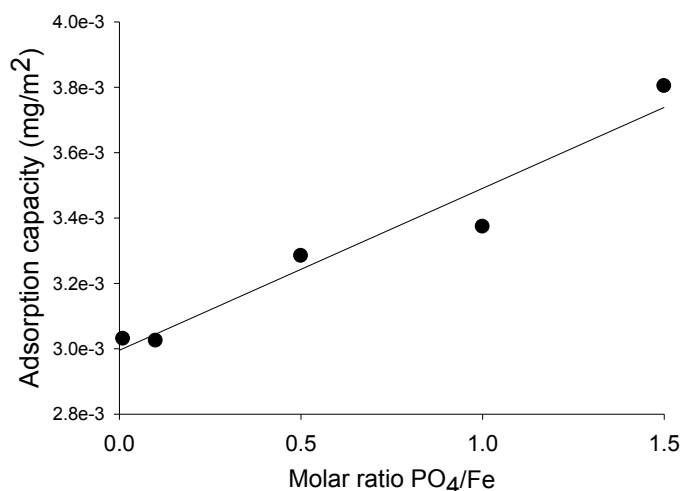


Figure 2.5 Surface adsorption capacity as a function of the molar ratio PO_4/Fe .

The linear equation is: $\text{adsorption} = 0.0005 \cdot \text{MR} + 0.003$.

In addition, the phosphorous content of modified materials increased with the MR, reaching a maximum of 0.3% at a MR of 1.5 (Figure 2.4.D). A mass balance that considered the phosphorous content in the material and in the rinsing water confirmed that the great majority (>99%) of phosphates used as capping agent were removed during the washing step. These results indicate that indeed phosphate acts as a capping agent by keeping IOHs available to adsorb arsenic.

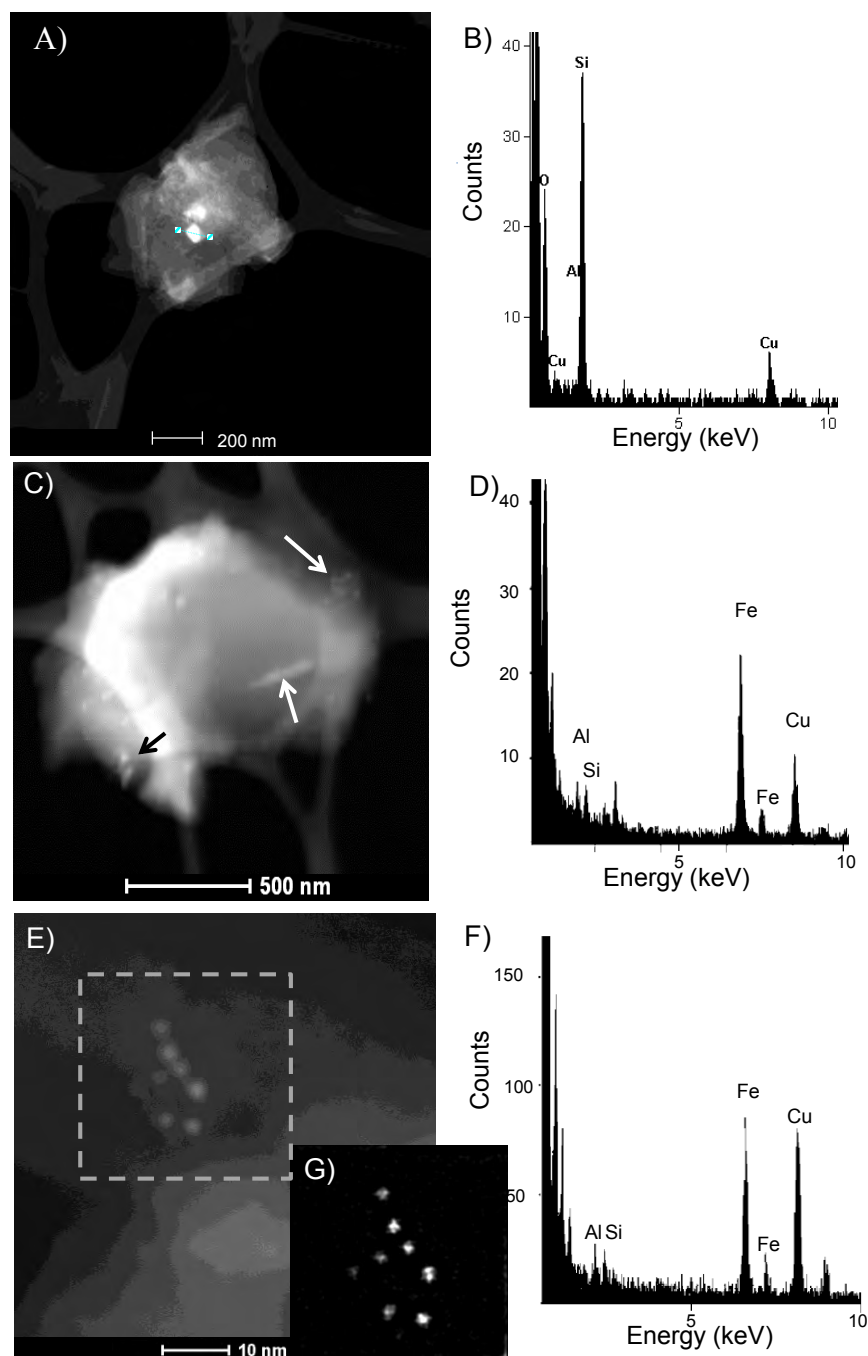
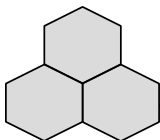
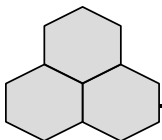


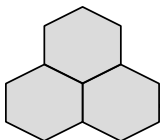
Figure 2.6 A) STEM image of GAC. B) EDS of GAC, (no iron was detected). C) STEM image of ACM, arrows indicate nanoparticles. D) EDS of ACM particles, indicating the presence of Fe. E) STEM image of ACM 1P: F) EDS of ACM 1P, indicating the presence of Fe ($K\alpha$ and $K\beta$ transitions). G) Fourier filtered image of selected area in E).



Moreover, when the As(V) adsorption capacity (expressed as mass adsorbed per square meter) of modified materials that involved phosphate is correlated with the molar ratio PO_4/Fe (Figure 2.5), a linear behavior is observed ($R=0.948$). These results suggest that a higher concentration of phosphate causes a decrease of IOHs particle size, and perhaps a better dispersion of these on the GAC surface, which increases the active surface area and hence the As(V) adsorption capacity (g/m^2).

Chang et al. [188] find a maximum arsenic adsorption capacity of 1.95 mg/g for impregnated granular activated carbon with ferrous chloride that had an iron content of 4.22 %. These same authors reported a decrease in adsorption capacity when the iron content increased in the modified materials. This was attributed to the decrease in adsorptive sites density as a result of pore blockage. The same effect was observed by Gu et al. [202] who reported a maximum arsenic adsorption capacity of 6.6 mg/g for activated carbon that had an iron content of 2.34 %.

Scanning transmission electron microscopy (STEM) studies were carried out for GAC, ACM and ACM 1P. Figure 2.6.A shows the image of GAC. EDS analysis confirmed the presence of aluminum and silica particles in GAC (Figure 2.6.B), which is expected since this material is of mineral origin. No iron was detected in GAC. When iron was added (ACM), nanoparticles of different sizes were observed: microparticles of about 300 nm and small nanoparticles of about 30 nm (Figure 2.6.C). EDS analysis indicates that these are iron particles (Figure 2.6.D). Furthermore, when the capping agent was added in a molar ratio of 1, the particles size considerably decreased; Figure 6E corresponds at the STEM image of ACM 1P, with an average particle size of 2 nm. EDS analysis corroborates that these



nanoparticles correspond to iron (Figure 2.6.F). To our knowledge, this is one of the smallest IOHs nanoparticles that have been introduced in GACs. With a Fourier filtrated image, (Figure 2.6.G) IOH nanoparticles in ACM 1P became more evident. In order to find out what is the contribution of iron oxyhydroxides on the surface charge of modified materials, natural goethite was included in the analyzes.

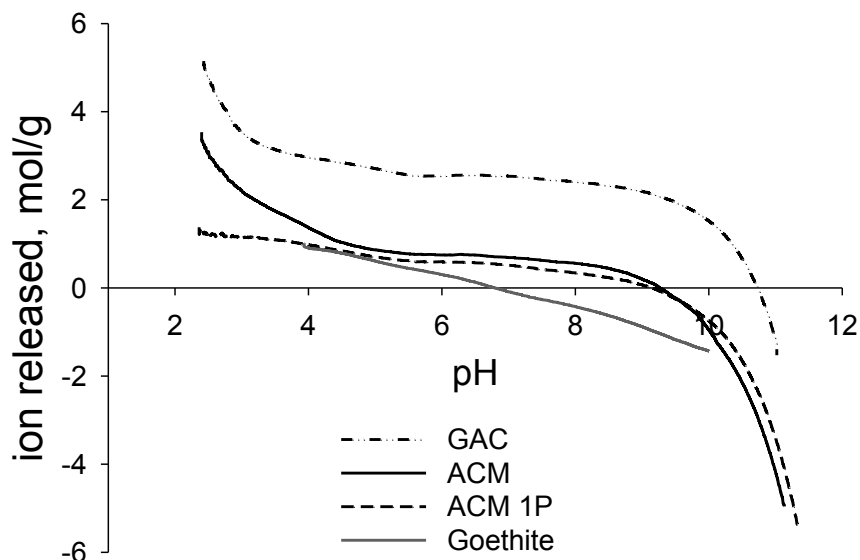
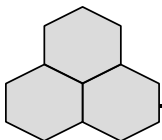


Figure 2.7 Surface charge distributions of studied materials at room temperature.

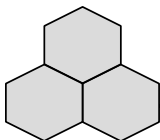
The surface charge distribution of GAC, ACM, ACM 1P and natural goethite is shown in Figure 2.7. The pH_{PZC} of GAC was 10.7, indicating the predominance of basic groups. However, after modification of the GAC, the pH_{PZC} was shifted to 9.3. This effect could be explained as follows: 1. As known, IOH particles have a strong association with oxygenated groups in activated carbon [199,202,204]. It is likely that IOH reacts with oxygen-containing groups (such as pyrone or chromene-like groups [94]), decreasing their density and hence lowering the pH_{PZC} . 2. IOH particles have a pH_{PZC} of about 7 [205] (as can be seen for natural goethite) and cause a more negative charge distribution when anchored on GAC. 3. GAC is in



contact with 9 M HCl ($\text{pH} < 1$) during forced hydrolysis of FeCl_3 . At these acidic conditions, some graphitic layers can be partially consumed, and when exposed to air, a higher amount of oxygen can be chemisorbed [206], forming acid groups that decrease the materials pH_{PZC} .

ACM and ACM 1P have very similar charge distributions but different adsorption capacities, which suggests that electrostatic attraction between $\text{As}(\text{V})$ and the materials surface is not as important as the concentration and particle size of IOHs. The main $\text{As}(\text{V})$ adsorption mechanism onto IOHs is due to inner sphere complexes, mainly the bidentate-binuclear kind between the $\text{As}(\text{V})$ tetrahedral and adjacent edge-sharing octahedral of the IOHs [207-210].

It is known that iron can form several allotropes of IOHs, and each of these have different adsorption capacities [211,212]. The XRD pattern of GAC (Figure 2.8.) shows an amorphous behavior which is characteristic of low graphitic carbons, in which the line broadening cannot be explained for the presence of graphitic microcrystallites [213]. Other peaks at 21, 35, and 68 2θ match with the XRD of goethite [214] and peaks at 31, 33, 36.8, 40.9, 50, 57.8 and 65 2θ can be attributed to hematite. However, due to the very low iron content of GAC, 0.2%, these peaks could also correspond to isomorphism impurities of aluminum $\alpha\text{-Al}_2\text{O}_3$ and $\alpha\text{-AlOOH}$ [83], which can also adsorb $\text{As}(\text{V})$ [215]. On the other hand, the XRD patterns of modified GAC samples (ACM) did not show an appreciable change compared to that of GAC, indicating that the IOH particles are either amorphous or very small to diffract. Finally, after the addition of H_3PO_4 (ACM 1P) as a capping



agent, the peaks of the isomorphism particles slightly decreased, probably due to the washing out of aluminum particles.

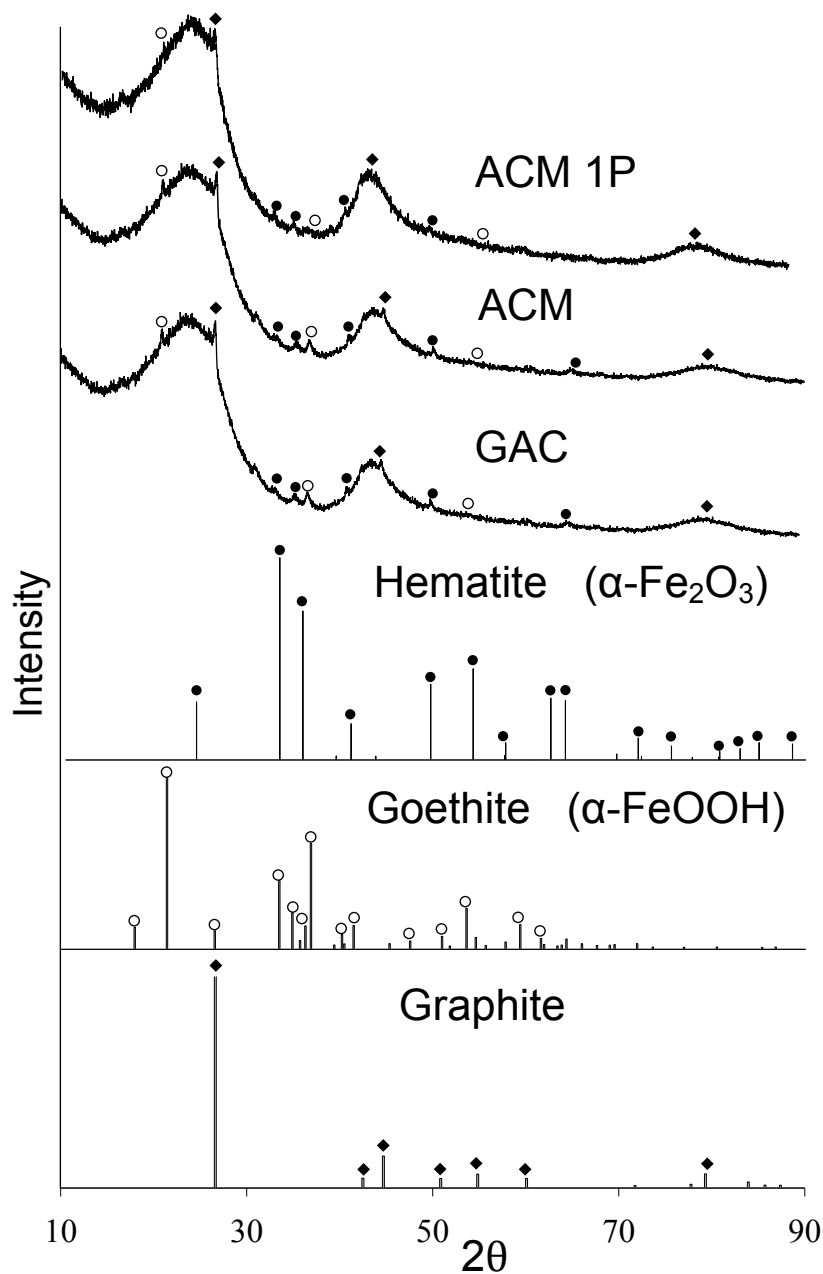
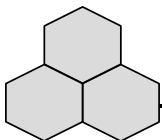


Figure 2.8 XRD patterns of studied materials with a step size of 0.02° 2θ at 10 s per step.



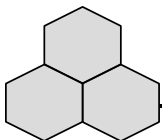
2.3.3 POSSIBLE CONTRIBUTION OF PHOSPHATE AS CAPPING AGENT

There are several pathways in which the phosphates coming from the phosphoric acid could influence the incorporation and grow of iron oxyhydroxides on the surface of activated carbon. The sequence of the possible mechanisms can be explained in the following four steps:

Step 1, Species distribution in solution.

The first step considers, if no phosphoric acid is present, the following species in solution: Fe^{3+} , FeCl^{+2} , $\text{Fe}_2(\text{OH})_2^{+4}$, $\text{Fe}_3(\text{OH})_4^{+5}$, Cl^- , FeCl^{+2} (Table 2.3). The iron predominant specie is FeCl^{+2} that coordinates with water molecules forming aquo-complexes. According Rose et al. [178] the chloride replaces a water molecule in the first coordination shell, leading to the formation of exa-aquo complexes from the shape: $[\text{FeCl} \cdot 5(\text{H}_2\text{O})]^{+2}$. The condensation reactions might proceed by the reactions described in Section 1.6.4. The chloride might be replaced during olation reactions or incorporate to the crystal structure instead of an oxygen atom [106].

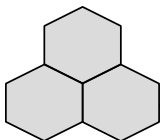
In the presence of phosphate there is a change in the species distribution of Fe depending on the molar ratio PO_4/Fe (see Table 2.3). As the concentration of PO_4^{3-} ions increases new species appear in solution and the concentration of the FeCl^{2-} complex decreases. At the MR PO_4/Fe of 1 there are not more complexes associated to chloride and only a 14% of the iron species are associated with phosphate. The iron hydroxo-complexes become stronger, that might be traduced in an easier dehydroxylation of the iron complex since its association is only with water molecules. Is clear that the addition of PO_4 causes a change in the thermodynamic conditions of the solution, it has been reported that the presence of



free Cl^- decreases the formation kinetics of the IOHs formation [178] and also since phosphate complexes are formed in the second coordination shell rather than in the first one [178], they are easier to displace. The combination of a decrease in the kinetic formation of IOHs due to free Cl^- ions and a decrease in the dehydroxylation energy of the hydroxo and phosphate complexes result in a better control of IOHs particles. Also it has been reported that the simply increase in the ionic strength of the solution results in a smaller particle size and an inhibition of Ostwald ripening [216].

Step 2, adsorption of species from solution in activated carbon.

When solution is contacted with the activated carbon, the anions are adsorbed in its surface through electrostatic interactions and Fe^{3+} cations are adsorbed by proton interchange with the oxygen functionalities. At the acidic conditions of the solution ($\text{pH} \sim 1$) most of oxygen functionalities in AC are protonated and the surface of the material is positively charged, then anions are attracted to the surface. These anions stabilize the positive charge of the surface of activated carbon and then the iron aquo-complexes can be bonded with oxygen functionalities. Without capping agent, 67% of the chloride species are free as Cl^- to stabilize the acidity of the surface (Figure 2.9 A) and some oxygen groups that remain protonated are not allowed to interact with the iron functionalities, additionally the FeCl^{2-} complex has one less active site for adsorption (Figure 2.9 C). In the presence of phosphate 100% of chloride and 70% of phosphate are present as free anions (Cl^- and HPO_4^{2-}) that might stabilize the positive charge of



the AC in a greater degree (Figure 2.9 B), resulting in a higher uptake of iron by oxygen groups (Figure 2.9 D).

Table 2.3 Species distribution of the solution employed during carbon modification.

Component	Specie	% of total concentration
No capping agent		
Fe	Fe ⁺³	0.194
	FeCl ⁺²	99.271
	Fe ₂ (OH) ₂ ⁺⁴	0.015
	Fe ₃ (OH) ₄ ⁺⁵	0.512
Cl	Cl ⁻¹	67.1
	FeCl ⁺²	32.9
At PO ₄ /Fe= 0.1 (0.3M H ₃ PO ₄)		
Fe	Fe ⁺³	0.079
	FeHPO ⁴⁺	1.617
	FeOH ⁺²	0.013
	Fe ₂ (OH) ₂ ⁺⁴	0.034
	Fe ₃ (OH) ₄ ⁺⁵	14.016
	FeCl ⁺²	75.908
	FeH ₂ PO ₄ ⁺²	8.333
Cl	Cl ⁻	74.843
	FeCl ⁺²	25.157
PO ₄ ³⁻	FeHPO ⁴⁺	16.089
	H ₂ PO ⁴⁻	0.395
	H ₃ PO ₄	0.583
	FeH ₂ PO ₄ ⁺²	82.932
At PO ₄ /Fe=0.5 (1.5 M H ₃ PO ₄)		
Fe	FeHPO ⁴⁺	36.578
	Fe ₃ (OH) ₄ ⁺⁵	48.027
	FeCl ⁺²	3.494
	FeH ₂ PO ₄ ⁺²	11.893
Cl	Cl ⁻	98.842
	FeCl ⁺²	1.158
PO ₄ ³⁻	FeHPO ⁴⁺	72.81
	H ₂ PO ⁴⁻	3.226
	H ₃ PO ₄	0.29
	FeH ₂ PO ₄ ⁺²	23.673
At PO ₄ /Fe=1 (3 M H ₃ PO ₄)		
Fe	FeHPO ⁴⁺	14.5
	Fe(OH) ²⁺	2.14
	Fe ₃ (OH) ₄ ⁺⁵	83.351
Cl	Cl ⁻	100
	PO ₄ ³⁻	14.43
PO ₄ ³⁻	HPO ₄ ⁻²	70.654
	H ₂ PO ⁴⁻	14.907

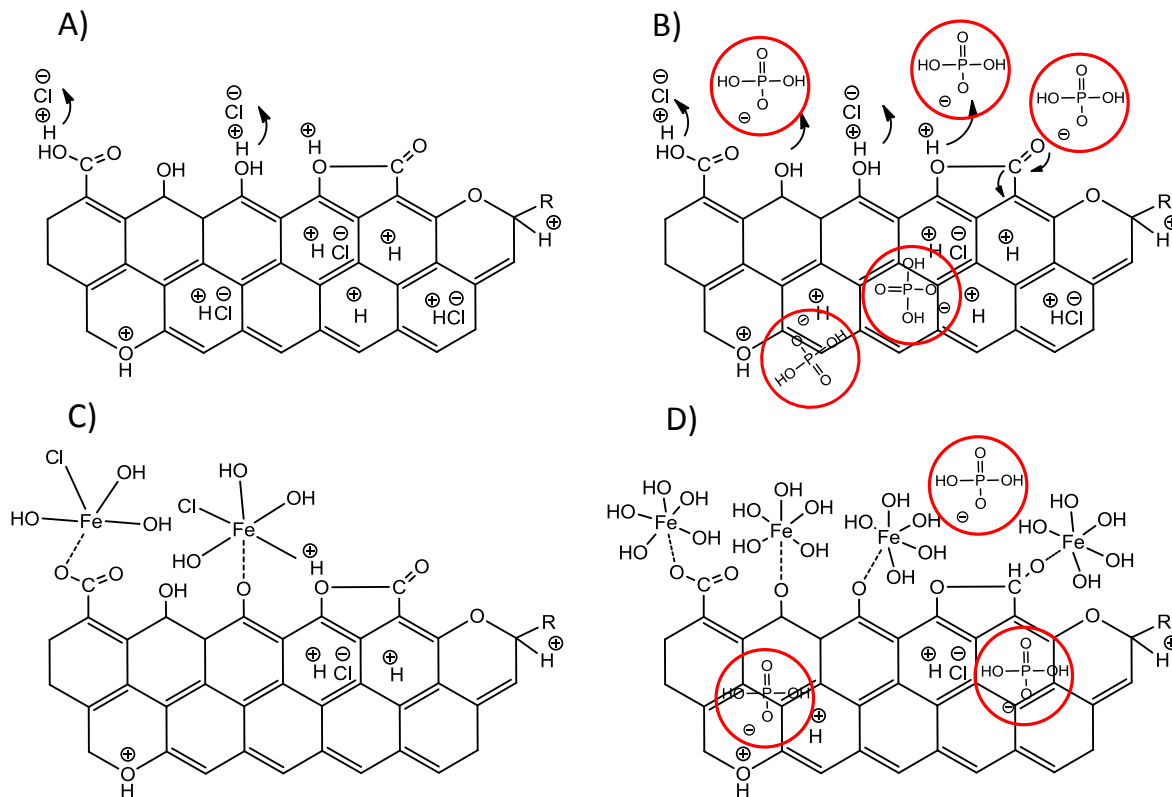
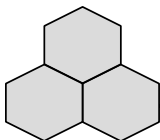
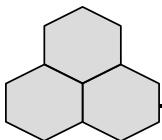


Figure 2.9 Adsorption and stabilization of the surface charge by anions **A)** without capping agent, **B)** in the presence of the capping agent. Adsorption of ferrous ions in the surface of activated carbon **C)** without the capping agent and **D)** in the presence of the phosphate. This effect contributes at a higher adsorption and to a better distribution of iron species on activated carbon.

Step 3, grow of IOHs and phosphate adsorption.

During the *olation* reactions IOHs particles start to grow up and condensate taking the oxygen groups in activated carbon as nucleation center (See [Figure 1.12](#)), in the presence of the capping agent some HPO_4^{2-} and H_2PO_4^- adsorb over the surface of the growing nanoparticles by interchanging a OH ligand coating a nucleation site and stabilizing the surface of the nanoparticles, allowing the particle



to become stable and condensate at smaller sizes (Figure 2.10). Since no iron phosphate particles were detected in the final material this indicates that phosphate species only adsorb over the surface of the IOH and are removed during the materials rinsing with double deionized water.

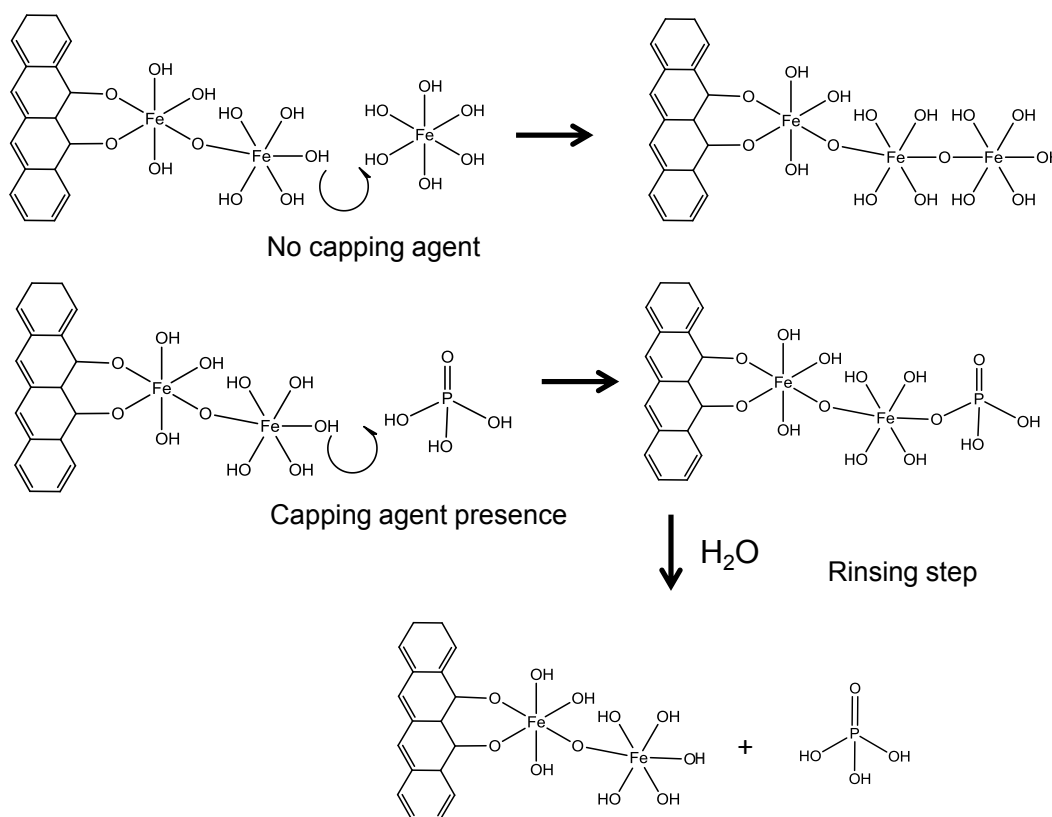
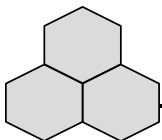


Figure 2.10 Adsorption of phosphate anions on the surface of the growing IOH nanoparticles.

Step 4, aging and phase transformation.

Studies related to the formation of nanoparticles by forced hydrolysis usually report the synthesis of well-defined crystalline forms; however, sometimes amorphous forms might be obtained. It has been reported that phosphate contributes to the aging of iron oxyhydroxides and to their phase transformation [217]. This effect



could not be confirmed in this study since the clarity XRD data was not enough, due to the low iron content in the modified AC, however, phase transformation by phosphate addition cannot be discarded.

2.4 CONCLUSIONS

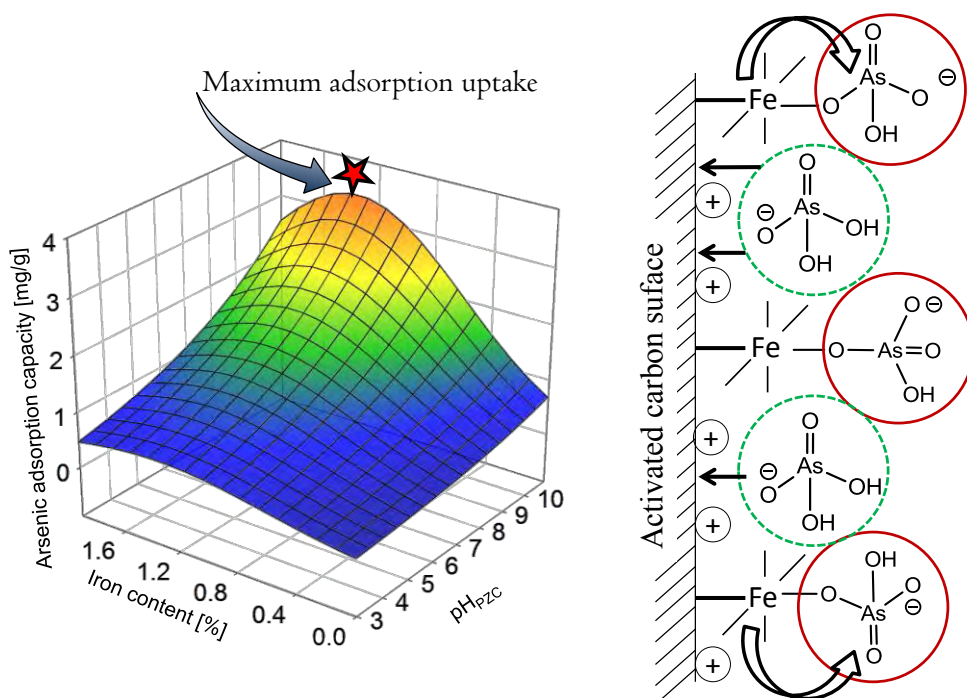
The present results demonstrate that the phosphate addition in forced hydrolysis of ferric chlorine reduces the particle size of anchorage IOHs on AC, which allows obtaining modified GACs with high arsenic(V) adsorption capacity. The best conditions for the synthesis were obtained at a MR of 1.0, 80°C and 60 h. As the MR increased the adsorption capacity increased exhibiting a plateau around at a MR of 1.0. Adsorption isotherms were better adjusted by Freundlich equation and a maximum As(V) adsorption capacity of 5 mg/g was reported at pH 7 and 25°C. Area BET passes through a maximum at a MR of 1 (900 m²/g) where iron content reaches a minimum (1%). The surface adsorption capacity has a lineal relation with the MR PO₄/Fe. Microscopy images corroborate the presence of IOH nanoparticles of about 2 nm in the surface of the ACM1P. The surface charge of the materials become more acidic after the modification and the capping agent presence do not change it. XRD studies suggest that formed particles are either amorphous or too small to diffract.

Nevertheless, these results were obtained in a particular activated carbon; in order to extend the modification technology and potentialize the arsenic(V) uptake by modified activated carbons it is necessary to study the role of the intrinsic properties of activated carbons over its adsorptive performance. This study is described in [Chapter 3](#).

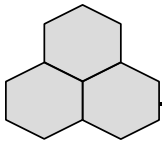
Chapter 3

Influence of Iron Content, Surface Area and Charge Distribution in the Arsenic Removal.

In order to efficiently remove arsenates from aqueous solution a basic surface charge and an iron content of about 1% in activated carbons is necessary, due to a dual stage mechanism: electrostatic interactions and ligands interchange.



This chapter was adapted from: *Influence of iron content, surface area and charge distribution in the arsenic removal by activated carbons*, Submitted to Journal of colloid and interface science.

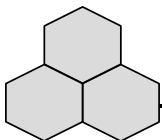


Abstract

In this chapter, the influence of textural and chemical features of several activated carbons (AC) modified with iron oxyhydroxide nanoparticles for the removal of arsenic(V) was studied. The surface area (S^{BET}), micropore volume, surface charge and iron content of 28 ACs were determined. Results showed that the SBET of materials range from 388 to 1747 m²/g, the point of zero charge (pH_{PZC}) from 3 to 11 and the iron content range from negligible to around 2%. A detailed data analysis demonstrated that the most important parameter of AC when removing arsenic(V) from water is the pH_{PZC} (52.5% of contribution); however, the presence of iron is indispensable for enhancing their adsorption capacity by 36.5%. A fitting equation indicated that in order to effectively remove arsenic from water a basic AC with an iron content of about 1% is desirable. Finally it is also suggested that the arsenate uptake by iron-modified AC is conducted by two simultaneous mechanisms: ligand interchange with iron oxyhydroxide particles and electrostatic attraction on basic AC.

3.1 INTRODUCTION

Numerous methodologies have been proposed to load iron on AC including impregnation [36,141,143,150,187,189,203], precipitation [146,184], salt evaporation [146,188], and chemical oxidation [187]. However, the adsorbents to

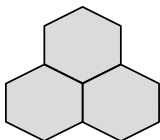


be used in water treatment systems must have chemical stability, which implies stable bonds between iron and the surface of activated carbon.

Recently Lodeiro et al. [187] modified activated carbon produced from sugar beet pulp by two iron incorporation protocols: impregnation and oxidation/impregnation. The authors founded that as iron is loaded there is an increase in the strong acidic moieties (and decrease in the pH_{PZC}) of the activated carbon reporting an extraordinary linearity between acidic functions and iron content determined by XPS. The authors reported that adsorption capacity is only function of iron content in carbons, regardless of the charge of materials and the speciation of arsenic. The iron content of modified-carbons is extraordinary high (5-32 %), leaving in doubt the chemical stability of such materials for water treatment.

A methodology of iron incorporation in activated carbon that has corroborated an stability in aqueous solution is the thermal hydrolysis of iron salts [151,153,218].

Chapter 2 demonstrated that by using H_3PO_4 during FeCl_3 hydrolysis is possible to anchor very small nanoparticles and with that increasing the arsenic adsorption capacity of AC. Recently Rios-Hurtado [219] surveyed the effect of the carbon oxidation on the anchorage of iron oxyhydroxides and its performance for As(V) removal finding that even when the oxidation of carbon promotes iron incorporation, the acidification of the modified activated carbon surface repels arsenate molecules. Those studies corroborate that arsenic adsorption capacity of activated carbons is function of many factors besides iron content and iron particle size.



Therefore, questions as to which of the intrinsic properties any activated carbon must have to be an efficient material for arsenic removal arise.

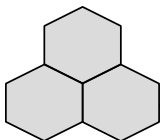
Hence, the objective of this study was to determine the contributions of the intrinsic properties of activated carbon: (surface area, micropore volume, surface charge distribution and iron content) on the removal of arsenic(V) from aqueous solution.

A set of 28 activated carbons from four different precursors that covers a large range of physicochemical features was studied. Some of the carbons were oxidized or basified to change their surface properties, and then these were modified with iron oxyhydroxides.

3.2 EXPERIMENTAL

3.2.1 MATERIALS AND CHEMICALS

The activated carbons studied (AC) were: bituminous Filtrasorb 400 (lot 2) from (GAC in chapter 1, named here CF to avoid ambiguity), NOBRAC AC obtained from the carbonization of coconut shell (CS) and wood based AC 8X30 (CW) both from Norit Company. Additionally, two activated carbons from agave bagasse were obtained; these materials were produced at 450°C under a flow of N₂ of 100 mL/min in a rotatory furnace (from Carbolite) with ZnCl₂ as activation agent [220] with a w/w ratio agave bagasse/ZnCl₂ of 1.2 for 60 min (CABZn1) and with a w/w ratio of 1.6 for 30 min (CABZn2). Before any oxidation/modification, all activated



carbons were reduced to a particle size of 250-500 μm (30 x 60 U.S. Mesh) and washed several times with double deionized water.

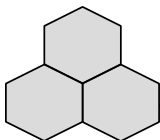
All chemical reagents used in this study ($\text{FeCl}_3 \cdot 6\text{H}_2\text{O}$, H_3PO_4 , Na_2HAsO_4 , HNO_3 , NaOH , HCl , H_2SO_4 , NaNO_3 , ZnCl_2 , NaHCO_3 and Na_2CO_3) were reagent grade and all solutions were prepared in double deionized water ($R > 18 \text{ M}\Omega \cdot \text{cm}$)

3.2.2 ACTIVATED CARBONS OXIDATION AND ALKALINE TREATMENT

The oxidation of the CF and CS activated carbons was conducted according to Rangel-Mendez and Streat (2002) [122], where 2 g of activated carbon were contacted with 80 mL of 8M HNO_3 at 80°C during 0.5, 2.0 and 5.0 h. The reactor was cooled down immediately after the solution was decanted, and materials were rinsed with double deionized water until constant pH. The oxidized materials are named with an extra Xh where X stands for the oxidation time.

Alkaline treatment was carried out over CF prior to iron incorporation. This method was modified from the one used by Liu (2012) [143], where 1 g of activated carbon was mixed with 50 mL of a solution containing 0.1M of a basic reagent. The solution was maintained under constant mechanical stirring for 24 h at room temperature and rinsed until constant pH was reached. The basic reagents used were H_2CO_3 (CFNaCa), NaHCO_3 (CFNaBi) and NaOH (CFNaOH).

After any treatment (oxidation or basic), once the rising solution reached a constant pH, the modified materials were dried at 90°C for 24 h.



3.2.3 IRON MODIFIED ACTIVATED CARBONS

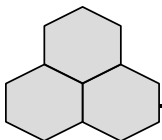
The ACs were modified by means of thermal hydrolysis of FeCl_3 salt as described in [Chapter 2](#), section 2.2.2 at 80°C for 60 in the presence of H_3PO_4 at a molar ratio Fe/PO_4 of 1. The materials were named with an extra MP to indicate that they were modified with iron.

3.2.4 ADSORBENTS CHARACTERIZATION

The surface area, micropore volume and iron content of materials were determined as reported in [Chapter 2](#), section 2.2.3.

Surface charge, point of zero charge, and pK_a distribution

The material surface charge was determined after a potentiometric titration carried out in a Metler Toledo P70 automatic titrator [\[221\]](#). The experimental procedure was as follows: 100 mg of material were contacted with 50 mL of 0.01 M NaNO_3 . Equilibrium was reached by stirring the solution overnight. Next, a certain amount of 0.1M HCl was added until the solution reached a pH of 3. Once the pH was constant, the solution was titrated with 0.1M NaOH. A blank containing only the electrolyte and the same amount of HCl was also titrated. During titration, the solution was continuously purged with N_2 in order to avoid interferences by atmospheric CO_2 . A difference in the volumes needed to reach a certain value of pH in the sample and blank yields the ions released curve also, referred as charge distribution ([equation 2.1](#)) and the point of zero charge pH_{PZC} .



The pKa distribution was obtained from the ions released curve by using the SAEIUS software according to the method proposed by Bandosz et al. [222].

Microscopy images

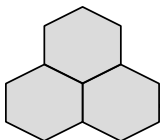
Scanning electron micrographs (SEM) were obtained in a high resolution field emission FEI HELIOS 600 NANOLAB microscope with a secondary electrons detector and operated at an acceleration voltage of 5 KeV. Before analysis, the sample were slightly grounded and deposited in a carbon conductive tape, double coated that was held in a SEM mount holder. Images were acquired without sample metal coating.

3.2.5. ARSENIC(V) ADSORPTION TEST

Adsorption experiments were carried out in 25 mL glass flasks, in which 20 mg of activated carbon were immersed in a solution that contained 4 ppm of As(V). The pH was kept constant at 7 by adding 0.1 N NaOH or HNO₃. The later was conducted as described in Chapter 2 in section 2.2.3. Arsenic(V) adsorption isotherms were obtained for the best materials, the procedure was similar to the one described previously, but the starting concentrations were set in the range of 0.2-1.2 mg/L.

3.2.6. STATISTICAL ANALYSES

Student t-test, multiple regression and dominance analyses were performed by using the SAS 8.0 software (SAS Institute Inc., Cary, NC, USA), the latter using the DA macro available at <https://pantherfile.uwm.edu/azen/www/damacro.html>.



3.3 RESULTS AND DISCUSSION

3.3.1 MATERIALS CHARACTERIZATION

Oxidation of activated carbons as well as an alkaline treatment caused chemical changes in the adsorbent materials. Most of the chemical activity of activated carbons is contributed by the presence of oxygen active sites in the carbon layers [118]; whereas in iron-modified materials it is hypothesized that iron bonds with oxygenated groups modifying the chemical behavior of ACs. Since the pH_{PZC} indicates the net zero charge of ACs, this parameter describes the overall contribution of the groups operating on the activated carbons and their ability for attracting charged ions to their surface. Figure 3.1 provides the pH_{PZC} of the activated carbons studied before and after iron modification. The oxidation of carbon F400 caused a drastic decrease to its point of zero charge (pH_{PZC}) from 10.9 to 3.2 (in CF5.0h), as a result of the insertion of oxygenated groups of an acidic nature on its surface. In coconut carbon, after 0.5 h of oxidation, the pH_{PZC} of the CS was shifted from pH 10.8 to 6 while in CF0.5h this parameter was shifted from pH 10.9 to 4.6. These results are in agreement with those obtained by the SAEIUS software which yielded the pK_a of dissociated surface groups. As can be observed in Figure 3.2, the oxidation of CF and CS increased the number and the contribution of groups having a pK_a value in the range of pH 3-11. These results also showed that new acidic groups were introduced in activated carbons by the action of the oxidant agent. Moreover, the concentration of these groups increased with the oxidation time.

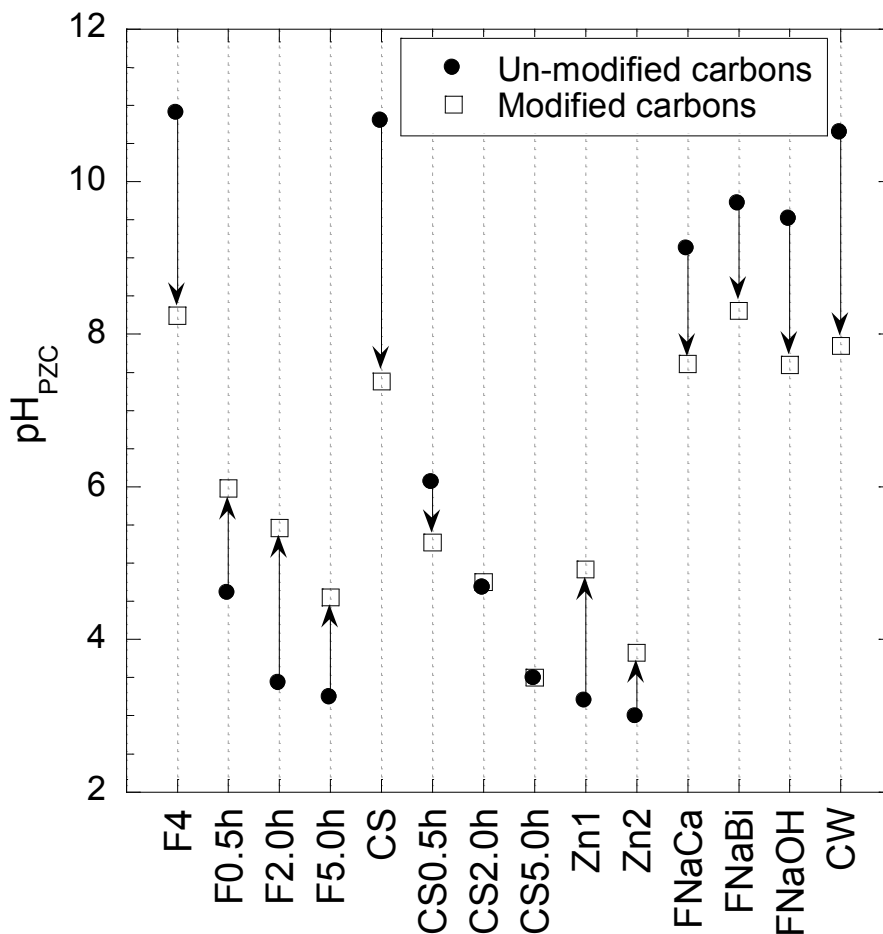
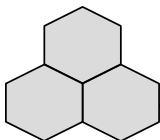
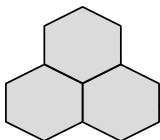


Figure 3.1 Point of zero charge (pH_{PZC}) of un-modified and modified activated carbons.

The alkaline treatments of carbon F-400 caused a slight decrease on its pH_{PZC} , (from 10.9 to around 9); since at the conditions of the treatment it is not expected to modify the surface chemistry of AC, this decrease in the pH_{PZC} might be due to the removal of naturally present impurities like Si or Al (Figure 3.1). On the other hand, the charge distribution of agave bagasse carbons is predominantly acidic, which is attributed to the oxidizing agent ($ZnCl_2$) that has been reported infers a



strongly acidic character in activated carbons [223]. The surface charge of the CW is mainly basic having a pH_{PZC} of 10.6.

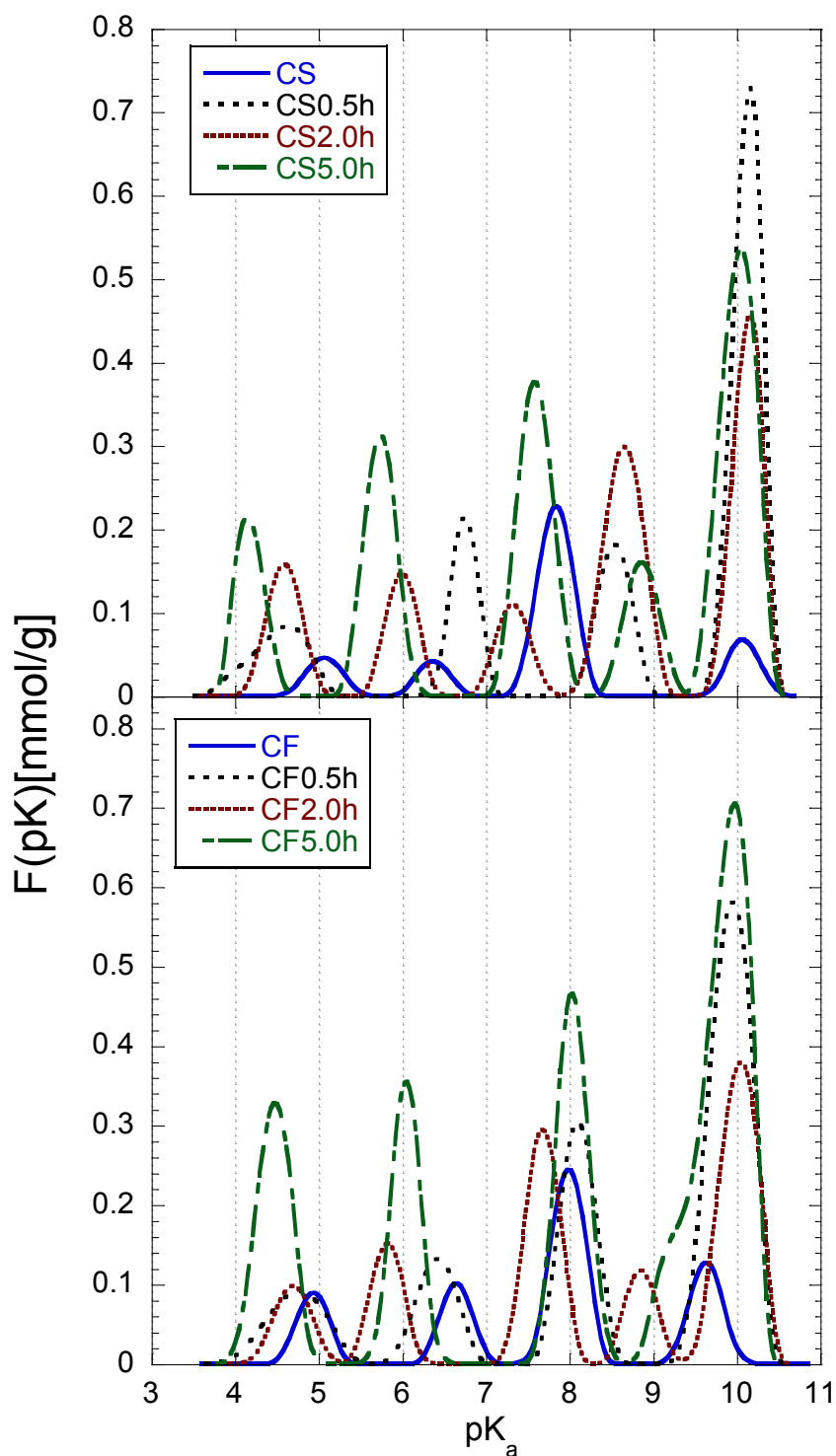


Figure 3.2 pK_a distribution of dissociated groups on the surface of the CS and CF.

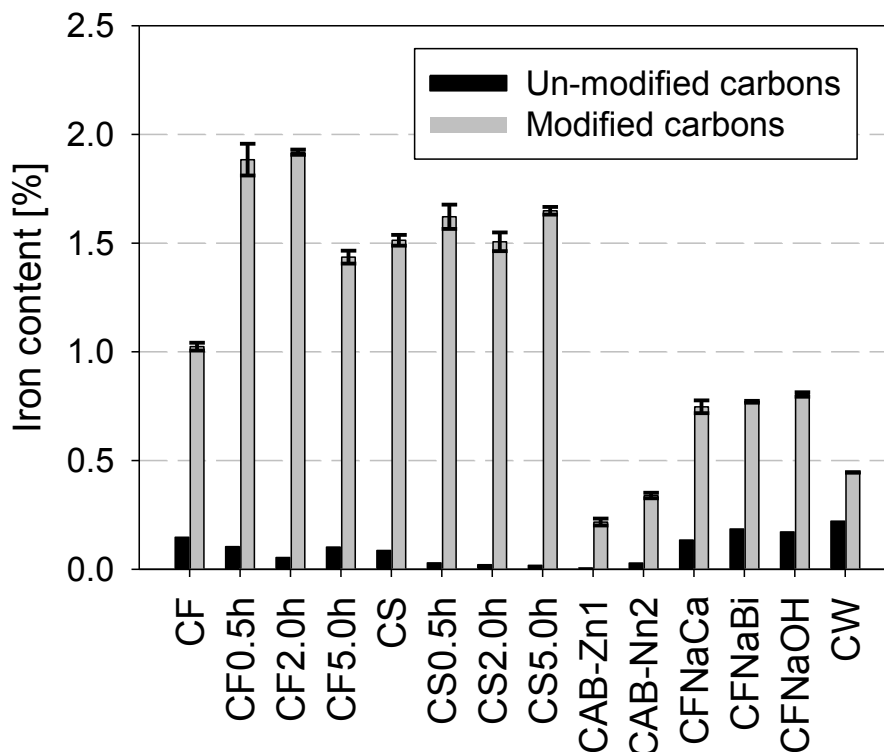
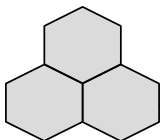
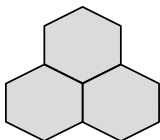


Figure 3.3 Iron content of activated carbons before and after modification.

After iron modification, there is a shift in the pH_{PZC} of the materials as a result of the incorporated iron particles. Acid materials such as agave bagasse carbons and oxidized CS and CF tend to become more positive, while the pH_{PZC} of basic carbons, such as un-oxidized CS, CW, and CF, decreased up to 3 pH unites. The latter is due to the incorporation of iron oxyhydroxide nanoparticles having a neutral or semi-neutral character [224] and to the interaction of iron oxyhydroxide nanoparticles with either acidic or basic containing oxygen groups in activated carbons surface [189,199]. As seen in Figure 3.1, the pH_{PZC} of the whole set of studied activated carbons ranges from 3 to 11, which allows to correlate the ACs surface charge with As(V) uptake. However, even when anions (as arsenate) are

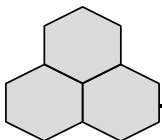


attracted by electrostatic forces to the AC surface, they specifically adsorb on the incorporated iron particles [83].

The iron content of raw materials and modified activated carbons is summarized in Figure 3.3. Depending on its precursor, the iron content of raw AC (as in coconut shell and agave bagasse) ranges from very low to around 0.2% in CW. On the other hand, as oxidation time of CS and CW increases, there is a decrease in the iron content of materials caused by the acidic etching of HNO_3 that dissolves inorganic impurities of ACs. The basic treatment of F400 did not cause a remarkable change on its iron content, since the alkaline reagents do not solubilize the iron naturally present in this AC.

Table 3.1 Textural features of materials studied.

Un-modified AC	S^{BET} [m ² /g]	V^{micro} [cm ³ /g]	Iron-modified AC	S^{BET} [m ² /g]	V^{micro} [cm ³ /g]
CF	929	0.268	CF-MP	863	0.250
CF0.5h	999	0.281	CF0.5h-MP	846	0.2419
CF2.0h	919	0.265	CF2.0h-MP	864	0.244
CF5.0h	930	0.264	CF5.0h-MP	824	0.234
CS	667	0.237	CS-MP	388	0.140
CS0.5h	570	0.208	CS0.5h-MP	479	0.173
CS2.0h	565	0.200	CS2.0h-MP	348	0.125
CS5.0h	604	0.215	CS5.0h-MP	491	0.173
CABZn1	1747	0.400	CABZn1-MP	1515	0.360
CABZn2	1306	0.274	CABZn2-MP	1054	0.236
CFNaCa	1019	0.297	CFNaCa-MP	959	0.281
CFNaBi	1056	0.306	CFNaBi-MP	932	0.275
CFNaOH	1037	0.299	CFNaOH-MP	957	0.287
CW	980	0.268	CW-MP	886	0.241



Moreover, in iron-modified materials, the highest iron content was observed in the CF2.0h-MP (1.9%), and the lowest in the CABZn1-MP (0.21%). The iron percentages are in the range of other reported modified activated carbons by hydrolysis of Fe(III) salts [151-153]. Basic washed and iron-modified carbons presented lower iron content than CF-MP (around 25%), which is hypothesized to be caused by the interaction of oxygen active groups with basic reagents, preventing iron incorporation.

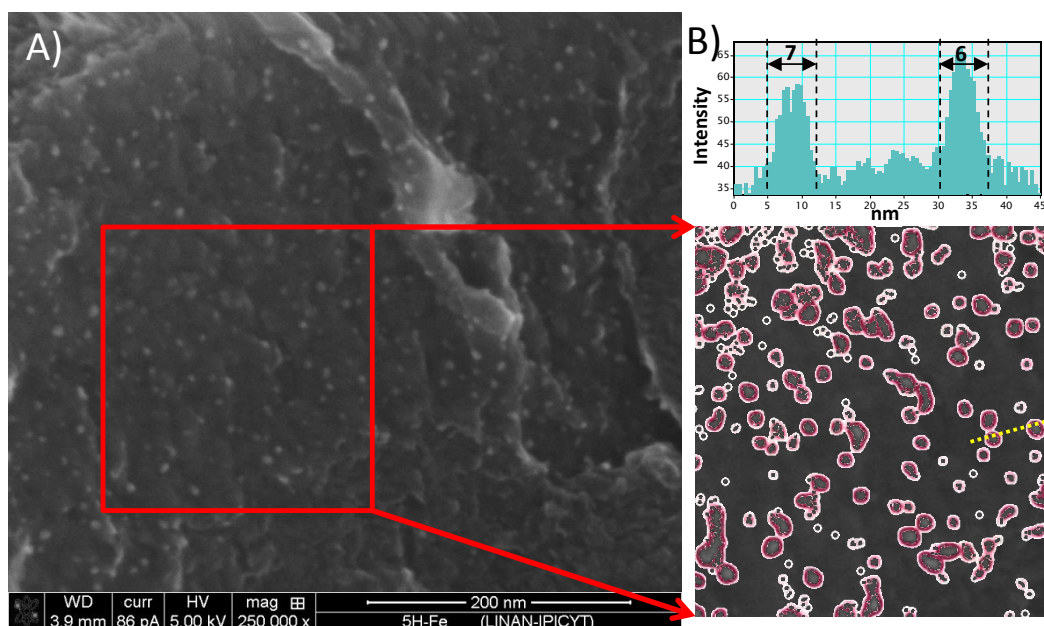
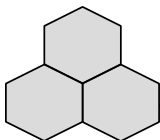


Figure 3.4 A) SEM image of the surface of CS5.0h-MP, B) Colored contour of iron nanoparticles inside the red square. The particles inside yellow line are in the range of 6-7 nm.

As mentioned before, the iron content of the AC is important for As(V) removal, though its incorporation on the AC might block pores, decreasing their surface area



and the number of available sites for As(V) adsorption. For this reason, the determination of the surface area is important.

The results of surface area and micropore volume of the studied adsorbents are summed up in [Table 3.1](#). Raw carbons have a large surface area that ranges from 667 (CS) to 1747 m²/g (Zn2).

On the other hand, from all raw activated carbons the coconut shell carbon has the lowest S^{BET} ; nevertheless, its micropore volume (V^{micro}) is high (0.237 cm³/g, 81% of total), indicating that this material is mainly microporous. The other two ACs (F400 and 8X30) have similar ranges of micropore volume (0.268 cm³/g) and surface area (> 900 m²/g). The oxidation of CF did not cause any major change to its textural properties, and the slight increase in S^{BET} after alkaline treatment can be explained for the pores opening during the removal of inorganic species as previously mentioned.

After iron modification, a decrease in S_{BET} and V^{micro} is noticed in all activated carbons, attributed to pore reduction by the incorporation of iron nanoparticles (See [Figure 3.4](#)). The lessening in textural properties is a result of the amount and size of iron particles incorporated. With the exception of CS and CS2.0h, all materials showed a drop in surface area of less than 20%. The overall surface area of the ACs under study ranges from 388 to 1747 m²/g.

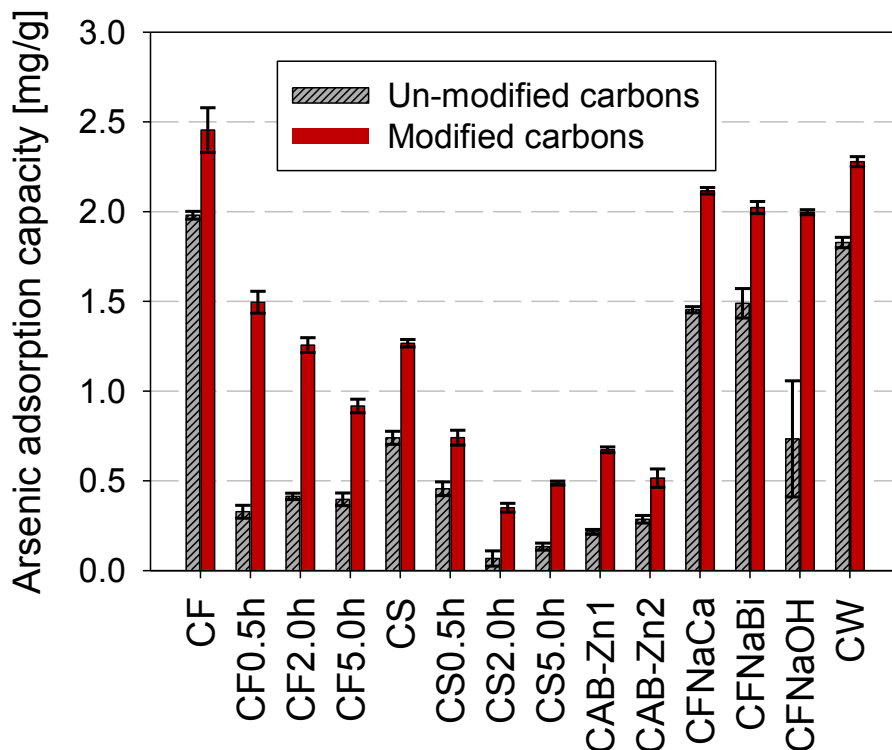
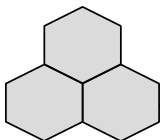
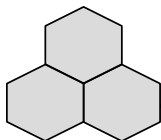


Figure 3.5 Arsenic(V) adsorption capacity of modified and unmodified activated carbons carried out at a starting concentration of 4 ppm As(V), pH 7 and 25°C.

Iron was introduced in the carbon matrix as small nanoparticles of about 6-7 nm as shown in [Figure 3.4](#). Since Iron particle size plays a relevant role during As(V) uptake as established in [Chapter 2](#), and since to all materials were produced under the same conditions, it is hypothesized that all of them present similar iron particle size and this variable might be eliminated from the analysis.

The materials characterization indicates that the 28 ACs have enough physicochemical differences to correlate them with their As(V) adsorption capacity.



3.3.2 ARSENIC ADSORPTION TEST

The arsenic(V) adsorption capacities of the 28 ACs under study are reported in [Figure 3.5](#). Raw activated carbons like CF and CW present high arsenic(V) adsorption capacities (around 2 mg/g) that might be due to their mainly basic surface charge distribution. Moreover, materials with low iron content and acidic surface, like CABZn carbons, present low arsenic capacities (<0.7 mg/g). The oxidation of CF and CS reduced their arsenic adsorption capacity due to the acidification of their surface. The basic treatment of CF also reduced the arsenic uptake, which is attributed to the slight change in surface charge.

Table 3.2 Paired Student's t-test of transformed Q As(V) values.

Factors	Log _e Mean	SD	N	t Value	df	p	95%	CL mean
Un-modified	-0.6973	1.0103	14					
Modified	0.1084	0.6467	14					
Difference	-0.8057	0.4844		-6.2229	13	<0.001	-1.0854	-0.5260

After iron modification, all activated carbons increased their As(V) adsorption capacity. The highest arsenic adsorption capacities were obtained by CF-MP (2.45 mg/g) and CW-MP (2.28 mg/g). Moreover, the maximum enhancement in adsorption capacity (3.5 times) was obtained by CF0.5h. A Student's paired t-test ($\alpha = 0.05$) between unmodified and modified materials demonstrated that iron treatment of carbons indeed increases their arsenic(V) adsorption capacity, corroborating the importance of iron when removing As(V) from aqueous solution ([Table 3.2](#)).

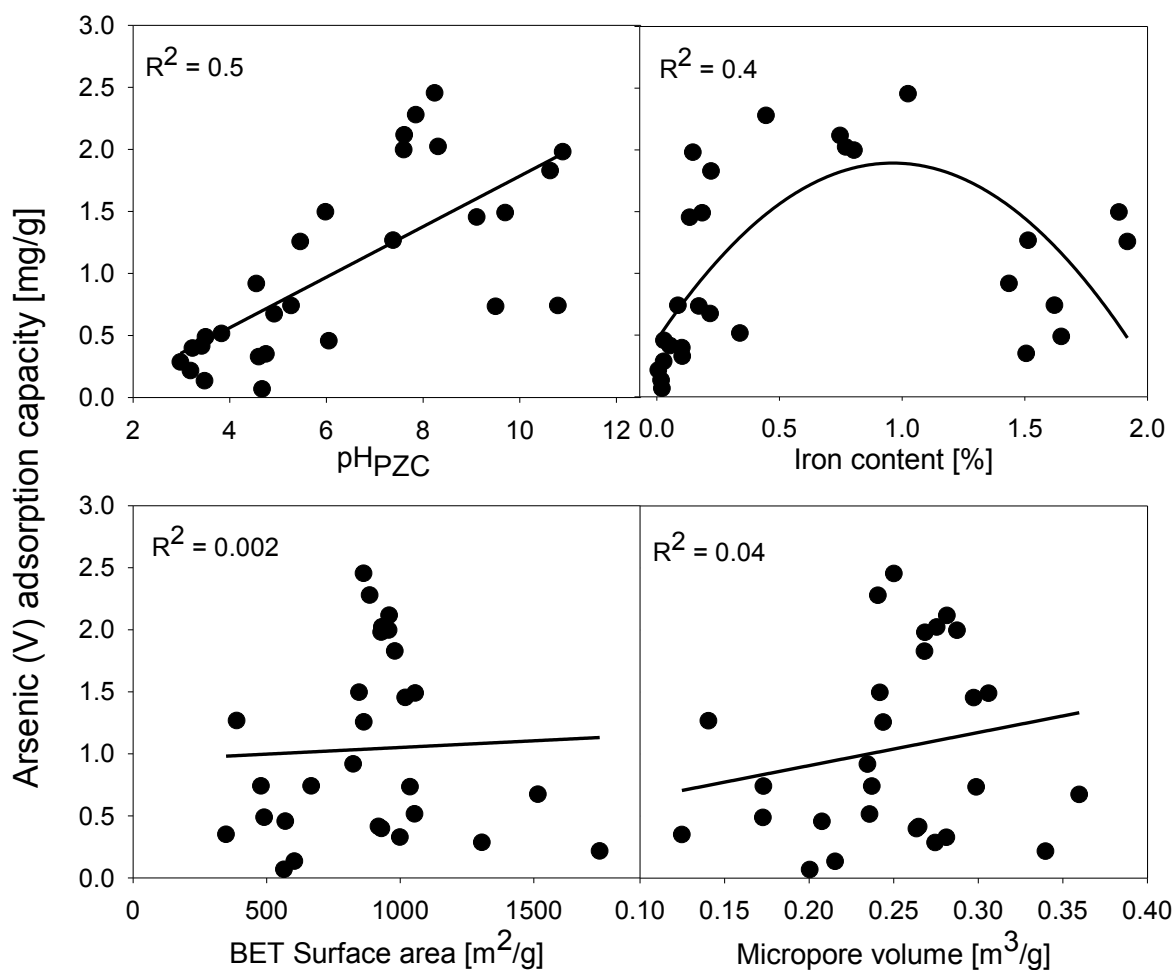
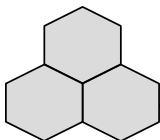
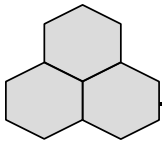


Figure 3.6 Relationships between arsenic adsorption capacity of the adsorbents under study and their pH_{PZC} , surface area, micropore volume and iron content.

Even when the benefit of incorporating iron into the carbon matrixes during arsenic uptake is demonstrated, its sole presence does not explain the arsenic adsorption capacities obtained.

Materials having high iron content but an acidic surface showed lower adsorption capacities than materials with basic properties and less iron content. For example, the CF2.0h-MP has the highest iron content (1.9%) and presents an arsenic

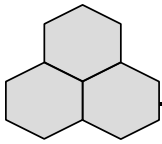


adsorption capacity of 1.26 mg/g, lower than the CF-MP (2.45 mg/g) that has half the iron content. Another important case is CS5.0h-MP, which even with an iron content of 1.65%, its adsorption capacity is just 0.5 mg/g. Therefore, there are other important factors besides iron content that influence the arsenic uptake in ACs.

In order to determine which features of the activated carbons have a higher influence on As(V) uptake, the adsorbent properties (pH_{PZC} , BET surface area, micropore volume and iron content) were plotted against their adsorption capacity (QAs(V)): [Figure 3.6](#) reports these results.

As observed above, no clear trend was found among the variables under study and arsenic adsorption capacity, there was an increasing trend between QAs(V) and pH_{PZC} ($R^2=0.5$); on the other hand the textural features do not correlate linearly. Furthermore, the iron content showed a quadratic relationship with $R^2=0.4$, passing for a maximum of QAs(V) at an iron content of around 1%, which suggested the inclusion of the Fe(%) quadratic term in the Multiple Regression Analysis (MRA). The MRA was used to estimate the relationship among the mentioned factors with QAs(V).

The analysis of residuals ([Appendix B](#)) showed non-normal distribution of errors and/or non-linear relationship between the response variable and factors, therefore, a logarithmic transformation to the response variable was applied for multiple regression analysis. The resultant equation has the form $\ln(y) = b_0 + b_1x_1 + b_2x_2 + \dots + b_nx_n$. To increase the data adjustment, the textural features were included



in the model, although these did not show linear correlation with the response variable. The best equation was selected according to adjusted R^2 and the Akaike Information Criterion (AIC) [225], which offers a trade-off between the variance explained (R^2) and the number of parameters in the model (complexity of model).

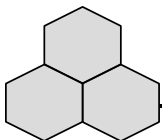
Table 3.3 Results of the multiple regression analysis showing the factor coefficients of the variables and the selection criteria. The selected equation is denoted by *.

Intercept	Variables in model					Selection criteria		
	pH _{PZC}	S ^{BET}	V ^{mic}	Fe %	Fe % ²	R ²	R ² adjusted	AIC
*-4.05	0.214		6.62	2.39	-0.884	0.833	0.804	-45.311
-3.96	0.221	0.0003	5.14	2.38	-0.879	0.834	0.796	-43.468
-3.487	0.245	0.0010		2.32	-0.873	0.824	0.794	-43.898

The results of the MRA are summarized in Table 3.3. The selected model corresponds to the equation 3.1., (model details can be found in Appendix B):

$$\ln Q_{As(V)} = -4.054 + 0.214 * pH_{PZC} + 6.615 * V^{micro} + 2.392 * Fe(\%) - 0.884 * (Fe\%)^2 \quad (3.1)$$

It is worth mentioning that the equation only predicts the arsenic(V) adsorption capacity based on the pH_{PZC}, V^{micro} and Fe(%) of the AC, obtained at the experimental conditions of temperature, pH and starting As(V) concentration. The 3D plot reported by the model is shown in Figure 3.7 A, where QAs(V) is described as a function of pH_{PZC} and iron content (an average micropore volume of 0.24 m³/g was selected to represent the QAs(V) in a 3D plot). The model revealed that the properties of a activated carbon to efficiently remove arsenic(V) are a basic pH_{PZC}



and an iron content of about 1%. This equation explained 83% ($p < 0.01$) of the variability of the adsorption capacity; [Figure 3.7 B](#) shows the fitting of the model versus observed data. The Dominance Analysis (DA) [\[226\]](#) yields the numeric contribution of the variables (pH_{PZC} , iron content, S^{BET} and micropore volume) in the model to the response variable (adsorption capacity). According to the DA ([Appendix B](#)), the most important variable was the pH_{PZC} since its additional contribution to R^2 was greater than that of iron content and micropore volume in all the subset models. The overall pH_{PZC} contribution in total R^2 was 52.5%, while iron content, linear and quadratic, contributes in 36.4% ([Figure 3.7 C](#)). The model predicted a maximum adsorption capacity of 3.4 mg/g for an activated carbon that should have a pH_{PZC} of 11 and an iron content around 1%.

The highest adsorption capacities were obtained with CF-MP and CW-MP, and because of this, their corresponding adsorption isotherms at low arsenic(V) concentration were obtained. The adjusted adsorption isotherms and the Langmuir parameters are provided in [Appendix B](#).

As previously mentioned, it is important to consider that modified materials prepared by the impregnation method contain high iron contents, but there is no guarantee that strong bonds between the ACs surface groups and the incorporated iron particles will form. Hence, hydrodynamic forces might promote the release of iron particles saturated with hazardous arsenic. On the other hand, thermal hydrolysis promotes the formation of covalent bonds between oxygen-containing carbon surface groups and iron nanoparticles, which allows a safe use of the modified ACs in water treatment systems.

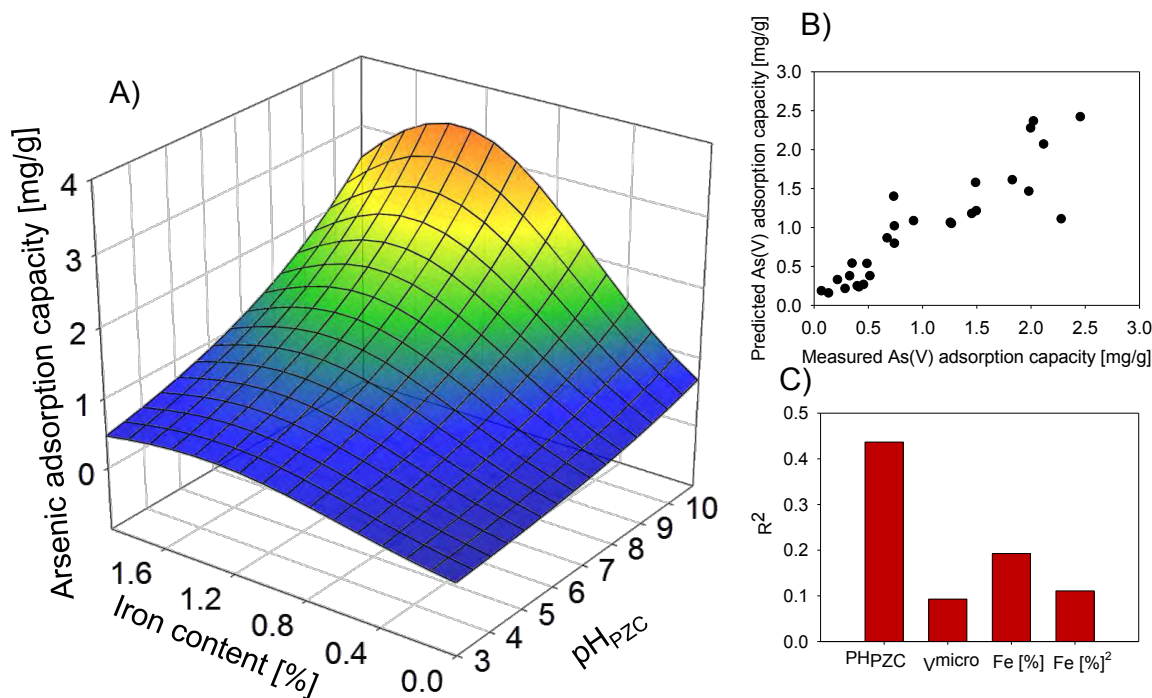
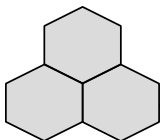
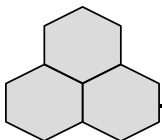


Figure 3.7 A) Developed empiric model that describes the arsenic adsorption capacity as a function of the iron content and pH_{PZC}. B) Predicted versus measured adsorption capacity. C) Importance of activated carbon features over the arsenic adsorption capacity.

3.3.3 EFFECT OF THE ADSORBENT SURFACE CHARGE ON As(V) UPTAKE

Even when the arsenic(V) adsorption mechanism on modified activated carbons is mainly carried out over the incorporated iron oxyhydroxide nanoparticles (by interchange of OH ligands), as has been widely reported [210,227,228], the material's electrostatic charge also plays a key role during As(V) uptake. As mentioned before (Figure 3.8 A), electrostatic repulsion between the surface of acidic materials (pH_{PZC} <7) and As(V) anions (H₂AsO₄⁻ and HAsO₄²⁻ at pH 7)



occurs; if these ionic molecules have difficulties to overcome these electrostatic forces they cannot interact to a higher extent with iron particles and hence adsorption occurs to a lesser extent. On the other hand, basic materials efficiently attract arsenate molecules allowing an interaction with iron oxyhydroxide nanoparticles, and with basic surface groups by electrostatic interactions ([Figure 3.8 B](#)). Since OH ligand interchange is stronger than electrostatic interactions, it is expected that a slight shift in solution pH will change the surface charge of materials removing weakly adsorbed As(V) molecules. To prove this point, desorption experiments were carried out at pH 10 for CF-MP and CW-MP that have a negative surface charge under these conditions ([Figure 3.9](#)).

The desorption percentages are 49.6 and 31.7 % for the CW-MP and CF-MP, respectively. This indicates that a considerable amount of adsorbed molecules is bonded by weak interactions. Moreover, the iron content of CF-MP is higher than that of CW-MP; therefore, more molecules are strongly adsorbed on this material. This corroborates the importance of activated carbon surface charge when adsorbing arsenic(V) from aqueous solution.

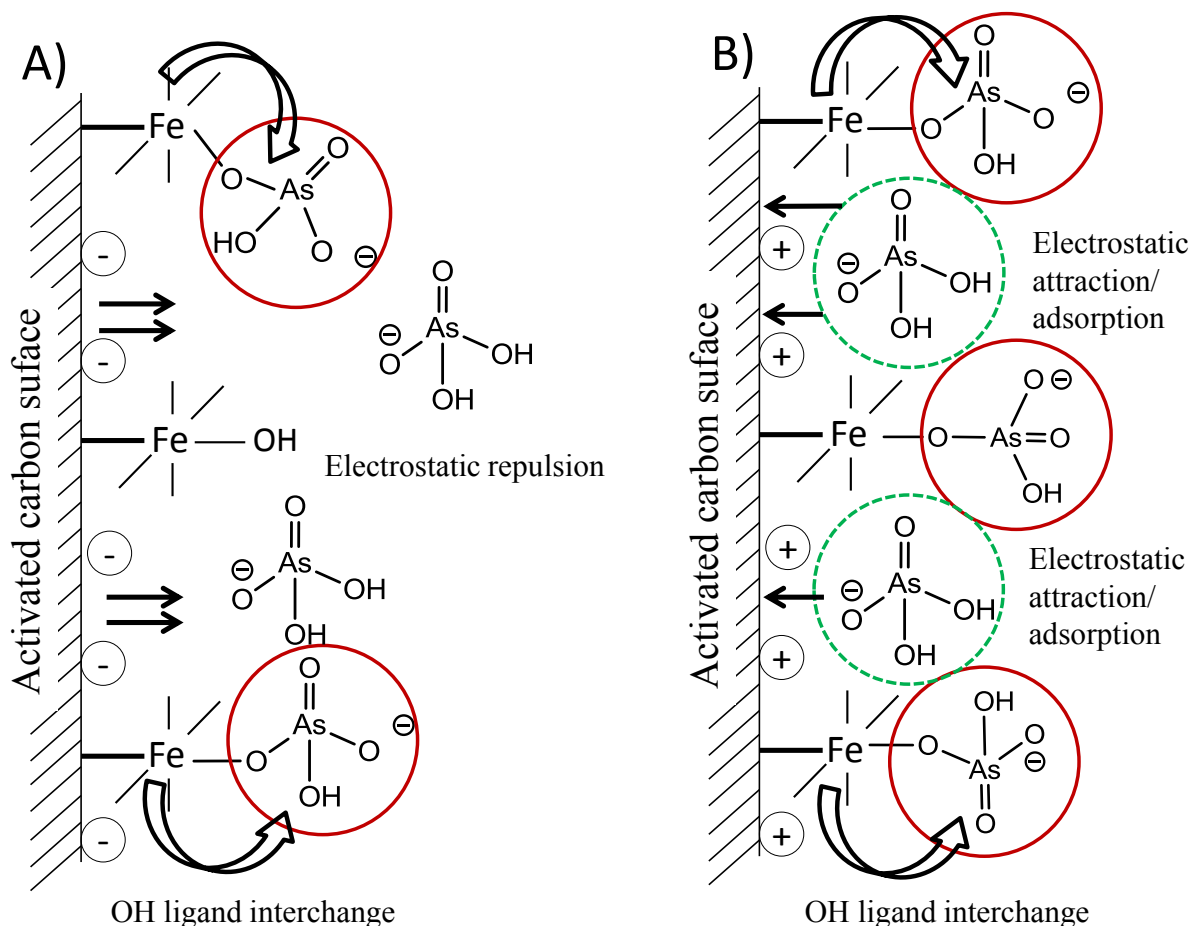
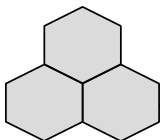


Figure 3.8 Arsenate (As(V)) adsorption mechanism on modified activated carbons with: **A) Acidic properties.** Most of the carbon surface remains negatively charged causing an electrostatic repulsion of anions preventing the adsorption of some arsenates onto iron oxyhydroxide particles. **B) Basic properties.** The positive surface charged attracts arsenates allowing their interaction with iron oxyhydroxide particles and with basic groups by electrostatic interactions.

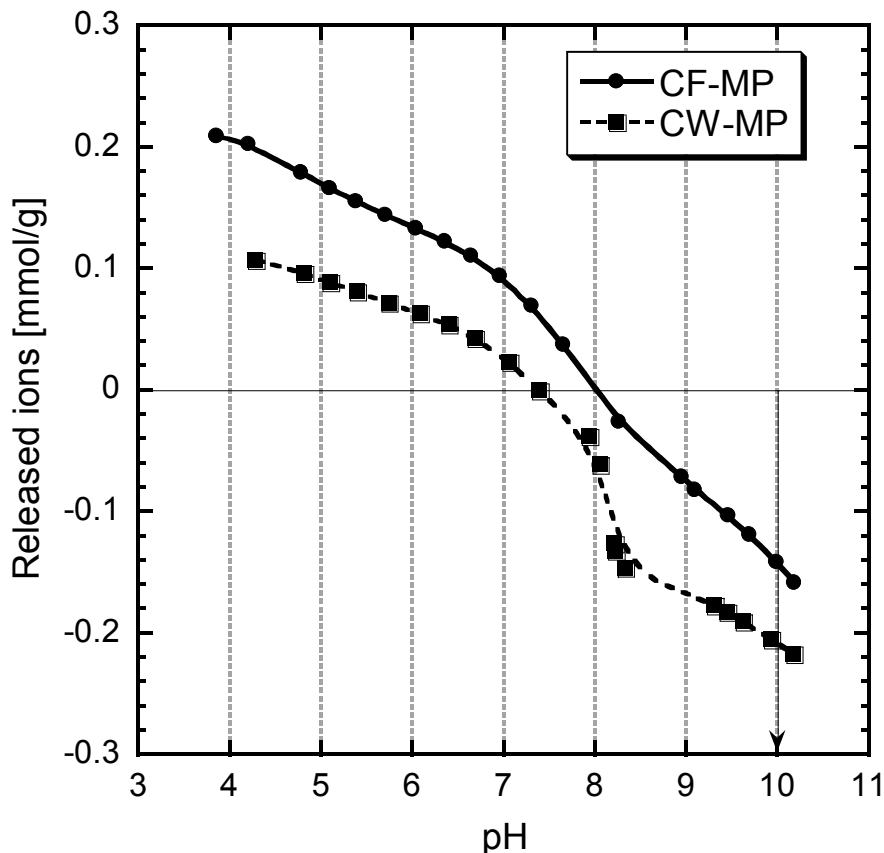
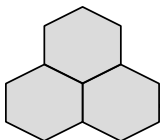
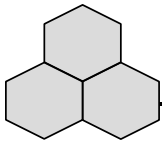


Figure 3.9 Surface charge distribution of CF-MP and CW-MP at 25°C.

3.4. Conclusions

A set of 28 activated carbons having different textural and chemical properties were evaluated for As(V) removal. Characterization results indicate that the pH_{PZC} ranges from 3 to 11, the iron content from negligible to around 2%, and the surface area from 388 to 1747 m^2/g . The best arsenic(V) adsorption capacities were obtained for CF-MP ($\text{pH}_{\text{PZC}} = 8.10$, $\text{Fe}(\%) = 1.0$, $S^{\text{BET}} = 863 \text{ m}^2/\text{g}$) and CW-MP ($\text{pH}_{\text{PZC}} = 7.58$, $\text{Fe}(\%) = 0.44$, $S^{\text{BET}} = 886 \text{ m}^2/\text{g}$). A detailed analysis of experimental data demonstrated that the most important parameter for As(V) uptake is the pH_{PZC} (contributing in a 52.5%) of activated carbons, followed by the iron content that

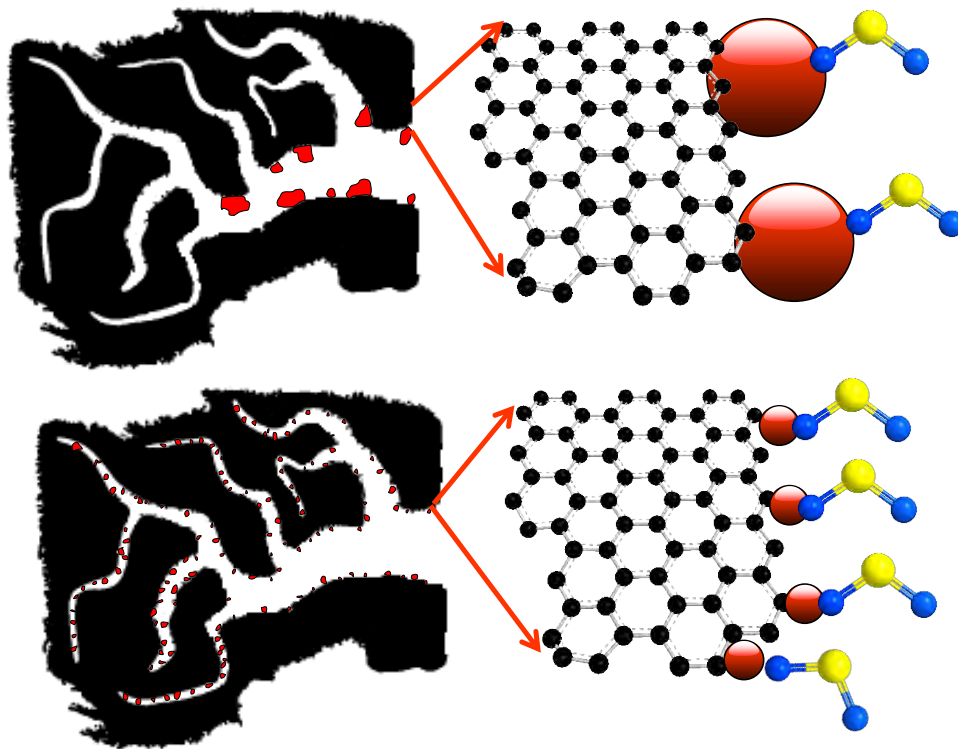


contributes in a 36.4% to the total arsenic adsorption capacity. An fitting equation that describes arsenic adsorption capacity as function of pH_{PZC} and iron content suggests that the best characteristics for arsenic removal of activated carbons (as modified in this study) is a basic surface with a pH_{PZC} of 11 and an iron content of about 1%. Finally, it is proposed that two adsorption mechanisms can be carried out simultaneously in iron-modified activated carbons: a ligand interchange between arsenates and iron oxyhydroxide nanoparticles and electrostatic attraction with basic surface groups.

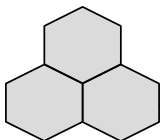
Chapter 4

Role of Iron Particle Size in the Reactive Adsorption of SO_2

Iron oxyhydroxide nanoparticles, synthesized by a capping agent, enhance the SO_2 reactive adsorption of activated carbons.



This chapter was adapted from: *Reactive adsorption of SO_2 on activated carbons with deposited iron nanoparticles*, 2013, *Journal of Hazardous Materials*, 246-247, 300-309.

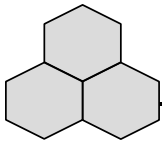


Abstract

The effect of iron particle size anchored on the surface of commercial activated carbon on the removal of SO_2 from a gas phase was studied. Nanosize iron particles were deposited using forced hydrolysis of FeCl_3 with or without H_3PO_4 as a capping agent. Dynamic adsorption experiments were carried out on either dry or pre-humidified materials and the adsorption capacities were calculated. The surface of the initial and exhausted materials was extensively characterized by microscopic, porosity, thermogravimetric and surface chemistry. The results indicate that the SO_2 adsorption capacity increased two and half times after the prehumidification process owing to the formation of H_2SO_4 in the porous system. Iron species enhance the SO_2 adsorption capacity only when very small nanoparticles are deposited on the pore walls as a thin layer. Large iron nanoparticles block the ultramicropores decreasing the accessibility of the active sites and consuming oxygen that rest adsorption centers for SO_2 molecules. Iron nanoparticles of about 3-4 nm provide highly dispersed adsorption sites for SO_2 molecules and thus increase the adsorption capacity of about 80%. $\text{Fe}_2(\text{SO}_4)_3$ was detected on the surface of exhausted samples.

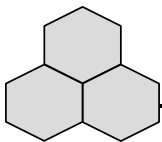
4.1 INTRODUCTION

One of the most widespread technologies used for the removal of sulfur dioxide is adsorption. Several adsorbents have been investigated and modified for the



effective removal of SO_2 from a gas phase, among them activated carbon is often used as a SO_2 removal medium. It has been demonstrated that SO_2 can be oxidized to SO_3 and then in a reaction with water, sulfuric acid is formed [47]. This leads to the acidification of the activated carbons surface which is traduced in several operation issues. Therefore carbons that have a basic surface and small pores [47,61] were found as the most suitable for SO_2 separation from air. Recently Furmaniak et al. [53] studied and corroborated by means of experimental data and Monte Carlo simulations, the importance of carbon functionalities for SO_2 physisorption

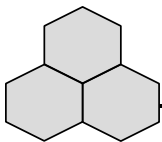
On the other hand, the reactions between SO_2 and iron oxyhydroxides surfaces have been investigated by several research groups [181,182,229-231]. Baltrusaitis and coworkers [181] found that SO_2 can be bound to the surface of hematite ($\alpha\text{-Fe}_2\text{O}_3$) and goethite ($\alpha\text{-FeOOH}$) forming adsorbed sulfite and sulfate. Furthermore, it has been reported that iron oxyhydroxides promote SO_2 transformation by oxidation/photolysis [182]. Faust et al.[230] proposed a mechanism of surface complex formation by a ligand exchange with surface hydroxyl groups. Davini, in his studies of the adsorption capacity of materials consisting carbon and iron derivatives [52], find that the SO_2 adsorption capacity increased from 35 mg/g to 79 mg/g with an increase in the iron content from 0 to 1.28 %. This was attributed to the presence of basic surface sites on carbon and to iron that promotes SO_2 transformation into more stable species. This latest finding highlights the benefits of carbon-iron adsorbents for SO_2 adsorption. However, in the majority of the



cases, when carbon materials containing iron have been studied as SO₂ adsorbents, the particle size of iron oxyhydroxides was not discussed.

The size of metal particles can be considered as a determinant factor for the adsorption of various molecules on activated carbon. When nanoparticles are deposited on the surface, the pores can be still accessible and both physical adsorption and chemisorption can enhance a separation process. [Chapter 2](#) reported that it is possible to anchor iron nanoparticles of about 2-3 nm at the surface of carbon by using phosphate as a capping agent. The decrease in the particle size allowed increasing the uptake of arsenic from aqueous solution up to 40 %, without an increase in the iron content of the materials. These iron-containing materials can be very efficient media for SO₂ adsorption from ambient air since iron nanoparticles can exhibit special catalytic properties due to their quantum confinement [\[168\]](#).

Taking into account the above, the objective of this study was to evaluate the effect of two different nanoparticle sizes of iron oxyhydroxides (denominated as ACM and ACM 1P in [Chapter 2](#)), anchored on activated carbons for the removal of SO₂ from a gas phase. The introduction of very small nanoparticles is expected to enhance the SO₂ adsorption capacity via providing highly dispersed active sites for the adsorption/reactive adsorption process. The interactions between the surface of the materials and SO₂ are analyzed based on the extensive characterization of porosity and surface chemistry.



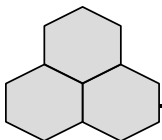
4.2 EXPERIMENTAL

A commercial activated carbon used in this study was Filtrasorb 400 (lot 3) that receives the treatment described in [section 2.2.1](#). The Filtrasorb carbon was treated to anchor two different particle sizes of iron oxyhydroxides on its surface as described in [Chapter 2](#) for the ACM and ACM 1P.

4.2.1 SO₂ DYNAMIC ADSORPTION EXPERIMENTS

The SO₂ adsorption was carried out in a glass column of 370 mm high and internal diameter of 0.9 cm. The packed volume of carbon was 2 cm³. The inlet concentration of SO₂ (Praxair, 5000 ppmv, purity 99.98 %) was kept constant at 1000 ppmv by diluting with air; the flow was 450 mL/min. Since our objective is to study the adsorption at ambient conditions the experiments were performed in moist and dry air. In the moisture conditions, the samples were pre-humidified by 2 h under a flow of 400 mL/min of humid air (Containing 75 % of water). After the pre-humidification, samples were weighted and water uptake was calculated. In dry conditions, materials were dried for 12 h before experimentation and any moisture in the challenge gas was removed with a desiccator before being fed. [Figure 4.1](#) shows the schematic representation of the experimental setup.

The concentration of SO₂ was monitored in a MultiRAE Plus PGM-50/4 gas detector with a detection limit of 20 ppm. Once the maximum concentration was reached at the column outlet, the SO₂ feed was closed and a flow of 360 mL/min of air was passed through the column and the SO₂ desorption was monitored. During all experiments the concentration of H₂S was recorded using the detector



(MultiRAE). Exhausted adsorbents in moist and dry conditions are referred with E-M and E-D, respectively. All experiments were conducted at ambient conditions.

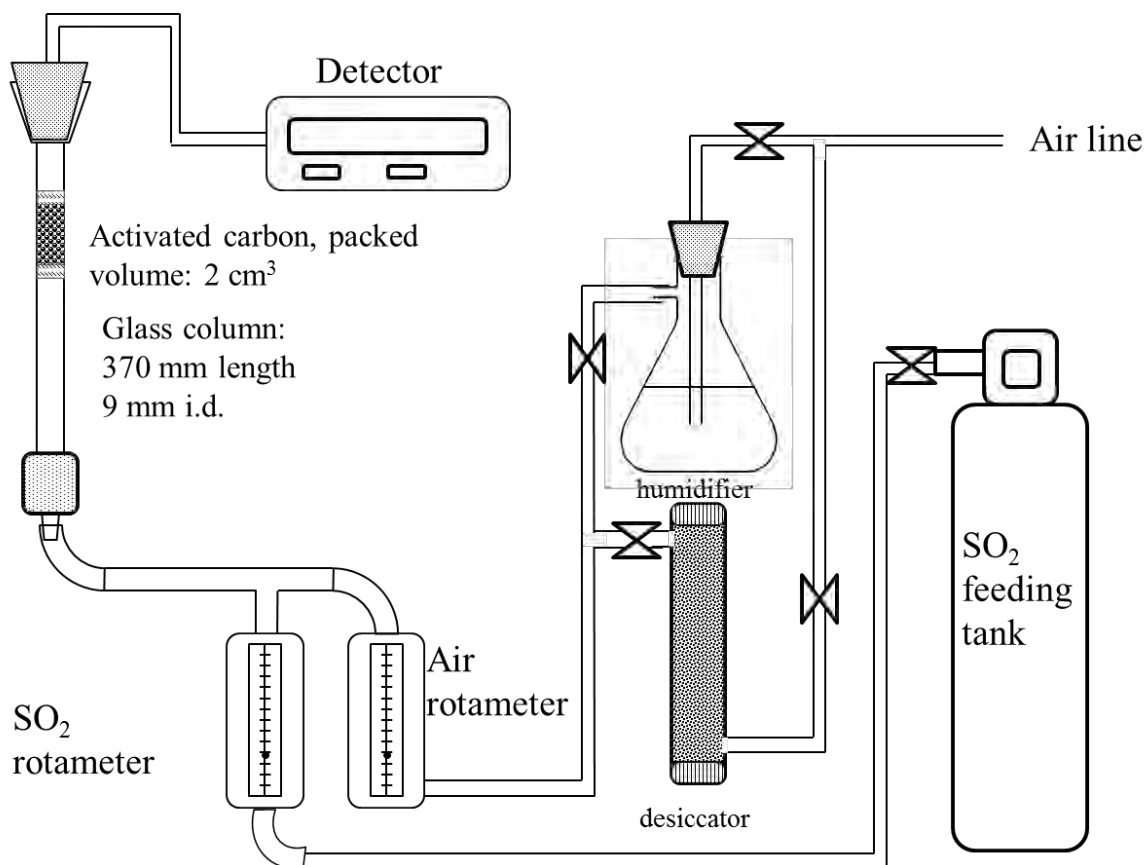
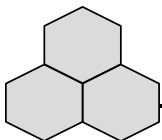


Figure 4.1 Experimental setup to adsorb SO₂.

4.2.2 MATERIAL CHARACTERIZATION

Thermogravimetric analyses

Thermal analyses were carried out in a SDT 2960 from TA instruments. The heating rate was 10 °C/min and the final temperature was 1000°C. The analyses were performed under a constant flow of 100 mL/min of nitrogen.



Potentiometric titration

The pK_a distributions and proton binding curves were obtained after potentiometric titration measurements in a DMS titrino 881 from Metrohm. The titration was carried out in the same way that the reported in the section 3.2.5. After titration, the proton binding isotherm $Q(pH)$ [222] and pK_a distribution [232] were obtained by determining the pK_a values of individual site by solving the next equation:

$$Q(pH) = \int_{-\infty}^{\infty} q(pH, pK) f(pK) dpK \quad (\text{eqn. 4.1})$$

Where $f(pK_a)$ is the distribution of acidic sites in terms of their pK_a values. The distribution was evaluated using the SAIEUS method. Integration of this function leads to the number of groups represented by each pK_a values.

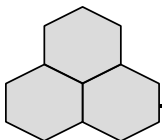
Other characterization techniques

Transmission electron images, porosity and surface area determination and iron content were obtained according the methodology described in [section 2.2.3](#)

4.3 RESULTS AND DISCUSSION

4.3.1 MATERIALS CHARACTERIZATION

After modification, the iron content in ACM increased to 1.39% and in ACM 1P to 1.12%. As can be seen in the TEM images in [Figure 4.2](#), the iron nanoparticles in ACM are in the range of 15-30 nm; however, when the particles are synthesized in the presence of a capping, there is a remarkable decrease in the particle size from



30 to 3 nm on the surface of ACM 1P. Nitrogen adsorption isotherms for the materials studied are collected in [Figure 4.3](#). All of them represent type I, which is characteristic of microporous materials. There is also a very small H4-like hysteresis loop that is related to slit-like pores. The BET surface area of the unmodified carbon is 1051 m²/g and after iron modification a decrease of 7 % in the surface area is found for ACM ([Table 4.1](#)). The DFT approach show a decrease of 6 % in the total pore volume for ACM as a result of the iron nanoparticles deposition, mainly in pores bigger than 0.7 nm, and, as a consequence, ultramicropores of 0.5 nm are formed ([Figure 4.4](#)).

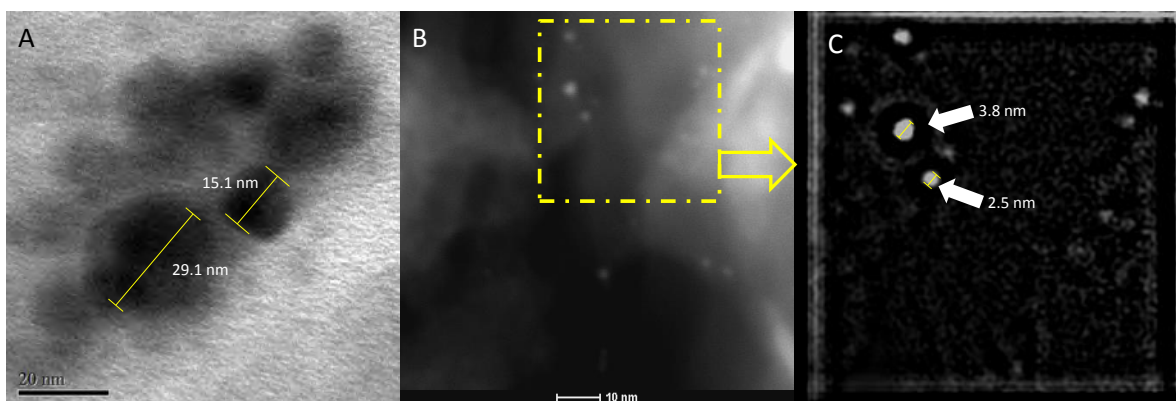
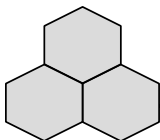


Figure 4.2 A) TEM image of AC-M, B) STEM image of AC-MP and C) Fourier Transform image of the dotted area in Figure B; the arrows indicate iron nanoparticles of about 2.5-4 nm.

Potentiometric titration results (strength and the number of acidic groups) collected in [Table 4.2](#), demonstrate that after modification the surface of carbons become acidic as a result of iron nanoparticles addition of acidic nature [205]. The surface of Filtrasorb is strongly affected by the iron presence. The pK_a distributions for the ACM (and ACM 1P) reveal the peaks at pK_a 6 and 10 linked to mono and poly-



nuclear species of Fe(III) [233]. In the ACM 1P the apparition of a peak at pK_a 7 is associated to the second dissociation constant of $H_2PO_4^-$. The latter species was used as a capping agent during the iron deposition.

Table 4.1 Surface areas and pore volumes of the initial and exhausted samples.

Material	S_{BET} [m ² /g]	V_t [cm ³ /g]	V_{mic}^{DFT} [cm ³ /g]	$V_{<0.7nm}^{DFT}$ [cm ³ /g]	V_{meso}^{DFT} [cm ³ /g]
AC	1051	0.527	0.329	0.145	0.052
ACM	980	0.510	0.308	0.146	0.052
ACM 1P	879	0.424	0.280	0.132	0.030
Samples after adsorption in moist conditions					
AC E-M	698	0.356	0.22	0.085	0.03
ACM E-M	748	0.390	0.234	0.094	0.039
ACM 1P E-M	773	0.401	0.241	0.099	0.042
Samples after adsorption in dry conditions					
AC E-D	987	0.499	0.310	0.135	0.049
ACM E-D	941	0.478	0.301	0.137	0.045
ACM 1P E-D	857	0.432	0.267	0.127	0.038

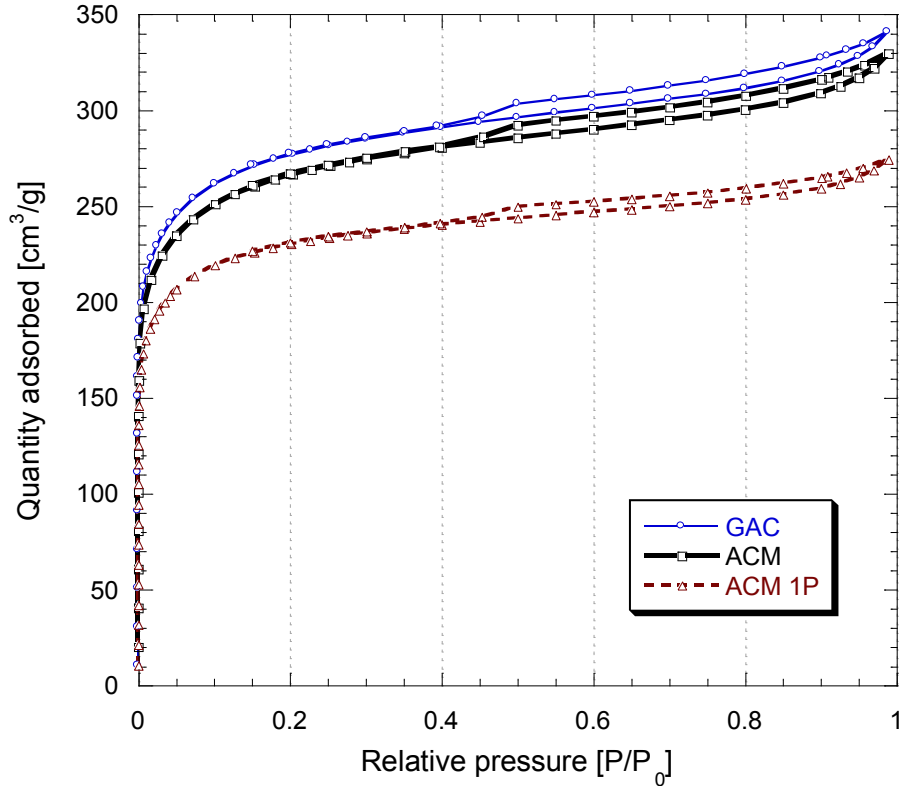
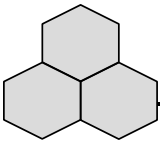
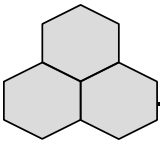


Figure 4.3. Nitrogen adsorption isotherms of studied materials.

4.3.2 DYNAMIC ADSORPTION EXPERIMENTS

Figures 4.5 shows the breakthrough curves of SO_2 in moist and dry conditions, respectively. A comparison between both figures indicates that the breakthrough point occurs after longer time when water is preadsorbed on the carbon. In moist conditions, SO_2 is detected immediately after disconnection of the challenge gas whereas in dry conditions there is a big gap in the measured concentration between the adsorption and desorption branches. That gap represents the time when SO_2 was released and our sensor was not able to measure its concentration since it was higher than its upper concentration limit. Based on this behavior we can conclude that adsorption forces are much stronger in moist than in dry



conditions since in the former the concentration of SO₂ was much lower when the bed was purged with air.

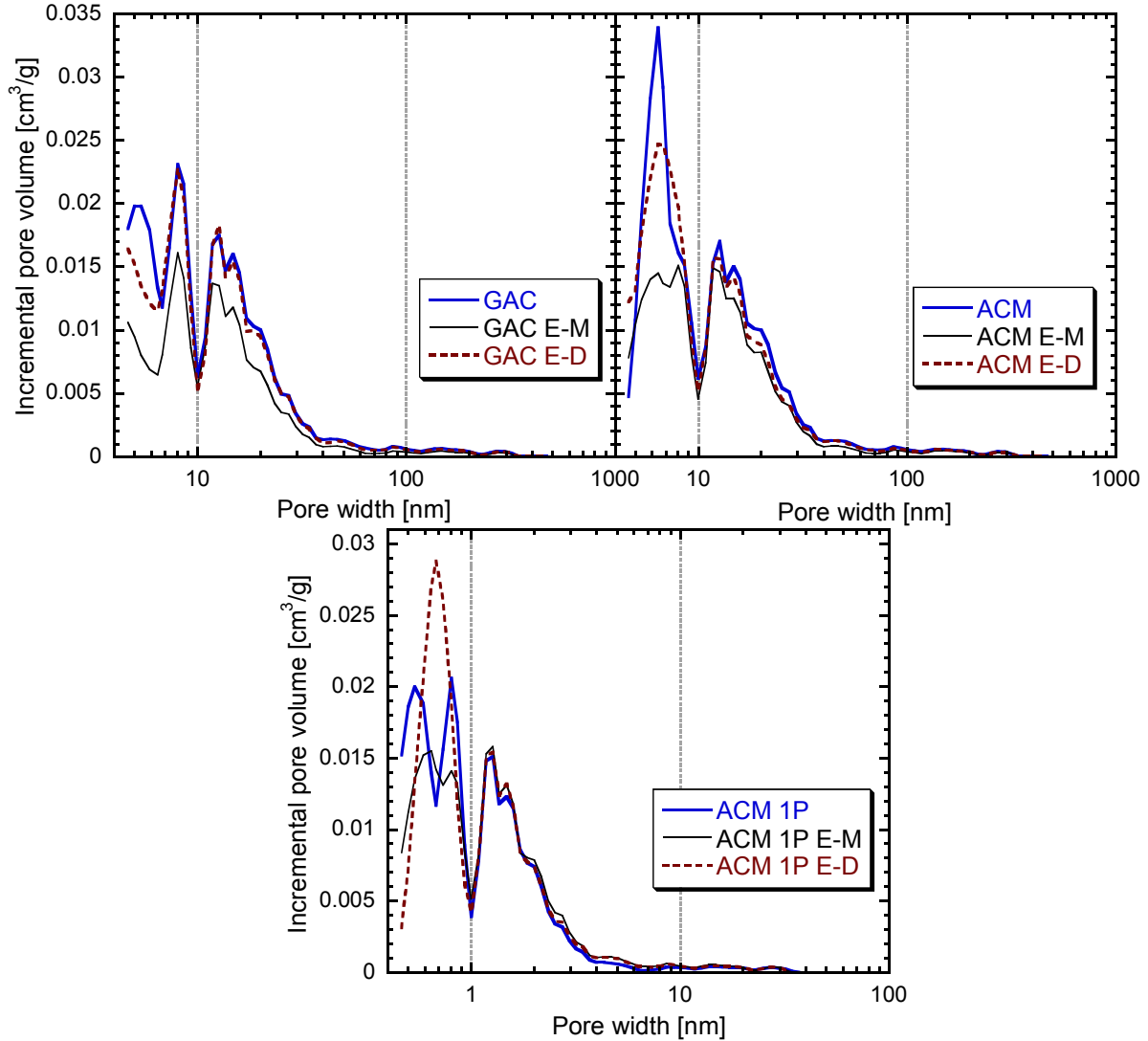


Figure 4.4 Pore size distributions for the initial samples and those exposed to SO₂ in moist and dry conditions.

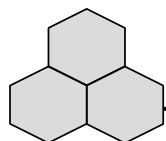


Table 4.2 pK_a positions, number of groups (in parentheses (mmol/g)), and surface pH values for the initial and exhausted samples.

Sample	pH	pK _a 3-4	pK _a 4-5	pK _a 5-6	pK _a 6-7	pK _a 7-8	pK _a 8-9	pK _a 9-10	pK _a 10-11	All
AC	8.6		4.64 (0.076)		6.45 (0.060)	7.52 (0.041)	8.68 (0.039)	9.98 (0.137)	10.89 (0.015)	0.368
ACM	5.78		4.68 (0.064)		6.29 (0.120)	7.84 (0.061)	8.46 (0.042)	9.27 (0.064)	10.16 (0.194)	0.546
ACM 1P	6.22	3.8 (0.019)	4.7 (0.040)		6.14 (0.076)	6.95 (0.013)	8.23 (0.06)	9.70 (0.14)		0.351
AC E-M	2.62		4.72 (0.111)		6.53 (0.124)		8.20 (0.111)	9.61 (0.140)	10.46 (0.112)	0.598
ACM E-M	2.98		4.49 (0.105)		6.14 6.65 (0.077) (0.035)		8.03 8.86 (0.093) (0.045)	9.91 (0.190)		0.545
ACM 1P E-M	2.94		4.57 (0.68)	5.29 (0.002)	6.35 (0.105)		8.02 (0.107)	9.29 (0.104)	10.23 (0.2546)	0.633e
AC E-D	7.01		4.59 (0.058)		6.54 (0.110)	7.61 (0.020)	8.68 (0.076)	9.95 (0.173)		0.437
ACM E-D	4.27	3.22 (0.043)	4.27 (0.039)		6.08 (0.046)		8.42 (0.038)		10.08 (0.211)	0.379
ACM 1P E-D	4.61				6.11 (0.036)	7 (0.004)	8.43 (0.026)	9.84 (0.116)		0.182

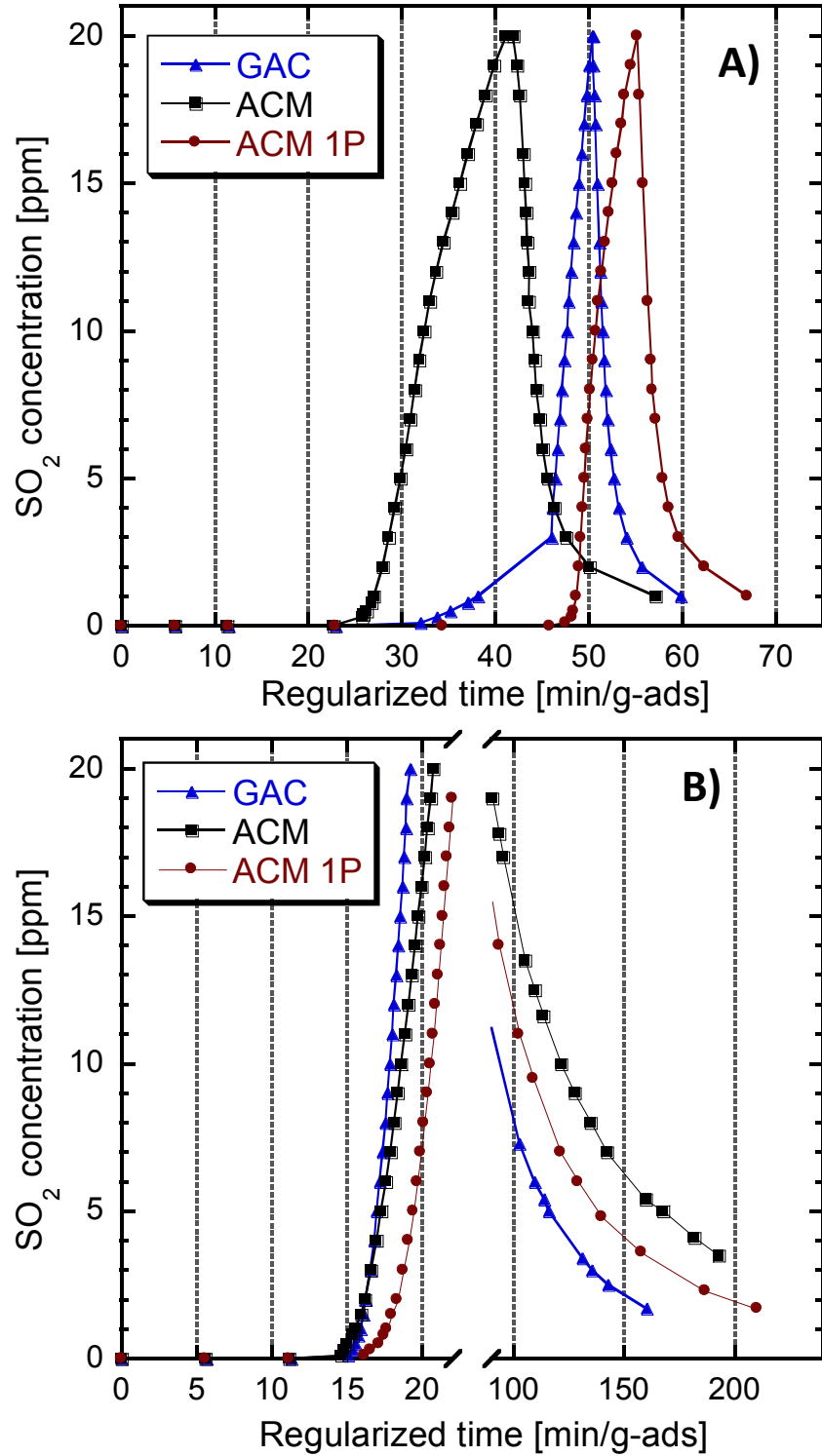
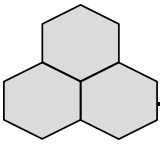
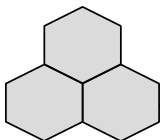


Figure 4.5 SO₂ breakthrough curves for the studied materials measured in moist (A) and dry (B) conditions.



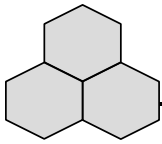
The calculated adsorption capacities for the materials studied are collected in [Table 4.3](#). The adsorption capacity of ACM at the breakthrough point is around 24 % lower than that of the unmodified carbon. Thus the iron deposition on the surface of ACM is not beneficial for SO₂ adsorption. On the other hand, for ACM 1P there is a 78 % and 10 % increase in the SO₂ adsorption capacity compared to Filtrasorb at the breakthrough point and at 20 ppm, respectively. Since both modified samples have similar iron contents (~1%), the increase in the adsorption capacity of ACM 1P might be caused by differences in the deposition of iron species on the surface and in the accessibility of active sites.

Table 4.3 SO₂ adsorption capacities of the materials studied and water uptake during the prehumidification.

Material	Q _{SO2} BP	Q _{SO2} 20	Q _{H2O}	Q _{SO2} BP	Q _{SO2} 20
	[mg-SO ₂ /g]	ppm [mg-SO ₂ /g]	[mg-H ₂ O/g]	[mg-SO ₂ /m ²]	ppm [mg-SO ₂ /m ²]
GAC E-M	32	60	119.7	0.030	0.057
ACM E-M	26	49	170.3	0.027	0.050
ACM 1P E-M	60	66	223.0	0.068	0.075
GAC E-D	18	23	-	0.017	0.023
ACM E-D	18	25	-	0.018	0.027
ACM 1P E-D	19	27	-	0.022	0.032

Q= Adsorption capacity

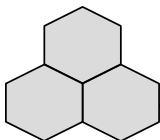
BP= Breakthrough point



When the adsorption capacity per unit of surface area is analyzed ([Table 4.3](#)), the performance of ACM 1P is more than 2 and 2.5 times better than those measured on GAC and ACM, accordingly. These results suggest that iron nanoparticles of 3-4 nm enhance SO₂ retention. Some sulfur dioxide was converted to H₂S and its detected concentration during the breakthrough tests was 2 ppm. This indicates some reducing capability of the carbons studied.

After adsorption of SO₂ in moist conditions a 50 % decrease in the volume of micropores, was found for Filtrasorb due to the decrease in the volume of ultramicropores less than 0.7 nm ([Table 4.1](#), [Figure 4.4](#)). The specific surface area decreased about 40 %. After adsorption in dry conditions a change in surface area is very small, which can be linked to the small amount of the adsorbed molecules.

In the case of ACM after SO₂ adsorption in moist conditions, the volume of ultramicropores less than 0.7 nm decreased from 0.146 to 0.094 cm³/g (50 %). Pore size distributions ([Figure 4.4](#)) suggest that iron particles, anchored in ultramicropores, react with SO₂ blocking the pores and thus 40 % decrease in the surface area is found. For ACM 1P a decrease in the surface area after SO₂ adsorption is less pronounced than those for GAC and ACM. The volumes of ultramicropores and micropores decrease only 33 % and 16 %. Since the SO₂ adsorption capacity in this material is the highest, the results indicate that adsorbed molecules are better dispersed on the surface of ACM 1P than those on the other two carbons studied. Thus the small size of nanoparticles of about 3-4 nm can be responsible for more efficient occupation of the adsorption sites. After adsorption in dry conditions all materials exhibit a very small decrease in the surface area owing



to the small amount adsorbed. This suggests difference in the mechanisms of SO_2 retention.

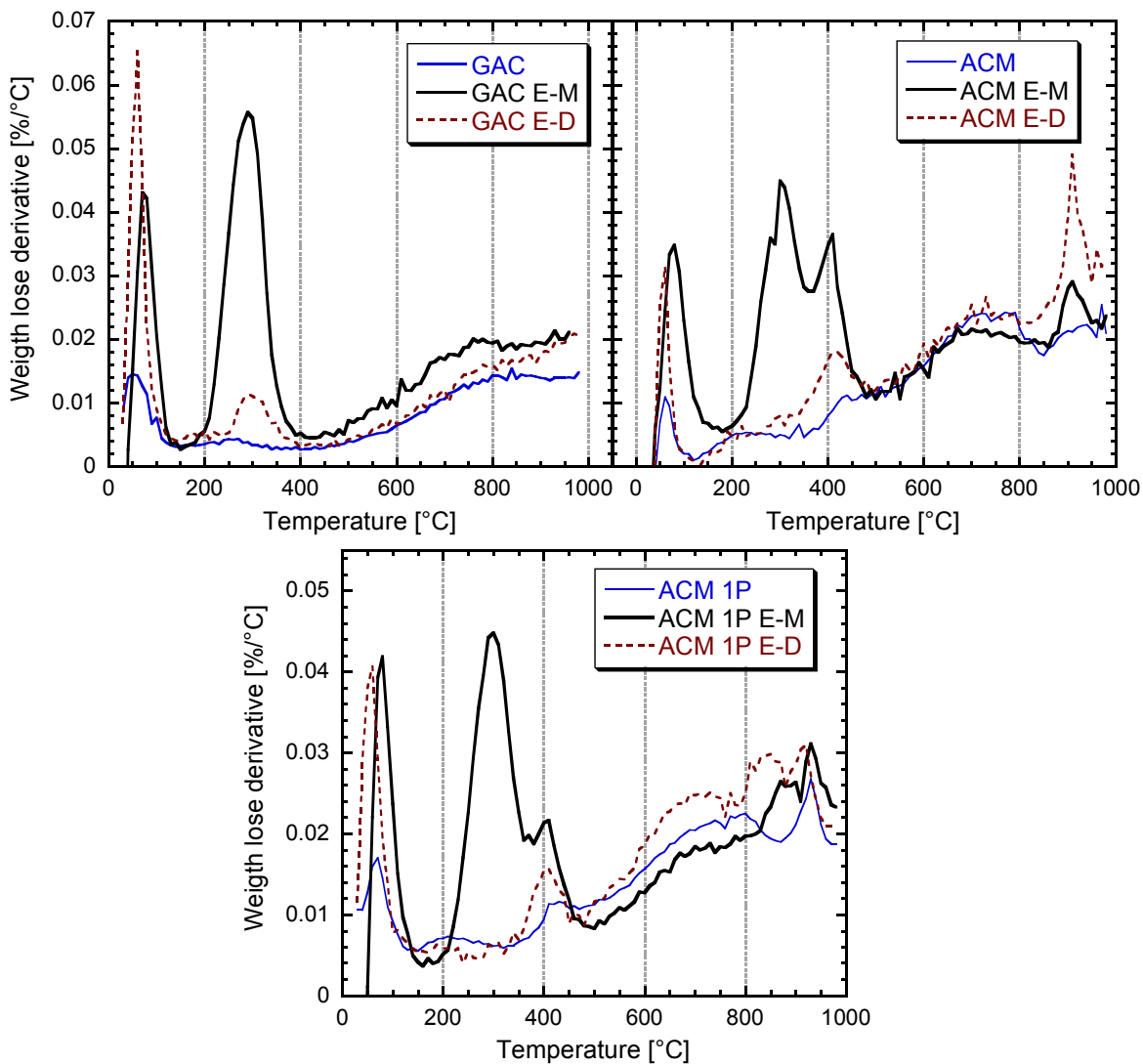
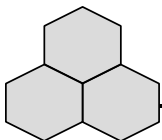


Figure 4.6 The DTG curves for the initial samples and those exposed to SO_2 in moist and dry conditions.

The DTG curves for the materials studied are collected in [Figure 4.6](#). Even though heating alters the materials, when the experiments are done on the initial and exhausted samples, and the weight lost patterns are compared the valuable



information about the changes in the materials chemistry as a result of reactive adsorption can be obtained. The curve for ACM revealed three peaks at 420, 600 and 900 °C. They are linked to the iron dehydroxylation ($\text{FeO}(\text{OH}) \rightarrow \text{Fe}_2\text{O}_3$), iron reduction ($\text{Fe}_2\text{O}_3 \rightarrow \text{FeO}$) and to the complete reduction of Fe^{II} to Fe^0 [234], respectively. After SO_2 adsorption, the DTG curve for the unmodified carbon in moist conditions show two peaks. The first one, at a temperature lower than 100 °C (Figure 4.7 A) represents water and weakly physisorbed SO_2 on the surface [48]. The second one, between 200 and 400 °C, is attributed to H_2SO_4 desorption [235], indicating that SO_2 is oxidized on the surface of this carbon [61]. The iron containing samples also show the peaks corresponding to desorption of physisorbed SO_2 and H_2SO_4 . An increase in the intensity of the peaks at 420 °C is noticed and linked to the removal of iron sulfate (melting point 480 °C) which is the product of surface reactions [181].

All exhausted samples exposed to SO_2 in dry conditions exhibit a major peak on the DTG curves at < 100 °C. It is linked to a large amount of SO_2 weakly adsorbed on the surface of carbons. The intensity of the peak representing H_2SO_4 (200-400 °C) for the unmodified carbon is very low owing to the absence of water in the gas stream. Nevertheless, its appearance can be linked to the presence of physically adsorbed water from the ambient air. Moreover, the iron-containing samples do not reveal the peak at 290 °C related to sulfuric acid. This indicates that in the absence of water SO_2 molecules are either weakly adsorbed or retained on the surface as a part of iron-containing species.

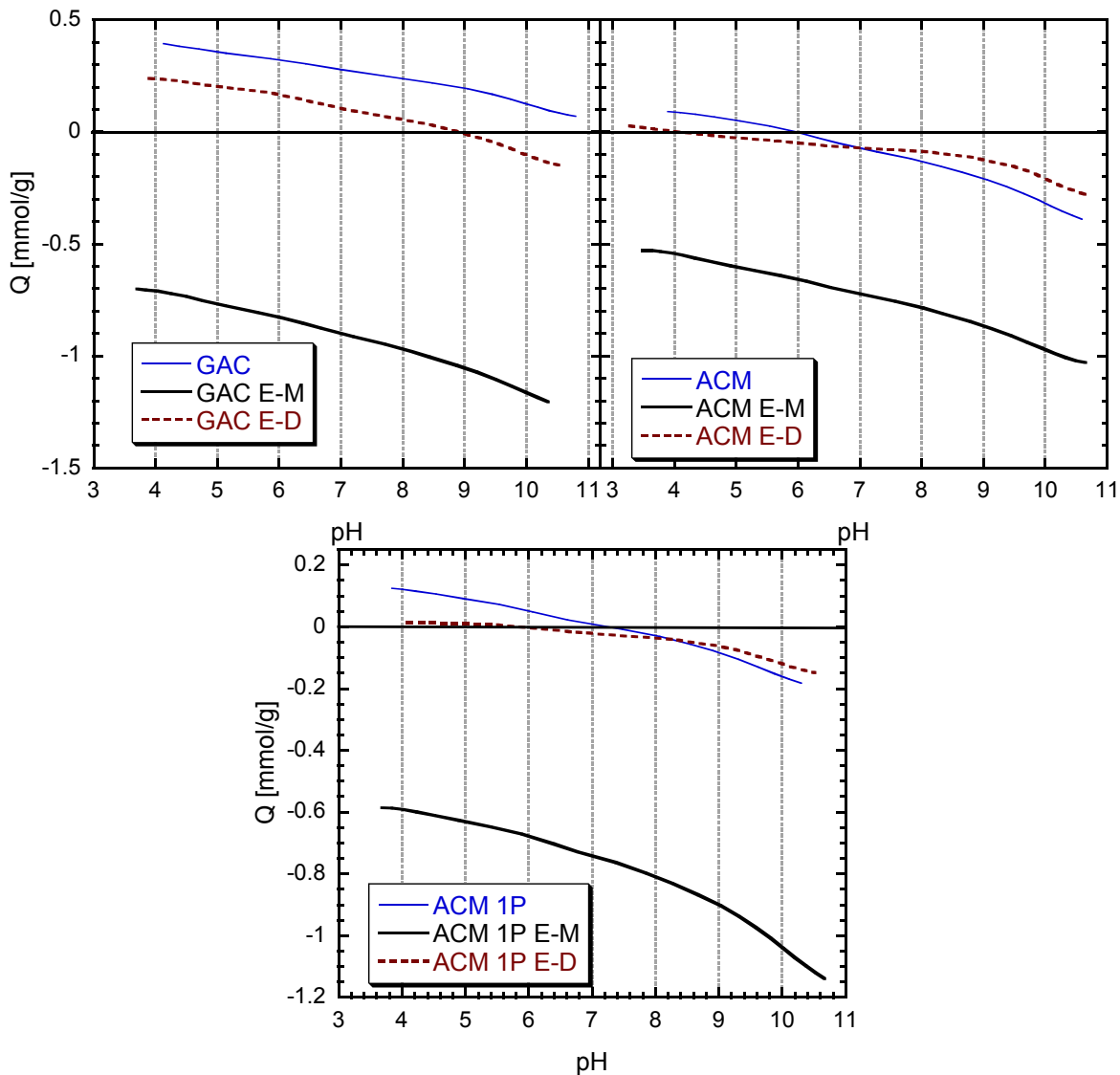
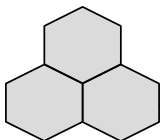
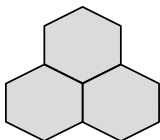


Figure 4.7 Proton binding curves of the materials before and after exposure to SO₂ in moist and dry conditions.

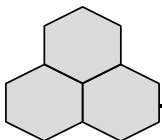
After adsorption in moist conditions, the pH of all samples decreases (Table 4.2). For Filtrasorb 400 the pH changes from 8.6 to 2.62, which is directly linked to H₂SO₄ formation on the surface and its oxidative effect on the carbon matrix. Proton binding curves (Figure 4.7) also show that the surface of carbons becomes acidic after SO₂ adsorption. For the iron-containing carbons, the surface pH is shifted from 5.78 to 2.98 for ACM and from 6.22 to 2.94 for ACM 1P (Table 4.2). In



both cases the pH after adsorption is less acidic than that for Filtrasorb suggesting the presence of less H_2SO_4 deposited on the surface, which is in agreement with the thermogravimetric analysis results.

The pK_a distributions of the species present on the surface of carbons are collected in [Table 4.2](#). In the case of Filtrasorb after adsorption in moist conditions the contribution of peaks at pK_a 8 and 10 increases. It is noteworthy that both exhausted samples have almost the same amount of groups and the peaks at pK_a 7.5 disappear after exposure to SO_2 . These changes in the surface chemistry indicate that basic groups are involved in the SO_2 adsorption process in the presence water, which is in agreement with the results published in the literature [\[50\]](#). This process causes a decrease in the surface pH of more than 6 units. After adsorption in dry conditions the groups at pK_a 10 are no longer detected. Since such groups might be associated with pyrone and chromene-like species [\[94\]](#), this finding suggests that under the shortage of water in the system SO_2 reacts with basic groups causing a decrease in the overall pH of the surface from 8.6 to 7.

The iron-containing samples do not follow the same trend as that found for Filtrasorb 400. For ACM after exposure to SO_2 new species at pK_a 6.6 and 8 appear. Their appearance is linked to surface oxidation and/or formation of iron salts. The contribution of groups at pK_a 9 increases and the groups at pK_a 10 disappear. Since the groups at 10 are also linked to iron hydroxides [\[233\]](#), the results suggest that both weakly acidic (basic) groups of carbon and iron species interact with SO_2 during its uptake. In dry conditions, there is the appearance on



new species at pK_a 3, the numbers of species represented by pK_a 7 and 9 decreased.

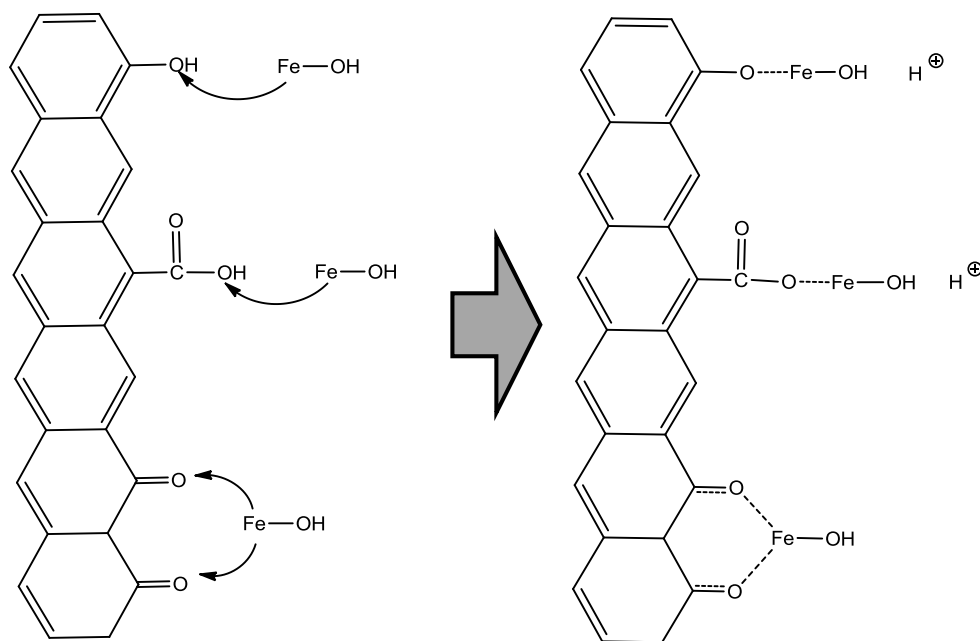
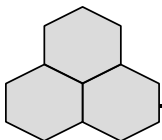
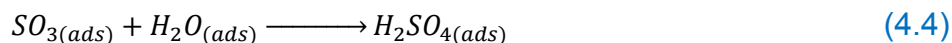
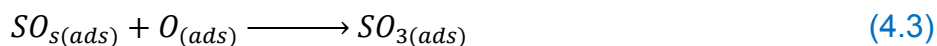


Figure 4.8 Schematic representation of the anchorage of iron oxyhydroxides on oxygenated groups of the carbon matrix.

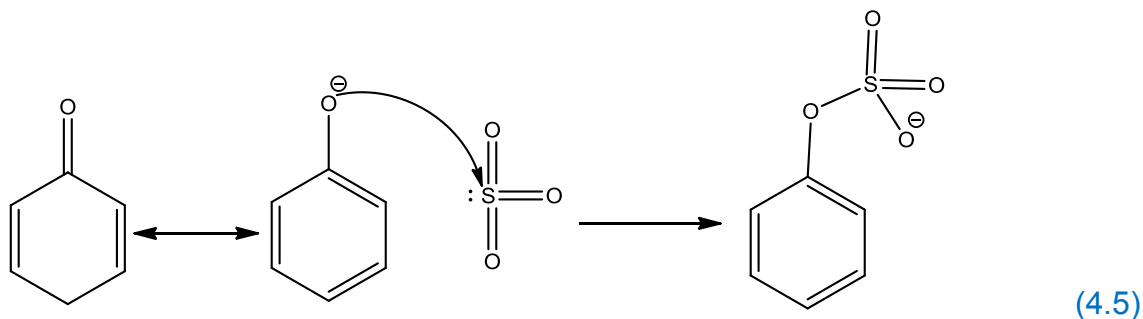
For ACM 1P E-M there is an increase in the contribution of groups at pK_a 6, 8 and 9. All of them have comparable quantities of about 0.1 mmol/g. Moreover, a large new peak at pK_a of 10 appears which might be indicative of the deposition of new compounds on the surface. The pK_a distribution for ACM E-D shows new species at pK_a 3. The amount of species represented by pK_a 7 and 9 decreased. For the ACM 1P E-D all groups below pK_a 6 and at 10 disappear. Since there are several differences between both iron-containing samples, it is plausible to assume that iron nanoparticles with different sizes interact with SO_2 differently.



Taking into account the above considerations, it is proposed that SO₂ bonds to the surface of our carbons according to several paths within two principal mechanisms: 1) on the surface of carbon matrix and 2) on the surface of iron oxyhydroxides. The following reactions have been reported as representing SO₂ reactions with the carbon matrix [47,57].

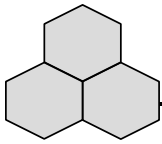


The SO₃ formed can be adsorbed on the negatively charged basic groups in carbon (mainly hydro-quinone and chromene-like [94]).

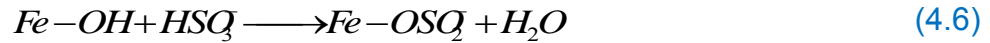


This reaction explains the consumption of basic groups in dry conditions.

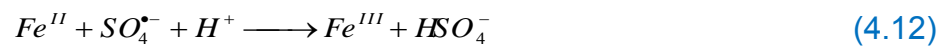
Since some H₂S was released during the breakthrough tests the carbon surface must contribute to SO₂ reduction. This process is naturally associated with the oxidation of carbon matrix which was shown by a decrease in the pH and the appearance of new species.



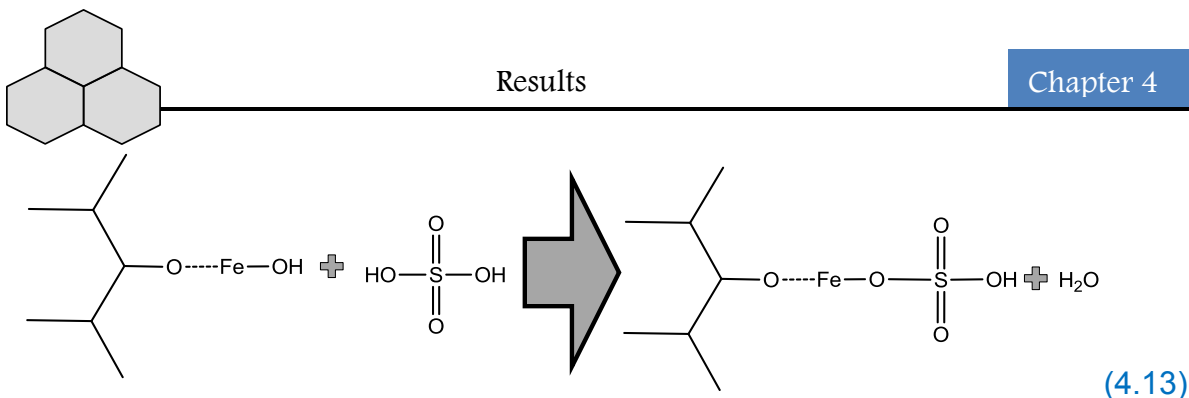
The adsorption of SO_2 on the surface of iron oxyhydroxides can occur without the electron transfer with iron sulfite as product [181,182]:



It has been proposed that sulfite can be transformed to sulfate by means of free-radical reactions [182].



Since both adsorption mechanism should co-exist on the surfaces of AC-M and ACM 1P the predominance of one or another will depend of the availability of the high-energy adsorption centers for the adsorbate molecules. For example, instead of [reaction 4.5](#) it is possible that iron oxyhydroxides can react with H_2SO_4 formed on the carbon. This should lead to the appearance of iron sulfate:



This reaction, along with [reactions 6-11](#) explain the presence of iron sulfate on the surface of ACM and ACM 1P after adsorption.

However, since iron oxyhydroxides can bond to the carbon matrix via oxygenated groups [\[236\]](#) ([Figure 4.8](#)) their presence can also lead to a decrease in the number of SO_2 adsorption sites. Thus in the case of ACM iron deposition have a negative effect on sulfur dioxide adsorption, owing to the screening of surface groups by iron nanoparticles of about 30 nm. However, on the surface of ACM 1P a large number of small iron nanoparticles increase the number of adsorption centers and their distribution, causing an enhancement in the SO_2 adsorption capacity ([Figure 4.9](#)).

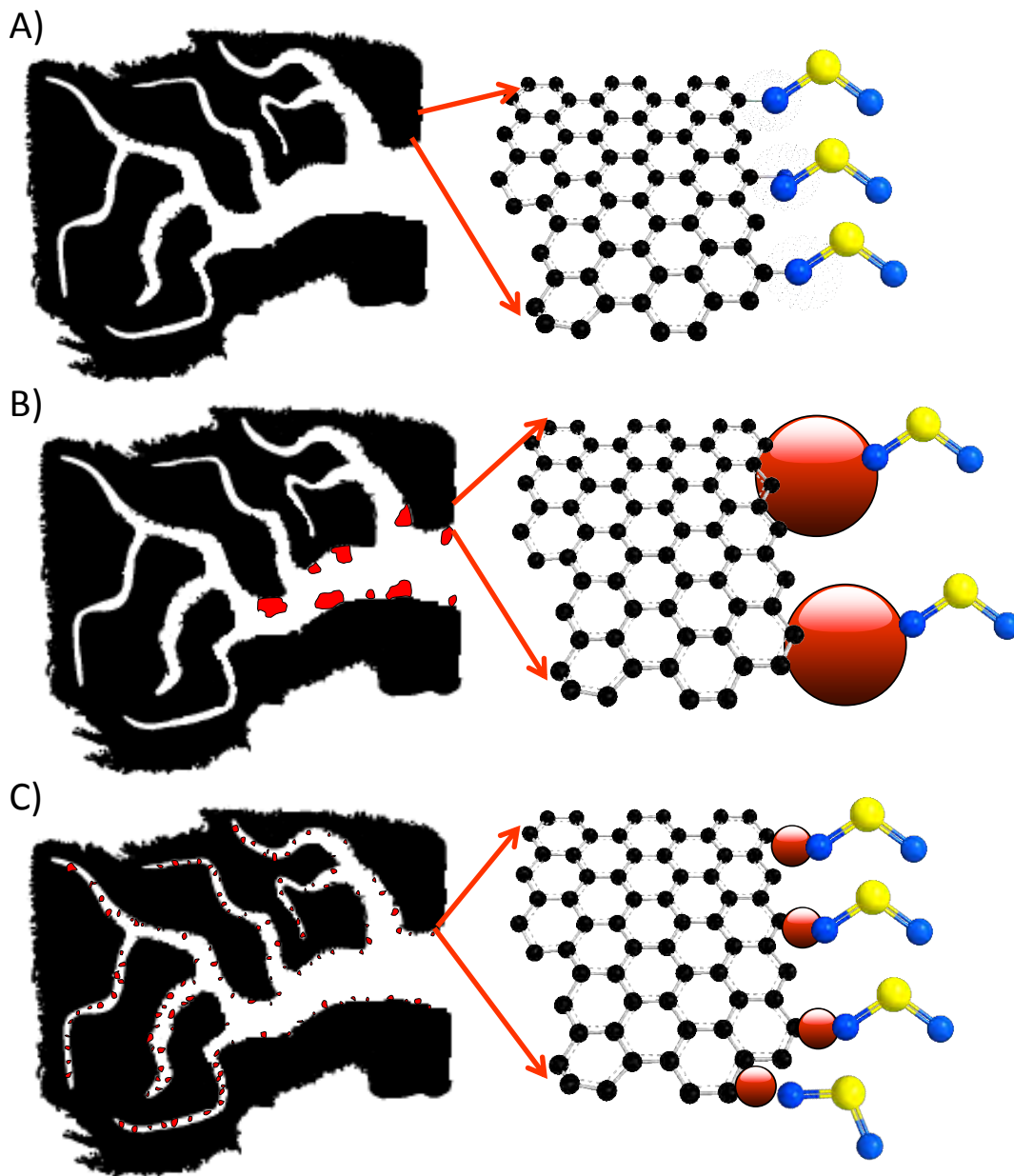
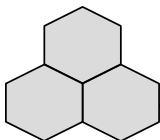
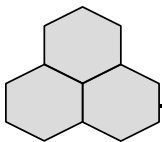


Figure 4.9 Role of the iron particle size in the SO_2 uptake. **A)** adsorbed SO_2 interacts with chemisorbed oxygen and water to form H_2SO_4 . **B)** Iron deposition causes a decrease in the adsorption capacity, owing to the screening of surface groups by larger iron nanoparticles. **C)** Capping agent utilization decreases iron nanoparticle size, and thus increases the number of adsorption centers and their distribution.



4.4 CONCLUSIONS

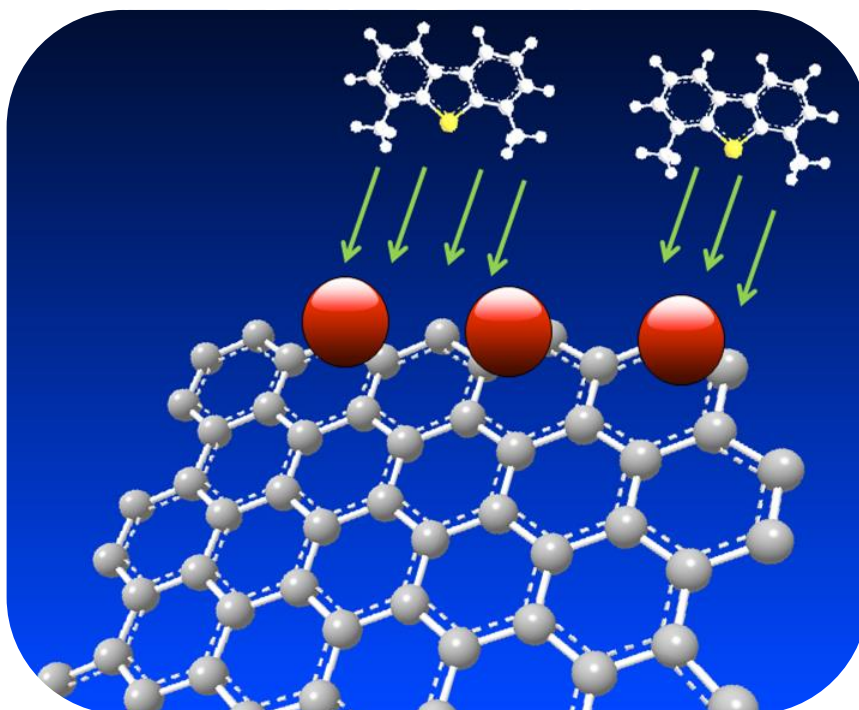
The results presented in this paper demonstrate that the anchorage of very small iron nanoparticles of about 3-4 nm on the surface of activated carbon increases the amount of SO₂ adsorbed of about 25%. It happens owing to the high dispersion of the adsorption centers with the high affinity for SO₂ bonding. On the surface of carbons sulfur dioxide is either weakly, as SO₂ gas, or strongly, as sulfuric acid, deposited in the pore system. Water is needed to form the later. The sulfuric acid formation dramatically improves the performance of carbons. For the iron-containing materials, iron sulfate Fe₂(SO₄)₃ is suggested as the main product of surface reactions. Formation of this species is linked to a less decrease in surface pH after exposure of sample to SO₂ in moist conditions and to the decrease in the numbers of OH group associated with iron hydroxide. Potentiometric results demonstrated that weakly acidic groups (basic) with pK_a about 10 are involved in the uptake of SO₂, which leads to the increase in the surface acidity. Moreover, modified materials present a smaller decrease in surface pH after adsorption that makes them attractive for real applications.

As mentioned before in the [Introduction](#) section of this thesis, the removal of sulfur compounds from fuels streams is of great interest nowadays: this study is presented in [Chapter 5](#).

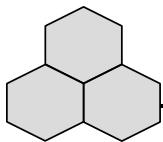
Chapter 5

Desulfurization of Model Diesel Fuel: Effect of Tert-Butylbenzene and Naphthalene Concentrations.

The incorporation of iron oxyhydroxide nanoparticles on activated carbon increases the desulfurization of model diesel, only at low aromatics concentrations, and provides an oxidation center for adsorbed molecules.



This chapter was adapted from: *Desulfurization of model diesel fuel on activated carbon modified with iron oxyhydroxide nanoparticles: Effect of tert-butylbenzene and naphthalene concentrations*, 2013, *Energy and Fuels*, 27 (9), 5380-5387.

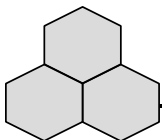


Abstract

The GAC and ACM 1P were tested in a continuous process, as a diesel fuel desulfurization medium. Model diesel fuel (MDF) was prepared as a mixture of decane-hexadecane, with 20 ppm of sulfur from dibenzothiophenes (DBT) and 4,6-dimethyldibenzothiophene (DMDBT), and different concentrations of tert-butylbenzene and naphthalene. The calculated selectivities and adsorption capacities for DBT and DMDBT were analyzed at different concentration of aromatics. The results indicate that while the concentration of naphthalene greatly affects the adsorption capacity of both DBT and DMDBT, the concentration of tert-butylbenzene affects only DMDBT uptake. At low concentration of aromatics, iron-containing carbon performs better than unmodified carbon and further oxidized species were identified on the surface of the iron modified activated carbon. This indicates that iron is acting as an acidic center attracting basic DBT and DMDBT and as an oxidant, for the adsorbed species. With an increase in the content of aromatics in MDF, the difference in the desulfurization performance between the studied materials diminishes. After thermal regeneration of the iron containing sample, 95 % of the pore volume is recovered, and only a 10 % loss in the DBT and DMDBT adsorption capacity is found.

5.1 INTRODUCTION

Activated carbon has been reported as a material having a high adsorption capacity for dibenzothiophenes, the predominant sulfur compounds in diesel [237].

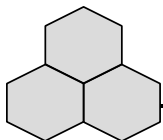


However, the main constraint of carbon is its lack of selectivity for sulfur compounds. Therefore, physical and chemical modifications of carbon surfaces are used to improve their adsorption capacities and selectivities [127,194,234,238-242].

It has been demonstrated that iron oxyhydroxide nanoparticles addition improves the adsorption capacity of sulfur species and participates in dibenzothiophene (DBT) and 4,6 dimethyldibenzothiophene (DMDBT) catalytic degradation [234].

Important surface features identified as governing desulfurization are: high specific surface area, heterogeneous structure with micropores mainly less than 10 Å in diameter [234], and surface chemistry enhancing the specific interactions of S-rings compounds. However, for an efficient desulfurization, it is also important to consider the presence of secondary compounds naturally present in diesel oil.

According to Xiao et al. [131], typical diesel fuel contains paraffins (65-75 %), mono-aromatic hydrocarbons (15-25 %), di-aromatic hydrocarbons (5-10%), and other compounds at ppm level (nitrogenated, sulfur-containing, additives). All of these affect the adsorption performance of activated carbons depending on the nature of various interactions. The addition of metal species can change these interactions and thus alter the adsorption capacity and selectivity for DBT and DMDBT [234]. The extent of these effects may depend on the composition and concentration of secondary components of diesel oil. Since mono- and di-aromatics have a major presence in the components an understanding of how these compounds interact with the adsorbents' performance is the first step in developing highly efficient materials for diesel fuel desulfurization.



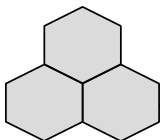
Based on the above, the objective of this paper is to evaluate the performance of activated carbon modified with iron oxyhydroxide nanoparticles in the desulfurization of a model diesel. The nature of interactions between the surface of activated carbon and mono- and di-aromatics present in model diesel is analyzed based on a study of surface chemistry and porosity. These interactions are expected to have a major effect on the adsorption capacity and selectivity of desulfurization process.

5.2 EXPERIMENTAL

5.2.1 EXPERIMENTAL SETUP

Model diesel fuel (MDF) was prepared by adding tert-butylbenzene (TBB >99%), and naphthalene(> 99%) –two chemicals that are often used to represent mono- and di-aromatics compounds-[131,243,244] in a mixture of 1:1w/w decane-hexadecane that simulates paraffin compositions. Dibenzothiophene (DBT > 99%) and 4,6-dimethyldibenzothiophene (DMDBT >99%) were added in a concentration of 10 ppm-sulfur each. In order to evaluate the desulfurization effect of the model diesel composition, four different model diesel fuels were prepared with different aromatics concentrations. The details of the concentration of these MDFs are listed in [Table 5.1](#). The selected concentrations correspond to Model Diesel Fuel with High Concentration (MDFHC), Low concentration (MDFLC) and two medium High and Low (MDFMH and MDFML) aromatics concentrations.

Dynamic adsorption experiments were performed in a polyethylene column with a 4 mm inside diameter and a 60 mm length; the packed volume was 0.7 mL. The



MDF was fed with a peristaltic pump at a constant flow of 5 mL/h. A contact time of 10 min was maintained. The materials studied in this research were the same to those reported in Chapter 4: GAC and ACM 1P.

The concentrations of sulfur- and aromatics-compounds were analyzed in a Waters 2690 HPLC with a photodiode array detector. Separation of compounds was performed in a Lichrosphere RP-18 column (100 Å, 5 µm, .0 mm×15 mm, EM Separations, Gibbstown, NJ). The gradient method utilized was: 10 µL of sample was injected at a constant flow of 1 mL/min; to separate naphthalene and tert-butylbenzene the starting composition was 80% methanol-20% H₂O, after 7 min the composition was changed to 100% methanol to separate DBT and DMBT over 8 min, maintained for 5 min and then changed back to 80% methanol for 5 min to remove decane and hexadecane from the column. All adsorption experiments were carried out at 25 °C. After adsorption, materials were dried at 100°C for 24 h before analysis was begun. A thermal regeneration of exhausted sample was carried out at 500°C for 2 h under a constant flow of nitrogen of 100 mL/min. The regeneration samples are referred to with the suffix: R.

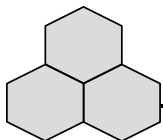
5.2.2. MATERIAL CHARACTERIZATION

X-Ray Fluorescence (XRF) analyses

XRF analyses were performed in a SPECTRO Model 300T Benchtop Multi-Channel Analyzer from ASOMA Instruments, Inc. The acquisition conditions were: voltage 9.0 kV, current 280 mA, and count time 100 s.

Mass extraction experiments

In order to qualitatively determine the compounds present on the surface of carbons substrates after adsorption, an extraction with furan was carried out. 0.05



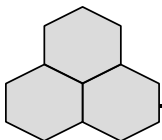
g of material were equilibrated with 5 mL of furan for 5 days. Then, the solution was filtered and injected into a mass spectrometer (MS) Q-TRAP 400 (Applied Biosystems). The MS parameters used are: ion spray voltage of 5500 V (highest sensibility); Collision energy and collision energy spread of 10 and 40 V, respectively; the declustering potential was 80 V, Nitrogen gas was used as a curtain gas and a collision gas.

Other characterization techniques

The pK_a distributions and proton binding curves were determined according to section 4.2.2 reported in [Chapter 4](#), differential thermogravimetric curves (DTG) were obtained by using the methodology reported in section 4.2.2, [Chapter 4](#), and the porosity and specific surface area were carried out according to the methodology included in section 2.2.3, [Chapter 2](#).

Table 5.1. Composition of the different model diesel fuels.

Compound	MDFMH Weight [%]	MDFLC Weight [%]	MDFML Weight [%]	MDFHC Weight [%]
Decane	43	47.8	47.5	38.5
Hexadecane	43	47.8	47.5	38.5
Naphthalene	7	2	2	8
Tert-butylbenzene (TBB)	8	2.2	4.7	20
Dibenzothiophene (DBT)	10 ^a	10 ^a	10 ^a	10 ^a
4,6 Dimethyldibenzothiophe ne (DMDBT)	10 ^a	10 ^a	10 ^a	10 ^a
[a] Expressed in parts per million of sulfur [ppm] ...				



5.3. RESULTS AND DISCUSSION

The breakthrough curves for DBT and DMDBT for each model diesel fuel (MDF) are presented in [Figure 5.1](#). For the sake of comparison, the adsorption capacities and selectivities were calculated from the breakthrough curves at an arbitrarily chosen equivalent bed volume (EBV), volume of treated effluent/volume of adsorbent packed of 65. At This value some materials start to be exhausted. For all MDFs used, the breakthrough points of naphthalene and TBB could not be detected (only those for MDFLC are reported in [Figure 5.2 A](#)), indicating a low affinity for adsorption of mono- and di-aromatics by these carbon surfaces and/or fast adsorption and saturation of the surface active centers.

In all cases, DBT appears in the column outlet sooner than does DMDBT. Its smaller size than that of DMDBT (diameters of 5.5 Å [\[245\]](#) and 6 Å for DMDBT [\[246\]](#)) probably result in faster diffusion. For the F400, the order for the removal of DBT ([Figure 5.1 A](#)) is: MDFMH<MDFHC<MDFLC<MDFML and for the removal of DMDBT ([Figure 5.1 B](#)) is MDFHC<MDFMH<MDFML<MDFLC. This indicates that naphthalene and TBB affect the adsorption of thiophenic compounds differently. For the ACM 1P, the order for the removal of DBT and DMDBT ([Figure 5.1 C](#) and [5.1 D](#)) is the same as that for GAC. However, there is a greater difference between the breakthrough curves at the same concentration of naphthalene. This suggests that materials containing iron interact with aromatics in a different way than does the unmodified carbon. The best total sulfur adsorption capacity (2 mg/g) was found for MDFLC, in which the breakthrough point was around 15 EBV. These results can be compared with similar studied in activated carbon (see [Table 1.7](#)).

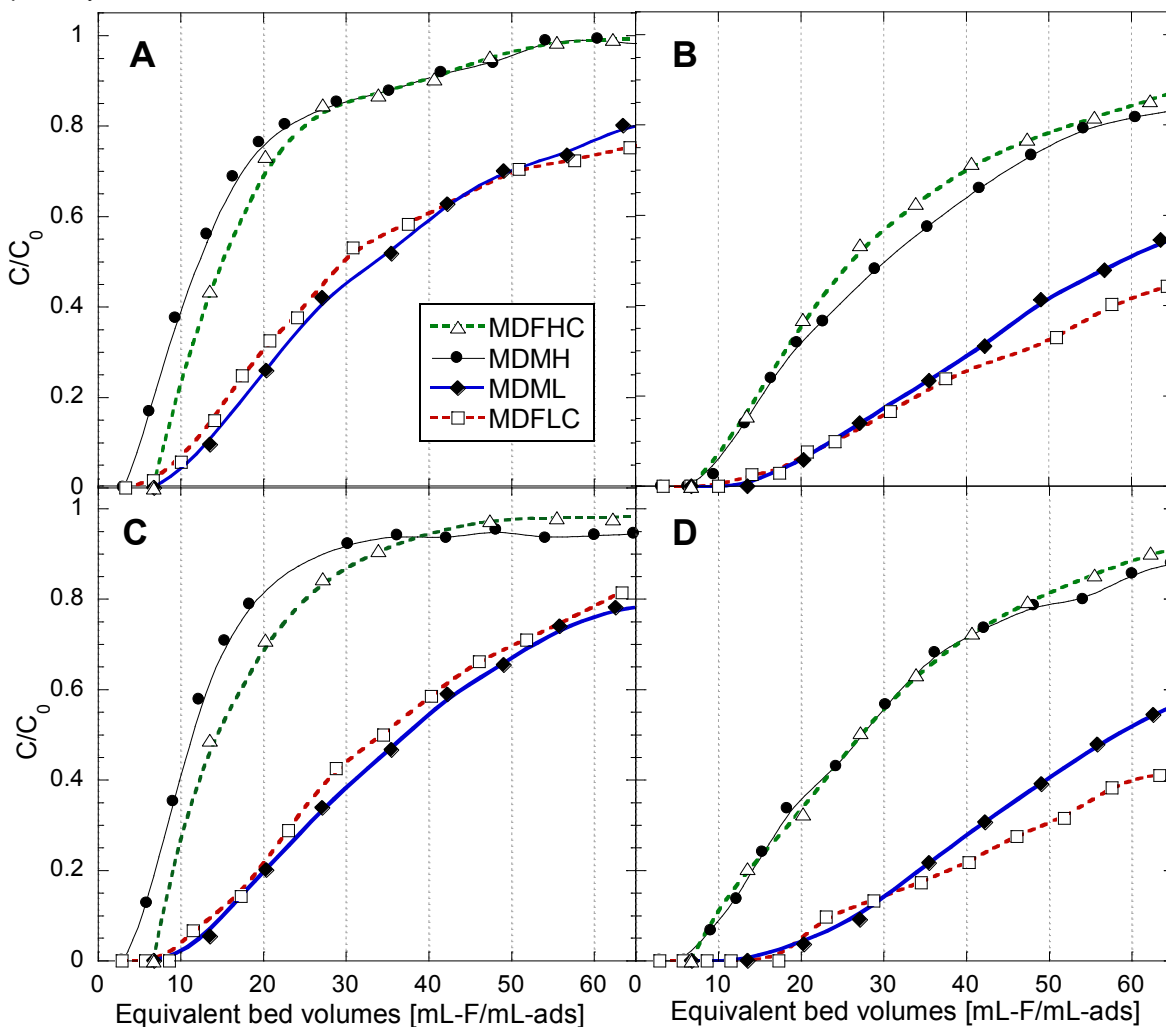
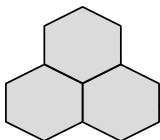
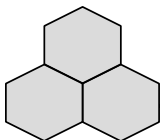


Figure 5.1 Breakthrough curves of **A)** DBT on GAC, **B)** DMDBT on GAC, **C)** DBT on ACM 1P and **D)** DMDBT onto ACM 1P.

Selectivities and adsorption capacities are summarized in [Table 5.2](#). Selectivities were calculated using naphthalene as the reference compound, at EBV of 65. The selectivity was calculated with the following:

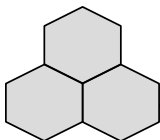
$$\alpha_{i-n} = \frac{Cap_i}{Cap_n} \tag{eqn. 5.1}$$

Where Cap_i is the molar adsorption capacity of the compound i at EBV of 65 and Cap_n is the adsorption capacity of naphthalene at EBV of 65



As shown in [Table 5.2](#), in all cases the adsorption capacities for DBT are about 40-50% lower than those for DMDBT. The ACM 1P shows a higher adsorption capacity for DBT than GAC. The capacity in MDFMH it is 10% higher, in MDFLC - 15% higher, and in MDFML - 5% higher than those adsorbed by F400. For DMDBT these differences between the performance of F400 and ACM-1P are 34% in MDFLC and 6% in MDFML for the favor of the iron containing material. With an increase in the concentration of naphthalene and TBB, the modified activated carbon behaves similar to the as received one. This indicates that iron oxyhydroxide nanoparticles improves the adsorption capacity of thiophenes only at low aromatics concentrations (2% naphthalene and 2.2% TBB). The adsorption capacities for naphthalene and TBB were very low in all measurements (~ 1 mg/g). At low aromatics concentrations, the ACM 1P sample has a strong affinity for thiophenes and a high selectivity is measured (~ 23 and 18 for DMDBT and DBT, respectively). This is consequence of a low adsorption capacity for naphthalene at low concentration. With an increase in the aromatics concentration, there are more naphthalene molecules adsorbed and the selectivity decreases. The selectivities of the DBT and DMDBT in MDFHC are around 10 times lower than those observed for MDFLC. This emphasizes the importance of aromatics concentration in the MDF for the desulfurization process.

In order to determine the real impact of each aromatic on the adsorption capacity, a factorial multivariable analysis was performed using Minitab 16. The results indicate the significance of each variable in the response parameter. Adsorption capacities of DBT and DMDBT were correlated as a function of naphthalene and TBB concentrations. The dependences are presented as contour plots in [Figure](#)



5.3. In all cases, the numeric effect of naphthalene is higher than that of TBB, indicating that naphthalene concentration is a critical issue for the uptake of thiophenes [131]. Contour plots for DBT exhibits a semi linear behavior underlying the importance of the naphthalene concentration. On the other hand, plots related to DMDBT adsorption reflect a great interference of the presence of both naphthalene and TBB in MDF.

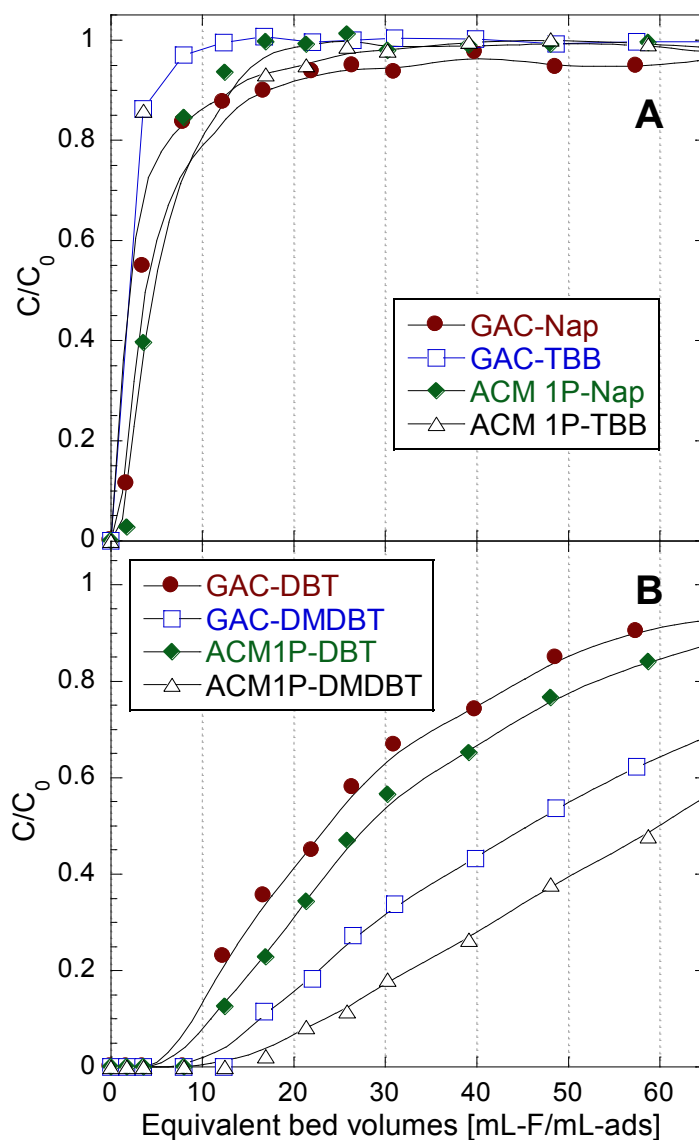
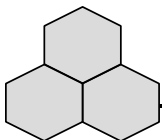


Figure 5.2. Breakthrough curves of A) naphthalene and TBB from MDFLC and B) of DBT and DMDBT on regenerated materials exposed to MDFLC.



A decrease in the thiophenes adsorption capacity caused by the naphthalene concentration was also observed by Xiao and co-workers [131]. The maximum uptake reported was 1 $\mu\text{mol/g}$ of DMDBT, against 35 $\mu\text{mol/g}$ in this study; however, the former value was obtained in batch and at very high sulfur concentrations (398 ppm). The effect of mono-aromatic concentration was also observed by Bu and co-workers [130], who found a total saturation of the carbon materials after exposure to 20 mL of treated fuel (lower than that in this study).

Owing to the good performance of our carbon materials in MDFLC, the adsorbents after exposure to this model diesel fuel were selected for regeneration and, then a second adsorption cycle in the same MDF was carried out, breakthrough curves are shown in Figure 5.2 B. The performance of both carbon materials is different, indicating that after regeneration, materials containing iron lose the beneficial effects of their surface features. This indicates that active sites, likely iron species, are deactivated after desulfurization. Perhaps due to the strong interactions of remaining compounds with the surface and/or iron reduction by carbon or sulfur compounds at the high temperature of regeneration. Also deactivation of iron oxyhydroxide nanoparticles after the thermal treatment may occurred by sintering or dehydroxylation reaction. Figure 5.4 shows a comparison between the adsorption capacities of DBT and DMDBT after and before regeneration. Generally, the adsorption capacity of the materials decreased less than 15% compared to the initial ones. In the case of DBT on F400, an increase after adsorption is apparent. This suggests that some sulfur groups were incorporated onto the carbon surface during the regeneration process, thus improving the performance [247].

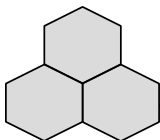


Table 5.2 Summarized of the adsorption capacities and selectivities of breakthrough curves.

Compound	α_{i-n} [mmol _i /mmol _n]	Adsorption capacity at the breakthrough point [mg/g]	Adsorption capacity at 65 EBV [mg/g]	Adsorption capacity at 65 EBV [μmol/g]	Total S adsorption capacity at 65 EBV [mg/g]
MDFHC					
ACM 1P					
Naphthalene	1	0.56	1.07	7.7	
TBB	1	0.66	0.97	8	
DBT	1.7	1.61	2.40	13	1.12
DMDBT	2.9	2.01	4.70	22	
GAC					
Naphthalene	1	0.54	1.08	7.8	
TBB	1	0.56	1.01	8.0	
DBT	1.7	1.69	2.47	13	1.16
DMDBT	2.88	2.11	4.82	23	
MDFMH					
ACM 1P					
Naphthalene	1	0.182	0.222	1.7	
TBB	0.49	0.0285	0.115	0.85	
DBT	5.3	0.674	1.68	9.2	0.86
DMDBT	10.3	1.160	3.80	18	
GAC					
Naphthalene	1	0.169	0.198	1.5	
TBB	0.5	0.045	0.101	0.76	
DBT	5.5	0.70	1.56	8.4	0.80
DMDBT	12.7	0.802	4.18	19.7	

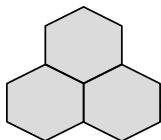


Table 5.2 Continuation.

Compound	α_{i-n} [mmol _i /mmol _n]	Adsorption capacity at the breakthrough point [mg/g]	Adsorption capacity at 65 EBV [mg/g]	Adsorption capacity at 65 EBV [μmol/g]	Total S adsorption capacity at 65 EBV [mg/g]
MDFML					
ACM 1P					
Naphthalene	1	0.138	0.22	1.71	
TBB	2	0.165	0.47	3.5	
DBT	16	1.90	5.18	28.1	1.94
DMDBT	19	3.76	6.90	32.5	
GAC					
Naphthalene	1	0.15	0.22	1.73	
TBB	2	0.16	0.46	3.4	
DBT	15	1.85	4.86	26.3	1.87
DMDBT	18.5	2.84	6.82	32.1	
MDFLC					
ACM 1P					
Naphthalene	1	0.081	0.192	1.5	
TBB	0.3	0.028	0.067	0.5	
DBT	18.4	1.63	5.09	28	2.004
DMDBT	23.2	2.47	7.41	35	
GAC					
Naphthalene	1	0.065	0.199	0.77	
TBB	0.5	0.34	0.097	0.72	
DBT	13.2	1.41	3.79	20.5	1.88
DMDBT	21.5	1.97	7.077	33	

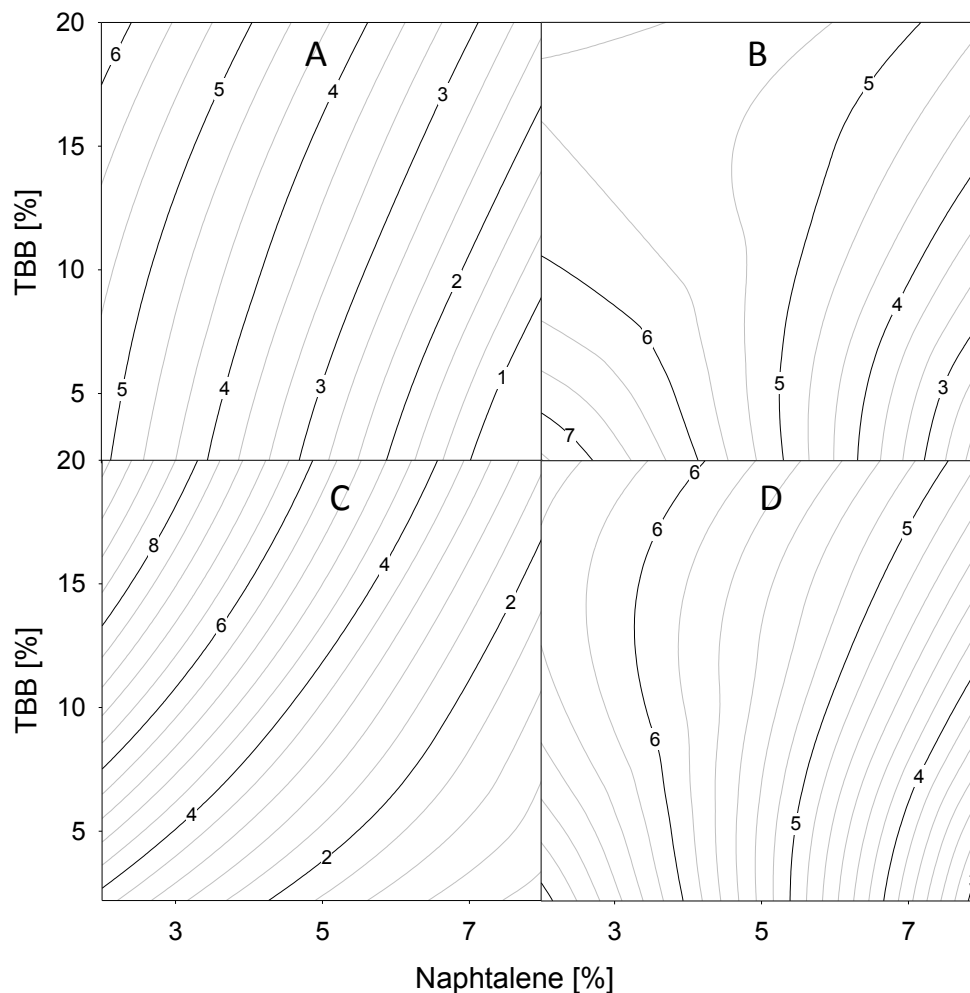
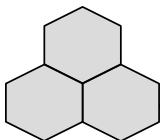
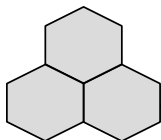


Figure 5.3 Contour plots that reflect the effects of naphthalene and tert-butylbenzene on the adsorption capacities of **A)** DBT on ACM-1P, **B)** DMDBT on ACM 1P, **C)** DBT on ACF, and **D)** DMDBT on ACF. Inside numbers indicate the sulfur uptake in mg-S/L.

The DTG curves for the initial and spent samples are shown in [Figure 5.5](#). The curve for the initial F400 exhibits a broad peak around 600 °C, which indicates that basic oxygenated groups [\[248\]](#) have been removed from the carbon surface [\[249\]](#). After exposure to MDFs two major peaks appear in the DTG curves. The first peak, between 250 and 350 °C corresponds to desorption of all non-sulfur compounds



present in MDFs. The boiling points for decane, hexadecane, naphthalene, TBB, DBT, and DMDBT are 174, 287, 218, 169, 332, and 365 °C, respectively [235,250,251]. Since all non-sulfur-containing compounds have similar boiling points, it is difficult to separate them during thermal analysis. The second peak at 470 °C is attributed to the removal of sulfur compounds and their surface reaction products that have higher boiling points than DBT and DMDBT [234]. All samples follow a similar trend in the adsorption capacities. The materials after adsorption of MDF with the highest aromatic concentration, exhibit more intense peaks in the DTG curves between 250 and 300 °C than those after adsorption of MDF of the small aromatics concentrations. For the DTG curves for the samples with the high sulfur adsorption capacity, a peak at 470 °C is more pronounced than that on the curves for the least performing samples. Except MDFHC, in all other cases the peak between 250 and 300°C has lower intensity than the one at 470°C.

Table 5.3 Parameters of surface area and pore volume of materials.

Sample	S_{BET} [m ² /g]	V_t [cm ³ /g]	$V_{<10\text{\AA}}$ [cm ³ /g]	V_{micro} [cm ³ /g]	V_{meso} [cm ³ /g]
GAC	1051	0.527	0.21	0.329	0.052
GAC-MDFLC	98	0.091	0	0.015	0.021
ACM 1P	879	0.424	0.183	0.279	0.033
ACM 1P-MDFLC	83	0.103	0	0.020	0.025
ACM 1P-R	831	0.421	0.157	0.260	0.027

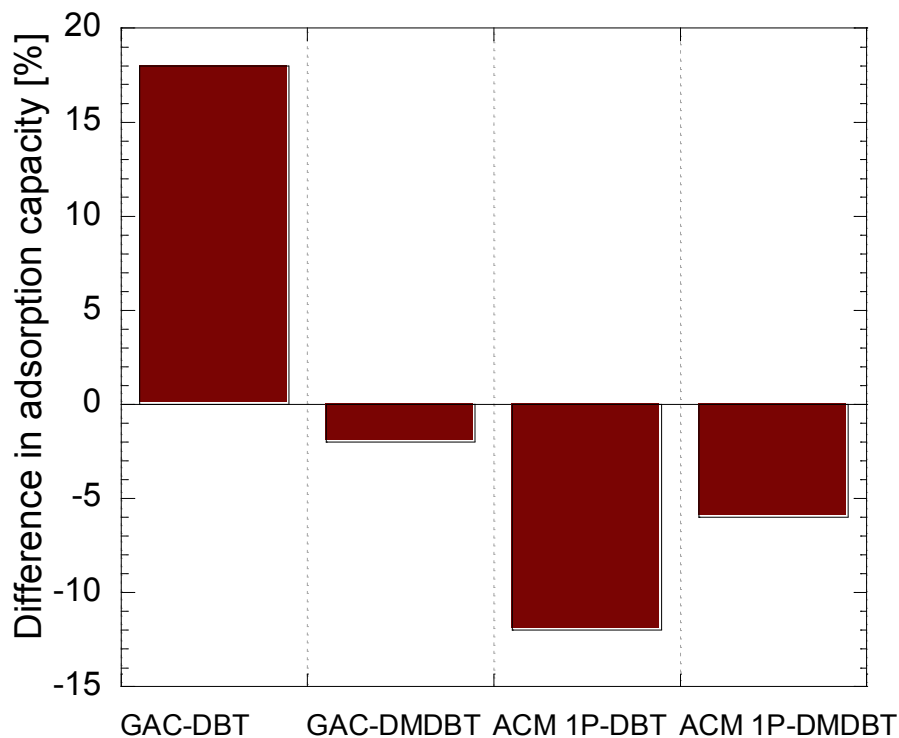
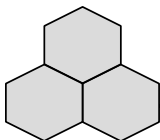
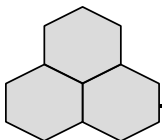


Figure 5.4 Comparison of the differences between the adsorption capacities of the initial and regenerated samples.

For the carbon modified with iron, a peak at about 420 °C is observed which probably represents dehydroxylation of iron oxyhydroxides [83]. The peak around 600°C can be attributed to the reduction of Fe(III) to Fe(II). The complete reduction of iron is observed at a temperature higher than 900°C [252]. After adsorption, there are significant differences between peaks seen on the DTG curves for the samples exposed to different MDFs. As with GAC, the most intense solvent peak corresponds to the most concentrated solution (MDFHC), while MDFLC, MDFMH and MDFML have similar intensities (around 0.07 %/°C). This is expected since on the GAC carbon material, the adsorption capacity of aromatic compounds is the highest (0.55 mg/g of naphthalene and 0.6 mg/g of TBB). For the DTG curves for



the iron-containing samples, after adsorption a new peak appears at ~ 850 °C. This temperature might be too low to link the peak to the complete reduction of iron. Interestingly, the area of this new peak increases with a decrease in the area of the peak at 450 °C. A plausible explanation of this is that iron is acting as an oxidant [234], creating new compounds strongly adsorbed on the carbon surface that require more energy to be desorbed. Strong adsorption of these new compounds/polymers adsorbed on the carbon surface can also contribute to the decrease in the adsorption capacity of ACM 1P after regeneration.

The parameters of the porous structure for the materials studied are presented in Table 5.3. The surface area of F400 is about 1000 m²/g, and the material is predominantly microporous. After modification, the surface area decreases by about 20%, mainly due to a volume contraction of ultra-micro pores (<10 Å). The changes in the porosity (Figure 5.6) suggest the formation of a thin layer of nanoparticles in the pores of activated carbon. After adsorption, almost all pores are blocked by solvents and aromatics, decreasing the surface area by about 90% for F400 and 95% for ACM 1P. However, after regeneration, there is a recovery of almost all porosity to 95% of the original area. The chemical stability of iron species in carbon materials after regeneration was studied by X-Ray fluorescence (Figure 5.7). After iron modification, an increase of the band at 7.05 KeV is observed, which is related to iron deposited on the activated carbon surface. After regeneration, the iron peak is still present, indicating that the thermal regeneration does not affect the presence of iron on the surface. This result, along with physisorption studies, demonstrates that these carbon materials have a sufficiently robust structure to endure the regeneration process.

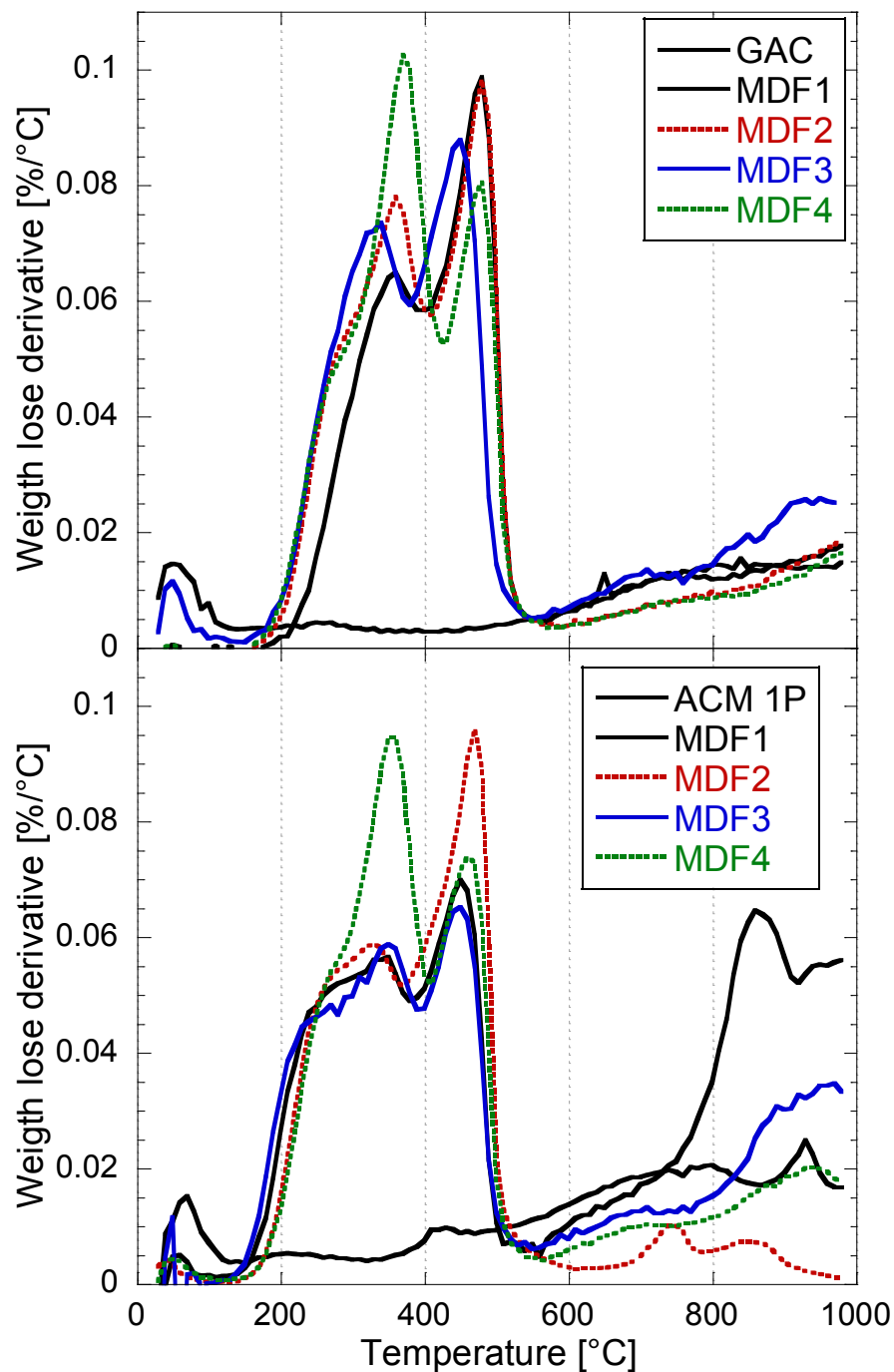
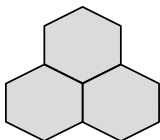


Figure 5.5 DTG curves in nitrogen for GAC and ACM 1P before and after exposure to the different MDFs.

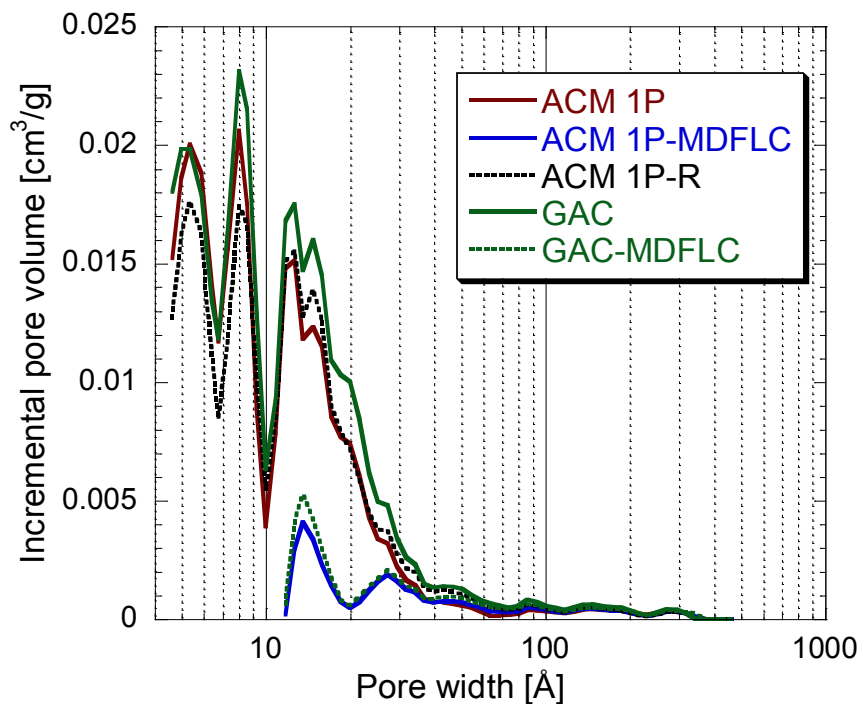
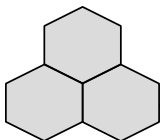


Figure 5.6 Pore size distributions for the materials before and after adsorption from MDFLC and for ACM 1P after regeneration.

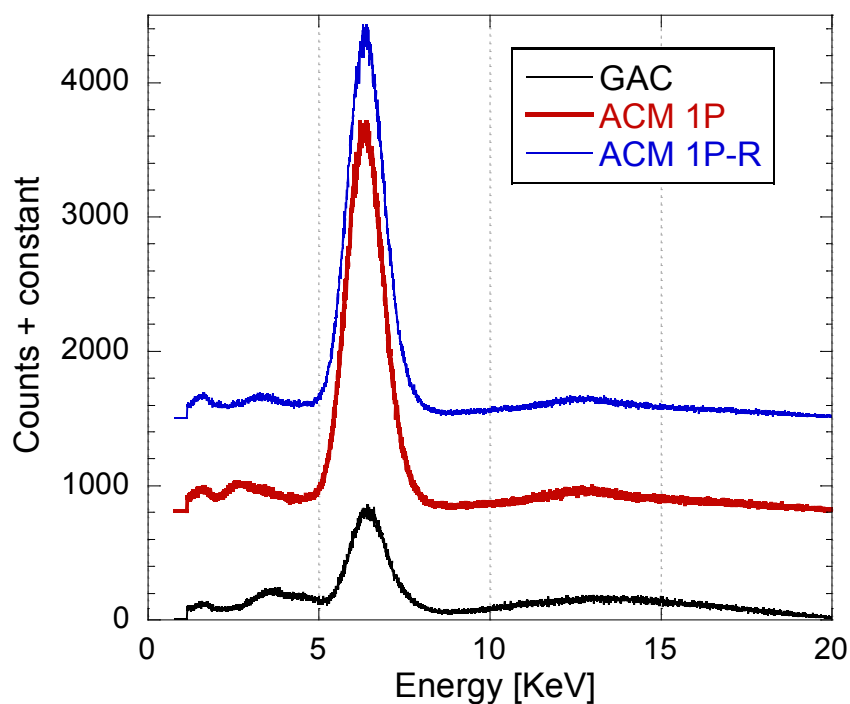
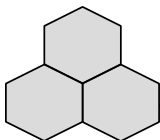


Figure 5.7 XRF for materials before and after regeneration.



In order to better understand the effect of the iron oxyhydroxides deposition on the interactions between compounds of MDF and carbon, the selected materials after MDFs exposure were further characterized by potentiometric titration to examine changes in surface chemistry caused by adsorption and, extraction of adsorbed species from the surface, followed by their identification by MS.

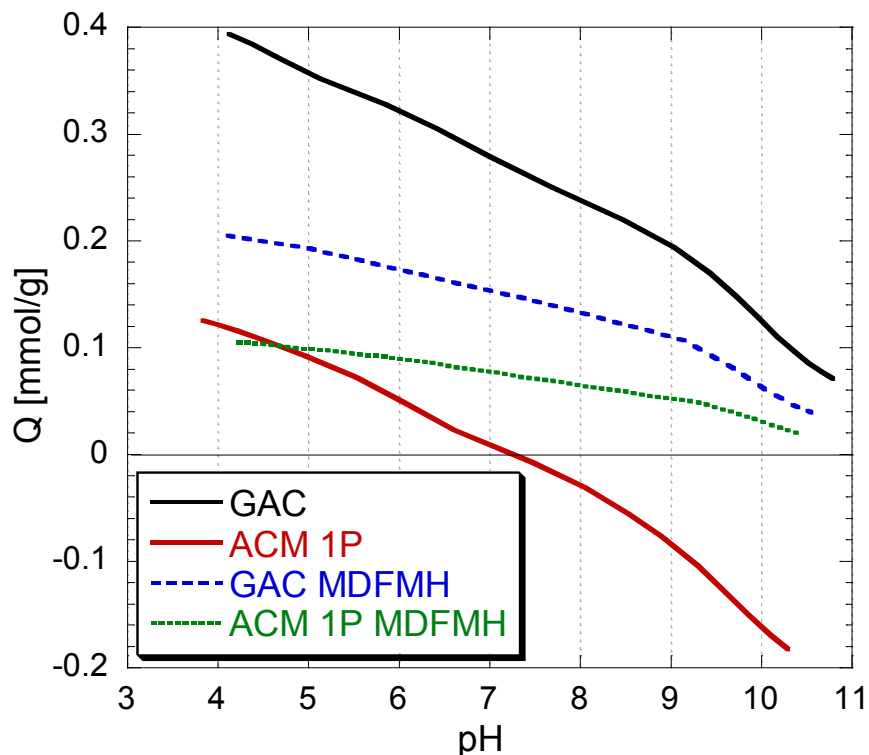
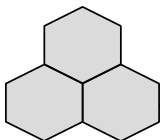


Figure 5.8 Proton binding curve of studied materials before and after exposure to MDFMH.

Proton binding curves for the initial materials are given in [Figure 5.8](#). The surface of F400 is basic and after modification with iron its acidity increases owing to the properties of the deposited iron oxyhydroxide nanoparticles [224]. The pK_a distributions ([Figure 5.9](#)) suggests that after modifications, there is a decrease in the number of carboxylic groups ($pK_a = 4.5$), indicating that acidic groups are involved in iron deposition. For ACM 1P a peak at $pK_a 7$ likely corresponds to the



second deprotonation of H_3PO_4 , which is expected since this reagent was used as a capping agent in the materials synthesis. The peaks at pK_a 6.1 and 9.7 can be attributed to the presence of mono- and poly-nuclear Fe(III) (hydroxy) iron species [233]. After adsorption, the surface of the materials becomes more basic, and the number of groups decreased. After adsorption of MDFMH two peaks are observed at pK_a 6.45 and 10. These peaks are also present in the distributions of the initial samples, however, their intensities are lower. For the material containing iron, a new peak at pK_a of 4.01 appears. This may be attributable to the changes in the acidity of the carbon surface as a result of the participation of surface species in DBT and DMDBT oxidation [246].

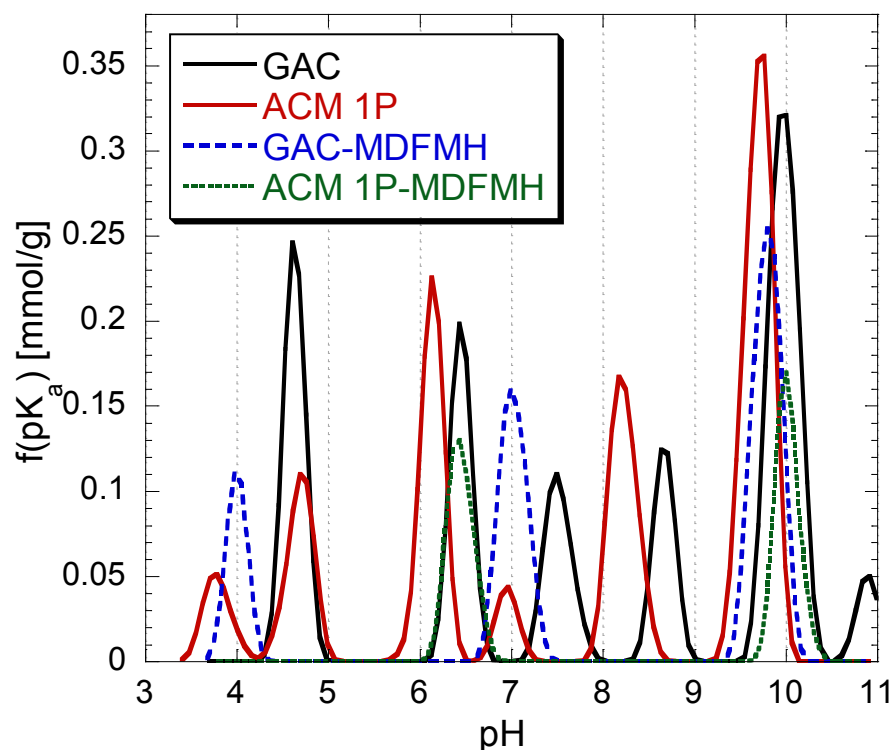


Figure 5.9 pK_a distribution of materials in Figure 5.8.

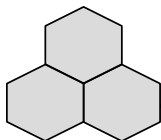
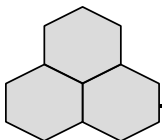


Table 5.4 Species identified after furan extraction from the surfaces of samples after exposure to MDF.

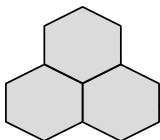
Sample	Products	m/z of fragments (intensity, %)	ions
GAC	DBT	185.04(100)	153.04(15.4)
		143.04(6.2)	141.04(70.7)
	DMDBT	213.5(9.6)	211.9(100) 198(48.8) 180.16(19.2) 165.8(39.2)
ACM1P	DBT-sulfoxide	201.04(32.1)	185.8(28.51)
		172.9(32)	171(69) 158.2(16.7)
		145.2(35.8)	141.5(28.5)
		115.04(100)	
ACM1P	DBT	185.2(7.4)	153.04(29.9)
	DMDBT	213.5(17.8)	211.8(100) 198(53.5)
		179.9(26.6)	166(44.7)
	DBT-sulfoxide	201.12(100)	185.04(35.6)
173.04(14.7)		171.04(27.1) 158(4)	
145.04(15.6)		141.04(11.9) 115.04(21.7)	
DBT-sulfone	217.1(82)	216(7.7) 187(69)	
	170.9(10.2)	143 (12.8) 135(100)	
DMDBT-sulfoxide	228.96(100)	212.08(43) 211(55)	
	200(41.7)	185(13.3) 176(42)	
	165(13)	152(51.7) 141(52)	
	126(42)	115(48)	

The mass spectra for the extracts from the carbon surfaces are presented in [Appendix B. Table 5.5](#) summarizes the analysis of mass to charge ratio (m/z) fragments and the intensities of the peaks representing DBT, DMDBT, and their oxidized counterparts. After adsorption, the mass spectrum indicates the presence of DBT-sulfone and DBT-sulfoxide. The appearance of any of these compounds depends on the properties of activated carbon sample in which the mass extraction



was carried out. For example mass spectra for GAC after MDF exposure shows that DBT is oxidized to sulfoxide, while in the case of ACM 1P oxidation to sulfoxide and further to sulfone has taken place. These results suggest that the addition of iron oxyhydroxide nanoparticles to the carbon surface promotes more probable oxidation of absorbed compounds which is demonstrated by appearance of the sulfone [253]. Moreover, for this sample, in addition to DBT, DMDBT is also partially oxidized to sulfoxides.

Plausible explanations why the deposition of iron oxyhydroxide nanoparticles on the carbon surface improves the adsorption of thiophenic species are enhanced specific interactions between the modified surface and DBT and DMDBT, and steric obstacles affecting adsorption at certain concentrations of aromatics. Naphthalene and TBB have conjugated aromatic rings and adsorb on the activated carbon surface via π - π interactions with the electrons in the graphitic layers. When the iron oxyhydroxide nanoparticles are present, they disturb the favorable orientation of the rings on the surface (parallel to the surface), decreasing the affinity for aromatic compounds. Moreover, the presence of iron oxyhydroxides promotes oxidation of sulfur compounds. These newly formed species are more polar than DBT and DMDBT and therefore can be strongly adsorbed on surface polar sites. The presence of iron also increases the surface acidity, which results in specific acid-base interactions with the slightly basic DBT and DMDBT. This increases not only the amount adsorbed but also the selectivity of a desulfurization process. It is important to mention that the coordination between iron and sulfur could also be feasible, as reported in the literature [254].



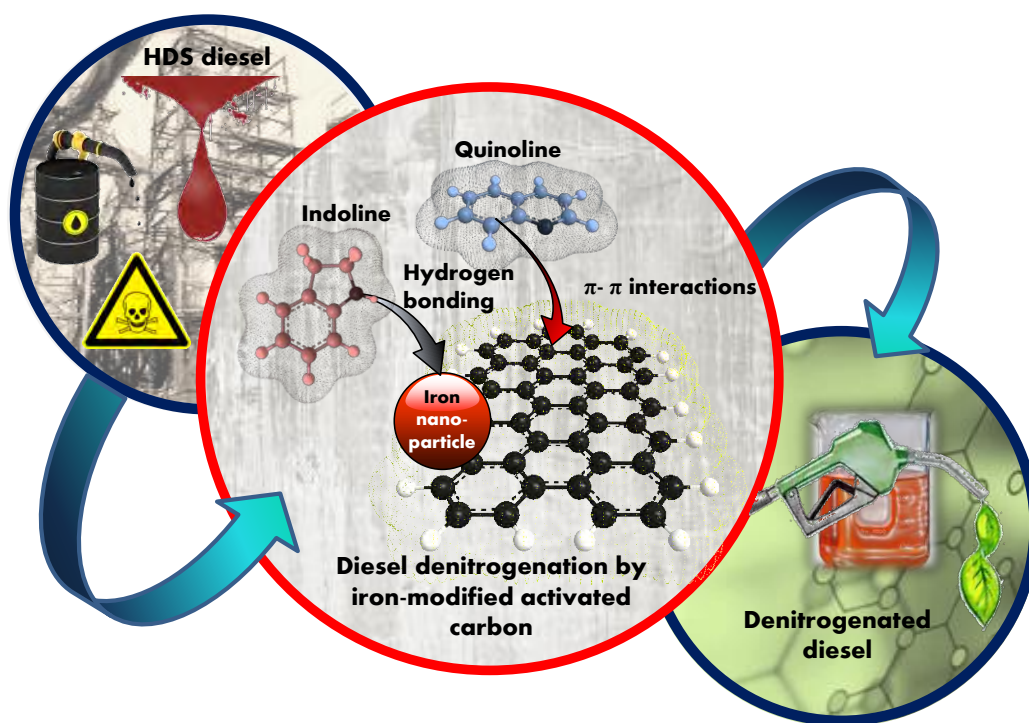
5.4. CONCLUSIONS

The presented results show that naphthalene concentration in diesel fuel is an important factor affecting the desulfurization process on activated carbons. This compound, even in low concentration, dramatically decreases the performance of carbons in dynamic conditions. This negative impact of naphthalene can be lessened in carbons by the addition of iron oxyhydroxide nanoparticles. Even though modification with iron decreases the porosity of about 20%, the desulfurization performance is enhanced compared to that of the unmodified carbon. The iron species decrease the interactions of aromatics with carbon surface, improving the selectivity for sulfur compounds. The latter is related to the acidity of iron compounds. Their presence on the surface can also create an obstacle for energy-efficient localization of aromatic ring via π - π interactions. Another beneficial effect of iron is oxidation of thiophenes to sulfoxides and sulfones which can interact with carbon polar groups and the deposited nanoparticles. However, in order to achieve such an improvement in the desulfurization performance, the fuel should have low naphthalene concentrations. A simple thermal regeneration process at 500 °C was able to recover most of the active sites in the materials and the desulfurization performance decreased only 10%. Other compounds that have major influence in the desulfurization performance of materials are nitrogenized compounds (such as quinoline and indoline); since denitrogenation is also of outmost interest the next step of the research was to evaluate the denitrogenation capacity of the materials employed here, as described in [Chapter 6](#).

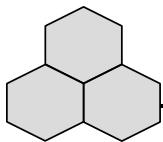
Chapter 6

Model Diesel Denitrogenation: Sulfur Compounds Effect.

Activated carbon modified with iron oxyhydroxide nanoparticles has the capacity of denitrogenating model diesel fuel, mainly by removing non-planar nitrogen molecules.



This chapter was adapted from: *Model diesel denitrogenation by modified activated carbon with iron nanoparticles: Sulfur compounds effect*, 2013, Chemical Engineering Journal 230, pp. 439-446.

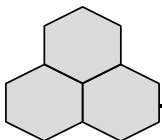


Abstract

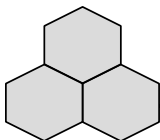
In this chapter, iron-modified activated carbon was studied for the removal of nitrogen compounds (indoline and quinoline) naturally present in diesel. Model diesel was simulated using a mixture of decane and hexadecane that also contained the previously used sulfur compounds dibenzothiophene and 4,6 dimethyldibenzothiophene. The results showed that iron enhances the indoline uptake of carbon by 30%, while quinoline adsorption also increased, but to a lesser extent. Increased iron denitrogenation capacity was also observed during the quinoline-indoline competition experiments; the iron-modified sample showed a 30% and 9% increase in indoline and quinoline uptake, respectively. When nitrogen and sulfur compounds compete for adsorption sites, the indoline and quinoline uptake in the iron materials increased. In contrast, carbon desulfurization performance decreased in iron-modified materials, indicating that these adsorbents are more selective for nitrogen than for sulfur compounds. The improved performance of the modified activated carbon was attributed to $\pi-\pi$ interactions between quinoline and activated carbon and to the nitrogen in indoline and iron oxyhydroxides.

6.1 INTRODUCTION

As mentioned in [Chapter 5](#) there is a growing interest in the development of materials capable of performing either diesel fuel denitrogenation and/or



desulfurization. Denitrogenation has garnered attention because ultra-low nitrogen levels in commercial diesel fuel are required by environmental organizations around the world [66] to abate the impact of nitrogen oxides (NO_x) released to the environment [255,256]. However, its interest is also due to desulfurization technologies are often affected by the presence of nitrogen compounds [22,131,257]. Recent studies on the ultra-deep desulfurization of model diesel have demonstrated that the presence of even small amounts of nitrogen aromatic compounds has an inhibitory effect on sulfur removal [72-75]. Similarly to desulfurization, adsorption under normal conditions has been proposed as a suitable process for deep denitrogenation of diesel fuel [27,76-78,193]. As the next step in the development of high cleaning fuels adsorption materials is necessary to evaluate the denitrogenation capacity of the materials studied in Chapter 5, and determine if they can either remove nitrogen and sulfur in a single stage or that are capable of removing nitrogen compounds selectively, prior to desulfurization. Adsorptive denitrogenation by activated carbon has attracted attention recently [237,258,259], owing to the following facts: carbons are generally cheaper than catalysts, can operate under normal temperature and pressure conditions, do not need hydrogen, and may be easily regenerated. Almarri et al. [258] studied the interactions among quinoline, indole, and oxygenated groups present in carbon. It was found that the type and amount of oxygen groups play a decisive role in nitrogen compound uptake. Stronger acidic moieties were more relevant for quinoline adsorption, whereas carbonyl and quinone contributed to the indole uptake.



Recently, Xiao et al. [131] found an interesting relationship between total oxygen concentration in carbon and nitrogen removal capacity. The authors modified commercial activated carbon with ammonium persulfate and H_2SO_4 at different times and temperatures, in order to selectively anchor carboxylic groups without significant change to its material porosity. Their results showed that carboxylic and anhydride groups bear the greatest responsibility for nitrogen uptake. These two studies illustrate the importance of the chemical surface of carbons and the nature of nitrogen molecules for fuel denitrogenation.

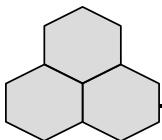
Therefore, the incorporation of oxygen functionalities provided from the anchored iron oxyhydroxide nanoparticles might enhance not only the desulfurization capacity of GAC, but also its denitrogenation capacity.

The purpose of this work is to evaluate the influence of iron nanoparticles on the model diesel denitrogenation when they are anchored on the surface of activated carbon, considering the importance of both carbon surface acidity and nitrogen's ability to bond with specific metal oxide groups created on the carbon surface. The effect of sulfur compounds on denitrogenation was also investigated. Hence similar materials to the employed in Chapter 5 were synthesized and studied.

6.2. EXPERIMENTAL

6.2.1. MATERIALS AND CHEMICALS

All chemicals were reagent grade with the following purities: uinoline ($\geq 98\%$), indoline ($\geq 99\%$), decane ($\geq 99\%$), n-hexadecane ($\geq 99\%$), dibenzothiophene (\geq



99%), and 4,6-dimethyldibenzothiophene ($\geq 99\%$), all provided by sigma-Aldrich. $\text{FeCl}_3 \cdot 6\text{H}_2\text{O}$ ($\geq 98\%$) was provided by Fermont and H_3PO_4 (85.6%) was acquired from J.T. Baker. The materials studied were GAC and ACM1P that were synthesized according to the methodology described in [section 2.2.3](#).

6.2.2. MATERIALS CHARACTERIZATION

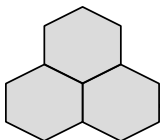
Ash content and inorganic composition

The ash content was obtained in a Versa Therm HS thermogravimetric analyzer from Thermo Cahn. 30 mg of material were heated from room temperature to 900°C at a heating rate of $10^\circ\text{C}/\text{min}$. The weight loss was recorded as a function of temperature. At the final temperature, all organic components in materials were volatilized, and the ash percentage was calculated as the ratio of the initial and final weights.

The inorganic composition of materials was obtained after digesting their ashes in a microwave (Milestone, Ethos 1). 40 mg of ashes were mixed with 20 mL of a $\text{HNO}_3:\text{H}_2\text{SO}_4$ (5:1) solution. The microwave port was hermetically closed and heated at $10^\circ\text{C}/\text{min}$ from room temperature up to 150°C for 1 h. Next, the solution was diluted to 50 mL and all dissolved elements were simultaneously analyzed by ICP-AES (Varian spectrometer 730-ES).

Other characterization techniques

Materials were characterized by: surface area and porosity as described in [section 2.2.3](#) and surface charge distribution by the method described in [section 3.2.4](#).



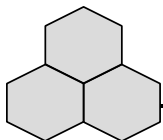
6.2.3. ADSORPTION ISOTHERMS

Model diesel fuel was simulated by a mixture of 1:1 w/w of decane-hexadecane. Nitrogen concentration was obtained by adding several concentrations of quinoline [76,191] and indoline, which are nitrogen compounds that can inhibit desulfurization to a great extent [260]. Competition experiments of quinoline and indoline were achieved by mixing these compounds at equimass concentrations. The effect of sulfur compounds on nitrogen compound removal in model diesel was simulated by adding 25 ppm-S of dibenzothiophene (DBT) and 25 ppm-S of 4,6-dimethyldibenzothiophene (DMDBT).

The procedure for obtaining the adsorption isotherms was as follows: in a 25 mL flask, several masses of GAC or ACM 1P were placed into contact with 10 mL of model diesel containing the adsorbates at the desired concentration. Flasks were closed and placed in a stirred incubator at 25 °C. After equilibrium was reached (10-15 days), the solutions were filtered and analyzed by HPLC. The adsorbed mass was calculated by means of the equation 1.1.

6.2.4. COMPOUNDS DETERMINATION

Compound analysis was conducted by high performance liquid chromatography (HPLC, 1200 series, Agilent Technologies) equipped with a diode array detector (DAD). The column for compound separations was a Purosphere STAR, Hibar 250-4,6, RP-18e (5 μ m). The following isocratic method was used: 10 μ L of sample were injected into the column at a constant flow of 0.6 mL/min. The mobile phase concentration was 10% water and 90% methanol. The compound retention time



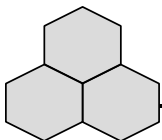
and wavelength were as follows: indoline (5.7 min, 254 nm), quinoline (6.2 min, 254 nm), DBT (14.5 min, 235 nm), and DMDBT (26 min, 235 nm). At the end, the composition was changed to 100% methanol to elute decane and hexadecane.

6.3. RESULTS AND DISCUSSION

6.3.1. MATERIAL CHARACTERIZATION

Micrograph images ([Figure 6.1](#)) shows very small nanoparticles across the surface of the ACM 1P. Such nanoparticles are in the range of 1 to 10 nm and are associated with oxygen as shown in the elemental mapping.

Surface area and pore volumes of materials are summarized in [Table 6.1](#) and the incremental surface area distribution in [Figure 6.2](#). The specific surface area of raw activated carbon increased by 4% after iron modification, which is linked to a slight increase in micropore volume of activated carbon. This increase is attributed to the porosity created among the nanoparticles incorporated (see [section 2.3.2](#) in [Chapter 2](#)). Due to the nanosize of anchored particles, the porosity generated in carbon is reflected in an increase of micropore surface. The incremental surface area distribution in [Figure 6.2](#) shows two effects after iron deposition. Zone 1 shows a narrowing of ultra-micropores ($<7\text{\AA}$) due to the incorporation of iron nanoparticles. Zone 2 (micropores from 7 to 20 \AA) shows that the deposition of particles increased the surface area, due to the effect mentioned above. Nonetheless, these results should be taken with caution because the use of N_2 as adsorbate could have some disadvantages when measuring ultra-micropores with reference to other gases like Ar [\[261\]](#) or CO_2 [\[262,263\]](#). Since iron is present as



very small nanoparticles, it is believed that the active adsorption sites related to iron are mainly present in the activated carbon pores.

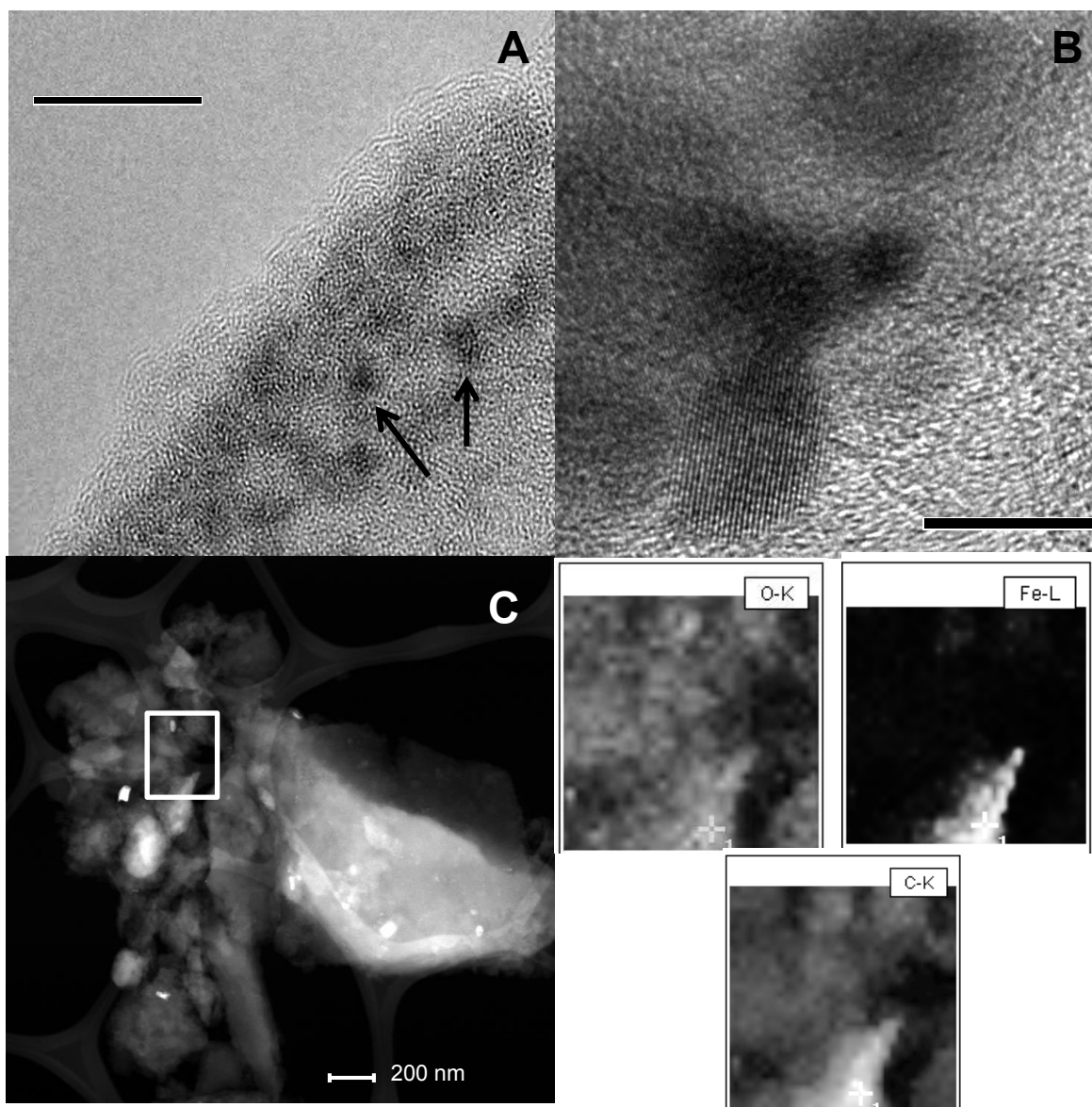


Figure 6.1 Electron transmission images of the ACM 1P material. **A)** and **B)** images show the presence of nanoparticles ranging from 1 to 10 nm. The elemental mapping of the marked zone in **C)** corroborates the presence of iron that is associated with oxygen of the adsorbent material.

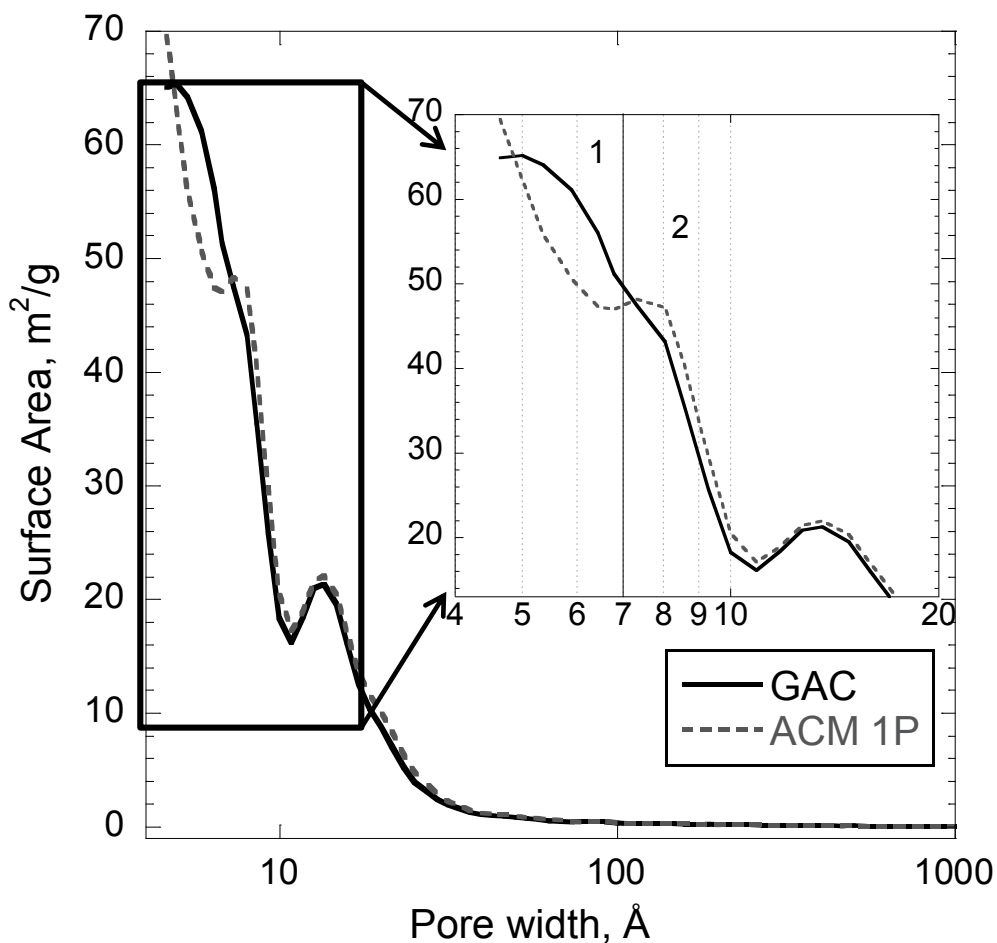
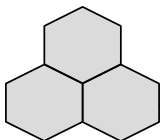
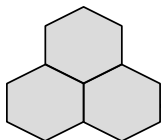


Figure 6.2 Surface area distribution of GAC and ACM 1P described by DFT.

Moreover, the slight difference in porosity between GAC and ACM 1P (see [Table 6.1](#)) allows us to suggest that the differences in adsorption capacities between these two adsorbent materials can be attributed to the presence of iron nanoparticles on the surface of ACM 1P.

The ash content of activated carbon changed from 7.20 % to 9.45% after iron deposition. A detailed analysis of raw (bituminous) activated carbon revealed that most of the natural inorganic impurities consist of Al, Ca, Fe, and Na ([Table 6.2](#)). After modification, the iron content increased from 0.20 to 2.35% ([Table 6.2](#)). The



decrease in the percentages of Al and Ca indicates that most impurities were washed during iron modification. Because of this, it is expected that the contribution of those inorganic elements to the adsorption of aromatic compounds will be negligible.

The charge distribution of the materials studied is provided in [Figure 6.3](#). The surface of activated carbon F-400 (GAC) is basic, with a point of zero charge at pH 11. After modification, the material became more acidic as a result of the anchorage of iron acidic particles: the point of zero charge of ACM 1P is 8.3. The change in the material surface charge will affect the degree to which molecules are adsorbed depending on their acidity. Basic moieties will be more attracted by the ACM 1P than by the GAC

Table 6.1 Physical surface properties of studied materials.

Sample	S^{BET}	S^{DFT}	V_{total}	V_{micro}	V_{meso}	S_{micro}	S_{meso}
	[m ² /g]	[m ² /g]	[cm ³ /g]	[cm ³ /g]	[cm ³ /g]	[m ² /g]	[m ² /g]
GAC	952	722	0.474	0.303	0.074	676	35
ACM 1P	995	724	0.504	0.314	0.087	670	41

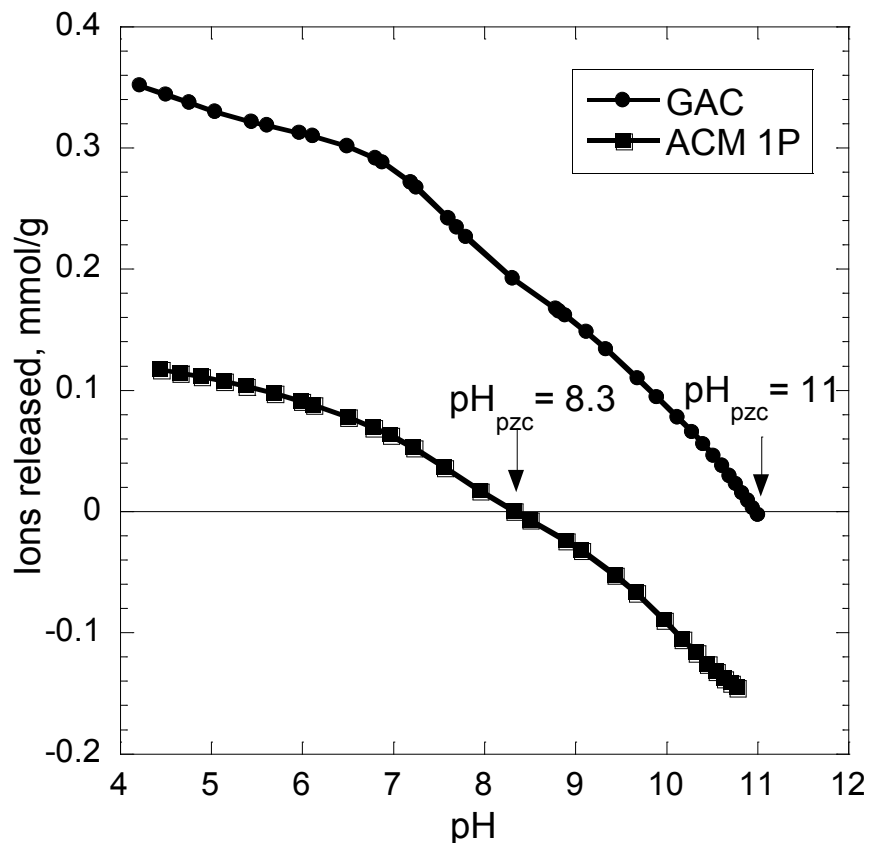
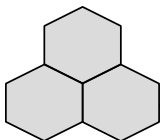
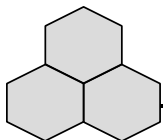


Figure 6.3 Proton-binding curve for released ions from the surface of studied materials.

6.3.2. ADSORPTION EXPERIMENTS

The adsorption isotherms were correlated to the Freundlich and Langmuir models. In order to determine which model has a better correlation, the variance (R^2) parameter was calculated. The Freundlich and Langmuir parameters as well as the R^2 and the standard deviations of experiments are provided in [Table 6.3](#). In all cases organic molecule adsorption is best described by the Freundlich model, perhaps because of the material's heterogeneity; hence, the adsorption isotherm reported in [Figures 6.4-6.6](#) was adjusted by this model. For the sake of



comparison, all isotherms are reported in mass concentration of the two molecules studied; in order to calculate the nitrogen concentration corresponding to each of these two organic molecules, it is necessary to consider that quinoline and indoline have 10.8% and 11.75% N, respectively.

6.3.2.1 Single adsorption of indoline and quinoline

The isotherms of single indoline and quinoline adsorption onto GAC and ACM 1P are reported in [Figure 6.4](#). Raw activated carbon had a similar adsorption capacity for both nitrogen compounds: the indoline uptake was barely higher than that of quinoline. For example, at a quinoline concentration of 1000 mg/L (7.74 mmol/L), the molar adsorption capacity (quinoline molar weight: 129.16 mg/mmol) was 0.480 mmol/g, while at the same indoline concentration the molar indoline adsorption capacity (indoline molar weight: 119.16 mg/mmol) was 0.443 mmol/g. After modification, the presence of iron nanoparticles increases the indoline uptake to a greater extent. At an indoline equilibrium concentration of 1000 mg/L, the GAC had an adsorption capacity of 58.4 mg/g, whereas the ACM 1P (iron modified) removed 30% more. This synergistic effect of iron addition is observed also for the quinoline adsorption though to a lesser extent (about 6%), as can be seen in [Figure 6.4](#).

Table 6.2 Elemental content of studied materials.

Sample	Elemental content [%]							
	Al	Ca	Cu	Fe	K	P	Mg	Na
GAC	0.26	0.14	0.002	0.33	0.04	ND	0.019	0.266
ACM 1P	0.11	0.01	0.004	2.35	0.03	ND	0.003	0.004

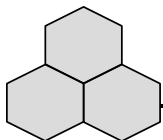
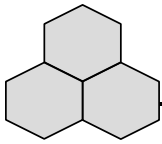


Table 6.3 Langmuir and Freundlich parameters and Standard deviation of adsorption experiments.

Adsorption isotherm	Langmuir parameters		R ²	Freundlich parameter		R ²	Std Desv
	b	Q _{max}		K	n		
GAC							
Single indoline	14.62	61.98	0.922	10.43	4.01	0.987	0.135
Single quinoline	6.42	64.62	0.944	5.51	2.98	0.988	0.059
Competitive indoline	9.55	47.90	0.980	9.26	4.54	0.978	0.009
Competitive quinoline	3.87	58.36	0.969	3.68	2.76	0.996	0.009
Thiophene indoline	1.28	78.01	0.957	0.64	1.62	0.982	0.97
Thiophene quinoline	22.75	62.7		1.66	2.1	0.991	0.96
ACM 1P							
Single indoline	62.09	74.32	0.943	16.93	4.55	0.978	0.318
Single quinoline	11.96	63.16	0.948	7.87	3.42	0.984	0.175
Competitive indoline	8.81	75.26	0.882	8.81	3.37	0.981	0.078
Competitive quinoline	5.69	59.21	0.965	5.04	3.03	0.993	0.022
Thiophene indoline	3.35	63.39	0.947	2.09	2.13	0.972	0.97
Thiophene quinoline	29.00	45.40	0.981	11.03	4.69	0.988	0.96



6.3.2.2 Competitive adsorption of indoline-quinoline

Figure 6.5 shows the adsorption isotherms of nitrogen compounds when indoline and quinoline are present at the same mass concentration at the beginning of the experiment. The indoline adsorption capacity of GAC and ACM 1P decreased to about 27 % and 11 %, respectively, compared to their corresponding single isotherm (Figure 6.3). This indicates that ACM 1P has a 32 % higher adsorption capacity (at 1000 mg/L) than GAC (Figure 6.4). The quinoline uptake decreased about 20% for both materials due to competitive adsorption; however, ACM 1P had a 9% higher adsorption capacity than GAC.

6.3.2.3 Effect of sulfur compounds on indoline and quinoline uptake

In order to study the effect of sulfur compounds on the denitrogenation capacity of carbon, several equimassic concentrations of quinoline and indoline were mixed with a constant sulfur concentration of 50 ppm, as mentioned in the experimental section. Simultaneously, the uptake of sulfur compounds (DBT and DMDBT) was monitored and correlated as a function of total nitrogen concentration in the starting solution.

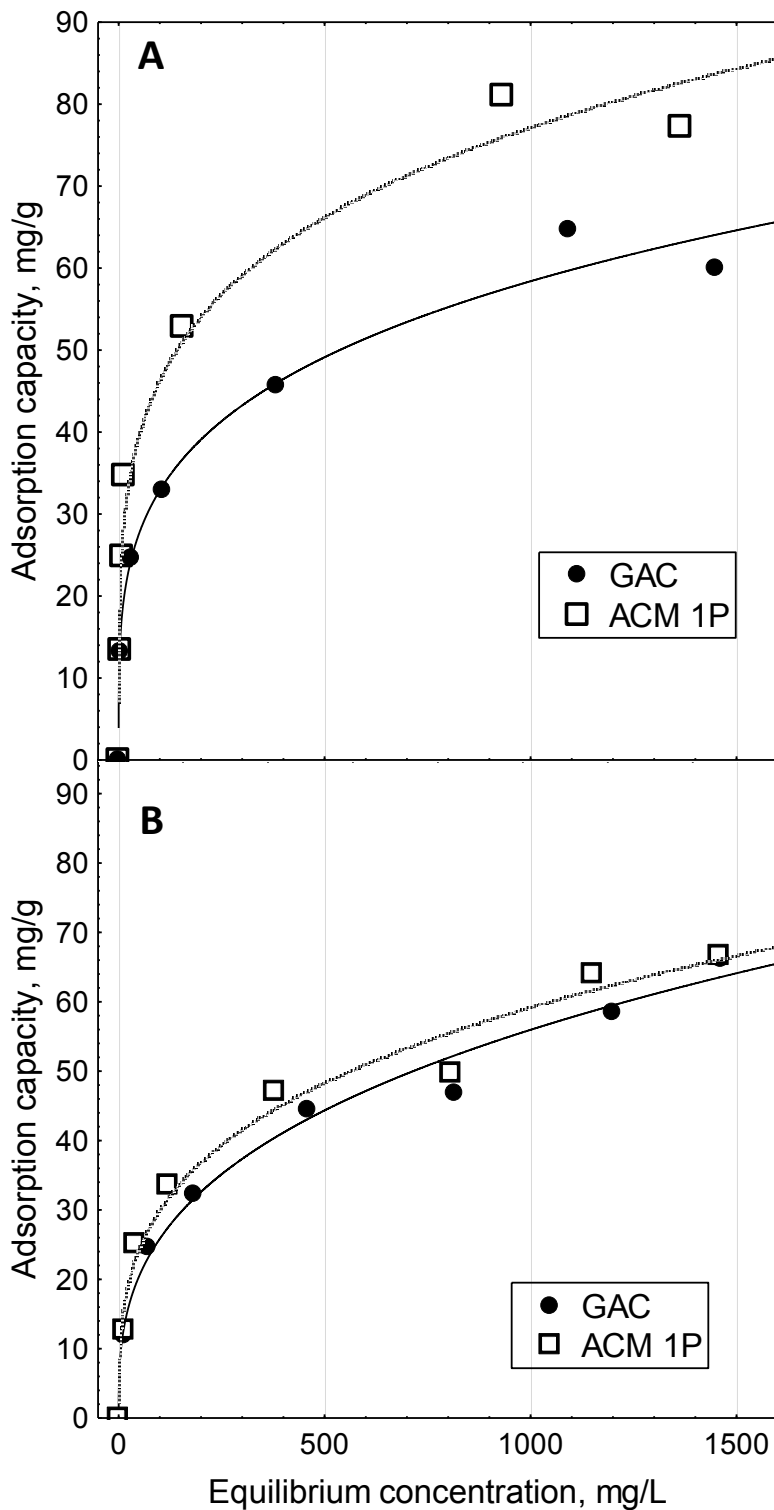
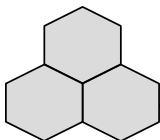


Figure 6.4 Single adsorption isotherms of **A)** indoline and **B)** quinoline over studied materials at 25°C.

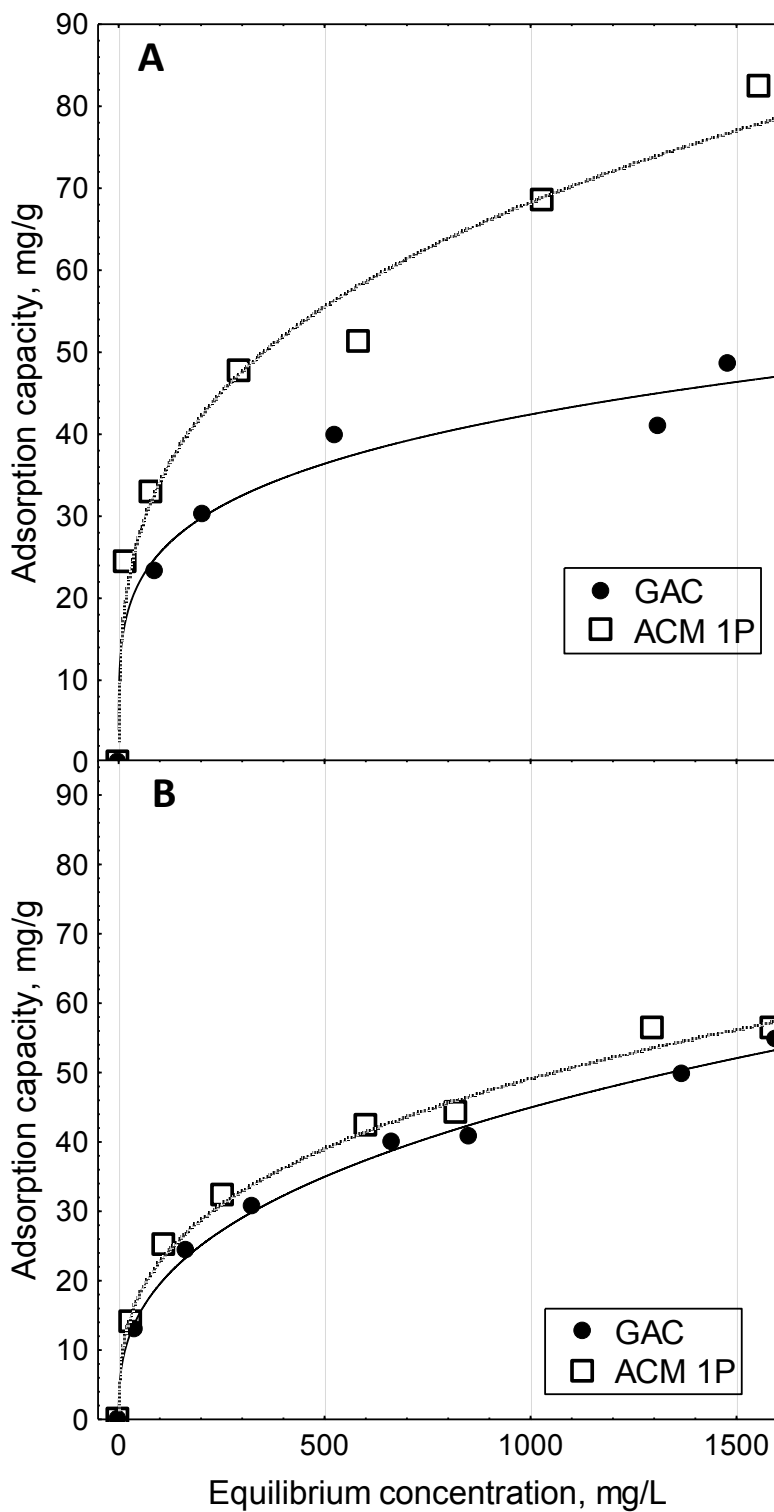
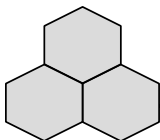


Figure 6.5 Competitive adsorption isotherms of **A)** indoline and **B)** quinoline at 25°C.

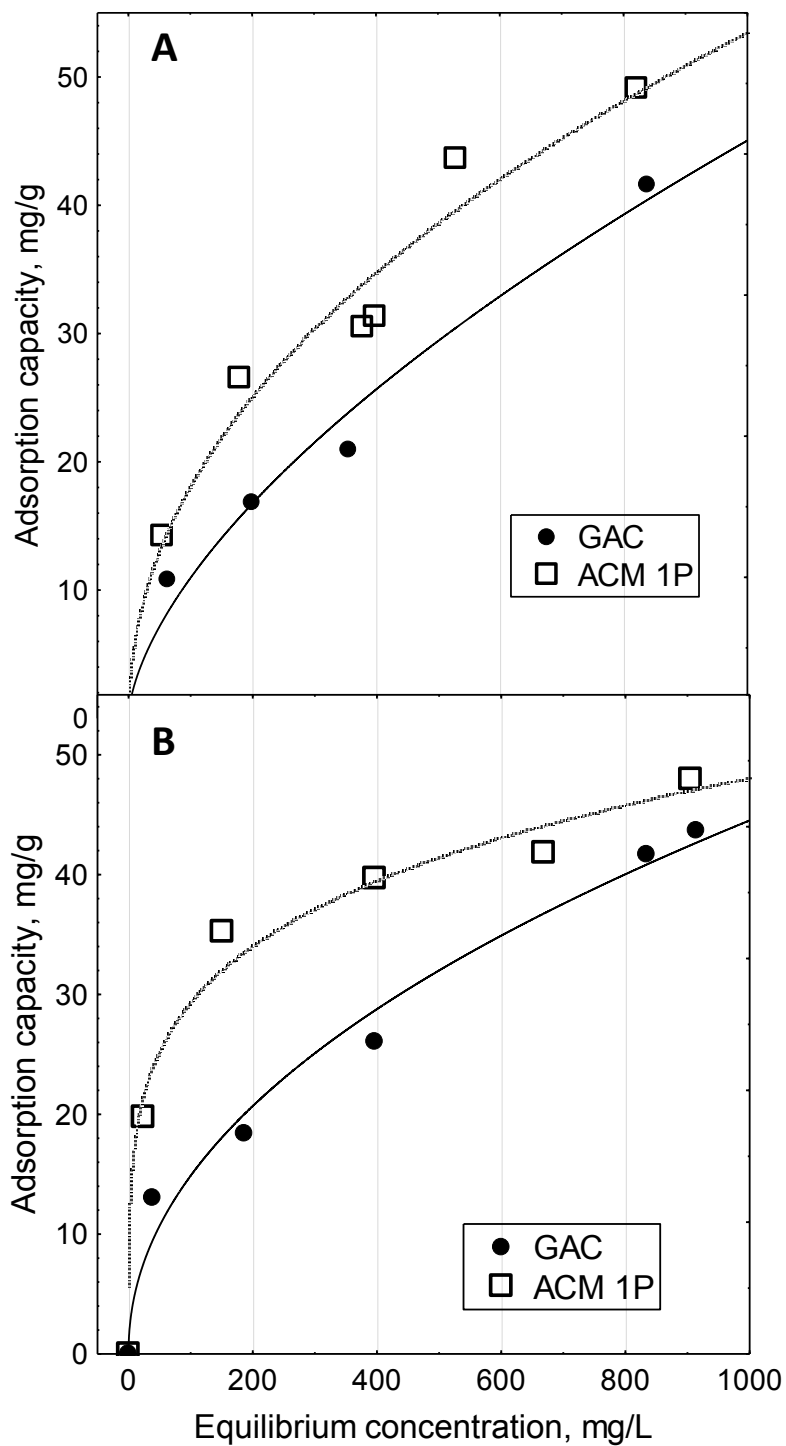
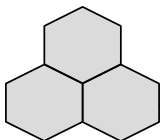
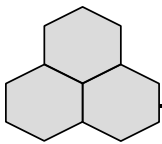


Figure 6.6 Adsorption isotherms of **A)** indoline and **B)** quinoline in competition with 50 ppm-S.



Denitrogenation results in Figure 6.6. showed that, when sulfur compounds are present in the starting solutions, the iron-modified material has a higher indoline and quinoline adsorption capacity than raw activated carbon. For indoline, at a concentration of 1000 mg/L, the ACM 1P adsorption capacity is 53.5 mg/g, while for GAC it is 45 mg/g, representing an increase of about 20%. Moreover, quinoline was removed in a larger quantity. Such an increase is greater at low indoline concentrations and became less intense at high concentrations. For example, at an equilibrium concentration of 500 mg-N/L the adsorption capacity of ACM 1P is 30% higher than that of GAC, whereas at 1000 mg-N/L the difference is just 8%.

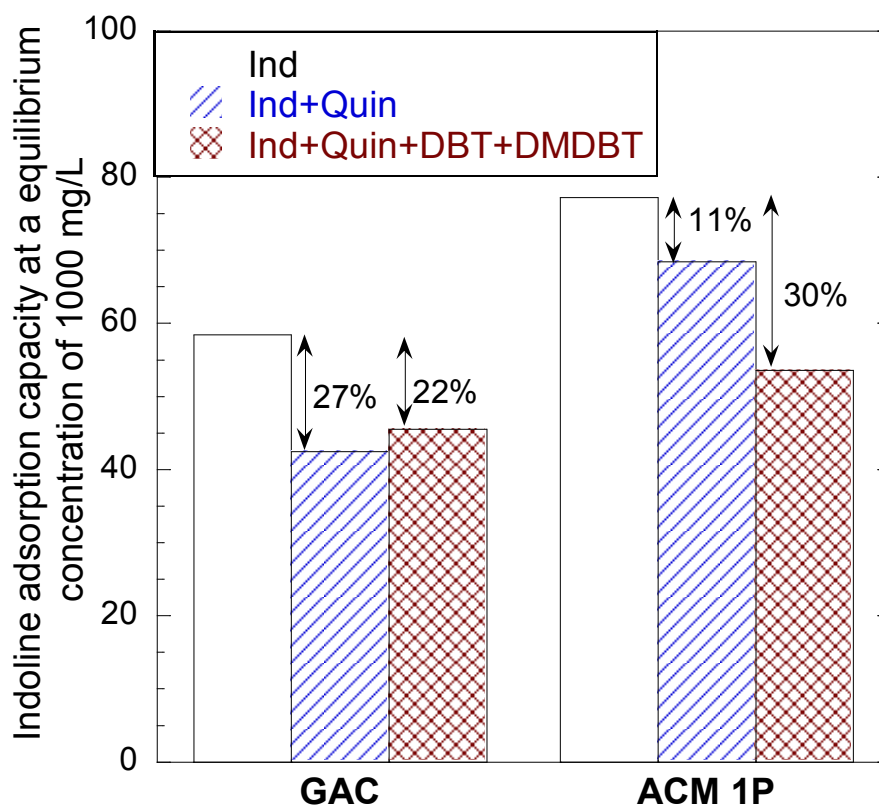


Figure 6.7 Adsorption capacities of indoline and quinoline of GAC and ACM 1P in presence of a nitrogen contaminant and two sulfur compounds.

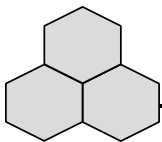
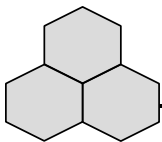


Figure 6.7 summarizes the adsorption capacity of quinoline and indoline in single and competitive experiments. The adsorption capacity of GAC for quinoline-indoline in competition was not affected by the presence of sulfur compounds, indicating that there is not competition for active adsorption sites between nitrogen and sulfur compounds. On the other hand, the decrease in indoline uptake for ACM 1P during sulfur competition was higher than when nitrogen compounds were present. These results suggest that in the presence of iron, sulfur compounds affected nitrogen compound uptake (mainly indoline). This might be attributed to competition of sulfur and nitrogen compounds for specific iron sites in carbon, or to hysteric hindrance of sulfur adsorbed molecules onto the surface of activated carbon.

On the other hand, the materials under study also showed considerable removal of sulfur compounds in the presence of different nitrogen concentrations (Figure 6.8). It was found that desulfurization strongly depends on nitrogen concentration. As the total nitrogen concentration (nitrogen from quinoline and indoline) increased in the model diesel fuel, the desulfurization capacity of both carbons (GAC and ACM 1P) decreased. Moreover, the iron-doped sample had a lower desulfurization capacity than the unmodified carbon. It has been reported that iron might enhance the desulfurization capacity of carbon [197,264]; however, those studies were conducted in the absence of nitrogen compounds. Our results indicate that iron is more akin to nitrogen than sulfur compounds. The decreased adsorption capacity of both sulfur compounds did not follow the same trend: the DBT uptake showed semi-linear behavior ($R^2 < 0.9$) for both materials, and the slope value (0.063



$\text{L}\cdot\text{mg}\cdot\text{mg}\cdot\text{N}^{-1}\cdot\text{g}^{-1}$) indicated that each milligram-per-liter of nitrogen increase caused a decrease of 0.063 mg of DBT per gram of material. At the highest nitrogen concentration (200 mg-N/L), the DBT adsorption capacity falls about 50% for the GAC and 66% for ACM 1P, compared with the experiments that did not contain nitrogen compounds.

On the other hand, the DMDBT adsorption capacity at the highest nitrogen concentration was 45% lower for GAC and 55% lower for ACM 1P than in the absence of nitrogen compounds. Moreover, as the nitrogen concentration increased the DMDBT adsorption capacity was rather more asymptotic than lineal, suggesting that at a very high nitrogen concentration (>200 mg/L), the DMDBT adsorption capacity of carbon materials will not be further reduced.

At the maximum nitrogen concentration, the total desulfurization and denitrogenation capacities of GAC were 5.08 mg-S/g and 10.12 mg-N/g, respectively, while for ACM 1P they were 3.33 mg-S/g and 11.5 mg-N/g. These results indicate that iron addition in activated carbons results in a higher denitrogenation capacity and in a lower desulfurization uptake. Because of this, we encourage the use of iron nanoparticles for enhancing the denitrogenation performance of adsorbent materials. The denitrogenation capacity in the presence of 50 ppm-S of iron modified carbon (0.821 mmol-N/g) was within the range of other carbon tested for diesel denitrogenation [191] and higher than other adsorbents such as activated alumina, aluminum silicate, and resins [265].

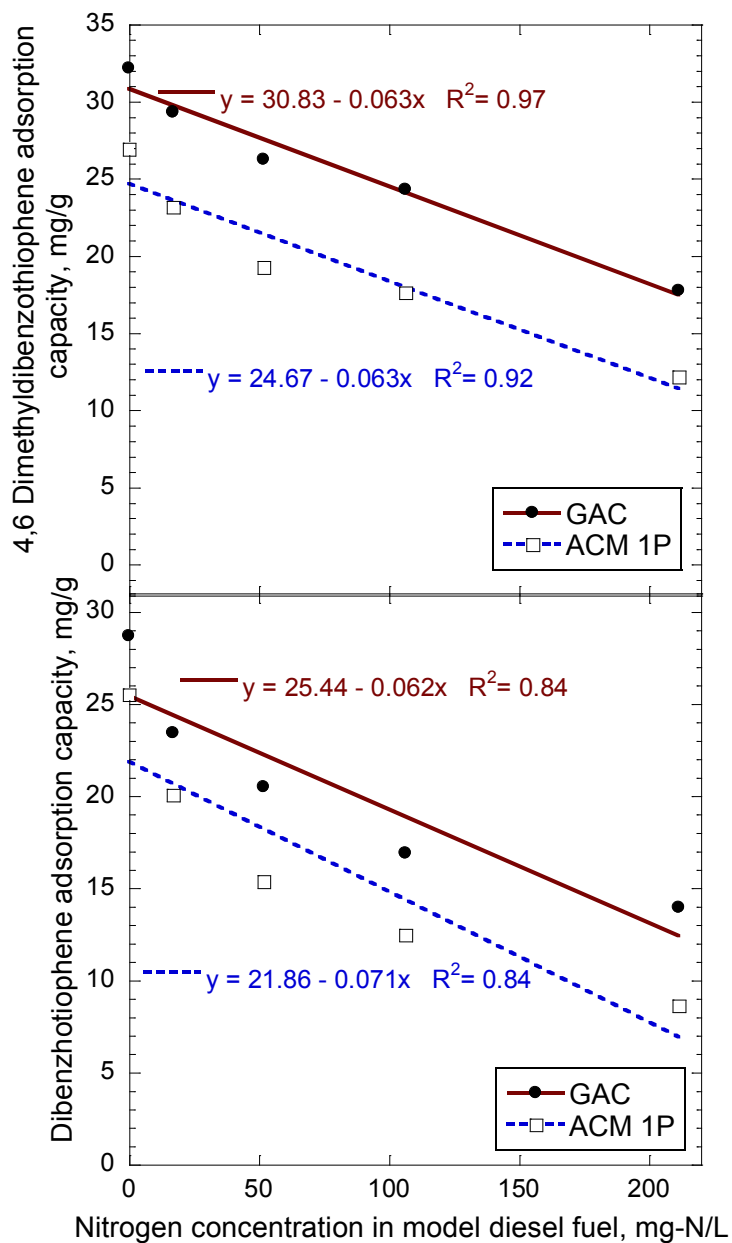
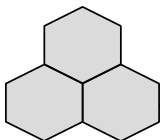
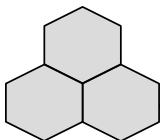


Figure 6.8 DBT and DMDBT adsorption capacities of carbon materials at several nitrogen concentrations.

It should be mentioned that the results reported herein did not take into consideration higher nitrogen concentration because the objective of our work was



to simulate usual nitrogen concentrations found in diesel fuel after hydrotreating [76,131].

6.3.3 ADSORPTION MECHANISM

Since both materials, GAC and ACM 1P, have almost the same textural properties, differences in adsorption capacity should be explained by chemical interactions between the material surface and the adsorbates.

In raw activated carbon, electronegative nitrogen may be bonded with either polar groups on the surface of carbon or with π - π interaction between quinoline aromatic ring and graphitic layers in carbon. Also, the surface of carbon contains oxygen groups like carboxylic and hydroxyl [266] that may promote the formation of hydrogen bonds with nitrogen [267]. Xiao et al. [131] reported that quinoline adsorption onto activated carbon is probably occurring by means of π - π interactions and hydrogen bonding, rather than by polar interactions with electronegative nitrogen.

The iron in the activated carbon is mainly present as a hydroxide [151,153,161] or an oxide [268,269] (collectively referred to as iron oxyhydroxides). Therefore, on iron-modified carbon, nitrogen molecules might be bonded on either the activated carbon or the iron oxyhydroxide surface. Since the presence of iron increases the indoline uptake to a higher extent than the quinoline uptake, it is believed that indoline is interacting mostly with the iron oxyhydroxides, whereas quinoline interacts mainly with the activated carbon sheets.

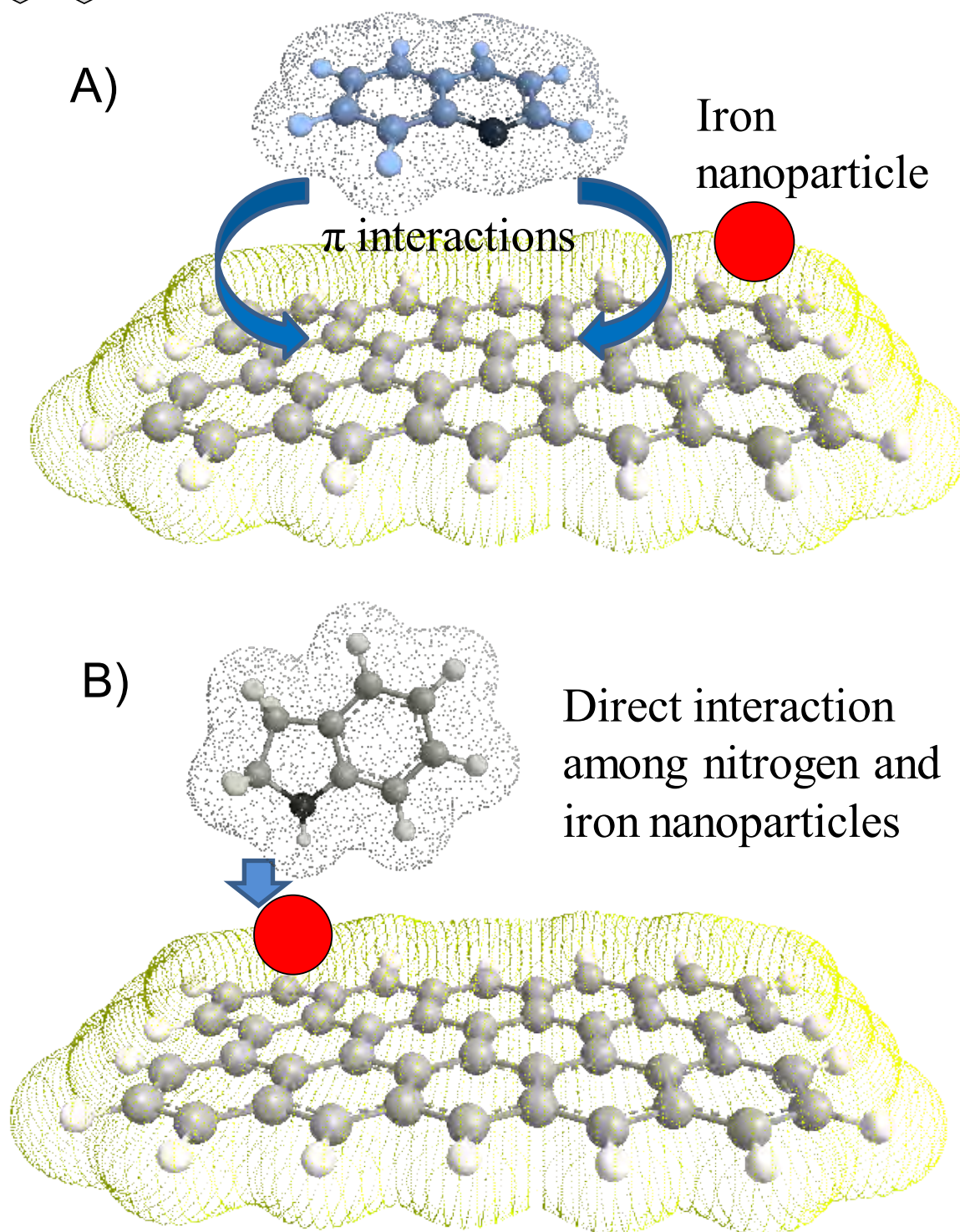
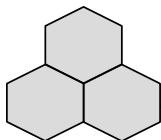


Figure 6.9 A) π - π interactions among quinoline and graphitic layers in carbon. B)

Nitrogen in indoline is more capable of interacting with iron nanoparticles.

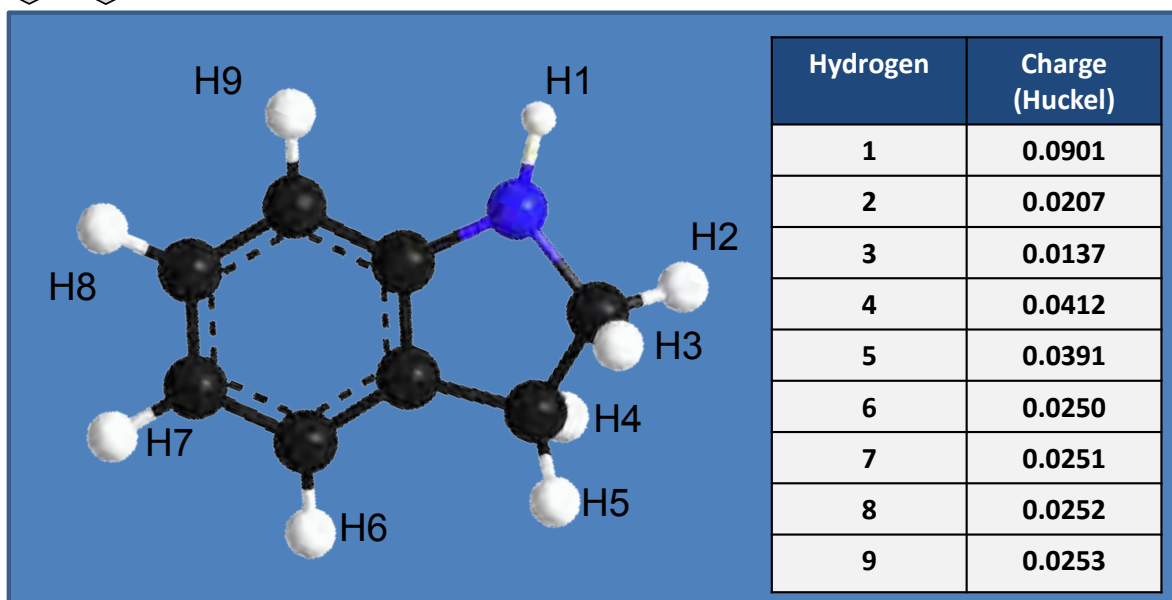
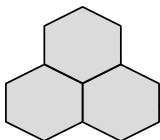
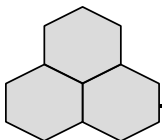


Figure 6.10 Charge of hydrogens in the indoline molecule, obtained in ChemBioDraw 12 (Hückel-charge calculation).

Due to their slightly basic chemical nature, nitrogen compounds were attracted to acidic surfaces [270], as is the case of the iron-modified sample. It is important to consider that quinoline is a planar molecule due to the sp^2 nitrogen configuration, while the sp^3 configuration of the indoline's nitrogen allows the rotation of the molecule, making polar interactions between the nitrogen and the carbon surface more feasible. Since quinoline approaches the carbon surface in a parallel manner, it is most likely that the predominant adsorption mechanism is governed by π - π interactions with carbon aromatic layers (Figure 6.9 A). On the other hand, since the indoline molecule approaches the adsorbent surface not only in a parallel manner (Figure 6.9 B), it is possible that nitrogen may be bonded with specific active sites. From all hydrogen atoms located in the indoline molecule, the one



next to the nitrogen atom has the higher charge and is more likely to form hydrogen bonds with the surface of carbon or iron oxyhydroxides (Figure 6.10).

6.4. CONCLUSIONS

Results indicated that iron-modified material has a higher adsorption capacity for nitrogen compounds than raw activated carbon. Of the two nitrogen compounds studied, indoline was more akin to iron particles.

Equimassic competition of quinoline and indoline is reflected in a decrease of about 30% in the uptake of both activated carbons; however, the adsorption capacity of the iron-modified carbon was 32% higher than that of GAC. Moreover, the iron-modified material has a higher capacity for nitrogen than for sulfur compounds. However, when sulfur is present in the starting solution, the iron-modified carbon has a 30% lower nitrogen adsorption capacity than GAC.

The increase in the uptake of indoline by iron-containing materials could be related to the non-planar shape of this molecule, which allows direct interaction among nitrogen and oxygen-containing surface groups. It is also hypothesized that such interactions might be governed by hydrogen bonding.

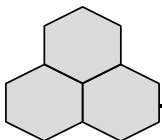
The results reported in this Chapter demonstrated that iron-modified materials are more effective for the removal of nitrogen than for sulfur compounds, however, the uptake of sulfur compounds is considerable, therefore, the modified materials reported herein are very attractive for the removal of nitrogen and sulfur compounds from diesel fuel.

Chapter 7

Final Remarks

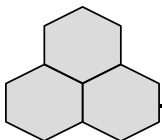
Arsenic and sulfur are prioritant pollutants whose presence determines the quality of water and air systems respectively. Due to the accelerated increase in anthropological activities and strict environmental regulations, nowadays the removal of those pollutants requires the implementation of highly efficient technologies. Arsenic removal and desulfurization (of gas and diesel fuel) by activated carbon is an attractive option for pollution control. However, some limitations related to the capacity and selectivity of activated carbons must be overcome.

The development of material sciences and especially in the field of nanotechnology allows to design and tailor materials so that their enhanced properties might be employed in several fields. This is the case of functionalized activated carbon with reactive iron oxyhydroxides nanoparticles, which have a large reactive surface area with special adsorptive properties.



One of the greatest challenges of iron nanoparticles formation is controlling the hydrolysis of Fe(III) that corresponds to a very low energy state and therefore nucleation and growth of Fe colloids are very spontaneous. Such constraints can be avoided by using complexing anions such as PO_4 that build stable bonds with Fe atoms and control the formation of Fe colloids.

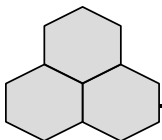
The results showed in [Chapter 2](#) demonstrated that by using phosphate during the FeCl_3 forced hydrolysis it is possible to reduce the particle size (from 30 to around 2 nm) of anchored IOH on activated carbon. The role of phosphate as a capping agent during activated carbon modification is proposed to be a conjunction of various effects: first, a change in the distribution of species in solution, promoting the formation of iron-hydroxyl rather than iron-chloride complexes that are easier to dehydroxylate. Second, the presence of a larger amount of free anions that stabilize the positive surface charge of activated carbons. During nucleation the positively charged iron aquo-complexes coordinate with oxygen functionalities in activated carbon using them as nucleation centers, and then a decrease in the positive charge of activated carbons leaves a higher amount of coordinated iron moieties. Third, by means of hydrolysis, olation, and propagation reactions the IOH start to polymerize; in order to grow, the dehydroxilated iron species need to attract iron-complexes; if phosphate species are present in solution (HPO_4^{2-}), those might be adsorbed instead of iron-complexes allowing the particle to become stable at smaller particle sizes and to condensate on the surface of the activated carbon. After that, phosphate is removed during the washing step leaving available the sites for molecules adsorption.



The decrease in IOH particle size depends on the thermodynamic conditions of the iron forced hydrolysis and on the concentration of phosphate during the materials synthesis. As the PO_4/Fe molar ratio (MR) increases there is an increase in the arsenic(V) uptake reaching a plateau at a MR of 1. The concentration of phosphate does not increase the mass percentage of iron incorporated on activated carbon, since as mentioned before, phosphate restricts the growing of iron oxyhydroxides on the surface of activated carbon. Therefore, the increase in adsorption capacity can be attributed to the decrease in the iron oxyhydroxides particle size that provides a large reactive surface area capable of efficiently remove arsenic(V) from aqueous solution; when the surface coverage of adsorbed molecules was plotted against PO_4/Fe molar ratio, a lineal trend was observed, indicating that, as phosphate increases in solution there is a better coverage of the carbons surface by arsenic(V) adsorbed molecules. As a result of the IOH particle size decrease an enhancement of 69% in the arsenic(V) uptake was recorded.

On the other hand, it has been reported that iron-modified activated carbons having diverse properties exhibit different arsenic adsorption capacities; therefore the effect of the intrinsic properties of activated carbons on the arsenic(V) adsorption capacity was studied ([Chapter 3](#)). In order to have physicochemical differences among adsorbents, several ACs were oxidized and then modified with iron to promote changes on their textural and chemical properties.

Since iron oxyhydroxides nucleates on the oxygen groups present on the surface of activated carbons, the incorporation of oxygen moieties allowed a higher loading of iron on the activated carbons surface; however, this increase does not cause an

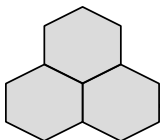


enhancement in arsenic(V) uptake, because when activated carbon is oxidized its surface contains a much higher concentration of negative charges that reject anions. This restricts the coordination of arsenate molecules with the incorporated iron oxyhydroxide nanoparticles.

A fitting equation predicts that the best conditions for arsenic removal are a basic surface charge to efficiently attract anions and an iron content of about 1%, probably due to a better coverage of the surface of activated carbon by iron nanoparticles. Moreover, it was found that the most important parameters of activated carbons for arsenic(V) removal were: first the point of zero charge that contributes in 52%, followed by the iron content that enhances the arsenic(V) uptake by 36%. Demonstrating that arsenic(V) removal by activated carbons depends in a greater extent on the adsorbents surface charge than in the amount of iron incorporated.

It was also proposed that the adsorption of arsenic(V) on modified activated carbons occurs in two stages: first an electrostatic attraction of negatively charged ions for the positively charged surface of activated carbon, followed by the specific adsorption of arsenates by interchange of ligands between hydroxyl groups in the arsenate aquo-complex and the incorporated iron oxyhydroxides nanoparticles.

Besides what was reported in Sections 2.5 and 3.5 in Chapters 2 and 3, the arsenic adsorption capacity of the best material (ACM 1P) can be compared with the results of other studies reported in the literature. Table 7.1 contains the



adsorption capacities of selected studies that were conducted in similar conditions as those reported in this study (pH 7 and As(V) concentration range in ppb level).

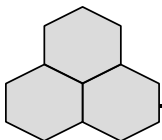
Table 7.1 Arsenic(V) adsorption capacities reported by iron-modified activated carbon.

Adsorption capacity [mg/g]	Reference
0.027	151
2	188
4.8	202
0.023	203
0.1	185
1.94	141
1.25 ¹	This work
5 ²	

1 At an As(V) equilibrium concentration of 1 mg/L

2 At an As(V) equilibrium concentration of 9 mg/L.

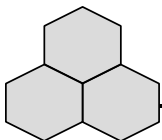
At an arsenic concentration of 1.0 mg/L the adsorption capacity of the material synthesized in this research is around 1.25 mg/g, greater than that of other materials reported in the literature with higher iron contents [151,185], but lower than other adsorbents modified by iron precipitation-impregnation. Gu et al. [202] prepared AC-Fe composites by oxidation-impregnation of a FeCl₂ salt, they found a remarkable adsorption capacity of 3.5 mg/g, at 1.0 mg/L measured at pH 4.7, with a material that had an iron content of 2.34%, higher than in the AC of this study. Moreover, Zhang et al. [141] obtained a similar As(V) adsorption capacity of 1.94 mg/g, with an activated carbon modified by FeCl₃ (impregnation), with an iron content of 8%. It is worth mentioning that the materials produced in this work, with



around 1% of iron content, have similar As(V) adsorption capacities as the reported by Lodeiro [187] with a 32% of iron.

However for a long-term operation it is vital to evaluate the material stability in column experiments. Considering a typical dynamic adsorption experiment with a packed volume of 10 cm³, a retention time of 30 min and a density of modified activated carbon of 0.45 Kg/L, the passed flow is 20 mL/h. Considering a natural water with an arsenic concentration of 50 µg/L, the As(V) adsorption capacity of ACM 1P is 0.5 mg/g, then the lifetime of the adsorbent packed bed will be 187.5 days. the latest without considering a loss in adsorption capacity in this time period. Most of the loss in arsenic(V) adsorption capacity could be due to arsenic leaching caused by IOH nanoparticles aging. Since IOH nanoparticles are attached to the AC surface by means of covalent bonds, then the aging of immobilized IOH nanoparticles by atom rearrangement is barely possible; on the other hand, at the pH of natural groundwater (6.5-8) iron nano particles will hardly undergo dissolution-recrystallization, then a great stability of ACM 1P is expected even in long-term operations.

Regarding the final destination of the exhausted modified-activated carbon, the adsorbent regeneration is not recommended, and hence its disposal is preferred. Therefore it is necessary to determine the chemical stability of the exhausted material with the objective of safe disposal. This information might be evaluated with the total leaching procedure (TLP) that provides valuable information on disposal strategies, which are available in the literature.



On the other hand, the potential of gas stream desulfurization by iron-modified activated carbons was proved in [Chapter 4](#). A gas stream of SO_2 was passed through a packed bed column containing raw and iron containing activated carbon modified with two iron particle sizes. The results showed that water presence is crucial for promoting the reactive adsorption of SO_2 . There was an increase in SO_2 uptake only when very small nanoparticles were present on the surface of the activated carbon. Large iron nanoparticles block the ultramicropores decreasing the accessibility of the active sites and consuming oxygen that rest adsorption centers for SO_2 molecules. Iron nanoparticles of about 3-4 nm provide highly dispersed adsorption sites for SO_2 molecules and thus increase the adsorption capacity of about 80%. When the SO_2 adsorption per surface unit was calculated, the material with the smallest iron nanoparticles was clearly superior.

It was proposed that during SO_2 reactive adsorption, adsorbed molecules are first oxidized by chemisorbed oxygen on the surface of the activated carbon forming H_2SO_4 and then these molecules react with iron, and $\text{Fe}_2(\text{SO}_4)_3$ is obtained on the surface. Also, the incorporation of iron oxyhydroxide nanoparticles on ACs not only leads to an increase of the SO_2 adsorption capacity, but also promotes less acidification of the adsorbent reducing the problem of the deuration system when adsorbing SO_2 .

The obtained adsorption capacity of ACM 1P can be compared with other commercial activated carbon materials as shown in [Table 7.2](#).

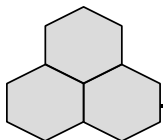
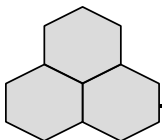


Table 7.2 Adsorption capacities of SO₂ by commercial activated carbons, taken from Reference [47].

Material	SO ₂ capacity [mgSO ₂ /gCA]
Centaur (catalytic carbon)	164
Vapure 612 (bituminous)	64.3
BAX-1500 (bituminous)	33.9
S208C (coconut shell)	48.2
VPR (polymer carbon)	24.6
ACM 1P	66 (this study)

The iron modified activated carbon also showed an important performance when removing sulfur compounds from diesel ([Chapter 5](#)). The results demonstrated that the iron oxyhydroxide nanoparticles anchored on activated carbon promote the uptake of dibenzothiophene (DBT) and 4,6 dimethyldibenzothiophene (DMDBT) from a simulated diesel fuel. This was observed only when low aromatic concentrations were employed (~ 2% w/w) because at this low aromatics concentration iron oxyhydroxides may disturb the parallel orientation of aromatic molecules adsorbing in activated carbon by means of the $\pi-\pi$ interactions that gains strength when higher concentrations of aromatics are present in solution, and also the high concentration gradient between the thiophenes and aromatics, makes the specific interactions between the former species and iron nanoparticles insignificant.

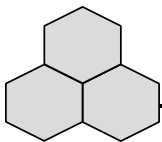


The compound that inhibits the sulfur compounds uptake to a higher degree is naphthalene (di-aromatic), due to the large number of carbon atoms in Sp² configuration that strongly adsorb over activated carbon creating steric hindrance for sulfur compounds to adsorb.

It was also determined that the adsorbed sulfur molecules interact with iron oxyhydroxides in several ways, sulfoxides and sulfones of DBT and DMDBT were identified in exhausted modified materials, suggesting that iron oxyhydroxide nanoparticle in activated carbon promotes further oxidation of adsorbed compounds that remain strongly adsorbed by polar-polar interactions and acid-base reactions with activated carbon.

Finally, in [Chapter 6](#), it was shown that nitrogen compounds (quinoline and indoline) greatly affected the uptake of DBT and DMDBT by activated carbons. This decrease in sulfur compounds uptake was higher in iron-modified material, revealing that the incorporated iron oxyhydroxide nanoparticles in activated carbon have a larger affinity for nitrogen than for sulfur compounds in diesel fuel.

The incorporation of iron nanoparticles promotes the uptake of indoline to a higher extent than the quinoline. It was hypothesized that the enhancement in the indoline uptake is linked to the non-planar shape of the indoline molecule given by the Sp³ hybridization of the non-aromatic nitrogen that allows the indoline molecule to rotate and adsorb by polar interactions or hydrogen bond on the surface of the iron oxyhydroxide nanoparticles and/or the activated carbon; on the other hand, the flat



shape of the quinoline molecule has a higher preference for adsorbing onto the graphitic layer of activated carbon by means of π - π interactions.

The obtained desulfurization capacity of ACM 1P was not as high as that of other materials, (see [Table 1.7](#)); however, the AC selectivity was high even at great aromatic concentration in MDF as shown in [Table 5.2](#). This means that the incorporation of iron into the matrix of highly efficient materials of desulfurization can be used as a strategy for increasing its selectivity. Moreover, since it was demonstrated that iron nanoparticles are more akin to nitrogen than to sulfur aromatic molecules, then the iron-modified material might be employed in a diesel denitrogenation stage prior to adsorptive desulfurization or hydrodesulfurization in a system similar to the one proposed by Moshida in [Figure 1.3](#).

The results presented in this doctoral thesis demonstrated the potential of the iron-modified activated carbon for the removal of arsenic from aqueous solution and sulfur from gas phase, and for the desulfurization and denitrogenation of model diesel fuel. This represents a significant advance in the development of efficient adsorbents, based on nanotechnology to remove key pollutants from liquid and gas phases.

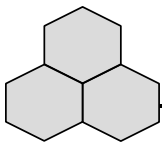
Chapter 8

Final Conclusions, Perspectives, and Scientific Products.

The Recent advances in nanotechnology and material science enable designing highly efficient adsorbents capable of removing several pollutants in various systems. This is the case of the functionalized activated carbon with iron oxyhydroxide nanoparticles, which combines the textural properties of activated carbon and the reactivity of iron oxyhydroxides.

This study demonstrated that it is possible to decrease the particle size, up to 2 nm, of iron oxyhydroxides anchored on activated carbon by using phosphate as capping agent during the ferric chloride forced hydrolysis, which in turn allowed the modified adsorbent to uptake various adsorbates from liquid and gas phase.

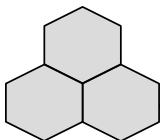
During the activated carbon modification, as the phosphate concentration increases the arsenic(V) adsorption capacity rises, reaching a plateau at a MR of 1. The optimum iron-modified activated carbon has a large surface area of 900 m²/g and a low iron content of about 1%, consisting in small nanoparticles of about 2 nm. Moreover, the decrease in iron particle size, from 30 to 2 nm, anchored on activated carbon brings an increase in arseni (V) uptake of about a 60%.



It was proven that a basic activated carbon charge is needed to obtain an efficiently adsorbent to remove arsenic from water, since a negatively charge surface repels arsenate anions preventing its specific adsorption on iron oxyhydroxide nanoparticles. The point of zero charge of the iron-modified activated carbon contributes in 52% to the arsenic(V) adsorption capacity, meanwhile the iron content enhances the arsenic(V) uptake in 36%. It is also proposed that two adsorption mechanisms can be carried out simultaneously in iron-modified activated carbons: a ligand interchange between arsenates and iron oxyhydroxide nanoparticles and electrostatic attraction with basic surface groups.

On the other hand, the functionalization of activated carbon with iron increases its reactive adsorption capacity of sulfur dioxide from gas phase. A higher number of oxygen-containing groups are embedded on the surface of activated carbon when the material is functionalized with iron oxyhydroxide nanoparticles in the presence of capping agent. As a result of the activated carbon functionalization a 80% increase in the dynamic uptake of SO_2 was recorded. Furthermore the incorporation of reactive iron oxyhydroxides enables the formation of $\text{Fe}_2(\text{SO}_4)_3$ on the adsorbents surface, which dismisses the acidification of the medium after SO_2 elimination.

The functionalization of activated carbons with iron nanoparticles was also effective for the oxidation of adsorbed sulfur compounds from model diesel fuel. Iron incorporation serves a dual purpose: it decreases the uptake of mono- and di-aromatics by disturbing the parallel orientation of molecules for adsorbing in activated carbon, and impedes the energy-efficient localization of the aromatic ring



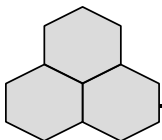
via π - π interactions and provides an oxidation center for adsorbed molecules; these two effects improve the selectivity of iron-modified activated carbon for sulfur compounds. However, in order to achieve such an improvement in the desulfurization performance, the fuel needs to have low mono and di-aromatic concentrations.

Finally, the presence of the nitrogen compounds indoline and quinoline decreases the adsorption capacity of the sulfur compounds dibenzothiophene and 4,6 dimethyldibenzothiophene by iron-modified activated carbon in model diesel. This is because iron oxyhydroxides adsorb non-planar nitrogen molecules as indoline. This study also suggests that it is feasible to perform denitrogenation and desulfurization of diesel fuel with the same material in a single or simultaneous stage.

8.2 PERSPECTIVES

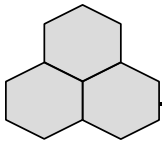
The results presented in this doctoral thesis demonstrated the potential application of iron-modified activated carbon to remove arsenic from water, SO_2 from gas, and sulfur and nitrogen compounds from diesel. However, there are several works that can be conducted for a better understanding of the interactions iron-oxygen-carbon surface and for the adsorption process.

In this thesis was postulated that oxygen acts as a nucleation center for the iron oxyhydroxide nanoparticles growing; this was strengthened in Chapter 2 when the



oxidation of carbon caused an increase of iron mass incorporation. However there are several questions related to this point: in which of the groups in activated carbon the iron is interacting to a greater extent. Due to the high reactivity of hydroxyl groups, the presence of iron oxyhydroxide nanoparticles might interfere the quantification of groups by Boehme and potentiometric titrations, hence, another spectroscopic tool should be used to elucidate which surface groups of carbon are associated to iron. For example, the use of X-Ray Absorption spectroscopy techniques as Extended X-Ray Absorption Fine Structure (EXAFS) and X-ray Absorption Near Edge Structure (XANES) might provide information about the second and third neighbors of iron and help to determine which of the oxygen groups in activated carbon promotes its incorporation. With this information, the selective incorporation of surface groups that promote the iron incorporation in AC might enhance the anchorage of iron oxyhydroxide nanoparticles.

Another question is what of the iron oxyhydroxide allotropic phases are present in the activated carbon surface after modification without and in the presence of the capping agent. Since the clarity of XRD data was not enough to give a clear conclusion about the crystal phases involved during activated carbon modification, due to the highly amorphous degree of the material and the low iron percentage in AC, the implementation of Mössbauer spectroscopy that is very sensitive to iron oxyhydroxides, might provide useful information about the kind of crystal structure anchored over the surface of the activated carbon. This could clarify if the

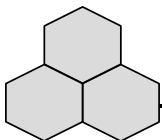


implementation of the capping agent also promotes a change in the phase of the iron particles incorporated on AC.

On the other hand, there are some works related to the arsenic removal that must be carried out in order to evaluate the feasibility of implementing the synthesized material in industrial scales, those studies are:

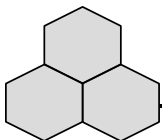
- Obtain the kinetics of adsorption of As(V) from aqueous solution over the modified activated carbon, and obtain an equation that allows to describe the most efficient retention time that should be employed for achieving a complete removal of arsenic(V) from aqueous solution.
- Once the adsorption kinetics is known then it is necessary to determine the volume that will be treated per mass of modified activated carbon in dynamic conditions. For that will be necessary to perform the adsorption of arsenic(V) in packed columns to obtain the breakthrough and saturation points. This study can be complemented by preparing a mixture of several anions (as PO_4^{3-} , SO_4^{2-} and NO_3^-) and study their interference during arsenic(V) removal: the inlet and effluent streams should be analyzed for pH, temperature and organic matter. Finally, it is necessary to perform the dynamic adsorption of arsenic(V) from well polluted water and to evaluate the performance of the modified material in a real scale.

Related to desulfurization experiments, there are other studies that will help to reinforce the results of this thesis and that could contribute to the understanding of the reactive desulfurization process and to the development of highly efficient materials for diesel purification. The adsorbents porosity is a key factor during



adsorptive desulfurization that is also modified with the decrease of the iron particle size; therefore, the study of the iron nanoparticle size during sulfur compounds uptake from diesel fuel might lead to reach an iron particle size and pore structure that maximizes the desulfurization of diesel fuels.

As demonstrated in Chapters 5 and 6, the presence of naturally present aromatic and nitrogen compounds in diesel affects the uptake of sulfur compounds, therefore it is important to study how the presence of other compounds as additives and moisture might hinder the desulfurization and denitrogenation performance of the activated carbon, and determine if the presence of iron oxyhydroxide nanoparticles attenuate this inhibition. This study can be accompanied for a survey of the denitrogenation of other compounds as indole and aniline that also are present in hydrotreated diesel. Also, if it is demonstrated that iron-modified materials have a larger capacity for the most representative nitrogen compounds rather than sulfur compounds, then a two stages denitrogenation-desulfurization process might be proposed, in which nitrogen compounds might be adsorbed in a first stage by iron modified activated carbon followed for a selective desulfurization in a second stage as shown in [Figure 1.3](#).



8.3 SCIENTIFIC PRODUCTS

8.3.1 LIST OF PUBLICATIONS

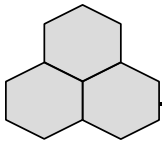
Arcibar-Orozco, J.A., Avalos-Borja, M., Rangel-Mendez, J.R., Effect of phosphate on the particle size of ferric oxyhydroxides anchored onto activated carbon: As(V) removal from water, *Environmental Science and Technology*, 2012, 46 (17), 9577-9583.

Arcibar-Orozco, J.A., Rangel-Mendez, J.R., Bandosz, T.J., Reactive adsorption of SO₂ on activated carbons with deposited iron nanoparticles, 2013, *Journal of Hazardous Materials*, 246-247, 300-309.

Arcibar-Orozco, J.A., Rangel-Mendez, J.R., Bandosz, T.J., Desulfurization of model diesel fuel on activated carbon modified with iron oxyhydroxide nanoparticles: Effect of tert-butylbenzene and naphthalene concentrations, 2013, *Energy and Fuels*, 27 (9), 5380-5387.

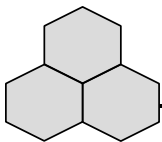
Arcibar-Orozco, J.A., Rangel-Mendez, J.R., Model diesel denitrogenation by modified activated carbon with iron nanoparticles: Sulfur compounds effect, 2013, *Chemical Engineering Journal* 230, pp. 439-446.

Arcibar-Orozco, J.A., Delgado-Balbuena J., Rios-Hurtado J.C., Rangel-Mendez, J.R., Influence of iron content, surface area and charge distribution in the arsenic removal by activated carbons, submitted to *Journal of colloid and interface science*.



8.3.2 ATTENDANCE TO CONFERENCES

- Participation in the "tercer foro interlocal de ciudades sustentables", San Luis Potosi, SLP Mexico 2011.
- Annual World conference on carbon 2011 in Shanghai China, with the oral presentation: "Influence of phosphate on the anchorage of nanoparticles of iron hydro(oxides) onto activated carbon and their effect on the arsenic(V) adsorption in a aqueous solution" and conference proceedings.
- First national conference of the IPICYT (2011) with the oral presentation: "Decrease of oxyhydroxide particle size onto activated carbon for arsenic removal". San Luis Potosi, SLP, Mexico.
- International Water Association-Mexico congress (Young water professionals) 2013 in San Luis Potosi, with the oral presentation "Enhanced arsenic(V) removal by modified activated carbon with iron oxyhydroxide nanoparticles".
- Annual World conference on carbon 2013 in Brazil, Rio de Janeiro, with the oral presentation: Effect of iron nanoparticles anchored on activated carbon in the desulfurization of model diesel fuel, and the poster: Removal of SO₂ by iron modified carbons: Effect of iron particle size.
- Second national conference of the IPICYT (2013) with the oral presentation: "Effect of iron nanoparticles anchored on activated carbon in the desulfurization of model diesel fuel". San Luis Potosi, SLP, Mexico.

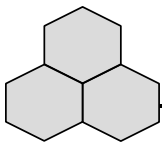


8.3.3 CONFERENCES PROCEEDINGS

Arcibar-Orozco, J.A., Rangel-Mendez, J.R., Influence of phosphate on the anchorage of nanoparticles of iron hydro(oxides) onto activated carbon and their effect on the arsenic(V) adsorption in aqueous solution, Annual World conference on carbon 2011, Shanghai, China.

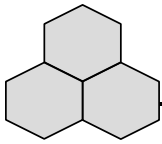
Arcibar-Orozco, J.A., Rangel-Mendez, J.R., Bandosz, T.J., Effect of iron nanoparticles anchored on activated carbon in the desulfurization of model diesel fuel, Annual World conference on carbon 2013, Rio de Janeiro, Brazil.

Arcibar-Orozco, J.A., Rangel-Mendez, J.R., Bandosz, T.J., Removal of SO₂ by iron modified carbons. Effect of iron particle size, Annual World conference on carbon 2013, Rio de Janeiro, Brazil.

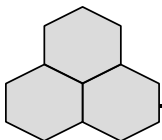


References

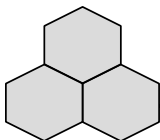
- [1] Bhattacharjee, Y., A Sluggish Response to Humanity's Biggest Mass Poisoning, *Science*, **2007**, 315, (5819), 1659-1661.
- [2] Mandal, B. K.; Suzuki, K. T., Arsenic round the world: a review, *Talanta*, **2002**, 58, (1), 201-235.
- [3] Berg, M., et al., Arsenic Contamination of Groundwater and Drinking Water in Vietnam: A Human Health Threat, *Environ. Sci. Technol.*, **2001**, 35, (13), 2621-2626.
- [4] Harvey, C. F., et al., Arsenic Mobility and Groundwater Extraction in Bangladesh, *Science*, **2002**, 298, (5598), 1602-1606.
- [5] Nordstrom, D. K., Worldwide Occurrences of Arsenic in Ground Water, *Science*, **2002**, 296, (5576), 2143-2145.
- [6] Chowdhury, U. K., et al., Groundwater arsenic contamination in Bangladesh and West Bengal, India, *Environ. Health Perspect.*, **2000**, 108, (5), 393-397.
- [7] Nickson, R., et al., Arsenic poisoning of Bangladesh groundwater, *Nature*, **1998**, 395, (6700), 338-338.
- [8] Smith, A. H., et al., Contamination of drinking-water by arsenic in Bangladesh: a public health emergency, *Bull World Health Organ*, **2000**, 78, (9), 1093-103.
- [9] Nickson, R. T., et al., Mechanism of arsenic release to groundwater, Bangladesh and West Bengal, *Appl. Geochem.*, **2000**, 15, (4), 403-413.



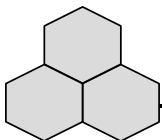
- [10] Berg, M., et al., Magnitude of arsenic pollution in the Mekong and Red River Deltas — Cambodia and Vietnam, *Sci. Total Environ.*, **2007**, 372, (2–3), 413-425.
- [11] Hanh, H. T., et al., Community exposure to arsenic in the Mekong river delta, Southern Vietnam, *J. Environ. Monit.*, **2011**, 13, (7), 2025-2032.
- [12] Wongyai, V. N. B. K., Environmental fluxes of arsenic from lignite mining and power generation in northern Thailand, *Environ. Geol.*, **2002**, 41, (8), 883-888.
- [13] Smedley, P. L.; Kinniburgh, D. G., A review of the source, behaviour and distribution of arsenic in natural waters, *Appl. Geochem.*, **2002**, 17, (5), 517-568.
- [14] Choong, T. S. Y., et al., Arsenic toxicity, health hazards and removal techniques from water: an overview, *Desalination*, **2007**, 217, (1-3), 139-166.
- [15] Hughes, M. F., Arsenic toxicity and potential mechanisms of action, *Toxicol. Lett.*, **2002**, 133, (1), 1-16.
- [16] Nagase, Y.; Silva, E. C. D., Acid rain in China and Japan: A game-theoretic analysis, *Reg Sci Urban Econ*, **2007**, 37, (1), 100-120.
- [17] Larssen, T., et al., Acid Rain in China, *Envir. Sci. Technol.*, **2006**, 40, (2), 418-425.
- [18] Xie, S., et al., Investigation of the effects of acid rain on the deterioration of cement concrete using accelerated tests established in laboratory, *Atmos. Environ.*, **2004**, 38, (27), 4457-4466.



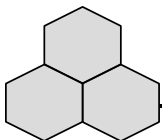
- [19] Kan, H. D., et al., Short-term association between sulfur dioxide and daily mortality: The Public Health and Air Pollution in Asia (PAPA) study, *Environ. Res.*, **2010**, 110, (3), 258-264.
- [20] Nelson, P. F., et al., Effects of vehicle type and fuel quality on real world toxic emissions from diesel vehicles, *Atmos. Environ.*, **2008**, 42, (21), 5291-5303.
- [21] Matti Maricq, M., Chemical characterization of particulate emissions from diesel engines: A review, *J. Aerosol Sci.*, **2007**, 38, (11), 1079-1118.
- [22] Stanislaus, A., et al., Recent advances in the science and technology of ultra low sulfur diesel (ULSD) production, *Catal. Today*, **2010**, 153, (1-2), 1-68.
- [23] EPA, Draft Regulatory Impact Analysis: Control of Emissions from Nonroad Diesel Engines. In 2003; p 1312.
- [24] Agency, U. S. E. P. <http://www.epa.gov/otaq/nonroad-diesel.htm>
- [25] EPA, Greenhouse Gas Emissions Standards and Fuel Efficiency Standards for Medium- and Heavy-Duty Engines and Vehicles In Transportation, D. o., Ed. 2011; Vol. 76.
- [26] Song, C., An overview of new approaches to deep desulfurization for ultra-clean gasoline, diesel fuel and jet fuel, *Catal. Today*, **2003**, 86, (1-4), 211-263.
- [27] Ma, X., et al., A new approach to deep desulfurization of gasoline, diesel fuel and jet fuel by selective adsorption for ultra-clean fuels and for fuel cell applications, *Catal. Today*, **2002**, 77, (1-2), 107-116.
- [28] Knudsen, K. G., et al., Catalyst and process technologies for ultra low sulfur diesel, *Appl Catal A*;, **1999**, 189, (2), 205-215.



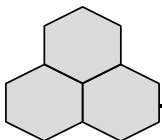
- [29] Whitehurst, D. D., et al., Present State of the Art and Future Challenges in the Hydrodesulfurization of Polyaromatic Sulfur Compounds. In *Advances in Catalysis*, D.D. Eley, W. O. H. B. G.; Helmut, K., Eds. Academic Press: 1998; Vol. Volume 42, pp 345-471.
- [30] Ma, X., et al., Hydrodesulfurization reactivities of various sulfur compounds in diesel fuel, *Ind Engi Chem Res.*, **1994**, 33, (2), 218-222.
- [31] Kartinen Jr, E. O.; Martin, C. J., An overview of arsenic removal processes, *Desalination*, **1995**, 103, (1-2), 79-88.
- [32] DeMarco, M. J., et al., Arsenic removal using a polymeric/inorganic hybrid sorbent, *Water Res.*, **2003**, 37, (1), 164-176.
- [33] Meng, X., et al., Treatment of arsenic in Bangladesh well water using a household co-precipitation and filtration system, *Water Res.*, **2001**, 35, (12), 2805-2810.
- [34] Sarkar, S., et al., Arsenic Removal from Groundwater and Its Safe Containment in a Rural Environment: Validation of a Sustainable Approach, *Environ. Sci. Technol.*, **2008**, 42, (12), 4268-4273.
- [35] Khan, A. H., et al., Appraisal of a simple arsenic removal method for ground water of Bangladesh, *J Environ Sci Hea-A*, **2000**, 35, (7), 1021-1041.
- [36] Payne, K. B.; Abdel-Fattah, T. M., Adsorption of arsenate and arsenite by iron-treated activated carbon and zeolites: effects of pH, temperature, and ionic strength, *J Environ Sci Hea-A*, **2005**, 40, (4), 723-749.
- [37] Mohan, D.; Pittman, J. C. U., Arsenic removal from water/wastewater using adsorbents--A critical review, *J. Hazard. Mater.*, **2007**, 142, (1-2), 1-53.



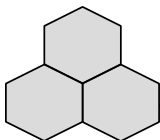
- [38] Singh, D. B., et al., Adsorption technique for the treatment of As(V)-rich effluents, *Colloids Surf. Physicochem. Eng. Aspects*, **1996**, 111, (1–2), 49-56.
- [39] Vithanage, M., et al., Arsenic binding mechanisms on natural red earth: A potential substrate for pollution control, *Sci. Total Environ.*, **2007**, 379, (2–3), 244-248.
- [40] Giménez, J., et al., Arsenic sorption onto natural hematite, magnetite, and goethite, *J. Hazard. Mater.*, **2007**, 141, (3), 575-580.
- [41] Dixit, S.; Hering, J. G., Comparison of Arsenic(V) and Arsenic(III) Sorption onto Iron Oxide Minerals: Implications for Arsenic Mobility, *Environ. Sci. Technol.*, **2003**, 37, (18), 4182-4189.
- [42] Auffan, M., et al., Enhanced Adsorption of Arsenic onto Maghemite Nanoparticles: As(III) as a Probe of the Surface Structure and Heterogeneity, *Langmuir*, **2008**, 24, (7), 3215-3222.
- [43] Lien, H.-L.; Wilkin, R. T., High-level arsenite removal from groundwater by zero-valent iron, *Chemosphere*, **2005**, 59, (3), 377-386.
- [44] Giles, D. E., et al., Iron and aluminium based adsorption strategies for removing arsenic from water, *J. Environ. Manage.*, **2011**, 92, (12), 3011-3022.
- [45] Gallegos-Garcia, M., et al., Arsenic Removal from Water by Adsorption Using Iron Oxide Minerals as Adsorbents: A Review, *Miner. Process. Extr. Metall. Rev.*, **2011**, 33, (5), 301-315.
- [46] Bandosz, T. J., Chapter 5 Desulfurization on activated carbons. In *Int Sci Technol*, Teresa, J. B., Ed. Elsevier: 2006; Vol. Volume 7, pp 231-292.



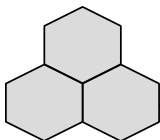
- [47] Bagreev, A., et al., Adsorption of SO₂ on Activated Carbons: The Effect of Nitrogen Functionality and Pore Sizes, *Langmuir*, **2002**, 18, (4), 1257-1264.
- [48] Bashkova, S., et al., Adsorption of SO₂ on Sewage Sludge-Derived Materials, *Envir. Sci. Technol.*, **2001**, 35, (15), 3263-3269.
- [49] Daley, M. A., et al., Adsorption of SO₂ onto oxidized and heat-treated activated carbon fibers (ACFs), *Carbon*, **1997**, 35, (3), 411-417.
- [50] Davini, P., Adsorption and desorption of SO₂ on active-carbon - the effect of surface basic groups, *Carbon*, **1990**, 28, (4), 565-571.
- [51] Davini, P., SO₂ adsorption by activated carbons with various burnoffs obtained from a bituminous coal, *Carbon*, **2001**, 39, (9), 1387-1393.
- [52] Davini, P., Influence of surface properties and iron addition on the SO₂ adsorption capacity of activated carbons, *Carbon*, **2002**, 40, (5), 729-734.
- [53] Furmaniak, S., et al., Influence of activated carbon surface oxygen functionalities on SO₂ physisorption – Simulation and experiment, *Chem. Phys. Lett.*, **2013**, 578, (0), 85-91.
- [54] Guo, J.; Lua, A. C., Microporous activated carbons prepared from palm shell by thermal activation and their application to sulfur dioxide adsorption, *J. Colloid Interface Sci.*, **2002**, 251, (2), 242-247.
- [55] Karatepe, N., et al., Sulfur dioxide adsorption by activated carbons having different textural and chemical properties, *Fuel*, **2008**, 87, (15-16), 3207-3215.
- [56] Kisamori, S., et al., Roles of Surface Oxygen Groups on Poly(acrylonitrile)-Based Active Carbon Fibers in SO₂ Adsorption, *Langmuir*, **1994**, 10, (4), 1241-1245.



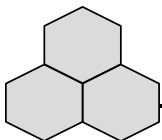
- [57] Lisovskii, A., et al., Adsorption of sulfur dioxide by active carbon treated by nitric acid: I. Effect of the treatment on adsorption of SO₂ and extractability of the acid formed, *Carbon*, **1997**, 35, (10–11), 1639-1643.
- [58] Lizzio, A. A.; DeBarr, J. A., Effect of surface area and chemisorbed oxygen on the SO₂ adsorption capacity of activated char, *Fuel*, **1996**, 75, (13), 1515-1522.
- [59] Mangun, C. L., et al., Adsorption of sulfur dioxide on ammonia-treated activated carbon fibers, *Carbon*, **2001**, 39, (11), 1689-1696.
- [60] Raymundo-Piñero, E., et al., Temperature programmed desorption study on the mechanism of SO₂ oxidation by activated carbon and activated carbon fibres, *Carbon*, **2001**, 39, (2), 231-242.
- [61] Raymundo-Piñero, E., et al., Factors controlling the SO₂ removal by porous carbons: relevance of the SO₂ oxidation step, *Carbon*, **2000**, 38, (3), 335-344.
- [62] Moreno-Castilla, C., et al., Activated carbons as adsorbents of sulfur dioxide in flowing air. Effect of their pore texture and surface basicity, *Langmuir*, **1993**, 9, (5), 1378-1383.
- [63] Yang, F. H.; Yang, R. T., Ab initio molecular orbital study of the mechanism of SO₂ oxidation catalyzed by carbon, *Carbon*, **2003**, 41, (11), 2149-2158.
- [64] Vasudevan, P. T.; Fierro, J. L. G., A Review of Deep Hydrodesulfurization Catalysis, *Catal Rev*, **1996**, 38, (2), 161-188.
- [65] Mochida, I., et al., Deep hydrodesulfurization of diesel fuel: Design of reaction process and catalysts, *Catal Today*, **1996**, 29, (1–4), 185-189.



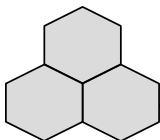
- [66] Song, C.; Ma, X., New design approaches to ultra-clean diesel fuels by deep desulfurization and deep dearomatization, *Appl Catal-B*, **2003**, 41, (1-2), 207-238.
- [67] Sie, S. T., Reaction order and role of hydrogen sulfide in deep hydrodesulfurization of gas oils: consequences for industrial reactor configuration, *Fuel Proc Technol*, **1999**, 61, (1-2), 149-171.
- [68] Hernandez, S. P., et al., High performance sorbents for diesel oil desulfurization, *Chem. Eng. Sci.*, **2010**, 65, (1), 603-609.
- [69] Ma, X., et al., Hydrodesulfurization Reactivities of Narrow-Cut Fractions in a Gas Oil, *Ind. Eng. Chem. Res*, **1995**, 34, (3), 748-754.
- [70] Kabe, T., et al., Hydrodesulfurization of sulfur-containing polyaromatic compounds in light oil, *Ind. Eng. Chem. Res*, **1992**, 31, (6), 1577-1580.
- [71] Gates, B. C.; Topsøe, H., Reactivities in deep catalytic hydrodesulfurization: challenges, opportunities, and the importance of 4-methyldibenzothiophene and 4,6-dimethyldibenzothiophene, *Polyhedron*, **1997**, 16, (18), 3213-3217.
- [72] Turaga, U. T., et al., Influence of nitrogen compounds on deep hydrodesulfurization of 4,6-dimethyldibenzothiophene over Al_2O_3 and MCM-41-supported Co-Mo sulfide catalysts, *Catal. Today*, **2003**, 86, (1-4), 265-275.
- [73] Rabarihoela-Rakotovao, V., et al., Deep HDS of Diesel Fuel: Inhibiting Effect of Nitrogen Compounds on the Transformation of the Refractory 4,6-Dimethyldibenzothiophene Over a NiMoP/ Al_2O_3 Catalyst, *Catal. Lett.*, **2009**, 129, (1-2), 50-60.



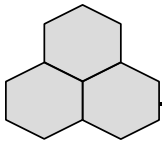
- [74] Yang, H., et al., Inhibition of nitrogen compounds on the hydrodesulfurization of substituted dibenzothiophenes in light cycle oil, *Fuel Process. Technol.*, **2004**, 85, (12), 1415-1429.
- [75] Laredo S, G. C., et al., Inhibition effects of nitrogen compounds on the hydrodesulfurization of dibenzothiophene, *Appl Catal., A: General*, **2001**, 207, (1–2), 103-112.
- [76] Macaud, M., et al., Novel Methodology toward Deep Desulfurization of Diesel Feed Based on the Selective Elimination of Nitrogen Compounds, *Ind. Eng. Chem. Res.*, **2004**, 43, (24), 7843-7849.
- [77] Hernández-Maldonado, A. J.; Yang, R. T., Denitrogenation of Transportation Fuels by Zeolites at Ambient Temperature and Pressure, *Angew. Chem.*, **2004**, 43, (18), 2321-2321.
- [78] Zhang, H.; Song, H., Study of Adsorptive Denitrogenation of Diesel Fuel over Mesoporous Molecular Sieves Based on Breakthrough Curves, *Ind. Eng. Chem. Res.*, **2012**, 51, (49), 16059-16065.
- [79] Sano, Y., et al., Two-step adsorption process for deep desulfurization of diesel oil, *Fuel*, **2005**, 84, (7–8), 903-910.
- [80] Thomas, W. J.; Crittenden, B., 3 - Fundamentals of adsorption equilibria. In *Adsorption Technology & Design*, Butterworth-Heinemann: Oxford, 1998; pp 31-65.
- [81] Noll, K. E., *Adsorption Technology for Air and Water Pollution Control*. Taylor & Francis: 1991.
- [82] Wade, L. G., *Química orgánica Volumen 2*. Pearson: 2012.



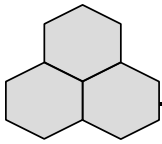
- [83] Cornell, R. M.; Schwetmann, U., *The Iron Oxides Structure, Properties, Reactions, Occurrences and Uses*. Weinheim, 2003.
- [84] Dzombak, D. A.; Morel, F. M. M., *Surface Complexation Modeling: Hydrous Ferric Oxide*. Wiley: 1990.
- [85] Vidic, R. D.; Siler, D. P., Vapor-phase elemental mercury adsorption by activated carbon impregnated with chloride and chelating agents, *Carbon*, **2001**, 39, (1), 3-14.
- [86] Sharma, M., et al., A review on reactive adsorption for potential environmental applications, *Adsorption*, **2013**, 19, (1), 161-188.
- [87] Seredych, M., et al., Enhancement in Dibenzothiophene Reactive Adsorption from Liquid Fuel via Incorporation of Sulfur Heteroatoms into the Nanoporous Carbon Matrix, *ChemSusChem*, **2011**, 4, (1), 139-147.
- [88] Langmuir, I., The constitution and fundamental properties of solids and liquids. II. Liquids.1, *J. Am. Chem. Soc.*, **1917**, 39, (9), 1848-1906.
- [89] Brunauer, S., et al., Adsorption of Gases in Multimolecular Layers, *J. Am. Chem. Soc.*, **1938**, 60, (2), 309-319.
- [90] Webb, P. A., et al., *Analytical methods in fine particle technology*. Micromeritics Instrument Corporation: 1997.
- [91] Freundlich, H. M. F., Over the adsorption in solution, *J. Phys. Chem.*, **1906**, 57, 385-471.
- [92] Foo, K. Y.; Hameed, B. H., Insights into the modeling of adsorption isotherm systems, *Chem. Eng. J.*, **2010**, 156, (1), 2-10.
- [93] Stumm, W.; Morgan, J. J., *Aquatic chemistry: chemical equilibria and rates in natural waters*. Wiley: 1996.



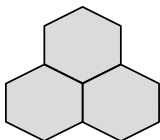
- [94] Fuente, E., et al., Basic Surface Oxides on Carbon Materials: A Global View, *Langmuir*, **2003**, 19, (8), 3505-3511.
- [95] Gouy, M., Sur la constitution de la charge électrique à la surface d'un électrolyte, *J. Phys. Theor. Appl.*, **1910**, 9, (1), 457-468.
- [96] Chapman, D. L., LI. A contribution to the theory of electrocapillarity, *Philosophical Magazine Series 6*, **1913**, 25, (148), 475-481.
- [97] Evanko, C. R.; Dzombak, D. A., Surface Complexation Modeling of Organic Acid Sorption to Goethite, *J. Colloid Interface Sci.*, **1999**, 214, (2), 189-206.
- [98] Ali, M. A.; Dzombak, D. A., Interactions of copper, organic acids, and sulfate in goethite suspensions, *Geochim. Cosmochim. Acta*, **1996**, 60, (24), 5045-5053.
- [99] Marmier, N., et al., Surface Complexation Modeling of Yb(III), Ni(II), and Cs(I) Sorption on Magnetite, *J. Colloid Interface Sci.*, **1999**, 211, (1), 54-60.
- [100] Hamdaoui, O.; Naffrechoux, E., Modeling of adsorption isotherms of phenol and chlorophenols onto granular activated carbon: Part I. Two-parameter models and equations allowing determination of thermodynamic parameters, *J. Hazard. Mater.*, **2007**, 147, (1-2), 381-394.
- [101] Hamdaoui, O.; Naffrechoux, E., Modeling of adsorption isotherms of phenol and chlorophenols onto granular activated carbon: Part II. Models with more than two parameters, *J. Hazard. Mater.*, **2007**, 147, (1-2), 401-411.
- [102] Yates, D. E.; Healy, T. W., Mechanism of anion adsorption at the ferric and chromic oxide/water interfaces, *J. Colloid Interface Sci.*, **1975**, 52, (2), 222-228.



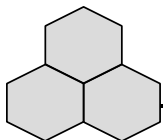
- [103] Davis, J. A.; Leckie, J. O., Surface ionization and complexation at the oxide/water interface II. Surface properties of amorphous iron oxyhydroxide and adsorption of metal ions, *J. Colloid Interface Sci*, **1978**, 67, (1), 90-107.
- [104] Bowden, J., et al., Describing the adsorption of phosphate, citrate and selenite on a variable-charge mineral surface, *Soil Research*, **1980**, 18, (1), 49-60.
- [105] Cowan, C. E., et al., Cadmium adsorption on iron oxides in the presence of alkaline-earth elements, *Env Sci Technol*, **1991**, 25, (3), 437-446.
- [106] Cornell, R. M.; Schwertmann, U., Adsorption of Ions and Molecules. In *The Iron Oxides*, Wiley-VCH Verlag GmbH & Co. KGaA: 2004; pp 253-296.
- [107] Stanić, T., et al., Adsorption of arsenic(V) by iron(III)-modified natural zeolitic tuff, *Env Chem Let*, **2009**, 7, (2), 161-166.
- [108] Chutia, P., et al., Adsorption of As(V) on surfactant-modified natural zeolites, *J. Hazard. Mater.*, **2009**, 162, (1), 204-211.
- [109] Hernández-Maldonado, A. J.; Yang, R. T., Desulfurization of Commercial Liquid Fuels by Selective Adsorption via π -Complexation with Cu(II)-Y Zeolite, *Ind. Eng. Chem. Res.*, **2003**, 42, (13), 3103-3110.
- [110] Srivastav, A.; Srivastava, V. C., Adsorptive desulfurization by activated alumina, *J. Hazard. Mater.*, **2009**, 170, (2-3), 1133-1140.
- [111] Qiu, H., et al., Critical review in adsorption kinetic models, *J. Zhejiang Univ. Sci. A*, **2009**, 10, (5), 716-724.
- [112] Ho, Y.-S., Review of second-order models for adsorption systems, *J. Hazard. Mater*, **2006**, 136, (3), 681-689.



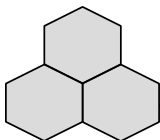
- [113] Cooney, D. O., *Adsorption Design for Wastewater Treatment*. Taylor & Francis: 1998.
- [114] Boyd, G. E., et al., The exchange adsorption of ions from aqueous solutions by organic zeolites. II. Kinetics, *J. Am. Chem. Soc.*, **1947**, 69, (11), 2836-2848.
- [115] Leyva-Ramos, R.; Geankoplis, C. J., Model simulation and analysis of surface diffusion of liquids in porous solids, *Chem Eng Sci*, **1985**, 40, (5), 799-807.
- [116] Bansal, R. C.; Goyal, M., *Activated Carbon Adsorption*. Taylor & Francis: 2010.
- [117] Marsh, H.; Reinoso, F. R., *Activated Carbon*. Elsevier Science: 2006.
- [118] Bandosz, T. J.; Ania, C. O., Chapter 4 Surface chemistry of activated carbons and its characterization. In *Interface Science and Technology*, Teresa, J. B., Ed. Elsevier: 2006; Vol. Volume 7, pp 159-229.
- [119] Harris, P. J. F., et al., Imaging the atomic structure of activated carbon, *J. Phys C.*, **2008**, 20, (36).
- [120] Dubinin, M. M., The potential theory of adsorption of gases and vapors for adsorbents with energetically nonuniform surfaces, *Chem Rev*, **1960**, 60, (2), 235-241.
- [121] Inagaki, M.; Tascón, J. M. D., Chapter 2 Pore formation and control in carbon materials. In *Interface Science and Technology*, Teresa, J. B., Ed. Elsevier: 2006; Vol. Volume 7, pp 49-105.



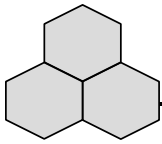
- [122] Rangel-Mendez, J. R.; Streat, M., Adsorption of cadmium by activated carbon cloth: influence of surface oxidation and solution pH, *Water Res.*, **2002**, 36, (5), 1244-1252.
- [123] Crittenden, J. C., et al., *Water Treatment - Principles and Design* (2nd Edition). In John Wiley & Sons.
- [124] Radovic, L. R., et al., Carbon materials as adsorbents in aqueous solutions. In 2000; Vol. 27, pp 227-405.
- [125] Lorenzen, L., et al., Factors affecting the mechanism of the adsorption of arsenic species on activated carbon, *Miner. Eng.*, **1995**, 8, (4-5), 557-569.
- [126] Mondal, P., et al., Effects of adsorbent dose, its particle size and initial arsenic concentration on the removal of arsenic, iron and manganese from simulated ground water by Fe³⁺ impregnated activated carbon, *J. Hazard. Mater.*, **2008**, 150, (3), 695-702.
- [127] Jiang, Z., et al., Activated Carbons Chemically Modified by Concentrated H₂SO₄ for the Adsorption of the Pollutants from Wastewater and the Dibenzothiophene from Fuel Oils, *Langmuir*, **2003**, 19, (3), 731-736.
- [128] Xiao, J., et al., Adsorption of Benzothiophene and Dibenzothiophene on Ion-Impregnated Activated Carbons and Ion-Exchanged Y Zeolites, *Energ. Fuel.*, **2008**, 22, (6), 3858-3863.
- [129] Baeza, P., et al., Adsorption of thiophene and dibenzothiophene on highly dispersed Cu/ZrO₂ adsorbents, *Appl Cat B.*, **2012**, 111-112, 133-140.
- [130] Bu, J., et al., Desulfurization of diesel fuels by selective adsorption on activated carbons: Competitive adsorption of polycyclic aromatic sulfur



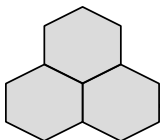
- heterocycles and polycyclic aromatic hydrocarbons, *Chem. Eng. J.*, **2011**, 166, (1), 207-217.
- [131] Xiao, J., et al., Effects of Aromatics, Diesel Additives, Nitrogen Compounds, and Moisture on Adsorptive Desulfurization of Diesel Fuel over Activated Carbon, *Ind. Eng. Chem. Res.*, **2012**, 51, (8), 3436-3443.
- [132] Xu, J.-h., et al., Nanoscale iron hydroxide-doped granular activated carbon (Fe-GAC) as a sorbent for perchlorate in water, *Chem Eng J.*, **2013**, 222, (0), 520-526.
- [133] Castro, C. S., et al., Iron oxide dispersed over activated carbon: Support influence on the oxidation of the model molecule methylene blue, *Appl Catal A.*, **2009**, 367, (1-2), 53-58.
- [134] Agarwal, B., et al., Use of iron-impregnated granular activated carbon for co-adsorptive removal of phenol and cyanide: insight into equilibrium and kinetics, *Chem Eng Comm*, **2013**, 200, (9), 1278-1292.
- [135] Wang, Z., et al., Equilibrium and kinetics of adsorption of phosphate onto iron-doped activated carbon, *Environ Sci Pollut Res*, **2012**, 19, (7), 2908-2917.
- [136] Liu, W., et al., Adsorptive removal of Cr (VI) by Fe-modified activated carbon prepared from *Trapa natans* husk, *Chem Eng J.*, **2010**, 162, (2), 677-684.
- [137] Stoyanova, D., et al., Catalytic activity of Fe/AC, obtained by impregnation of activated carbon in aqueous and non-aqueous media, to neutralize NO, *J Porous Mater*, **2009**, 16, (1), 1-7.



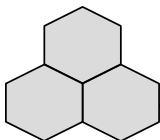
- [138] Rey, A., et al., Catalytic wet peroxide oxidation of phenol over Fe/AC catalysts: Influence of iron precursor and activated carbon surface, *Appl Catal B.*, **2009**, 86, (1–2), 69-77.
- [139] Zazo, J. A., et al., Optimizing calcination temperature of Fe/activated carbon catalysts for CWPO, *Catal Today*, **2009**, 143, (3–4), 341-346.
- [140] Shimada, H., et al., Dehydrogenation of isobutane to isobutene with iron-loaded activated carbon catalyst, *Appl Catal A.*, **1998**, 168, (2), 243-250.
- [141] Zhang, Q. L., et al., A method for preparing ferric activated carbon composites adsorbents to remove arsenic from drinking water, *J. Hazard. Mater.*, **2007**, 148, (3), 671-678.
- [142] Yu, M. R., et al., Application of activated carbon impregnated with metal oxides to the treatment of multi-contaminants, *Env Technol UK*, **2012**, 33, (14), 1553-1559.
- [143] Liu, X., et al., Arsenic Removal from Water by Iron-Modified Bamboo Charcoal, *Water Air Soil Poll*, **2012**, 223, (3), 1033-1044.
- [144] Jang, M., et al., Combined hydrous ferric oxide and quaternary ammonium surfactant tailoring of granular activated carbon for concurrent arsenate and perchlorate removal, *Water Res*, **2009**, 43, (12), 3133-3143.
- [145] Mondal, P., et al., A laboratory study for the treatment of arsenic, iron, and manganese bearing ground water using Fe³⁺ impregnated activated carbon: Effects of shaking time, pH and temperature, *J. Hazard. Mater*, **2007**, 144, (1–2), 420-426.
- [146] Chen, W., et al., Arsenic removal by iron-modified activated carbon, *Water Res.*, **2007**, 41, (9), 1851-1858.



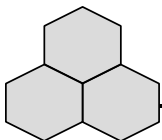
- [147] Ghanizadeh, G. H., et al., Application of iron impregnated activated carbon for removal of arsenic from water, *Iran J Envi Health Sci Eng*, **2010**, 7, (2), 145-156.
- [148] Deliyanni, E.; Badosz, T. J., Importance of carbon surface chemistry in development of iron-carbon composite adsorbents for arsenate removal, *J. Hazard. Mater*, **2011**, 186, (1), 667-674.
- [149] Mackenzie, K., et al., Colloidal activated carbon and CARBO-IRON - Novel materials for in-situ groundwater treatment, *Glob Nest J.*, **2008**, 10, (1), 54-61.
- [150] Hristovski, K. D., et al., Effect of synthesis conditions on nano-iron (hydr)oxide impregnated granulated activated carbon, *Chem Eng J*, **2009**, 146, (2), 237-243.
- [151] Fierro, V., et al., Arsenic removal by iron-doped activated carbons prepared by ferric chloride forced hydrolysis, *J. Hazard. Mater.*, **2009**, 168, (1), 430-437.
- [152] Vitela-Rodriguez, A. V.; Rangel-Mendez, J. R., Arsenic removal by modified activated carbons with iron hydro(oxide) nanoparticles, *J Environ Man*, **2013**, 114, (0), 225-231.
- [153] Nieto-Delgado, C.; Rangel-Mendez, J. R., Anchorage of iron hydro(oxide) nanoparticles onto activated carbon to remove As(V) from water, *Water Res*, **2012**, 46, (9), 2973-2982.
- [154] Ozaki, M., et al., Formation of monodispersed spindle-type hematite particles, *J. Colloid Interface Sci.*, **1984**, 102, (1), 146-151.



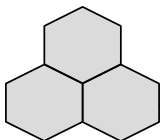
- [155] Flynn, C. M., Hydrolysis of inorganic iron(III) salts, *Chem Rev*, **1984**, 84, (1), 31-41.
- [156] Schultz, M., et al., Investigations on thermally forced hydrolysis and phase formation in aqueous iron(III) nitrate solutions, *J. Mater. Sci*, **1999**, 34, (9), 2217-2227.
- [157] Shang, Y.; van Weert, G., Iron control in nitrate hydrometallurgy by autoclave hydrolysis of iron(III) nitrate, *Hydrometallurgy*, **1993**, 33, (3), 273-290.
- [158] Sugimoto, T.; Muramatsu, A., Formation Mechanism of Monodispersed α -Fe₂O₃ Particles in Dilute FeCl₃ Solutions, *J Colloid Interface Sci*, **1996**, 184, (2), 626-638.
- [159] Chiu, C.-A., et al., Modeling temperature and reaction time impacts on hematite nanoparticle size during forced hydrolysis of ferric chloride, *Chem Eng J.*, **2012**, 210, (0), 357-362.
- [160] Fu, D., et al., Iron oxyhydroxide nanoparticles formed by forced hydrolysis: Dependence of phase composition on solution concentration, *Phys Chem Chem-Phys*, **2011**, 13, (41), 18523-18529.
- [161] Meyer, W. R., et al., Formation of colloidal particles of hydrous iron oxide by forced hydrolysis, *J. Non-Cryst. Solids*, **2000**, 273, (1-3), 41-47.
- [16] Kajiyama, A.; Nakamura, T., Hydrothermal synthesis of β -FeO(OH) rod-like particles with uniform size distribution, *Colloid Surf A:*, **2000**, 163, (2-3), 301-307.
- [163] Naono, H., et al., Micropore formation due to thermal decomposition of acicular microcrystals of β -FeOOH, *J. Colloid Interface Sci.*, **1982**, 87, (2), 317-332.



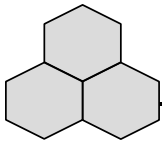
- [164] Woo, K., et al., Easy synthesis and magnetic properties of iron oxide nanoparticles, *Chem. Mater.*, **2004**, 16, (14), 2814-2818.
- [165] Angermann, A.; Töpfer, J., Synthesis of magnetite nanoparticles by thermal decomposition of ferrous oxalate dihydrate, *J Mat Sci.*, **2008**, 43, (15), 5123-5130.
- [166] Flynn Jr, C. M., Dense hydrolysis products from iron(III) nitrate and sulfate solutions, *Hydrometallurgy*, **1990**, 25, (2), 257-270.
- [167] Jolivet, J. P., et al., Iron oxide chemistry. From molecular clusters to extended solid networks, *Chem Comm.*, **2004**, 10, (5), 481-487.
- [168] Jolivet, J. P., et al., *Metal Oxide Chemistry and Synthesis: From Solution to Solid State*. Wiley: 2000.
- [169] Zhang, H., et al., Enhanced Adsorption of Molecules on Surfaces of Nanocrystalline Particles, *J Phys Chem. B.*, **1999**, 103, (22), 4656-4662.
- [170] Yean S, C. L., Yavuz CT, Mayo JT, Yu WW, Kan AT, Colvin VL, Tomson MB Effect of magnetite particle size on adsorption and desorption of arsenite and arsenate, *J. Mater. Res.*, **2005**, 20, (12), 3255-3264.
- [171] Stará, I.; Matolín, V., The influence of particle size on CO adsorption on Pd/alumina model catalysts, *Surf. Sci.*, **1994**, 313, (1-2), 99-106.
- [172] Zhang, G.; Liu, M., Effect of particle size and dopant on properties of SnO₂ based gas sensors, *Sensor Actuat B-Chem*, **2000**, 69, (1-2), 144-152.
- [173] Music, S., et al., Some factors influencing forced hydrolysis of FeCl₃ solutions, *Mater. Lett.*, **2003**, 57, (5-6), 1096-1102.



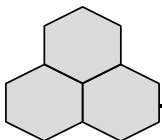
- [174] Kandori, K., et al., Effects of amino acids on the formation of hematite particles in a forced hydrolysis reaction, *J. Colloid Interface Sci.*, **2006**, 293, (1), 108-115.
- [175] Kandori, K., et al., Effects of vinyl series polymers on the formation of hematite particles in a forced hydrolysis reaction, *J. Colloid Interface Sci.*, **2005**, 283, (2), 432-439.
- [176] Kwon, S.-K., et al., Influence of silicon on local structure and morphology of $[\gamma]$ -FeOOH and $[\alpha]$ -FeOOH particles, *Corros. Sci.*, **2007**, 49, (3), 1513-1526.
- [177] Ishikawa, T., et al., Influences of metal ions on the formation of $[\gamma]$ -FeOOH and magnetite rusts, *Corros. Sci.*, **2002**, 44, (5), 1073-1086.
- [178] Rose, J., et al., Nucleation and Growth Mechanisms of Fe Oxyhydroxide in the Presence of PO₄ Ions. 1. Fe K-Edge EXAFS Study, *Langmuir*, **1996**, 12, (26), 6701-6707.
- [179] Ishikawa, T., et al., Influence of anions on the formation of $[\beta]$ -FeOOH rusts, *Corros. Sci.*, **2005**, 47, (10), 2510-2520.
- [180] Kandori, K., et al., Control on size and adsorptive properties of spherical ferric phosphate particles, *J. Colloid Interface Sci.*, **2006**, 300, (1), 225-231.
- [181] Baltrusaitis, J., et al., Adsorption of sulfur dioxide on hematite and goethite particle surfaces, *PCCP*, **2007**, 9, (41), 5542-5554.
- [182] Fu, H., et al., Heterogeneous Uptake and Oxidation of SO₂ on Iron Oxides, *J. Phys. Chem. C*, **2007**, 111, (16), 6077-6085.
- [183] Seredych, M., et al., Involvement of water and visible light in the enhancement in SO₂ adsorption at ambient conditions on the surface of zinc (hydr)oxide/graphite oxide composites, *Chem. Eng. J.*, **2013**, 223, 442-453.



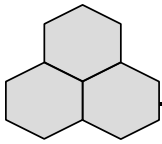
- [184] Tuna, A. Ö. A., et al., Removal of As(V) from aqueous solution by activated carbon-based hybrid adsorbents: Impact of experimental conditions, *Chem Eng J.*, **2013**, 223, 116-128.
- [185] Moreno-Piraján, J.; Giraldo, L., Activated carbon from bamboo waste modified with iron and its application in the study of the adsorption of arsenite and arsenate, *cent.eur.j.chem.*, **2013**, 11, (2), 160-170.
- [186] Asadullah, M., et al., Preparation of microporous activated carbon and its modification for arsenic removal from water, *J Ind Eng Chem.*, (In press).
- [187] Lodeiro, P., et al., Novel Fe loaded activated carbons with tailored properties for As(V) removal: Adsorption study correlated with carbon surface chemistry, *Chem Eng J*, **2013**, 215–216,, 105-112.
- [188] Chang, Q., et al., Preparation of iron-impregnated granular activated carbon for arsenic removal from drinking water, *J Hazard Mater*, **2010**, 184, (1–3), 515-522.
- [189] Deliyanni, E., et al., Impregnation of activated carbon by iron oxyhydroxide and its effect on arsenate removal, *J Chem Technol Biotechnol*, **2013**, 88, (6), 1058-1066.
- [190] Fallah, R. N.; Azizian, S., Removal of thiophenic compounds from liquid fuel by different modified activated carbon cloths, *Fuel Process. Technol.*, **2012**, 93, (1), 45-52.
- [191] Almarri, M., et al., Selective Adsorption for Removal of Nitrogen Compounds from Liquid Hydrocarbon Streams over Carbon- and Alumina-Based Adsorbents, *Ind. Eng. Chem. Res.*, **2008**, 48, (2), 951-960.



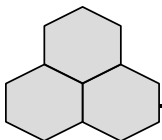
- [192] Yang, Y. X., et al., Selective dibenzothiophene adsorption on modified activated carbons, *Carbon*, **2007**, 45, (15), 3042-3044.
- [193] Seredych, M., et al., Textural and chemical factors affecting adsorption capacity of activated carbon in highly efficient desulfurization of diesel fuel, *Carbon*, **2009**, 47, (10), 2491-2500.
- [194] Selvavathi, V., et al., Adsorptive desulfurization of diesel on activated carbon and nickel supported systems, *Catal. Today*, **2009**, 141, (1-2), 99-102.
- [195] Wang, Y.; Yang, R. T., Desulfurization of Liquid Fuels by Adsorption on Carbon-Based Sorbents and Ultrasound-Assisted Sorbent Regeneration, *Langmuir*, **2007**, 23, (7), 3825-3831.
- [196] Xiao, J., et al., Adsorption of Dibenzothiophene on Ag/Cu/Fe-Supported Activated Carbons Prepared by Ultrasonic-Assisted Impregnation, *J Chem Engi Data*, **2010**, 55, (12), 5818-5823.
- [197] Seredych, M.; Bandosz, T. J., Adsorption of dibenzothiophenes on activated carbons with copper and iron deposited on their surfaces, *Fuel Process. Technol.*, **2010**, 91, (6), 693-701.
- [198] Reed, B. E., et al., As(III), As(V), Hg, and Pb Removal by Fe-Oxide Impregnated Activated Carbon, *J. Environ. Eng.*, **2000**, 126, (9), 869-873.
- [199] Muñiz, G., et al., Synthesis, characterization and performance in arsenic removal of iron-doped activated carbons prepared by impregnation with Fe(III) and Fe(II), *J. Hazard. Mater.*, **2009**, 165, (1-3), 893-902.
- [200] Chen, W., et al., Ammonia-tailoring of GAC to enhance perchlorate removal. I: Characterization of NH₃ thermally tailored GACs, *Carbon*, **2005**, 43, (3), 573-580.



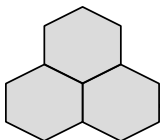
- [201] Brett, C., et al., A new approach in the use of SIT in determining the dependence on ionic strength of activity coefficients. Application to some chloride salts of interest in the speciation of natural fluids, *Chem. Speciation Bioavailability*, **2004**, 16, (3), 105-110.
- [202] Gu, Z., et al., Preparation and Evaluation of GAC-Based Iron-Containing Adsorbents for Arsenic Removal, *Environ. Sci. Technol.*, **2005**, 39, (10), 3833-3843.
- [203] Ghanizadeh, G., et al., Application of iron impregnated activated carbon for removal of arsenic from water, *Iran. J. Environ. Health Sci. Eng.*, **2010**, 7, (2), 145-156.
- [0] Pakuła, M., et al., Chemical and Electrochemical Studies of interactions between Iron(III) Ions and an Activated Carbon Surface, *Langmuir*, **1998**, 14, (11), 3082-3089.
- [205] Aredes, S., et al., The removal of arsenic from water using natural iron oxide minerals, *J. Clean. Prod.*, **2012**, 29–30, (0), 208-213.
- [206] Wang, Z. M., et al., Air oxidation effects on microporosity, surface property, and CH₄ adsorptivity of pitch-based activated carbon fibers, *J. Colloid Interface Sci.*, **2004**, 276, (1), 143-150.
- [207] Guo, X., et al., Mechanism of removal of arsenic by bead cellulose loaded with iron oxyhydroxide (β -FeOOH): EXAFS study, *J. Colloid Interface Sci.*, **2007**, 314, (2), 427-433.
- [208] McBride, M. B., A critique of diffuse double layer models applied to colloid and surface chemistry, *Clays Clay Miner.*, **1997**, 45, (4), 598-608.



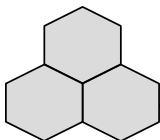
- [209] Alain, M., The mechanism of anion adsorption on iron oxides: Evidence for the bonding of arsenate tetrahedra on free $\text{Fe}(\text{O}, \text{OH})_6$ edges, *Geochim. Cosmochim. Acta*, **1995**, 59, (17), 3647-3653.
- [210] Sherman, D. M.; Randall, S. R., Surface complexation of arsenic(V) to iron(III) (hydr)oxides: structural mechanism from ab initio molecular geometries and EXAFS spectroscopy, *Geochimica et Cosmochimica Acta*, **2003**, 67, (22), 4223-4230.
- [211] Su, C.; Puls, R., Arsenate and Arsenite Sorption on Magnetite: Relations to Groundwater Arsenic Treatment Using Zerovalent Iron and Natural Attenuation, *Water, Air, Soil Poll*, **2008**, 193, (1), 65-78.
- [212] Sabbatini, P., et al., Iron oxide adsorbers for arsenic removal: A low cost treatment for rural areas and mobile applications, *Desalination*, **2009**, 248, (1-3), 184-192.
- [213] Marsh, H.; Rodríguez-Reinoso, F., *Activated Carbon*. Elsevier: 2006.
- [214] Gualtieri, A. F.; Venturelli, P., In situ study of the goethite-hematite phase transformation by real time synchrotron powder diffraction, *Am Mineral.*; **84**; (5-6), **1999**, Medium: X; Size: pp. 895-904.
- [215] Halter, W. E.; Pfeifer, H.-R., Arsenic(V) adsorption onto $[\alpha]\text{-Al}_2\text{O}_3$ between 25 and 70°C, *Appl. Geochem.*, **2001**, 16, (7-8), 793-802.
- [216] Vayssières, L., et al., Size Tailoring of Magnetite Particles Formed by Aqueous Precipitation: An Example of Thermodynamic Stability of Nanometric Oxide Particles, *J Colloid Interface Sci*, **1998**, 205, (2), 205-212.



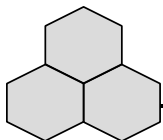
- [217] Gálvez, N., et al., Effect of phosphate on the crystallization of hematite, goethite, and lepidocrocite from ferrihydrite, *Clays Clay Miner*, **1999**, 47, (3), 304-311.
- [218] Rajbhandari, R., et al., Nanoporous Activated Carbon Derived from Lapsi (Choerospondias Axillaris) Seed Stone for the Removal of Arsenic from Water, *J Nanosci Nanotechnol*, **2012**, 12, (9), 7002-7009.
- [219] Rios-Huratado, J. C. Estudio del grado de oxidación de materiales microporosos para el anclaje de hidro(óxidos) de hierro: remoción de arsénico., Tesis de maestría, San Luis Potosi, San Luis Potosi, 2013.
- [220] Nieto-Delgado, C.; Rangel-Mendez, J. R., Production of activated carbon from organic by-products from the alcoholic beverage industry: Surface area and hardness optimization by using the response surface methodology, *Ind Crops Prod*, **2011**, 34, (3), 1528-1537.
- [221] Bourikas, K., et al., Potentiometric Mass Titrations: Experimental and Theoretical Establishment of a New Technique for Determining the Point of Zero Charge (PZC) of Metal (Hydr)Oxides, *J Phys Chem B.*, **2003**, 107, (35), 9441-9451.
- [222] Badosz, T. J., et al., Characterization of the surfaces of activated carbons in terms of their acidity constant distributions, *Carbon*, **1993**, 31, (7), 1193-1202.
- [223] Tsai, W. T., et al., Adsorption of acid dye onto activated carbons prepared from agricultural waste bagasse by ZnCl₂ activation, *Chemosphere*, **2001**, 45, (1), 51-58.



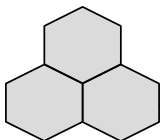
- [224] Parks, G. A., The Isoelectric Points of Solid Oxides, Solid Hydroxides, and Aqueous Hydroxo Complex Systems, *Chem. Rev.*, **1965**, 65, (2), 177-198.
- [225] Akaike, H., Information Theory and an Extension of the Maximum Likelihood Principle. In *Selected Papers of Hirotugu Akaike*, Parzen, E.; Tanabe, K.; Kitagawa, G., Eds. Springer New York: 1998; pp 199-213.
- [226] Azen, R.; Budescu, D. V., The dominance analysis approach for comparing predictors in multiple regression, *Psychol Methods*, **2003**, 8, (2), 129-48.
- [227] Jain, A., et al., Arsenite and Arsenate Adsorption on Ferrihydrite: Surface Charge Reduction and Net OH⁻ Release Stoichiometry, *Env Sci Technol*, **1999**, 33, (8), 1179-1184.
- [228] Goldberg, S.; Johnston, C. T., Mechanisms of Arsenic Adsorption on Amorphous Oxides Evaluated Using Macroscopic Measurements, Vibrational Spectroscopy, and Surface Complexation Modeling, *J Colloid Int Sci*, **2001**, 234, (1), 204-216.
- [229] Yin, S., et al., Reaction between sulfur dioxide and iron oxide cationic clusters, *Chin. Sci. Bull.*, **2009**, 54, (21), 4017-4020.
- [230] Faust, B. C., et al., Photocatalytic oxidation of sulfur dioxide in aqueous suspensions of α -iron oxide (Fe₂O₃), *J. Phys Chem-US*, **1989**, 93, (17), 6371-6381.
- [231] Kraft, J.; Van Eldik, R., Kinetics and mechanism of the iron(III)-catalyzed autoxidation of sulfur(IV) oxides in aqueous solution. 1. Formation of transient iron(III)-sulfur(IV) complexes, *Inorg. Chem.*, **1989**, 28, (12), 2297-2305.



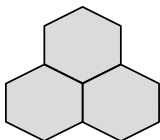
- [232] Jagiello, J., Stable Numerical Solution of the Adsorption Integral Equation Using Splines, *Langmuir*, **1994**, 10, (8), 2778-2785.
- [233] Bandosz, T. J., Structural and acidic properties of taeniolites modified by introduction of Fe⁺³ species, *Pol. J. Chem.*, **1998**, 72, (7), 1202-1214.
- [234] Seredych, M., et al., Role of microporosity and surface chemistry in adsorption of 4,6-dimethyldibenzothiophene on polymer-derived activated carbons, *Fuel*, **2010**, 89, (7), 1499-1507.
- [235] Weast, R. C., *CRC handbook of chemistry and physics*. CRC Press: Boca Raton, FL, 1981.
- [236] Zhang, G., et al., Preparation and evaluation of a novel Fe–Mn binary oxide adsorbent for effective arsenite removal, *Water Res.*, **2007**, 41, (9), 1921-1928.
- [237] Kim, J. H., et al., Ultra-deep desulfurization and denitrogenation of diesel fuel by selective adsorption over three different adsorbents: A study on adsorptive selectivity and mechanism, *Catal. Today*, **2006**, 111, (1-2), 74-83.
- [238] Yu, C., et al., Adsorption removal of thiophene and dibenzothiophene from oils with activated carbon as adsorbent: effect of surface chemistry, *J. Porous Mater.*, **2008**, 15, (2), 151-157.
- [239] Ania, C. O.; Bandosz, T. J., Metal-loaded polystyrene-based activated carbons as dibenzothiophene removal media via reactive adsorption, *Carbon*, **2006**, 44, (12), 2404-2412.



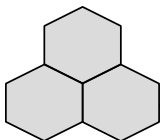
- [240] Yu, M., et al., Effect of thermal oxidation of activated carbon surface on its adsorption towards dibenzothiophene, *Chem. Eng. J.*, **2009**, 148, (2-3), 242-247.
- [241] Seredych, M., et al., Effect of the Incorporation of Nitrogen to a Carbon Matrix on the Selectivity and Capacity for Adsorption of Dibenzothiophenes from Model Diesel Fuel, *Langmuir*, **2009**, 26, (1), 227-233.
- [242] Seredych, M.; Bandosz, T. J., Selective Adsorption of Dibenzothiophenes on Activated Carbons with Ag, Co, and Ni Species Deposited on Their Surfaces, *Energ. Fuel.*, **2009**, 23, (7), 3737-3744.
- [243] Zhou, et al., Liquid-Phase Adsorption of Multi-Ring Thiophenic Sulfur Compounds on Carbon Materials with Different Surface Properties, *J. Phys. Chem. B*, **2006**, 110, (10), 4699-4707.
- [244] Zhou, A., et al., Effects of oxidative modification of carbon surface on the adsorption of sulfur compounds in diesel fuel, *App Catal B.*, **2009**, 87, (3-4), 190-199.
- [245] Seredych, M.; Bandosz, T. J., Adsorption of Dibenzothiophenes on Nanoporous Carbons: Identification of Specific Adsorption Sites Governing Capacity and Selectivity†, *Energ. Fuel.*, **2010**, 24, (6), 3352-3360.
- [246] Deliyanni, E., et al., Interactions of 4,6-Dimethyldibenzothiophene with the Surface of Activated Carbons, *Langmuir*, **2009**, 25, (16), 9302-9312.
- [247] Seredych, M., et al., Investigation of the Thermal Regeneration Efficiency of Activated Carbons Used in the Desulfurization of Model Diesel Fuel, *Ind. Eng. Chem. Res.*, **2011**, 50, (24), 14097-14104.



- [248] Figueiredo, J. L., et al., Modification of the surface chemistry of activated carbons, *Carbon*, **1999**, 37, (9), 1379-1389.
- [249] Salame, I. I.; Bandosz, T. J., Surface Chemistry of Activated Carbons: Combining the Results of Temperature-Programmed Desorption, Boehm, and Potentiometric Titrations, *J. Colloid Interface Sci.*, **2001**, 240, (1), 252-258.
- [250] Dean, J. A., *LANGE'S HANDBOOK OF CHEMISTRY*. McGRAW-HILL, INC.: New York, 1999.
- [251] Perry, R. H.; Green, D. W., *Perry's Chemical Engineers' Handbook*. McGraw-Hill: New York, 2008.
- [252] Hines, D., et al., Surface Properties of Porous Carbon Obtained from Polystyrene Sulfonic Acid-Based Organic Salts, *Langmuir*, **2004**, 20, (8), 3388-3397.
- [253] Che, Y., et al., Photooxidation of Dibenzothiophene and 4,6-Dimethyldibenzothiophene Sensitized by N-Methylquinolinium Tetrafluoroborate: Mechanism and Intermediates Investigation, *J. Phys. Chem. B*, **2005**, 109, (16), 8270-8276.
- [254] Kwon, J.-M., et al., Adsorptive Desulfurization and Denitrogenation of Refinery Fuels Using Mesoporous Silica Adsorbents, *ChemSusChem*, **2008**, 1, (4), 307-309.
- [255] EPA, U., Technical Bulletin: Nitrogen oxides (NO_x), why and how they are controlled. In Quality, O. o. a., Ed. Research Triangle Park, NC 27711, November, 1999.



- [256] Mushrush, G. W., et al., Post-refining removal of organic nitrogen compounds from diesel fuels to improve environmental quality, *Journal of Environmental Science and Health, Part A*, **2011**, 46, (2), 176-180.
- [257] Zeuthen, P., et al., Organic nitrogen compounds in gas oil blends, their hydrotreated products and the importance to hydrotreatment, *Catal. Today*, **2001**, 65, (2-4), 307-314.
- [258] Almarri, M., et al., Role of Surface Oxygen-Containing Functional Groups in Liquid-Phase Adsorption of Nitrogen Compounds on Carbon-Based Adsorbents, *Energ. Fuel.*, **2009**, 23, (8), 3940-3947.
- [259] Wen, J., et al., A critical study on the adsorption of heterocyclic sulfur and nitrogen compounds by activated carbon: Equilibrium, kinetics and thermodynamics, *Chem. Eng. J.*, **2010**, 164, (1), 29-36.
- [260] Beltramone, A. R., et al., Inhibition of the Hydrogenation and Hydrodesulfurization Reactions by Nitrogen Compounds over NiMo/Al₂O₃, *Catal. Lett.*, **2008**, 123, (3-4), 181-185.
- [261] Paulsen, P. D., et al., Applicability of adsorption equations to argon, nitrogen and volatile organic compound adsorption onto activated carbon, *Carbon*, **1999**, 37, (11), 1843-1853.
- [262] Lozano-Castelló, D., et al., Usefulness of CO₂ adsorption at 273 K for the characterization of porous carbons, *Carbon*, **2004**, 42, (7), 1233-1242.
- [263] Garrido, J., et al., Use of nitrogen vs. carbon dioxide in the characterization of activated carbons, *Langmuir*, **1987**, 3, (1), 76-81.



- [264] Arcibar-Orozco, J. A., et al., Desulfurization of model diesel fuel on activated carbon modified with iron nanoparticles: Effect of tert-butylbenzene and naphthalene concentrations, **2013**, *Energy Fuels*, 27 (9), 5380-5387.
- [265] Laredo, G. C., et al., Denitrogenation of middle distillates using adsorbent materials towards ULSD production: A review, *Fuel Process. Technol.*, **2013**, 106, 21-32.
- [266] Boehm, H. P., Surface oxides on carbon and their analysis: a critical assessment, *Carbon*, **2002**, 40, (2), 145-149.
- [267] Li, N., et al., Tailoring of surface oxygen-containing functional groups and their effect on adsorptive denitrogenation of liquid hydrocarbons over activated carbon, *AIChE J.*, **2012**.
- [268] Daichuan, D., et al., Preparation of uniform α -Fe₂O₃ particles by microwave-induced hydrolysis of ferric salts, *Materials Research Bulletin*, **1995**, 30, (5), 531-535.
- [69] Wang, W., et al., Structure and Morphology Evolution of Hematite (α -Fe₂O₃) Nanoparticles in Forced Hydrolysis of Ferric Chloride, *J Phys Chem C*, **2008**, 112, (25), 9203-9208.
- [270] Furimsky, E.; Massoth, F. E., Deactivation of hydroprocessing catalysts, *Catal. Today*, **1999**, 52, (4), 381-495.

Appendix A

Models that describe the adsorption kinetics in porous solids

Empiric models

These models assume that adsorption rate depends solely on the concentration of the adsorbate in solution and describe the adsorption processes with an empiric model, the most common and employed are the *pseudo-first* and the *pseudo-second order* kinetics ([Table A.1](#)).

Film diffusion models

Those models take into consideration that the adsorption rate is controlled by the transport of molecules from the bulk solution through the boundary layer to the surface of the solid. Those models are applicable for spherical non-porous solids in which the adsorption occurs immediately and can be described by the Langmuir equation. The film mass transference can be determined by the equation proposed by Cooney and the most common model is the one described by Boyd ([Table A.1](#)).

Intraparticle diffusion models

In pore diffusion models it is assumed that the adsorbate diffuses into the pores and is adsorbed on the walls of the pores of a spherical particle; also it is assumed

a dilute solution and local equilibrium. In those models the molecular transport is normally described by Fick's second law. The most commonly employed models are the following: 1. The *pore-volume diffusion with external mass transfer resistance* that assumes that intraparticle diffusion is only due to pore volume diffusion, particles are spherical, adsorption is instantaneous and the adsorption might be represented by the Langmuir equation, and 2. The *Homogeneous Solid Diffusion Model (HSDM)* with external mass transfer resistance that considers a dual mass transport mechanism through the boundary layer and surface diffusion of adsorbates. Both models are described in [Table A.1](#).

Model	Equation	Ref
Pseudo-first order	$\ln\left(\frac{X}{X-x}\right) = kt$	[111]
Pseudo-second order	$\frac{dq_t}{dt} = k_2(q_e - q_t)^2$	[112]
Film mass transference	$V_p\left(\frac{\partial q}{\partial t}\right) = k_f A_s (C - C_i)$	[113]
Boyd	$\ln\left(1 - \frac{q_t}{q_e}\right) = -Rt \quad \text{where} \quad R = \frac{3D}{r_0 \Delta r_0 k}$	[114]
Pore-volume diffusion with external mass transfer resistance	$\varepsilon_p \frac{\partial C_{s,r}}{\partial t} + \rho_p \frac{\partial q}{\partial t} = \frac{1}{r^2} \frac{\partial}{\partial r} \left[r^2 \left(D_{e,p} \frac{\partial C_{s,r}}{\partial r} \right) \right]$	[115]
Homogeneous solid diffusion model	$\rho_p \frac{\partial q}{\partial t} = \frac{1}{r^2} \frac{\partial}{\partial r} \left[r^2 \left(D_s \frac{\partial q}{\partial r} \right) \right]$	[111]

Appendix B

Supporting information of Chapter 2

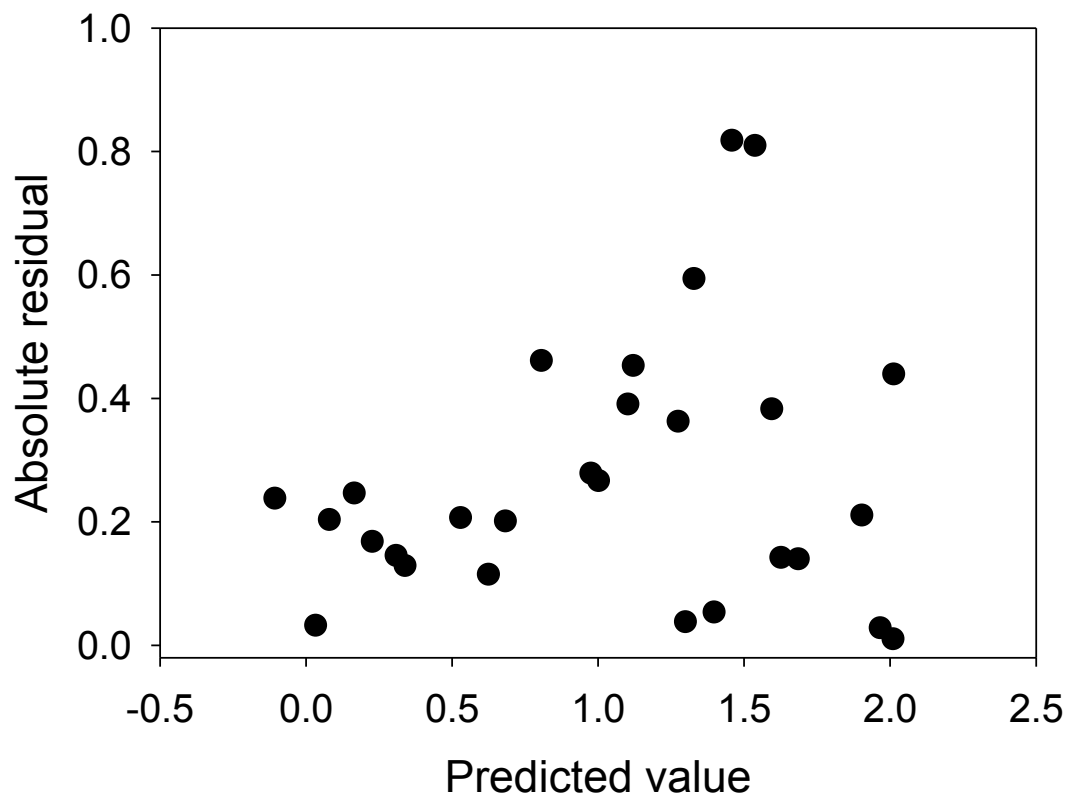


Figure A1. Results of the residual analysis

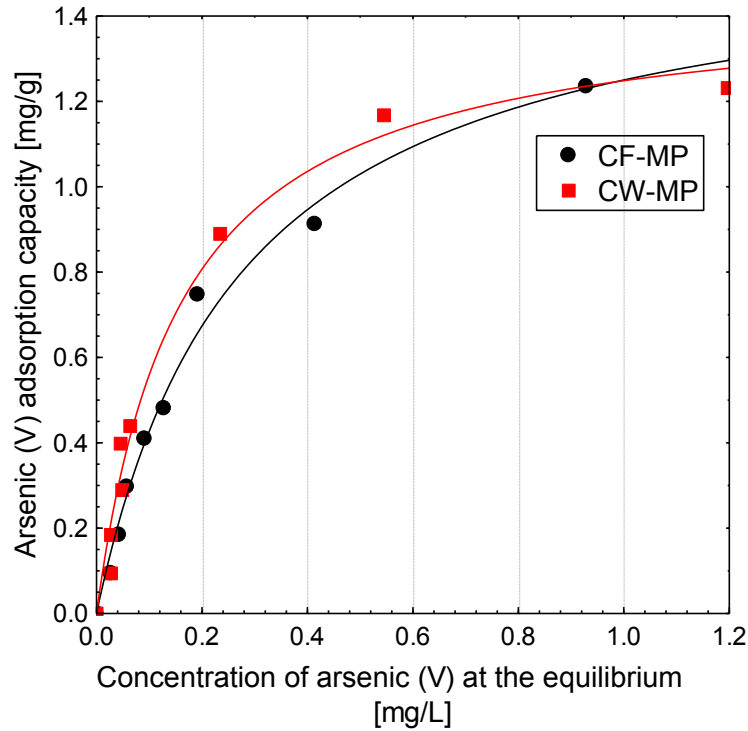


Figure B2. Arsenic(V) adsorption isotherms of best materials at pH 7 and 25°C.

Table B1. Paired Student's t-test of transformed Q As(V) values.

Factors	Log _e Mean	SD	N	t Value	df	p	95%	CL mean
Un-modified	-0.6973	1.0103	14					
Modified	0.1084	0.6467	14					
Difference	-0.8057	0.4844		-6.2229	13	<0.001	-1.085	-0.526

Table B2. Details of the empiric model

Parameter	DF	Estimate	SE	t value	p	Standardized estimate
Intercept	1	-4.054	0.506	-8.01	<.0001	0
pHPZC	1	0.214	0.033	6.44	<.0001	0.594
Fe%	1	2.393	0.54	4.43	0	1.722
Fe% ²	1	-0.884	0.302	-2.92	0.008	-1.146
v ^{Micro}	1	6.615	1.752	3.78	0.001	0.386

Table B3. Dominance analysis of QAs(V) data (n=28)

Factors in model	R ²	Additional contribution of			
		X ₁	X ₂	X ₃	X ₄
C⁽⁰⁾X_i	0.000	0.488	0.117	0.046	0.037
X₁	0.488	_____	0.170	0.118	0.004
X₂	0.117	0.541	_____	0.258	0.199
X₃	0.046	0.560	0.329	_____	0.136
X₄	0.037	0.455	0.279	0.145	_____
C⁽¹⁾X_i		0.519	0.259	0.173	0.113
X₁X₂	0.658	_____	_____	0.071	0.113
X₁X₃	0.606	_____	0.123	_____	0.084
X₁X₄	0.493	_____	0.278	0.198	_____
X₂X₃	0.375	0.354	_____	_____	0.157
X₂X₄	0.317	0.454	_____	0.215	_____
X₃X₄	0.182	0.508	0.350	_____	_____
C⁽²⁾X_i		0.439	0.251	0.161	0.118
X₁X₂X₃	0.729	_____	_____	_____	0.104
X₁X₂X₄	0.771	_____	_____	0.062	_____
X₁X₃X₄	0.690	_____	0.143	_____	_____
X₂X₃X₄	0.532	0.301	_____	_____	_____
C⁽³⁾X_i		0.301	0.143	0.062	0.104
X₁X₂X₃X₄	0.833	_____	_____	_____	_____
CXi		0.437	0.192	0.111	0.093

X₁=pHPZC, X₂=Fe%, X₃=Fe%², X₄=V^{micro}.

Table B4. Langmuir parameters of materials in Figure A2.

Sample	Langmuir parameter		R ²
	Q _{max} [mg/g]	b [L/mg]	
CF-MP	1.59	3.672	0.992
CW-MP	1.45	6.306	0.984

Appendix C

Mass spectra of adsorbed compounds in the surface of GAC and ACM 1P

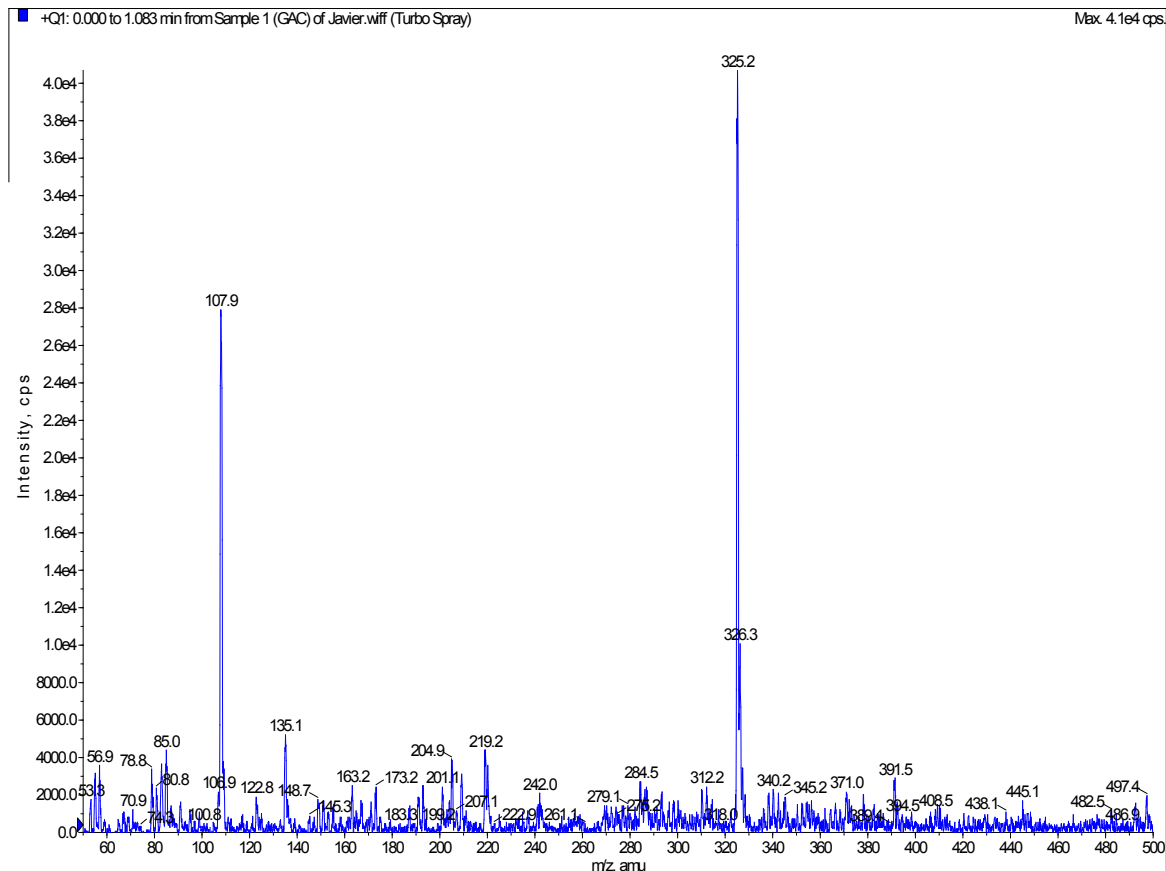


Figure C1. Mass spectra for ACF before MDF adsorption

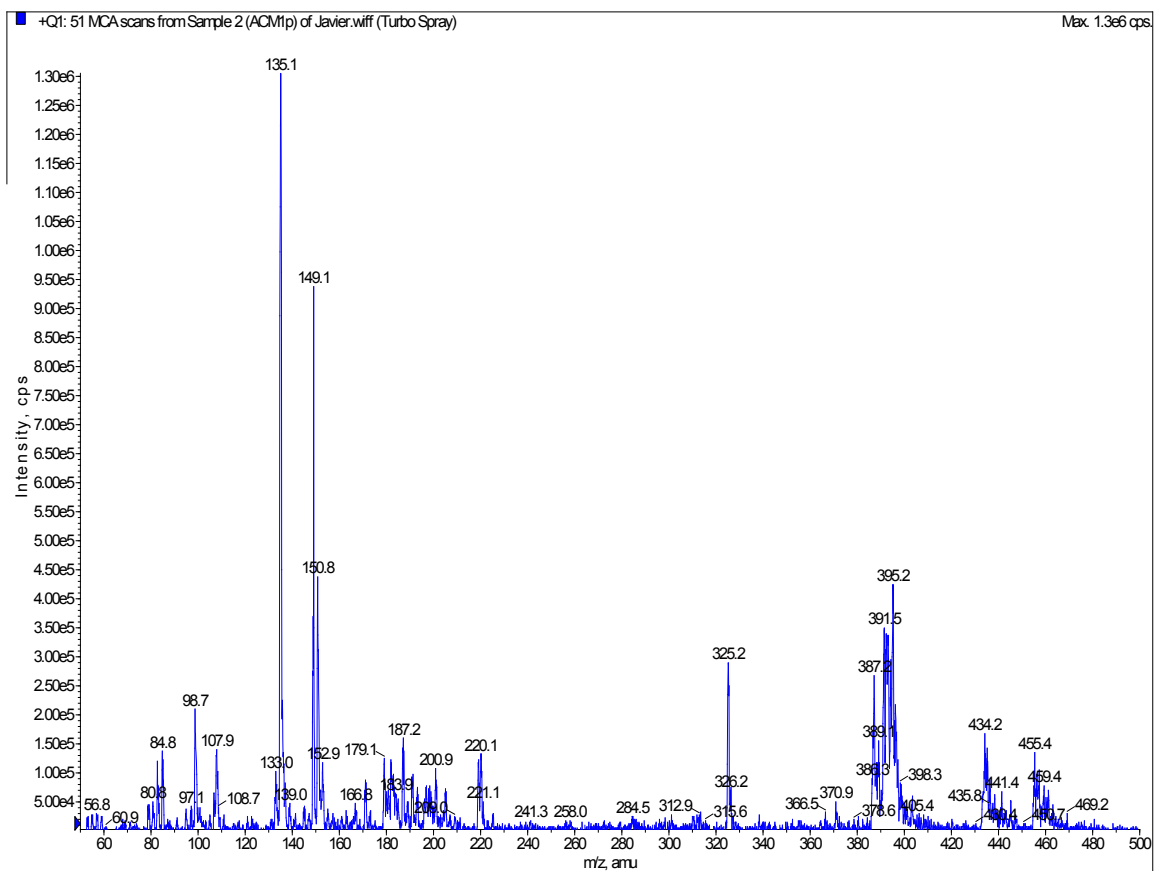


Figure C2. Mass spectra for ACM1P before MDF adsorption

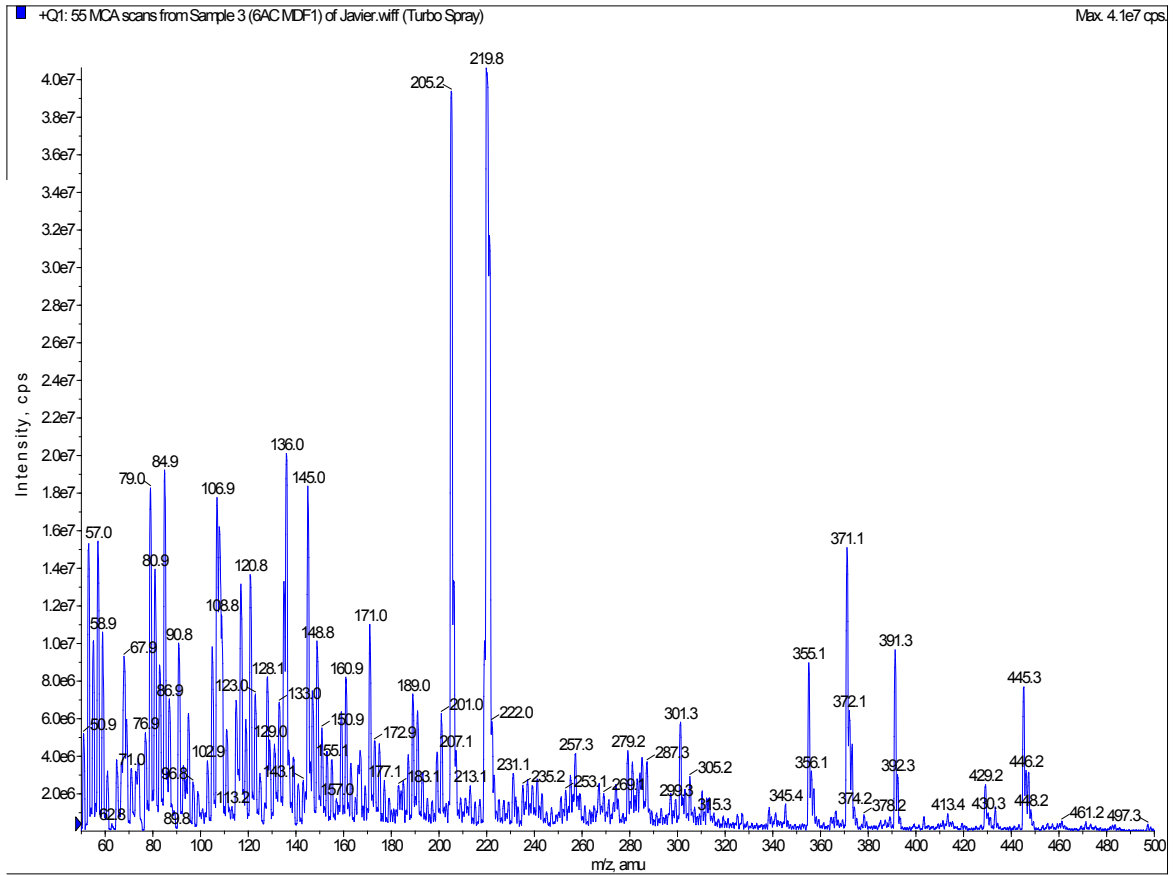


Figure C3. Mass spectra for GAC after MDF exposure

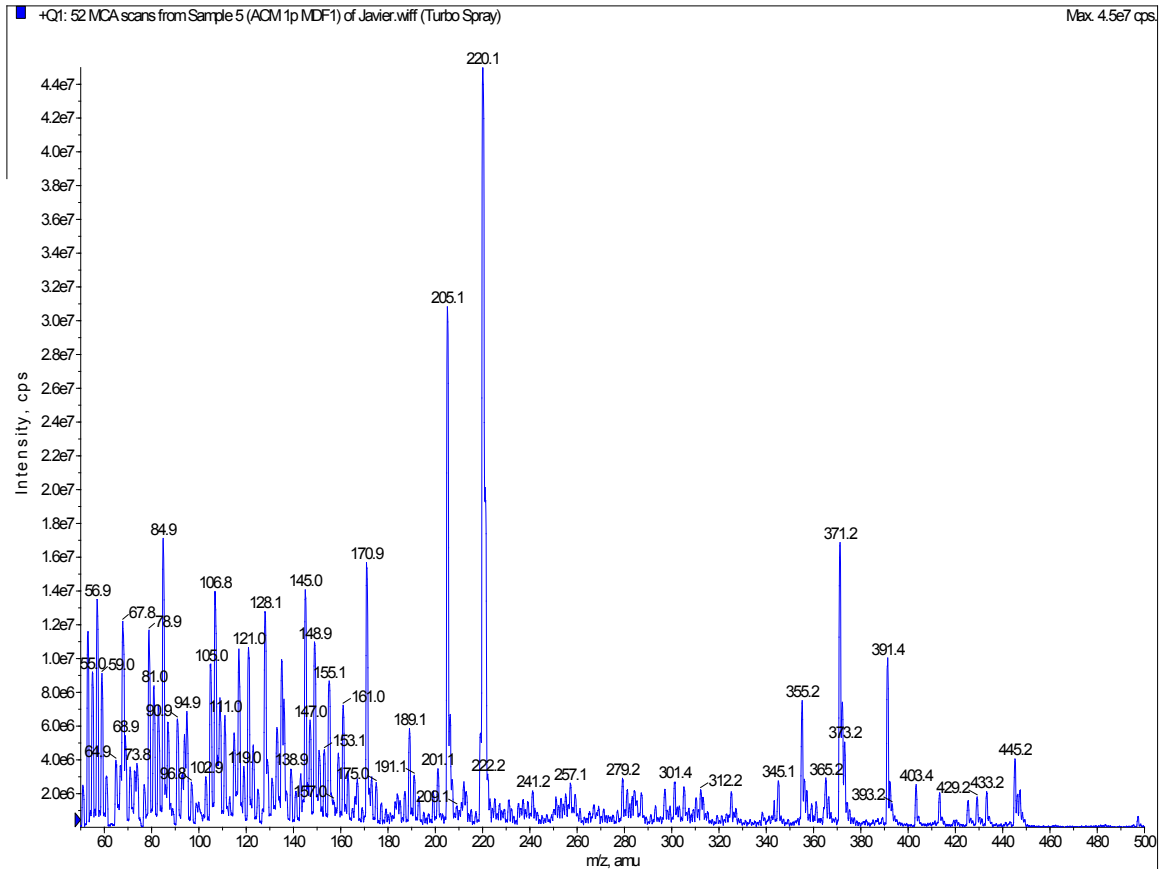


Figure C4. Mass spectra for ACM 1P after MDF exposure

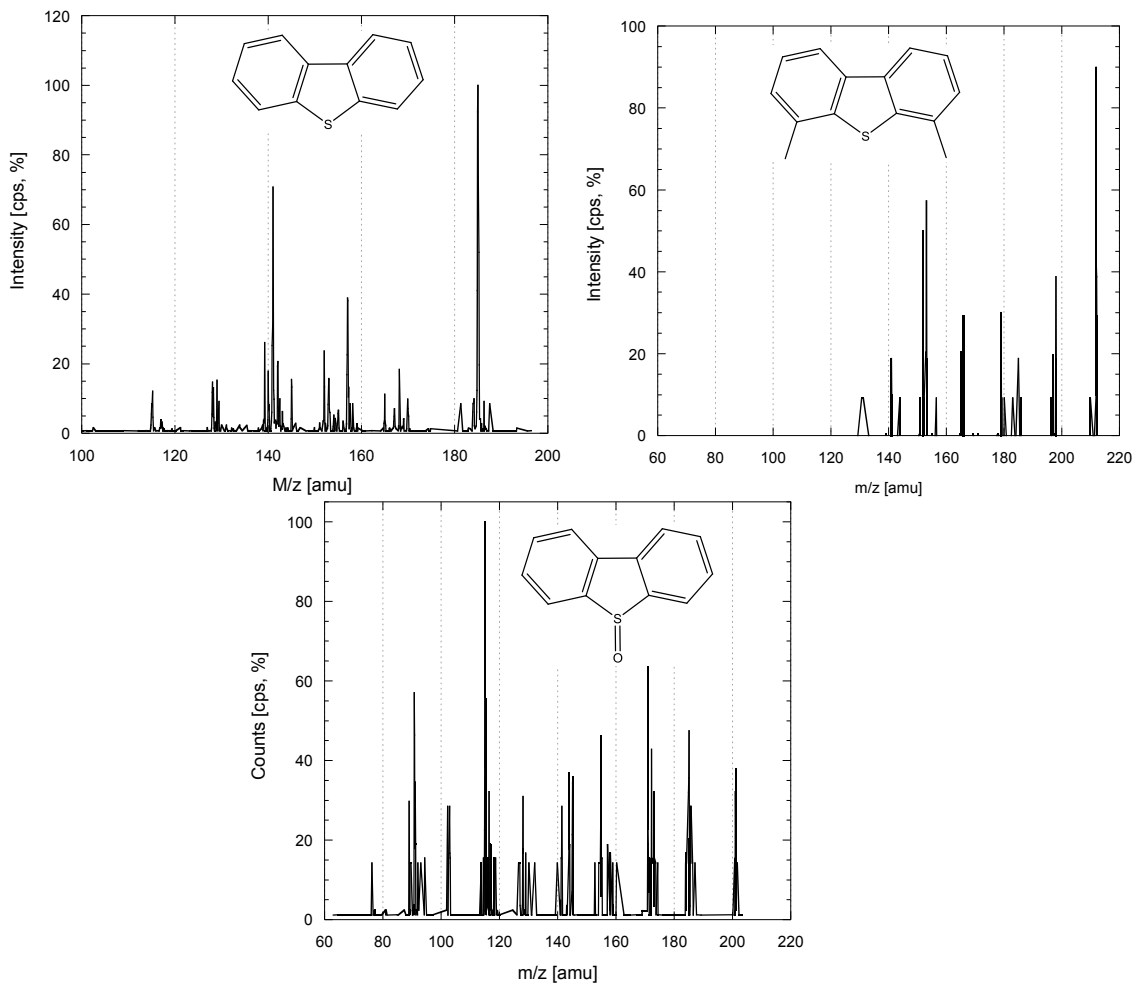


Figure C5. Mass spectra of DBT, DMDBT and DBT-sulfoxide after extraction from ACF.

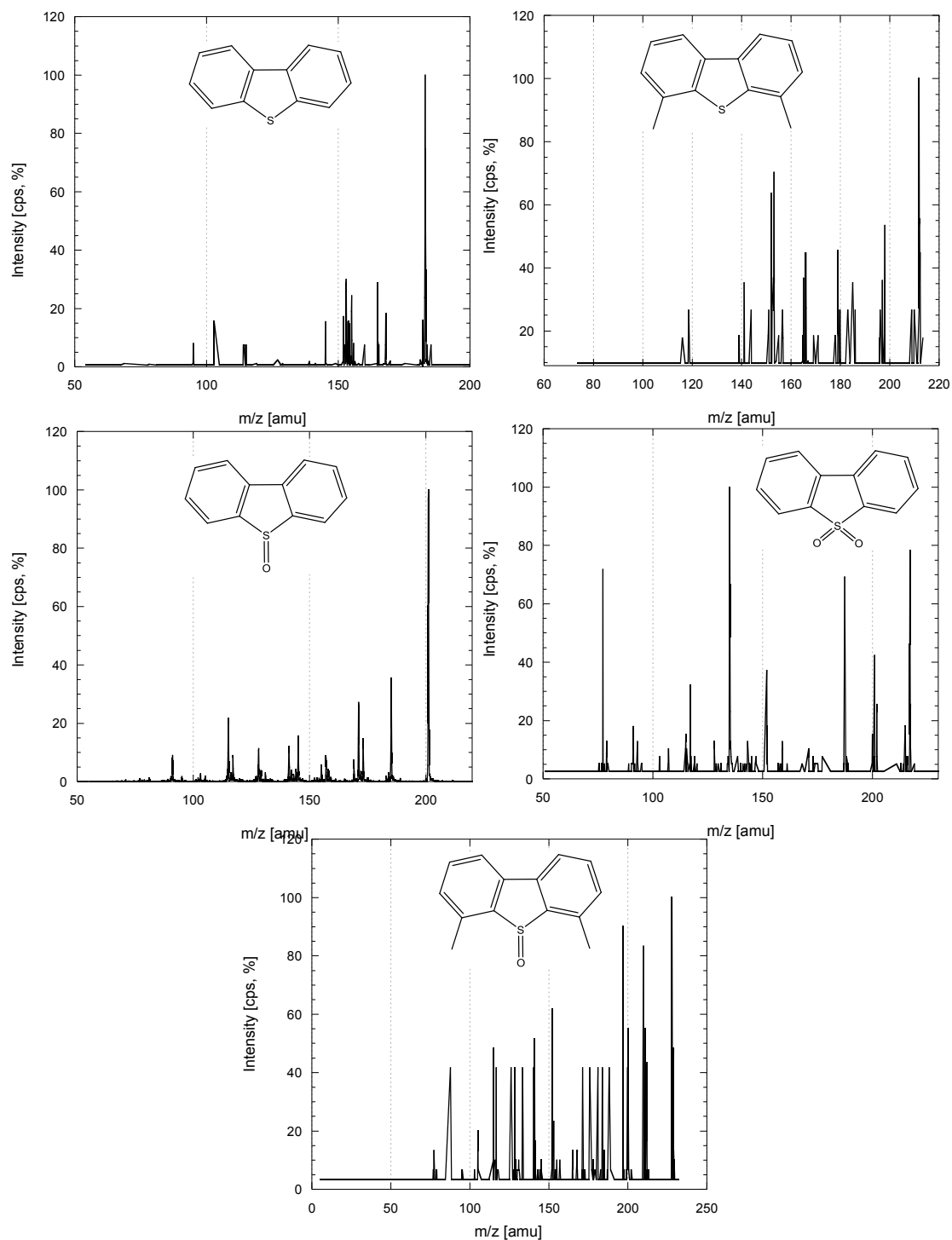


Figure C6. Mass spectra of DBT, DMDBT and DBT-sulfoxide, DBT-sulfone and DMDBT-sulfoxide after extraction from ACM1P.